Department of Pure and Applied Chemistry

BIOINSPIRED MATERIALS FOR ENZYME IMMOBILISATION AND TRANSPORT OF BIOMOLECULES

BY

ANA M. L. SOUSA

A thesis submitted to the Department of Pure and Applied Chemistry, University of Strathclyde, in part fulfilment of the regulations for the degree of Doctor of Philosophy in Chemistry.

2017

Declaration

This thesis is the result of the author's original research. It has been composed by the author and has not been previously submitted for examination which has led to the award of a degree.

Signed: Date:

Leave this world a little better than you found it and
when your turn come to die, you can die happy in
feeling that at any rate you have not wasted your time
but have done your best.

Baden-Powell

Acknowledgements

I do not have enough words to describe how thankful I am for this great experience that is my PhD. Everyone that I met during this journey was somehow important to define the person that I have become. However, I would especially like to thank:

Dr Aaron Lau for giving me this wonderful and challenging opportunity. I feel grateful for your guidance during all my PhD, for everything you taught me every day, for believing and trusting me with so many responsibilities and, most of all, for your support no matter the circumstances. Thank you for this painful, frustrating, amazing and joyful journey. I believe I am a better person and professional after doing this PhD with you.

My second supervisor Prof Peter Halling for all the support, for giving me feedback so promptly and for sharing all his expertise with me.

Prof Rein Ulijn and all his group for *adopting* me since the first day of my PhD. My first colleagues in Glasgow became my first friends in this city. They gave me all the support and showed me how good work should be done.

Dr Leonard Berlouis. My first PhD months were spent in your lab. Without your collaboration and patience I would not have been able to achieve those great shiny membranes and work with such accuracy (that ellipsometer is such a big tool!).

Prof Peter Cormack, thank you for allowing me to explore the polymerisation world. Definitely, you will be one of the academics who I will remember as reference of enthusiastic and confident speaker.

Dr Jakub Dostalek and all his group. My thesis has much more value due to our collaboration. Thank you for your availability and the opportunity to work in your lab and enjoy Vienna.

To all the staff in the stores of TG/TIC. You gave me good laughs and were very helpful. You were sign of more work and new projects, but it was great to have you on my side.

My undergrads: Catherine, Larissa, Maxence, Pedro, Matheus, Aimee, Hannah and Romain thank you for your hard work. Even a bad result in your project helped me finish my PhD. I learned from you so I could not forget to thank/congratulate you for your/our achievements.

Marwa and Kunal, thanks for encouraging, supporting me and for sharing all the good sweets that energised the writing of my thesis. I cannot forget to thank my lab/office buddy Raph! Always working together out of hours: it was good to know that you were always there.

Glasgow family: I was very proud seeing you graduating, sad leaving you, happy seeing you again, but more important I am glad that I met you all. Thanks for sharing all the frustration and happiness. Thanks for: inspiring me to work hard (Ivan); the greatest smile (Paula); all the silly videos (Flo); all the Italian input (Davide); your joy and entertainment (Kiko); being the kindest person (Laura); always being there to dry my tears (Mari); being so kind (Dan); all the new and crazy experiences (Nuno). Andreia: lucky me for having you as a flatmate! All the noisy, silent and “grey’s” moments with you were priceless; Inês, *muito obrigada por tudo*: all the random coffees, beers, walks, *coisinhas boas de* Portugal, *pela palavra amiga* that you always have ready to give and for helping me (a lot!) with the thesis.

Thank you a lot Glasgow LindyHoppers! Thanks, Ivan, Vivien, Jason, Athinais, Jack and Katie for being my buddies on the dance floor. Thanks Claire for all the good chats and cheering me up! Thank you to all my friends from Portugal that always made me feel special and gave me wonderful moments. Cristina, thank you a lot for reviewing my first ever cover letter that definitely had an enormous effect (this PhD!). Rob, thanks and *obrigada*!

Finally, I would like to thank my family that encouraged me to start this challenging journey and supported me all the time, no matter what. *Obrigada mãe e pai por acreditarem em mim e por me terem dado todo o apoio*. Thanks, my little nephews that always make me cry but make my heart warm. Thanks to my sisters-in-law and big thanks to Ângelo and Eduardo for inspiring me every day and for being so proud of me. Thanks Miguel for believing in me in every moment, for cheering me up in all the occasions that I did not feel that it was possible to finish a PhD and for being so *lado a lado* even when so many kilometers separated us. This thesis is definitely a result of your, my, our perseverance, passion, strength and determination.

The author

Publications

1 Molecular design of antifouling polymer brushes using sequence-specific peptoids

King Hang Aaron Lau, Tadas S. Sileika, Sung Hyun Park, **Ana M. L. Sousa**, Patrick Burch, Igal Szleifer, Phillip B. Messersmith

Adv. Mater. Interfaces., 2, 1, 140025 (2015)

2* Plant-based polyphenol coatings for surface functionalization with proteins and enzymes

Ana M. L. Sousa, Tai-De Li, Sabu Varghese, Peter J. Halling, and King Hang Aaron Lau

Adv. Funct. Mater. manuscript in preparation

3* Nanoporous alumina as optical waveguides for characterising molecular diffusion in nanopores

Ana M. L. Sousa, Jakub Dostalek, Peter J. Halling, King Hang Aaron Lau

ACS Appl. Mater. Interfaces, manuscript in preparation

4* Impedance measurements for anodic aluminium oxide (AAO) pore opening

Ana M. L. Sousa, Leonard Berlouis, King Hang Aaron Lau

joVE, manuscript in preparation

*Publication related to work in this thesis

Conferences and Outreach activities

2015 MC12 – 12th International Conference on Materials Chemistry
University of York, UK
Improving Biocatalysis with Polyphenol Functionalisation of Nanoporous Alumina Oxide – Poster presentation

2015 Image of Research
University of Strathclyde
Tasty Membranes – Image competition

2016 E-MRS – European Materials Research Society 2016 Fall Meeting
Warsaw University of Technology, Poland
Enzyme immobilization with bioinspired polyphenol and polydopamine surface functionalisation – Poster presentation
Characterising molecular diffusion through nanopores using nanoporous anodic alumina waveguides – Poster presentation, Best Student Presentation Award

2017 ACS meeting – 254th American Chemical Society National Meeting & Exposition
Washington, DC
Plant-based polyphenol coatings for surface functionalization with proteins and enzymes – Oral presentation
Characterizing molecular diffusion through nanopores using nanoporous anodic alumina waveguides – Poster presentation

Abstract

Protein and enzyme immobilisation on synthetic material surfaces enables a range of applications from biosensing to industrial biocatalysis. There are several immobilisation techniques, but common methods need multiple preparation steps or are material-dependent, which reduce the effectiveness and success of biosensing/industrial applications.

In this thesis, the possibility of using plant-based polyphenol coatings to immobilise a range of proteins and enzymes (avidin, immunoglobulin G, acid phosphatase, chymotrypsin, lactate dehydrogenase, horseradish peroxidase) on polymeric or oxide materials (cellulose, polyester, silica, alumina and stainless steel) was shown for the first time. Polyphenols are in abundance in nature and less costly than dopamine (common immobilisation agent). Polyphenols were more effective than physisorption and polydopamine coatings for certain combinations of materials and proteins. Several parameters that can influence the immobilisation procedure were evaluated showing that there is a dependence on the coating and immobilisation pH as well as the type of coating and material.

Polyphenol coatings were also used to functionalise nanoporous anodic aluminium oxide (AAO) membranes in order to measure molecular transport through nanopores. Inspired by the biological nanopores that enable the highly specific and efficient separation of a range of biomolecules, we used AAO membranes with a pore size matching the biological nuclear pore complex for controlling the diffusion of molecules through the pores. AAO membranes also match the requirements for optical waveguide spectroscopy (OWS) that was used to characterise and differentiate processes that occurred inside and above the nanoporous membranes. In a second approach, a nanoporous membrane was placed between two gaskets to be suspended on the flow cell. This work brings a new concept of how the molecular diffusion can be characterised, which is important for controlling the transport of biomolecules. It was possible to monitor *in situ* biocatalytic reactions as well as nanopore transport control by using a responsive polymer that was able to allow and restrict the transport of molecules.

Abbreviations

AAO	Anodic aluminum oxide
BSA	Bovine Serum Albumin
DOPA	3,4-dihydroxy-L-phenylalanine
HRP	Horseradish peroxidase
LDH	Lactate dehydrogenase
LCST	Lower critical solubility temperature
OWS	Optical waveguide spectroscopy
pDA	Polydopamine
PEG	Poly(ethylene glycol)
pPG	Pyrogallol or 1,2,3-trihydroxybenzene
PNIPAM	Poly(N-isopropylacrylamide)
pTA	Poly(tannic acid)
pTHPA	Poly(3,4,5-trihydroxyphenethylamine)
TIR	Total internal reflection
XPS	X-ray photoelectron spectroscopy

Table of Contents

1. Introduction

1.1 Project Motivation

Immobilisation of biomolecules on material supports is an advantage on several applications from biosensing to industrial biocatalysis. Proteins and enzymatic proteins on solid supports are conveniently handled and can be recovered because they are readily separated from the solution phase.[1] Protein immobilisation reduces waste and cost by reducing the need of purification[1,2] and through reuse of the enzymes.[3–5]

There are several immobilisation methods, however common methods can lead to non-specific binding and protein denaturation, which reduce the sensitivity and efficacy of biosensing/industrial applications.[6] Some other methods can be laborious, specific linkers can be costly, and commercially available methods are effective only on specific materials. For these reasons, it is desired to find a "universal" approach where any material can be functionalised and be used for immobilising biomolecules without changing the biochemical and physical properties of the biomolecules.

Nanoporous supports can be used for biomolecule immobilisation due to their high surface area. Some nanoporous supports also have another potential, which is mimicking the biological nanopores that are able to control and regulate the transport of proteins and RNA between the cell nucleus and the cytosol. Nevertheless, there is a lack of techniques able to characterise the transport of different molecules. Pore functionalisation to control the entry and exit of molecules is also less developed.

Optical waveguide spectroscopy (OWS) can be used to characterise and differentiate processes that occur inside and above the pore entrance. The use of OWS can be an attractive idea to characterise the functionalisation of nanoporous materials that can control the transport of biomacromolecules.

It would be advantageous to create a spontaneous and facile strategy to functionalise different materials for immobilising macromolecules and to develop and characterise molecular transport control through nanopores.

1.2 Project Aims

The main aims of this project are to develop a new strategy to immobilise enzymes on different materials and develop bioinspired, synthetic nanoporous structures that can control molecular transport through nanopores. The specific aims are:

- Create spontaneous and stable polyphenol films on a nanoporous material;
- Study the different parameters that influence the coating and immobilisation processes;
- Investigate polyphenol coatings for immobilising proteins;
- Characterise the diffusion of different molecules through nanoporous membranes;
- Control the transport of biomolecules;

A simple summary of the different main aims of this project is represented in Figure 1.1.

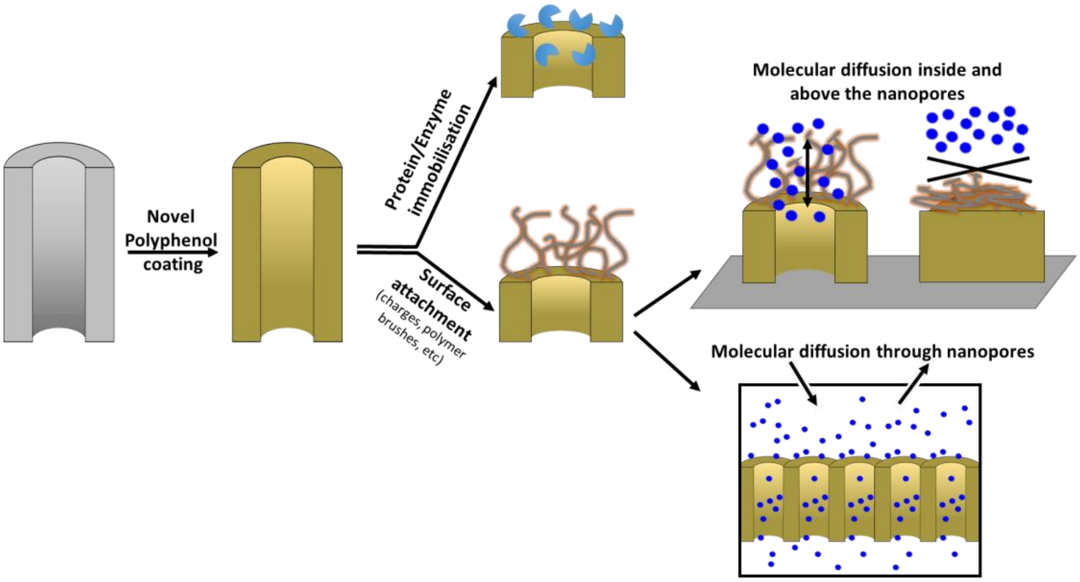

Figure 1.1 – Scheme highlighting the strategy adopted for functionalisation of nanoporous material with polyphenols for protein/enzyme immobilisation or for the attachment of polymer brushes or other molecules in order to characterise diffusion through nanoporous membranes. The enzymes and the grafted-polymer are represented by the blue pac-man and the brown spaghetti, respectively. Dark blue dots represent fluorophores.

1.3 Layout of the Thesis

The thesis starts with an overview of the literature about surface modification for biomolecules attachment, universal coating and surface immobilisation for biointerfacial applications. For surface immobilisation, antifouling surfaces and enzyme immobilisation will in particular be discussed. The different common methods used to achieve antifouling surfaces preventing protein adsorption will be described. The importance of immobilising enzymes as well as the considerations to take into account during enzyme immobilisation are discussed. This chapter subsection finishes with a discussion of the use of nanoporous supports for enzyme immobilisation. Novel concepts of enzyme immobilisation on nanoporous supports used to overcome some of the problems or to improve the enzyme immobilisation are summarised.

Chapter 3 depicts the use of plant-based polyphenol coatings for surface functionalisation with proteins and enzymes. The polyphenol coatings were used for protein immobilisation on alumina, regenerated cellulose, stainless steel, polyester and silica. The activity of the immobilised enzymes was measured and effectiveness of the polyphenol was compared to the activity of enzymes immobilised by dopamine coatings and physisorption method. Different parameters that influence both coating and immobilisation procedures were assessed.

The characterisation of the diffusion of different molecules through nanoporous alumina membranes is described in Chapter 4. This work was performed in Austrian Institute of Technology (AIT) using optical waveguide spectroscopy (OWS). With this technique, light can be confined at different depths of the nanopores and, for that reason, it was possible to distinguish processes that occurred inside and outside of the nanoporous AAO membranes. Polyphenol coatings were also used in this chapter to graft a polymer, (poly(ethylene glycol) PEG), for preventing adsorption events.

Chapter 5 shows a simple and versatile method for using an attenuated total reflection (ATR) setup for characterising the diffusion of molecules through a nanoporous membrane placed between two gaskets in a flow cell – suspended membrane. “Switch-on” of the transport of molecules as well as biocatalytic reactions were monitored *in situ* using this technique. The molecular transport was controlled by using a responsive polymer that was able to allow or restrict the passage of molecules.

Chapter 6 (conclusions and future work) highlights the achievements of this work, what challenges remained, and proposes some further work based on the main conclusions achieved and the latest developments.

In this thesis, there is supporting information of the chapters stated above in the appendices. In particular, the description of the fabrication steps of the nanoporous membrane that resulted on the membranes used in chapter 4 and 5 is given. An appendix about diffusion and other processes that occur during the measurements performed in chapter 4 and 5 was prepared to clarify and justify the analysis and interpretation of the data.

2. Literature Review

2.1 Surface modification for biomolecules attachment

2.1.1 Introduction

The surfaces of solid materials may need to be modified to give the desired properties for specific applications. The change of properties on the surface of a material is called "surface modification" in general. If functional groups are added to the surface, this is called "surface functionalisation". Surface modification will be used as a general term that also includes surface functionalisation. Surface modifications can alter physical, chemical and/or biological properties so that the interaction between the surface and the environment is improved for better performance or to give additional functionality to the material. The different characteristics that can be changed include surface energy, hydrophobicity/hydrophilicity (wettability), chemical inertness, roughness, surface charge, biocompatibility, conductivity and reactivity.[7,8] For example, on packing boards, surface oxidation is commonly applied to increase the surface energy and amount of polar groups for increasing the printability and durability of the ink.[9,10] The wettability of the surface is also an important factor on the adhesion (attraction of modifier to the surface) and cohesion (attraction between modifier atoms or molecules). The wettability can be controlled by altering the hydrophobic interactions (by adding or removing polar groups).[11] The roughness of the material can have an enormous impact on the surface area of the material. The introduction of a porous structure increases the surface area of the material and consequently allows more functional groups to be added on the surface.[9]

Surface modification should affect only a thin layer of the surface, because thick layers may alter the mechanical properties of the bulk material. Thick coatings can also suffer from delamination – layer coming off from the material. However, in some cases, a thicker layer is necessary in order to assure a total coverage of the surface for post functionalisation.[12]

The previous cases described the modification of surfaces for changing the function/applicability of the materials. In this thesis, there was a specific interest in chemical modification techniques that can be used for either immobilising or repelling biomolecules as these modified surfaces can be used in numerous applications in biotechnology, medicine, spectroscopy, and biocatalysis. For this reason, the next section (2.1.2) will describe common methods that can be used for coupling biomolecules.

Section 2.3 will describe some methods that have been used to prevent protein adsorption. The summary of all these methods is shown in Figure 2.1.

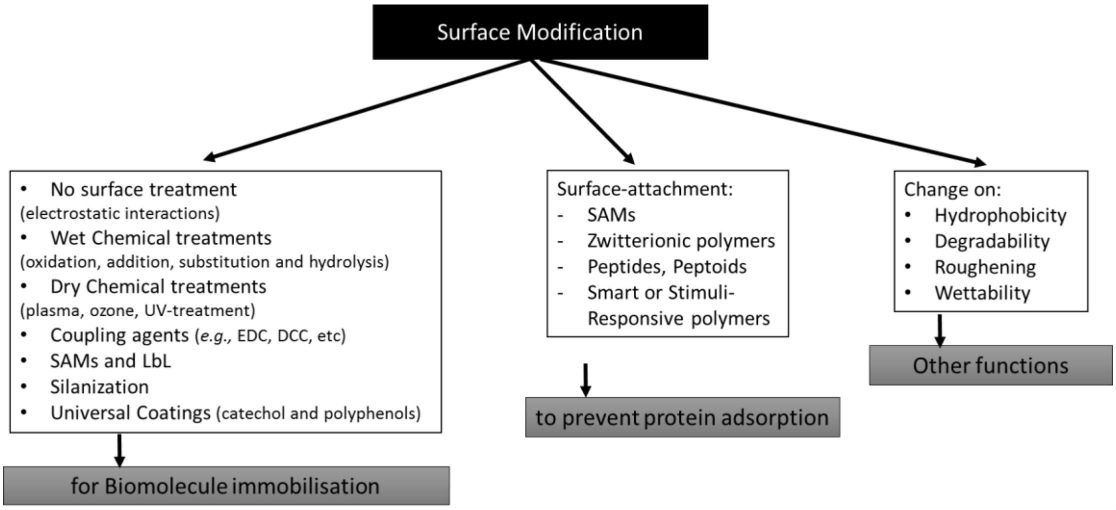

Figure 2.1 – Overall scheme of surface functionalisation techniques used to couple biomolecules to a surface, to prevent protein adsorption or to give other functionality to the surface material.

The attachment of molecules to a surface can be by physisorption and/or covalent coupling. Physisorption means that the biomolecules are adsorbed on the surface by non-specific intermolecular forces such as electrostatic, van der Waals or hydrophobic interactions. Despite the fact that most of these physisorbed interactions are weak, multiple weak interactions can secure the molecules to the surface strongly. Another interesting fact about physisorption is that desorption can occur over time. However, for some specific applications and materials, a covalent bond between the biomolecule and the surface is needed in order not to lose the biomolecules during their use. In some other cases, the biomolecule can be bound to the surface by a combination of physisorption interactions and covalent bonds because the biomolecules can have more than one type of chemical group to interact with the surface.

2.1.2 Common methods of surface modification for biomolecules attachment

Chemical treatments include oxidation, addition, substitution and hydrolysis. Wet or dry chemical treatments can be applied depending on the material and the functional groups that are desired to be on the surface.

- Wet chemical methods involve immersion of the material in a solution and its surface is altered during the treatment. A simple example is the wet chemical hydrolysis of polyester fabric. The fabric is immersed in a solution of sodium hydroxide (NaOH) for a certain time, resulting on the generation of reactive carboxylic acid groups that can interact with other (bio)molecules.[7]

- Dry chemical methods include plasma, ozone and UV treatments. In the simplest case, plasma treatments clean surfaces and increase their hydrophilicity which can be convenient for immobilisation of proteins (either by physisorption or covalent bonding).[13] Depending on the chemical nature of the base material, O_2-plasma can introduce carboxylic acid, peroxide and hydroxyl groups, and CO_2-plasma can also introduce carboxyl groups as well as hydroxyl, ester and carbonyl groups – ketones and aldehydes.[10] Ketone-activated surfaces can then interact with primary or secondary amine groups.[14,15] Nitrogen, ammonia and N_2/H_2-plasmas introduce primary, secondary, and tertiary amines and amides. Although no functional groups are introduced on the surface by Ar or He plasmas, free radicals are created on the surface that can initiate other processes (*e.g.*, coupling initiator molecules for grafting polymerisations).[16] A unique advantage of plasma treatment is that the top of the surface (nanometers) can be modified without using solvents or generating chemical waste. There can be less degradation and roughening of the material when compared to wet chemical treatments. As for disadvantages, this method is not very versatile in the sense that the optimal parameters for one specific material cannot be adopted for another system, and usually costly vacuum and power equipment is required for this technique.

Generally, ozone/UV treatments generate carbonyl and hydroxyl groups on polymeric and oxide surfaces, respectively.[7,9] The introduction of these functional groups can be used for further chemical coupling or silanization reactions. Using an ozone plasma, it is also possible to activate monomers or initiators for polymer grafting polymerisation (see section 2.3.1).[16]

Self-assembly monolayers (SAMs) are organic assemblies formed by spontaneous adsorption, rearrangement and chemical reaction of molecules species (usually) from the liquid phase onto solid surfaces. There are many advantages using this method over other techniques such as the simplicity of forming well-defined layers with different terminal chemical groups. SAMs is in principle not restricted to the type of surface and the end groups of the last layer can be used to tailor surface properties, if a suitable surface coupling chemistry can be found.[17–19] The way that biomolecules can then attach to SAMs depends on the nature of the functional groups on the monolayers and the biomolecule structure. Figure 2.2 shows an example of a SAMs that is able to covalently bond a biomolecule. These SAMs are composed of a thiol end group, a hydrophobic alkyl chain and oligo ethylene glycol (OEG) segments with a carboxylic acid at the end. The thiol group binds covalently to the gold surface, the alkyl chain is used to help to order the SAMs on the surface, OEG prevents physisorption of proteins to the alkyl chains and the carboxylic acid end group is used to bind amine-containing molecules covalently.

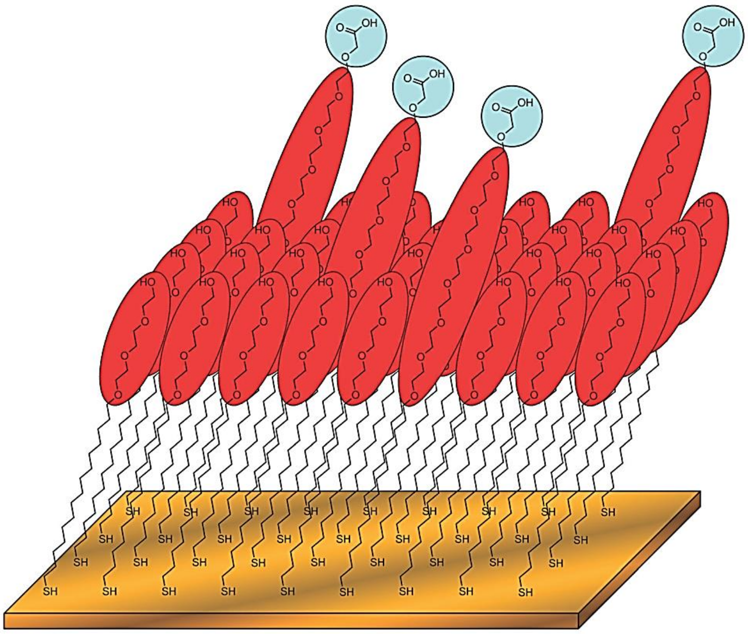

Figure 2.2 – Self-assembling monolayers (SAMs) on gold. Thiol groups (-SH) bind to the gold surface. Alkyl chains are used for assembly of the monolayer. Oligo ethylene glycol (PEG) groups (red) are used to avoid protein adsorption and the carboxylic groups (blue) are used for coupling to biomolecules containing amine groups. Copyright from [20].

Layer-by-layer (LbL) technique is the deposition of layers of polyelectrolytes with alternating charges on the surface of a material. The electrostatic interactions enable the modification of the surface and consequently the introduction of other layers. The first demonstration of this technique was with polyelectrolytes showing that LbL can control film composition, thickness and function on the nanoscale by changing the number, sequence and chemical nature of the polyelectrolyte layers.[21,22] An alternative LbL strategy is to exploit specific biorecognition interactions between molecules (*e.g.*, proteins). For example, Lazzara *et al.* attached avidin, a protein that is positively charged at neutral pH, to a negatively charged surface.[23] The next layer was added by using another protein that was functionalised with biotin (biotinylated-bovine serum albumin). This biotin has high affinity to avidin, so the two proteins were bounded by non-covalent interaction layer by layer. In sum, any molecule (polymer, protein, lipid) or surface that is functionalised with biotin can be paired with (strept)avidin proteins for LbL surface functionalisation.[24]

Coupling agents are organic molecules that aid in the formation of chemical bonds between two functional groups. For example, carboxylic acids (formed by plasma or other treatment) can react with carbodiimides to form highly reactive O-acylisourea derivatives that can then react with a nucleophile such as a primary amine. Two very commonly used and versatile carbodiimides are 1-ehyl-3-(3-dimethylaminopropyl)carbodiimide (EDC) and N,N'-dicyclohexylcarbodiimide (DCC) for aqueous and non-aqueous activations, respectively. N,N’-diisopropylcarbodiimide (DIC) is a convenient alternative to DCC because is easier to handle as a liquid, more soluble and its by product is soluble in most organic solvents.[25]

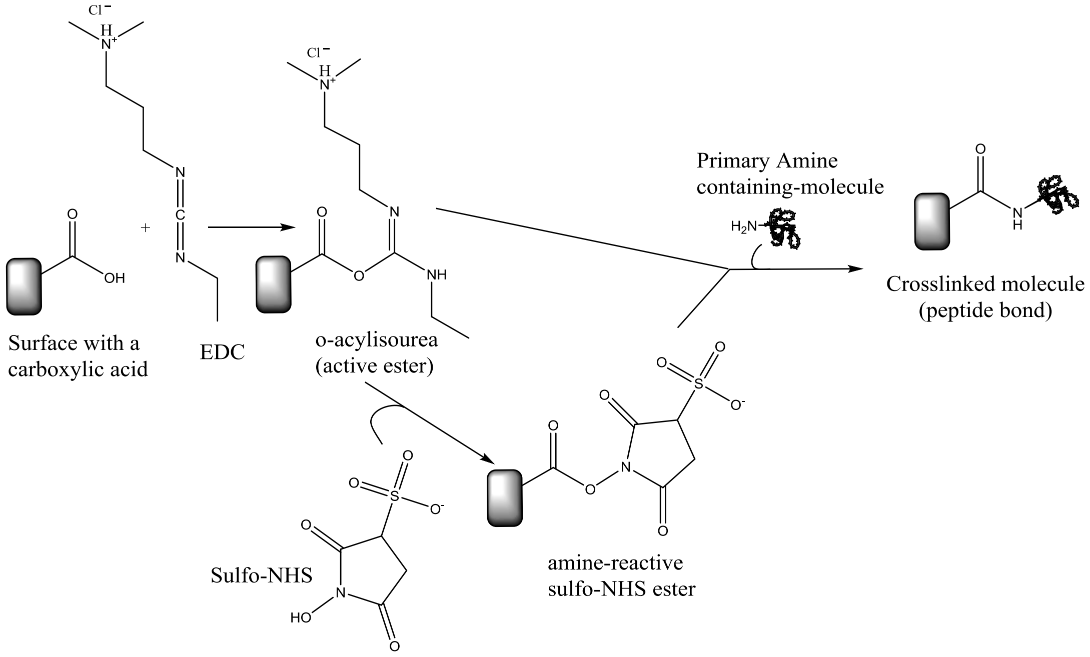

Figure 2.3 – Formation of activated carboxylic acid by carbodiimide coupling agent – 1-ethyl-3-(3-dimethylaminopropyl)carbodiimide (EDC). This intermediate can react with a nucleophile such as a primary amine or sulfo-N-hydroxysuccinimide (Sulfo-NHS) to form an amide bond with an amine-containing molecule. Adapted from [26].

EDC can be used in combination with *N*-hydroxysuccinimide (NHS) to improve coupling efficiency. NHS is coupled to the carboxylic groups by EDC forming NHS ester, which is more stable than the O-acylisourea intermediate (at physiological pH) (Figure 2.3). This is followed by reaction between the amine group (present in the biomolecules structure) and the reactive intermediate forming an amide bond.[26]

This carbodiimide crosslinker chemistry is very commonly used and a range of kits are commercially available. These kits are often used for amide conjugation to label carboxyl groups with amine compounds (*e.g.*, amine-biotin or amine-PEG) and to immobilise peptides to surface materials.

Other amide coupling reagents are phosphonium (*e.g.*, BOP, Benzotriazol-1-yloxy-tris(dimethylamino)-phosphonium hexafluorophosphate), aminium salts (*e.g.*, TBTU/HBTU, (N-[(1H-benzotriazol-1-yl)(dimethylamino)-methylene]-N-methylmethan aminium tetra/hexa-fluoroborate, and TATU/HATU, N-[(dimethylamino)-1H-1,2,3-triazolo-[4,5-b]pyridin-1-ylmethylene]-N-methylmethanaminium tetra/hexa-fluoro phosphate N-oxide) and triazenes.[25]

It is also possible to couple biomolecules through other functional groups, such as aldehydes and ketones. Aldehydes and ketones do not naturally occur in proteins or other biomolecules but aldehydes can be formed by oxidising sugar moieties (present in polysaccharides, glycoproteins, or in the ribose unit of RNA). A very common sugar oxidising agent is sodium periodate that forms activated-aldehydes that can then react with hydrazide or alkoxyamine reagents to form hydrazone and oxime bonds, respectively.[27]

To immobilise aldehyde-containing molecules on an amine-surface or to immobilise biomolecules with primary amine groups on an activated aldehyde surface, reductive amination reaction chemistry can be applied (Figure 2.4). The electrophilic carbon atom of the aldehyde attacks the nucleophilic nitrogen of the primary amine to form an unstable Schiff base. This structure is reduced by sodium cyanoborohydride ($NaCNBH_3$) to form an alkylamine (secondary amine).

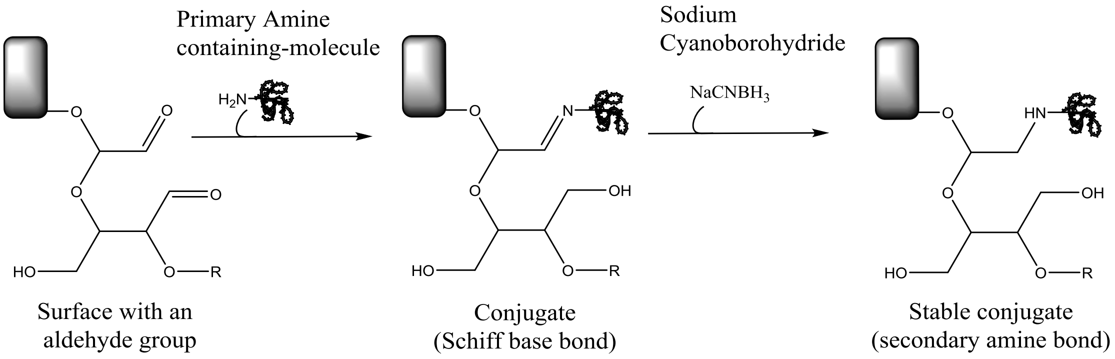

Figure 2.4 – Reductive amination reaction between an aldehyde and primary amine groups to form a covalent secondary amine bond. Cyanoborohydride ($NaCNBH_3$) is used as a reducing agent to stabilise the Schiff base bond. Adapted from [27].

Agarose is a common support material used for immobilising proteins and other biomolecules that contain primary amines. The secondary amine bond is used to bind the aldehyde-activated agarose with amine groups.[28]

Another common functional group present in proteins and other biomolecules for coupling to a functionalised surface is the sulfhydryl (-SH) group, also called a thiol. This group is found in (i) cysteine amino acid or (ii) amine groups can be converted to thiol groups. Iodoacetyl-activated surfaces are the commercially available supports for this type of coupling. Thiol groups can react with this activated surface forming a stable thioether bond. Despite the fact that this coupling is very specific for thiol groups, a slight change in the conditions of the reaction (*e.g.*, pH, time, concentration) promotes the binding to other functional groups.[29] Iodoacetyl-activated surfaces can be obtained by coupling the carboxylate of iodoacetic acid to an amine group to form an amide bond (by EDC coupling).[28] Amine-activated surfaces can be prepared by silanization.

Silanization is the process of adding a silane coating to a surface. The most common structure for a silane is a monomeric silicon-based molecule containing three constituents: a terminal functional or reactive group, an alkyl chain linker and the silane group. The functional group can be any number of groups, and commercially available silanes can have *e.g.*, a methylene, a halogen, a -OH group, a -NH_2 group, groups containing methyl or ethyl ethers, thiol, and others. The functional group can also be bonded to the silicon atom directly (without the linker in between), but the alkyl chain avoids steric effects.[30]

Silanization is favourable on surfaces like silica glass and oxides that contain hydroxyl groups (Figure 2.5). However, hydroxyl groups can be added before the silanization process by other techniques such as the ones described previously.

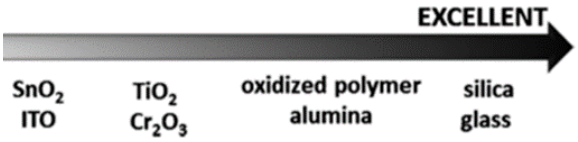

Figure 2.5 – Effectiveness of silane modification of various inorganic substrates. (ITO = indium tin oxide). Copyright from [19].

To coat a surface by silanization, different reactions occur (Figure 2.6). The first reaction is the hydrolysis of the silane *e.g.*, an alkoxysilane, to form a reactive intermediate. This intermediate interacts with more molecules by hydrogen bonding, and then a condensation reaction occurs to form a polymer matrix linked together by -Si-O-Si- bonds. This network interacts with the surface by hydrogen bonds, and another condensation reaction then occurs to result in the formation of covalently linked organosilane network to the surface.

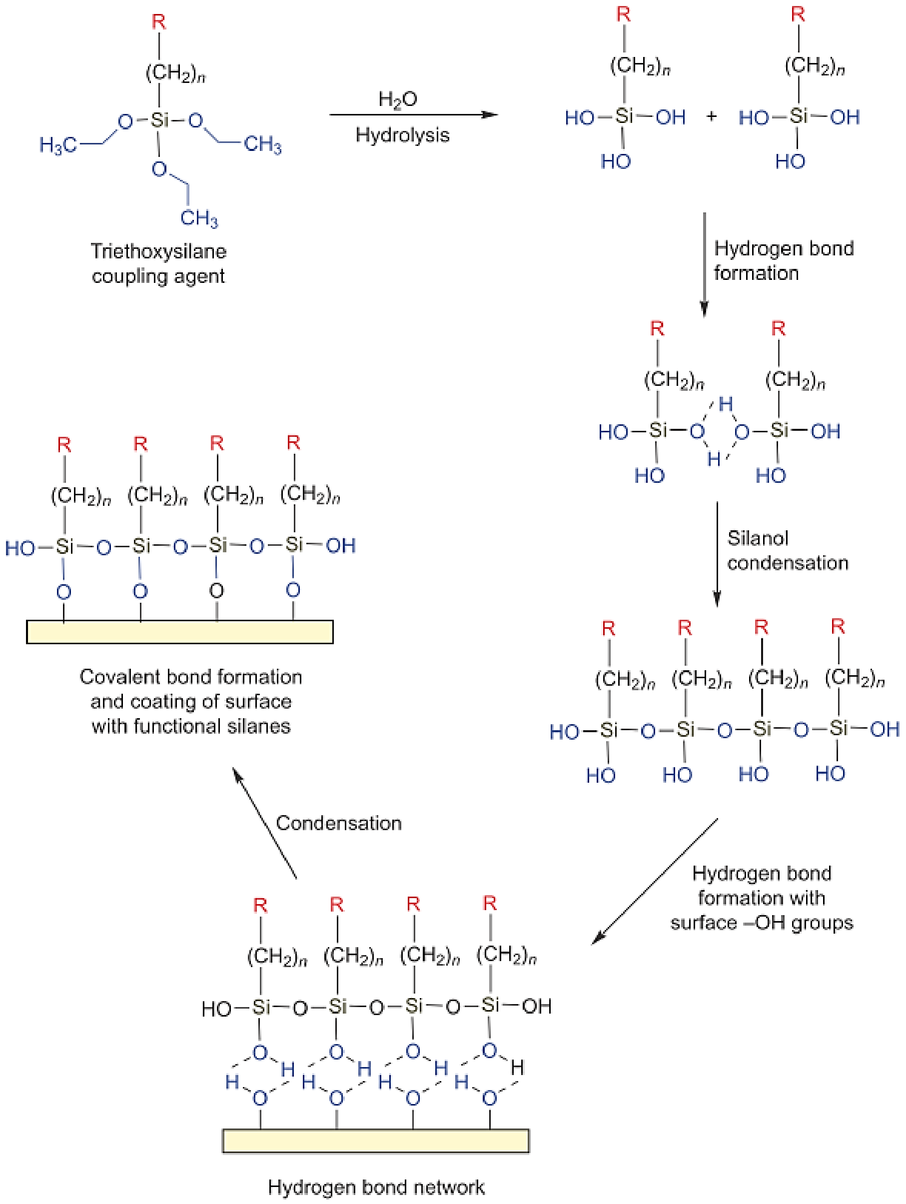

Figure 2.6 – Reactions involved between the silane and a surface. (1) Hydrolysis of the alkoxysilane groups to form highly reactive silanols (R – functional or reactive group). (2) Hydrogen bonds between the silanol molecules in solution and on the surface, forming a polymeric matrix. (3) Condensation reaction to covalently bind the polymerised coating to the surface of the material. Copyright from [30].

There are various types of silane deposition techniques. The reactions can be performed in solution or in the vapour phase. The solution can be aqueous, organic or a mixture of organic solvent with a small amount of water, typically at room temperature. Vapour phase deposition is normally carried out at high temperatures (50-120 °C).[19] The choice of reaction technique depends on the surface of the material, and the functional group of the silane molecule. Solubility, viscosity and polarity of the silane are other factors that need to be taken into account. A summary of the different silane groups, silanization reactions and the coupling with biomolecules is shown in Figure 2.7 and Figure 2.8.

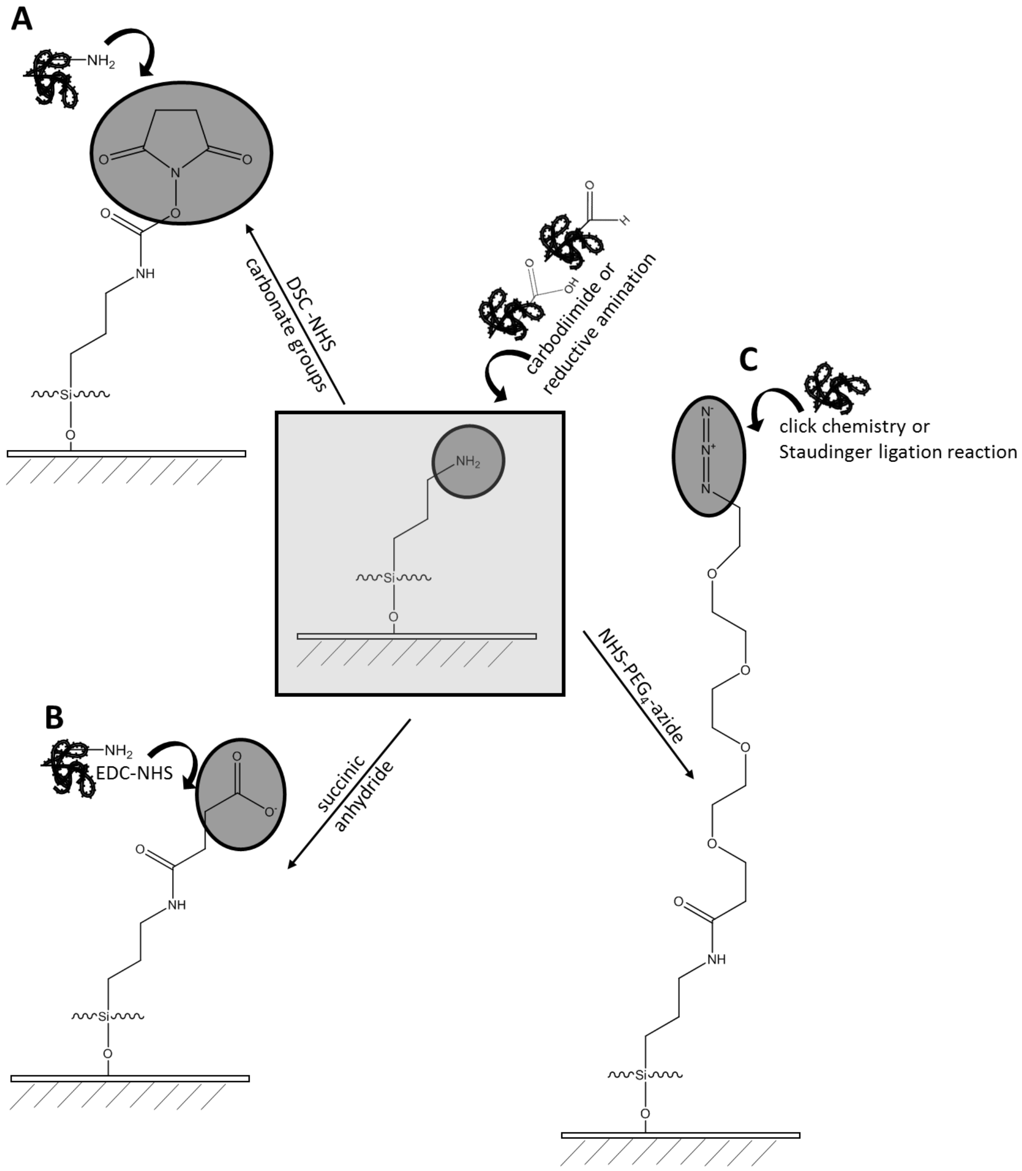

Figure 2.7 –Silane with an amine group as functional group can be used to couple biomolecules. Carboxylic acid- and aldehyde-containing biomolecules can react with this silane through carbodiimide or reductive amination. (A) Amino group can be activated by DSC (N,N’-disuccinimidyl carbonate) to react with the amines and create terminal NHS-carbonate groups, which then could be coupled to amine-containing molecules. (B) Amino group with glutaric anhydride generates terminal carboxylates for coupling of amine-containing molecules. (C) Amino group can be modified with NHS-PEG$_4$-azide that then can be used in a click chemistry or Staudinger ligation reaction to couple other molecules. Adapted from [30].

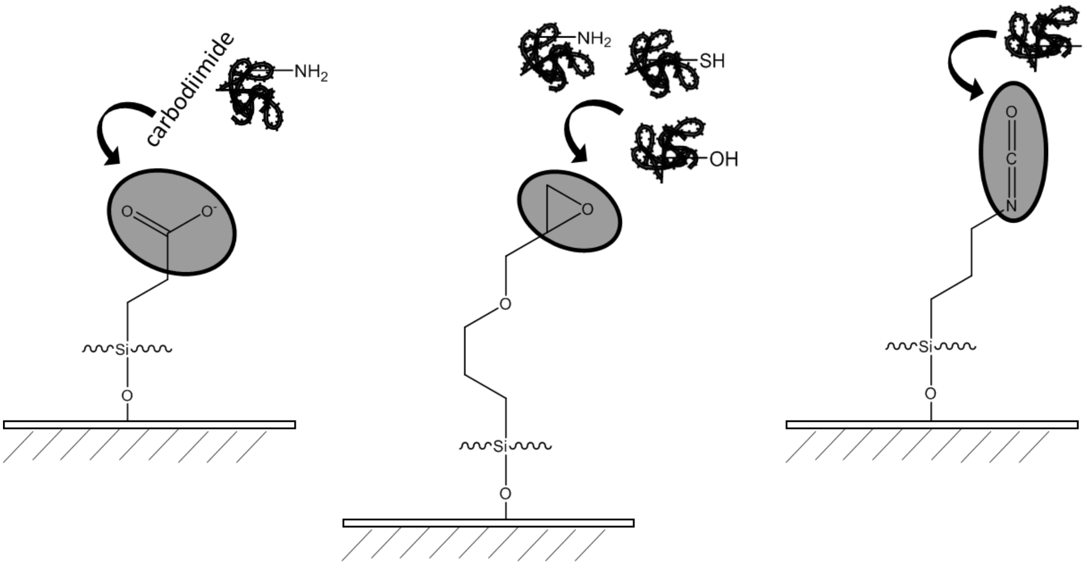

Figure 2.8 – Silanes with different functional groups. (A) Carboxylethylsilanetriol can be used to couple amine-containing biomolecules. (B) Epoxy-containing silane can couple amine-, thiol-, or hydroxyl-containing molecules. (C) Isocyanate-containing silanes can couple hydroxyl-containing molecules (reaction in a dry organic solvent). Adapted from [30].

To conclude this section, it is also important to mention that the interactions between a biomolecule and a surface can be modulated not only by surface chemistry but also by varying the conditions during the attachment, like the pH and the ionic strength. The pH influences the charges on both surfaces (molecule and material). If the biomolecule and material surfaces have the same charge then it is less likely that they will bind due to electrostatic repulsions. However, a high ionic strength can screen the charges so that the repulsions are minimised.[31] Protein concentration[32,33] and the flexibility/conformation of the protein[33] are other two factors that determine adsorption of these molecules (see discussion in section 2.3.2). Therefore, during the development of the surface modification method for biomolecule attachment it is important to test different conditions and parameters that influence the interactions between the material and the biomolecule surfaces.

2.2 Universal coatings

The different techniques described above for modifying and functionalising surfaces involve a lot of different chemical techniques and some of them require specific equipment and conditions. Most of the techniques are also material specific. It is highly desirable to find a versatile and straightforward method to modify surfaces that is independent of the material and can be used to attach biomolecules to a support material.

Mussel-inspired surface chemistry is a promising approach reported in 2007 that has been shown to be effective on many surfaces. It was already demonstrated that these coatings have reactive groups that can interact with (bio)molecules.[34,35] In the past few years, polyphenol plant-based coatings have also been shown to have many coating properties similar to these mussel-inspired coatings.[36] However, their use for the immobilisation of biomolecules is essentially unexplored. Here, we will briefly describe the interactions of mussel-inspired coatings with the surface of materials and biomolecules. For polyphenols, the parameters and conditions that influence the deposition of the coatings will be discussed because chemical characterisation of polyphenol coatings is not available yet.

2.2.1 Mussel-inspired surface modification

Adhesive proteins secreted by mussels are abundant in 3,4-dihydroxy-L-phenylalanine (DOPA) and lysine amino acids.[37] These two compounds form strong covalent and non-covalent interactions with surfaces.[38] DOPA is a precursor of catecholamines such as dopamine. Dopamine is a molecule that contains a catechol group and one amine group attached via an ethyl chain, so dopamine has been exploited as a structural mimic of these compounds responsible for mussel adhesive properties. Under alkaline condition, dopamine polymerises to polydopamine (pDA), which is able to adhere to virtually any kind of surface: noble metals (Au, Ag, Pt, and Pd), metals with native oxide surfaces (Cu, stainless steel, and NiTi shape-memory alloy), oxides [TiO_2, non-crystalline SiO_2, crystalline SiO_2 (quartz) Al_2O_3, and Nb_2O_5], semiconductors (GaAs and Si_3N_4), ceramics [glass and hydroxyapatite (HAp)], and synthetic polymers [polystyrene (PS), polyethylene (PE), polycarbonate (PC), polyethylene terephthalate (PET), PTFE, polydimethylsiloxane (PDMS), polyetheretherketone (PEEK), and polyurethanes [Carbothane (PU1) and Tecoflex (PU2)].[38,39]

The oxidation of dopamine to polydopamine and the exact chemical mechanism are not completely understood.[40–44] Dopamine monomers both on the surface and in solution can oxidise to form quinones at mildly basic pH and in the presence of an oxidizer (*e.g.*, oxygen). The dopamines and quinones can react with each other and self-polymerise (Figure 2.9). Subsequent rearrangements via intramolecular cyclisation of quinones, further oxidation and cross-linking reactions of dopamines and quinones lead to polydopamine.[38] Non-covalent interactions such as π-stacking, H-bonding, van der Waals and electrostatics can also result in the formation of polydopamine.[45]

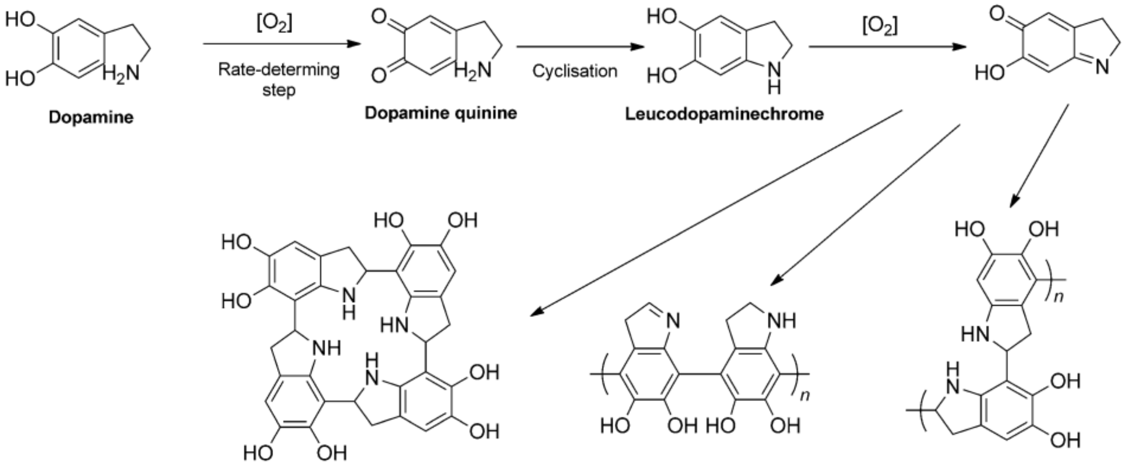

Figure 2.9 – Self-polymerisation of dopamine forming the stable tetramer of 5,6- dihydroxyindole (left) and polydopamines (middle and right). Copyright from [19].

The mechanism of catechol bonding with surfaces is also not clearly understood but likely involves several mechanisms (Figure 2.10). Catechol functionalises surfaces in a different way depending on the material (Figure 2.11).

The hydroxyl groups of the catechol can interact with other hydroxyl groups on the surface of a metal oxide by H-bond. For example, one -OH of the catechol may form a bond with one Ti atom forming a monodentate mononuclear complex (cat-I). From this cat-I intermediate, three combinations can be formed: (1) one Ti atom binds coordinatively with two O atoms of the catechol (cat-II), (2) a monodentate binuclear complex (cat-III), in which an adjacent Ti atom has lost an -OH group and can bind to the -OH group of the catechol, and (3) two -OH groups of the catechol can bind to two different Ti atoms, bidentate binuclear complex (cat-IV) or sometimes called as bridged bidentate structure.[40,46]

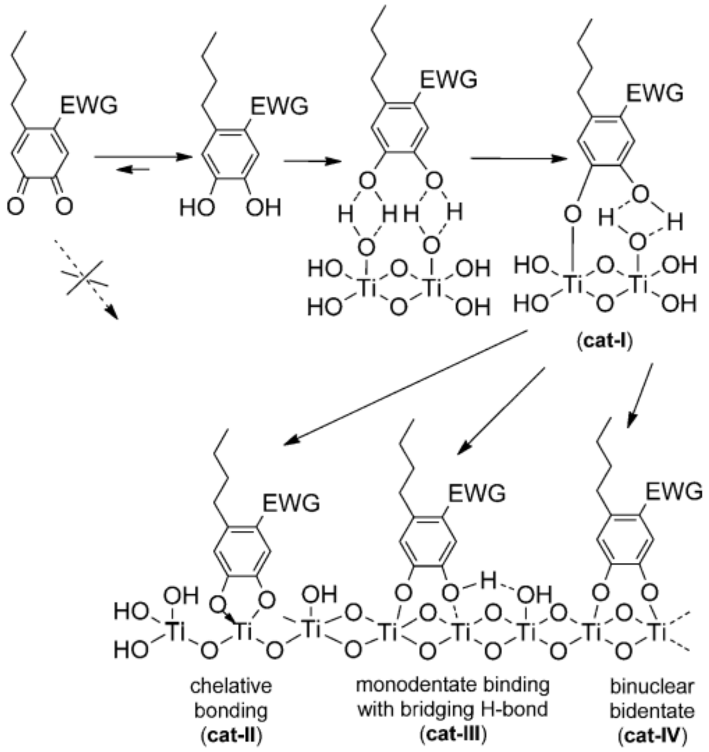

Figure 2.10 – Four possible configurations of catechol on titania surfaces. The introduction of the electron-withdrawing group (EWG) in catechol is to avoid the formation of unorganised thick polymer layers. Ortho-dihydroxyaryl compounds can attach to a hydroxy-terminated surface by monodentate mononuclear complex (Cat-I), chelative bonding (Cat-II), monodentate binuclear complex (Cat-III) or bidentate binuclear complex (Cat-IV). Copyright from [19,40,46].

The adhesion of catechol to titania (TiO_2) is much stronger than that on mica. On mica, the coating is formed by H-bonding interactions between the -OH groups of the catechol with the O atoms of the cleaved mica surface. These interactions are much less specific and they are weaker than the bidentate binuclear complexes formed by the catechol and catechol quinone groups with the TiO_2 surface (Figure 2.21).

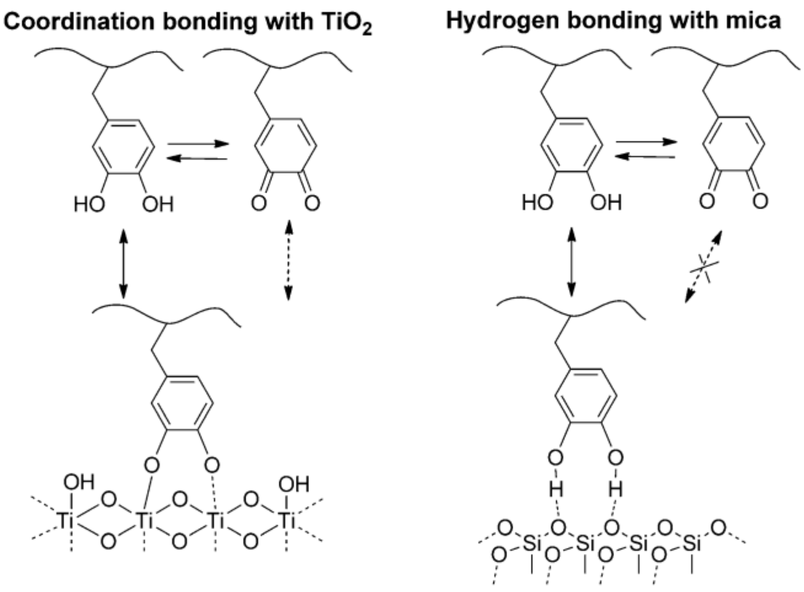

Figure 2.11 – Binding mechanism of dopamine to titania and mica surfaces. Catechol and catechol quinone groups can bind the TiO_2 surface forming bidentate binuclear complexes. On mica surfaces, only catechol groups can coat the surface by H-bonding interactions. Copyright from [19,40].

Dopamine molecules can also interact by electrostatic interactions between protonated amine group and the negatively charged native oxide of metals as well as other polar surfaces, by covalent and strong non-covalent interactions, as well as π-stacking and hydrogen-bonding.[41,47–49] These non-covalent intermolecular forces also occur with polymeric surfaces.[50] On organic materials, quinones formed from oxidation of the catechol can react and form covalent bonds with the surface.

Polydopamine coatings have the ability to react with a broad range of biomolecules. The crosslinking reaction of pDA with amino and/or thiol residues of the biomolecules are widely investigated.[19,39,40,51–54] Under alkaline conditions and at room temperature, the quinones can react with nucleophilic amino groups via Schiff base reaction and/or Michael addition. Thiol groups react with pDA through Michael addition reaction (Figure 2.12).

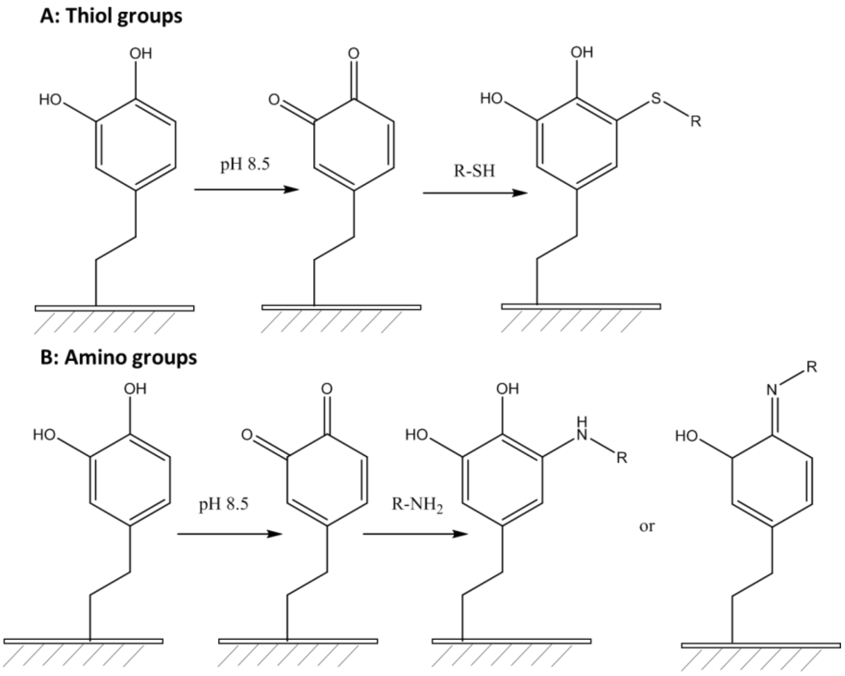

Figure 2.12 – Covalent bonding between amine or thiol groups and dopamine. Michael addition for thiol coupling, and Michael addition and Shiff base reaction involved in the coupling of the amino group. Adapted from [54].

Biomolecule coupling through this pDA coating shows several advantages compared to the techniques described previously. This procedure is not dependent on the solid support and the kind of biomolecule as long as the biomolecule has nucleophiles. The coatings are formed by a simple immersion of the materials in an aqueous solution. It also does not require multistep chemical activation processes or aggressive surface treatments. However, this procedure has some disadvantages; namely, dopamine is costly and the coating has a dark colour, which can limit its practical applications.[55]

2.2.2 Plant-based polyphenol surface modification

Polyphenols naturally occur in plants serving diverse chemical functions and have recently been found to form chemically reactive coatings on surfaces through multiple covalent and non-covalent interactions.[49,56] These coatings can be used as “green” immobilisation agents that act under mild and aqueous conditions. Polyphenol coatings are colourless, can be deposited at and around neutral pH and are derived in some cases from reagents a hundredfold less costly than dopamine.[55] The coatings can be prepared just by using unadulterated polyphenol-rich beverages such as tea and wine on tea or wine cups.[55] For these reasons, in this thesis, polyphenol molecules have been investigated and exploited for the first time in the context of surface modification for immobilising proteins and enzymatic proteins. Their use as anchors for surface grafted polymer brushes has been previously reported.[55]

Some examples of polyphenol structures are shown in Figure 2.13. Pyrogallol (PG) is a small synthetic polyphenol molecule with a benzene ring and three hydroxyl groups. Tannic acid (TA) is a natural high-molecular-weight polyphenol that is most commonly described as pentadigalloyl ester groups covalently attached to a central glucose core.[57] Due to this polyvalency, TA is a good comparison to PG, to assess how the number of trihydroxyphenyl moieties of the polyphenol affects surface modification.[55,58]

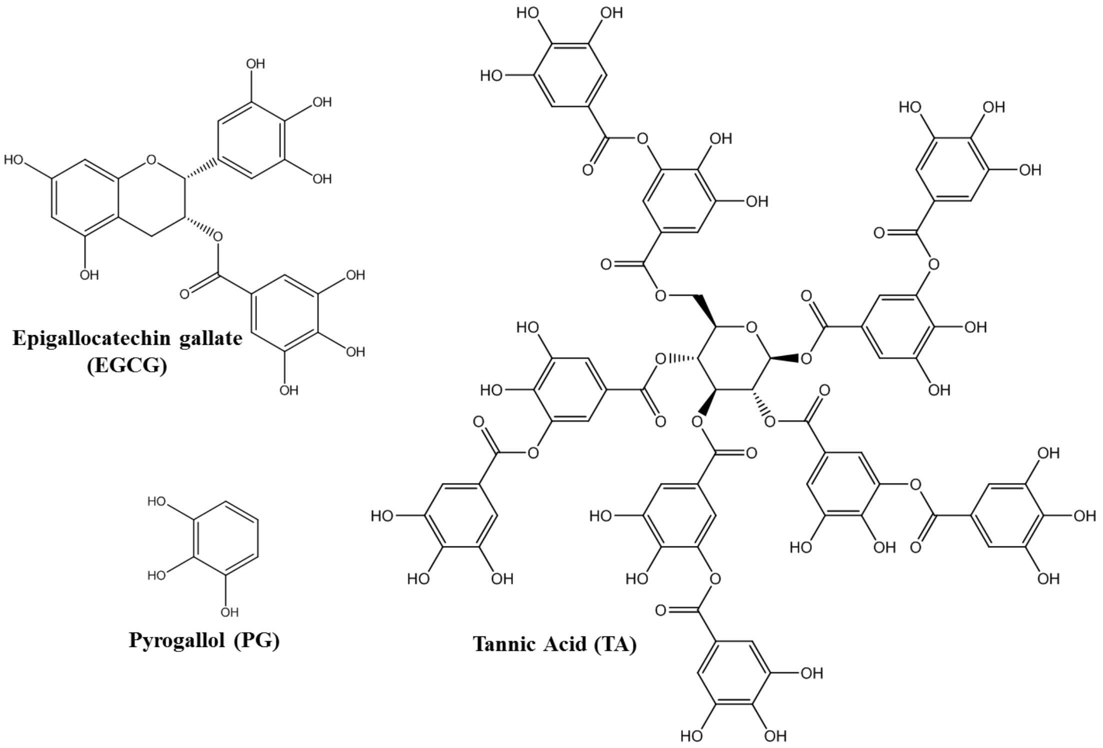

Figure 2.13 – Polyphenol structures: epigallocatechin gallate (EGCG), pyrogallol (PG) and tannic acid (TA).

Polyphenols possess significant abundance of dihydroxyphenyl (catechol) and/or galloyl/gallic acid groups. Dopamine has a dihydrophenyl (catechol) so for that reason, polyphenol coatings are assumed to exhibit similar interactions with material surfaces such as dopamine.[36] The coating formation of pDA and polyphenols is generally associated with the deprotonation and autoxidation of the precursors suggesting that there is a relatioship between the phenolic pKa and the coating pH. Barrett *et al.* suggests that successful coatings occur at pH values less the first phenolic pKa (by up to 2 pH units). For that reason, it was observed successful coatings of poly(tannic acid) pTA and pDA at pH 7 and 8.5 (first phenolic pKa of 7.7 and 10.6, respectively).[56,59]

The deposition of pDA and polyphenol coatings depend on many factors: (1) incubation time – increasing the incubation time increases the coating thickness up to a certain point; (2) pH – optimal coating pH generally is below the first phenolic pKa; (3) salt concentration which may influence on the protonation of phenols; and (4) polyphenol/catechol concentration – increasing the concentration increases the coating thickness (Figure 2.14).[55,56]

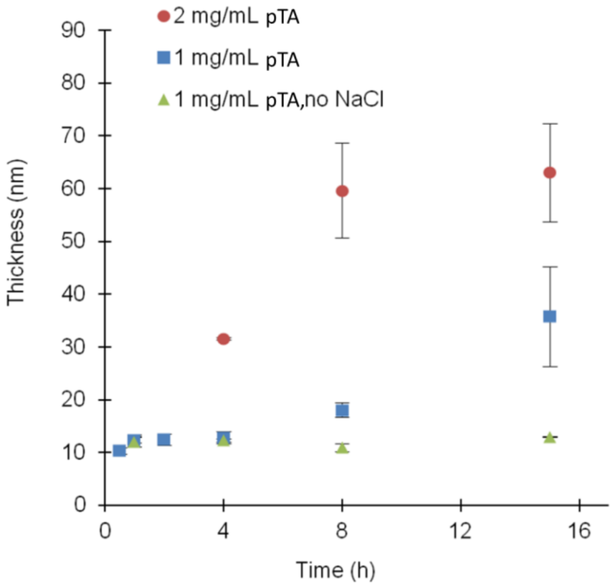

Figure 2.14 – Kinetics of poly(tannic acid) (pTA) coating deposition. Time dependence of pTA film deposition on TiO2 determined by ellipsometry. Coatings were deposited at the concentrations indicated either in water or buffered saline (0.6 M NaCl, pH 7.8). Copyright [55].

2.3 Surface immobilisation for biointerfacial applications

The following sections will describe some antifouling surfaces to prevent protein adsorption (section 2.3.1) and the different methods to immobilise proteins and enzymes (section 2.3.2). These two sections are important to give an overview of the different approaches that have been exploited and also to introduce the techniques used in the next chapters that focus on protein and enzyme immobilisation and molecular transport control where protein adsorption was avoided.

2.3.1 Antifouling surfaces for preventing protein adsorption

Protein adsorption on the surface of materials is in some cases inconvenient. When proteins attach to a surface, the material can lose its properties and the desired performance for its application.[60] For example, in biomedical applications, implants are introduced in the body and they need to be functionalised to minimise foreign body reaction/inflammation response that can lead to the rejection of the material. On the other hand, protein adsorption is useful for certain applications – as it will be discussed section 2.3.2.

Antifouling surface is a general term used for surfaces that resist fouling (*i.e.*, adsorption or attachment) by proteins, cells, bacteria, and marine organisms. In this section, the focus will be on surfaces that are able to prevent protein adsorption as we want to develop nanoporous structures that can control molecular transport through nanopores so adsorption events should be avoided. Antifouling surfaces minimise the intermolecular forces of interactions (van der Waals, hydrophobic and electrostatic forces) between the proteins and the surface of a material.[61] The hydration layer of the surface of a material may also be altered in order to repel proteins.[62] The interaction between the protein and the surface will depend on different conditions such as protein properties (charge, size, structural stability and steric conformation), protein concentration, surface properties (roughness, hydrophobicity) and external parameters (temperature, pH, ionic strength).[63]

There are a few major rules to obtain antifouling surfaces although exceptions have been observed. The surfaces should be hydrophilic and charge neutral to reduce electrostatic interactions and to form a hydration layer on the surface that cannot be easily displaced by non-specific biomolecule adsorption.[64–66] The surfaces should possess hydrogen bond acceptors, and the hydrogen bond donors should be accessible to water molecules but not to the hydrogen bond-forming groups of the proteins.[65,67]

In general, chemical strategies for creating antifouling surfaces involve the modification of surfaces with biological molecules or with the introduction of organic molecules using SAMs or polymer brushes.

SAMs were described in section 2.1.2 when surfaces were modified to attach biomolecules. SAMs also have the ability to repel proteins if the functional groups and layers structure can decrease protein adsorption. SAMs can cover the surface very effectively and it can be used to specify certain chemical interactions that satisfy the above antifouling design rules.[60] However, SAMs have some disadvantages, such as defects on the layer structures and chemical stability.[68] Creating SAMs with zwitterionic, peptides and oligosaccharide molecules have been exploited.[69] Peptide sequences can be selectively chosen to use amino acid residues that are hydrophilic, uncharged side-chains that can provide hydrogen bond acceptor groups.[60]

When polymer brushes are used to achieve antifouling surfaces there are other important points to take into account. Polymer brushes are long-chain polymers attached by one end to a surface. The grafting density and polymer chain length can enhance the resistance against protein adsorption by creating an entropic barrier.[66,70] Flexible and long polymer chains are more compressed during the approach of the protein toward the surface which leads to more steric repulsion.[64] The protein adhesion is reduced when the surface is completely covered with polymer chains (high density) because there is no surface area available for the proteins to attach. An intermediate surface density also allows chain mobility while ensuring complete surface coverage. On the other hand, too low surface density is not desirable, because the proteins can attach to the surface that is not covered.

2.3.1.1 Grafted-polymer brushes

Polymer brushes are attached to a surface by one of the grafting strategies that will be described below. These polymer brushes have the advantage to be stable for long time and there is control over the polymer length (it is possible to achieve greater film thickness if necessary).

There are three different regimes that grafted polymer chains can form (Figure 2.15). In low grafting density conditions, the distance between the attached chains is so large that neighbouring chains do not interact. If the interaction between the polymer and the surface is weak, the chains form a typical random coil “mushroom” conformation (Figure 2.15 A). When the interaction is strong, the polymer molecules assume a flat “pancake”-like conformation (Figure 2.15 B). Increasing the grafting density – covering the surface with a relatively dense initiator or monomer molecules layer – the growing polymer chains have less space to bend, so that the chains stretch away much more, giving a polymer brush regime (Figure 2.15 C).[71,72]

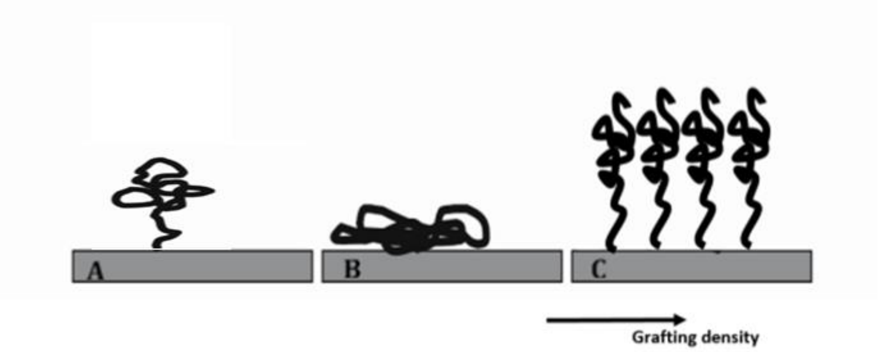

Figure 2.15 – Schematic illustration of different morphologies formed by grafted polymer chains: (A) mushroom, (B) pancake and (C) brush. Adapted from [73].

Many types of polymer and molecules can be attached to the surface such as hydrophilic or responsive polymers. Some examples are listed below.

Most hydrophilic materials that have been reported to have nonfouling properties include poly(ethylene glycol) (PEG), poly[oligo(ethylene glycol)] methacrylates (POEGMA), polyacrylamides, polyglycidols and polysaccharides.[63] Each monomer in PEG can strongly bind to one water molecule (H-bonding), forming a highly hydrated layer that leads to a steric hindrance to the proteins. PEG is non-toxic, non-immunogenetic and biocompatible.[63] Polyoxazolines can also be used due to their non-cytotoxic and low acute toxicity.[63]

Zwitterionic polymers have been used for antifouling due their high degree of ionic hydration. [74] These polymers have both positive and negative charges so the overall charge of these polymers is neutral.[63] The surface-bound water molecules are formed by ionic solvation, leads to a super-hydrophilic layer that does not allow proteins to adhere to the surface.[63]

Peptoids are peptidomimetic polymers that have a protein-like backbone with side chains on the nitrogen atom instead of the α-carbon [poly(N-substituted glycine)].[62] The surface structure and antifouling ability of peptoid-based materials can be easily tuned because the residue coupling is (mostly) independent from the side chain chemistry.[62] It is also easily convenient to prepare zwitterionic peptoids with differential spatial separation between charged groups, charge sequence order, and overall charge densities.

Smart or stimuli-responsive polymers have been used on material surfaces due to their ability to alter their chemical and/or physical properties upon exposure to external stimuli. Poly(N-isopropylacrylamide) (PNIPAM) is a thermoresponsive polymer with a lower critical solubility temperature (LCST) in water of 32°C. PNIPAM is soluble in water and possesses hydrophilic conformation at temperatures below the LCST. However, when the temperature increases, the polymer becomes water-insoluble and collapses to a hydrophobic structure.[60] When there is a high grafting degree and density (long chain and numerous polymer chains covering the surface), polymer brushes on nanoporous membranes allow the passage of molecules but when the temperature increase, the polymer shrinks, become more compact and resistant to diffusion decreasing the permeability and consequently restricting the passage of molecules.[17,75] There other polymers that can be responsive to the pH change. For example, polyvinylpyridine (PVP) brushes on mesoporous silica surfaces were able to block the passage of molecules at neutral or slightly alkaline conditions but when the pH was decreased the protonated brushes became swollen and permeable to the molecules.[76]

2.3.1.2 Surface grafting strategies

Surface grafting is a chemical modification technique where a macromolecular chain is attached to the surface of a material by covalent bonding or non-specific interactions. Tethering polymers to the surface can give distinctive properties to the material depending on the type of grafted polymer.

Polymer grafting can be divided into three classes, *i.e.*, “grafting-from”, “grafting-to” and “grafting-through” processes (Figure 2.16).

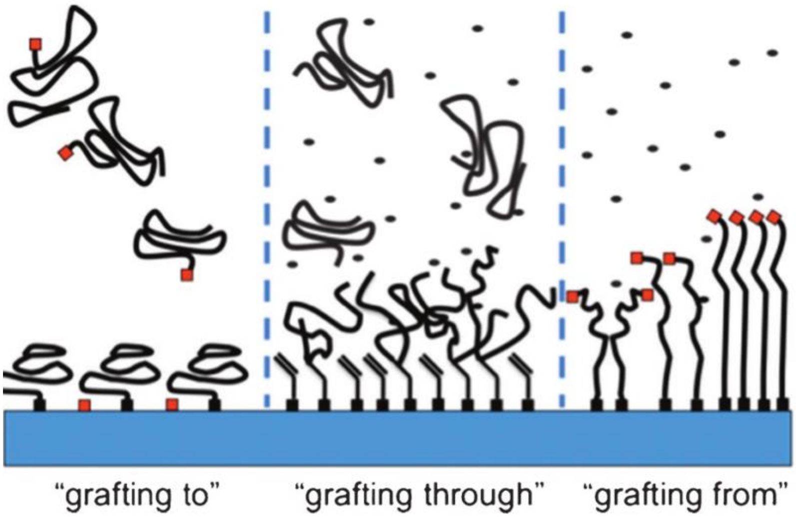

Figure 2.16 – Scheme of (left to right) the “grafting-to”, “grafting-through”, and “grafting-from” approaches to polymer immobilisation. Red squares represent reactive groups (initiator or covalent linker). Copyright [77].

Grafting-from

The grafting-from strategy involves a primary step of immobilising a polymerisation initiator at the surface of the material through chemical self-assembly or a covalent bond, and a secondary step of successive propagation of polymerisation from the surface.[72] Some techniques to initiate grafting from a surface are: (i) chemical, (ii) photochemical and/or via high-energy radiation, (iii) the use of plasma, and (iv) enzymatic.[78] Depending on the polymerisation conditions, the polymers on the surface can have a high grafting density, and they can have a thickness of more than 100 nm, because the small monomers or initiator can reach growing chains easier (compared with other grafting strategies).[79,80]

Stretched polymer chains are created when the initiation of the grafting-from approach is efficient and all of the chains grow at the same rate.[77] As an advantage, this strategy confers good control over the type of immobilised polymer chain and to the packing density of the grafted polymer on the surface. In other words, immobilising a particular initiator on a surface using different approaches and varying parameters such as initiator concentration, the type of initiator, or using inert monolayer components to produce diluted initiator layers, will influence the final structure and properties of the immobilised polymer chains. However, grafting-from polymerisation has some disadvantages such as (i) the primary step of initiator immobilisation at the surface can be difficult depending on the material composition/nature, (ii) complex experimental setup compared with the other strategies and (iii) it is limited to chain-growth polymerisations.[81]

Grafting-to

The grafting-to strategy involves the synthesis of a polymer in a solution that has an end-functional group obtained during polymerisation or through chemical transformation due to a post-polymerisation process.[77] The end-functionalised polymer chain can be attached to a surface by a covalent or non-covalent bond. The thickness of the polymer layer is limited due to the steric hindrance effects of the polymers – the initially grafted polymer chains form an entropic and steric barrier that prevents further polymer chains from diffusing through and coupling to the surface sites, limiting the ultimate grafting density.[72,79–81]

Grafting-through

The grafting-through strategy is based on the immobilisation of monomer groups, typically with vinyl ($H_2C{=}CH$) or acryl [$H_2C{=}CH{-}C(O)O{-}$] functions on a surface. These monomer groups can act as chemical anchors and propagation sites during polymerisation.[79,81] The major difference between this strategy and grafting-from is that in the former, the polymerisation starts to grow from the surface because an initiator is immobilised on the surface. In grafting-through, the polymerisation occurs in the bulk and covalent attachment of the polymer chains results during the propagation step if a surface-bound monomer is integrated into the growing chains (Figure 2.16 illustrates the differences). If more than one surface-bound monomer is incorporated into the growing chain, polymer loops are created.[81] This grafting technique can generate a high grafting density if short oligomeric segments, which have fewer diffusion limitations, are initially grafted through onto the surface.[80]

2.3.2 Enzyme immobilisation

Coupling biomolecules on the surface of a material is an advantage on handling biomolecules, for carrying out specific assays and on recovering biomolecules. This section will focus on enzyme immobilisation due to enzyme characteristics, properties and its use in biocatalysis applications (see also the introduction of chapter 3).

2.3.2.1 Enzymes and enzyme immobilisation

Enzymes are biological catalysts operating under mild conditions (*e.g.*, physiological pH and temperature). As catalysts, enzymes are not consumed during the reaction and can be recycled.[82] Most enzymes are proteins, with the exception of a small group of catalytic RNA molecules called ribozymes (ribonucleic acid enzymes).[83] The major difference between these two types of enzymes is its macromolecular structure. Enzymatic proteins are constituted of long chains of amino acids while ribozymes are made up of nucleic acid units (nucleotides).[84] In this thesis, only enzymatic proteins are considered and the term "enzyme(s)" will refer exclusively to such proteins. These macromolecules are highly effective as chemo-, regio- and stereo-selective catalysts on a range of chemical reactions.[82] They are biodegradable entities that are in some cases capable of much higher catalytic turnover rates than inorganic catalysts.[3,5,82] It is convenient to reuse enzymes however the process of recovering enzymes from the reaction mixture is difficult and can cause loss of activity and is highly expensive.[1] No activation or (de)protection of functional groups are generally necessary. Enzymatic reactions can be made in water and thus eliminate organic chemical waste streams, making enzymes environmentally and economically attractive.[5] However, most proteins, in their native form, denature easily in organic solvents or at extreme reaction conditions (pH, mechanical or heat treatment) and their performance can be compromised.

Enzyme immobilisation overcomes many of the issues described above. The attachment of enzymes on different types of supports can enhance enzyme performance, enable recovery, reuse and increase the range of enzyme applications.[85] There are additional advantages of using enzyme immobilisation, such as more convenient handling and enhancement of enzyme stability under storage and/or operational conditions in some cases. Also, immobilised enzymes are separated from the reactants in solution which simplify the purification of the product and enable enzyme reuse.[1,2] These benefits reduce waste contamination and cost. Consequently, the reactions can be more effective and cheaper.[3–5]

However, some methods to immobilise enzymes can damage the enzymes, reduce or cause a loss of their structural mobility, and decrease their activity. There are physical or covalent interactions between the enzyme surface and the support material (or carrier) that can change the enzyme conformation, mobility and accessibility. Consequently, the stability and activity of the immobilised enzyme are altered.[3] On the other hand, there are methods that are not effective and the amount of immobilised enzyme is too little because of electrostatic repulsions or insufficient quantity of functional groups to bind to the enzyme.

2.3.2.2 Conventional enzyme immobilisation methods

Immobilisation methods can be classified as: (1) physical or (2) covalent binding to a support, (3) entrapment, (4) encapsulation and (5) cross-linking.[86]

Physical binding to a support

The term physical adsorption describes non-specific binding by non-covalent interactions, such as van der Waals forces, hydrogen bonds, hydrophobic or electrostatic interactions, to bind, attach enzymes to a material surface.[87] The first example of artificial enzyme immobilisation was demonstrated in 1916 when it was found that the enzyme invertase physically adsorbed on charcoal or aluminium oxide ($Al(OH)_3$) have a similar activity compared to the enzyme in solution.[5,88] This type of binding is simple and easy to achieve because the purpose is to rely on the native physical properties of the support material (*i.e.*, it is not necessary to functionalise the surface). However, this binding can be too weak to keep the enzyme fixed to the carrier (*i.e.*, leaching), especially under conditions for catalytic reactions depending on the physicochemical conditions (*e.g.*, temperature and/or pH). Furthermore, the activity of the immobilised enzyme is strongly dependent on the isoelectric point (pI) of the enzyme and the support because small pH changes and hence changes in electrostatic interactions can result in different protein immobilisation loadings.[89] Besides the weak bonds between the enzyme and the support, surface-induced denaturation of the enzyme can occur. Multiple physical interactions may form between the enzyme and the surface, which can be strong in total, and lead to collapse and unfolding of the enzyme structure. The multiple physical bonds on the surface of the enzyme can also change the flexibility of the enzyme and/or hide the active site to the substrate, reducing the enzyme activity.

Covalent coupling to a support

Covalent coupling can in principle overcome the biggest problem of physical binding – enzyme leaching. The enzyme may be coupled through the reactive groups located on the enzyme surface. These include amino acid residues (lysine, arginine and histidine), carboxylic groups (glutamic or aspartic acid), or the sulfhydryl groups of cysteine residues (Figure 2.17). There is an extensive choice of organic linkers (as mentioned previously in section 2.1.2). The disadvantages of this method are the added chemical complexity and expense required to chemically activate the solid substrate and this procedure can involve multiple chemical steps. Also, as the enzyme is chemically modified, conformational and biochemical changes of the enzyme can occur, reducing or even eliminating catalytic activity. The enzyme is irreversibly attached in this approach, so if the enzyme loses their capabilities, the support cannot be recovered or reused (not easily). In this thesis, some of these problems will be investigated and mitigated (chapter 3).

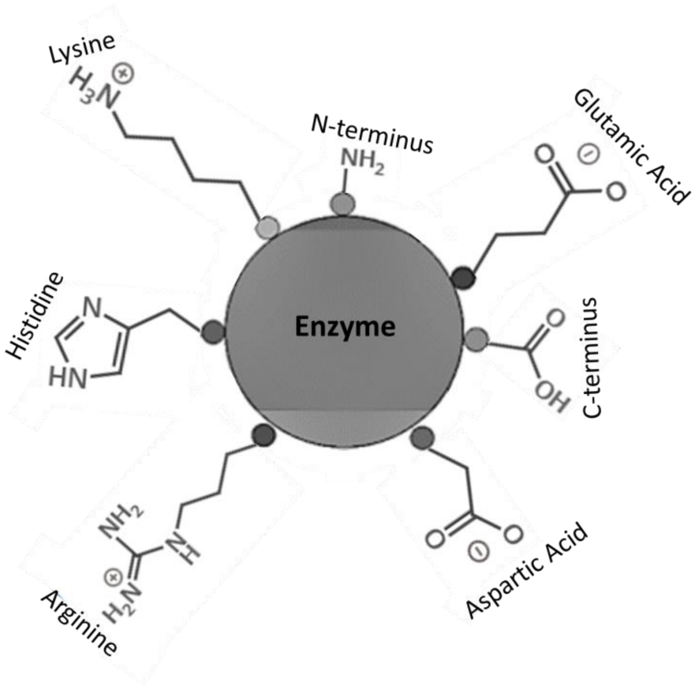

Figure 2.17 – Reactive amino acid residues of enzymes. Adapted from [90].

Similar to physical adsorption, the denaturation of the enzyme can also occur due to the multiple interactions between the enzyme and the support. Multipoint attachments can change the conformation of the enzyme until a certain point when the enzyme is unfolded, losing its activity. Moreover, if the active site of the enzyme is not available to the substrate due to reactions with the support material, the enzyme activity will be very low or absent.

Entrapment in matrices

When enzyme molecules are confined in a matrix formed by dispersing the enzyme in a fluid medium, followed by formation of an insoluble matrix around the confined enzymes, the process is called entrapment. In general, the entrapment matrix synthesis and the immobilisation process occur at the same time.[4] Conventionally the enzyme is entrapped in a polymeric matrix by dispersing the enzyme-polymer solution in an immiscible medium, followed by chemical or physical gelation. Using the entrapment method, the enzymes ideally do not lose their native conformations, but this process decreases the diffusion rate of substrates/products and not every enzyme is compatible with a given gelation process.[90]

Encapsulation in porous material supports

Another immobilisation method, where enzymes can also be confined in a support is encapsulation. In this case, the enzyme is immobilised in a ready-made support, for example, prefabricated nanoporous silica, and the enzymes are introduced into the pores. Conventionally, the enzyme is dissolved in a solution and is immobilised inside the porous structure as it diffuses into the pores. The enzyme can then either adsorb on the surfaces of pores that fit the size of the enzyme or freely diffuse inside larger pores with openings smaller than the enzyme to enclose them.[90,91] Both encapsulation and entrapment methods physically confine an enzyme inside a material support. However, when the polymeric matrix formation and enzyme immobilisation occur at the same time it is called entrapment. When the enzyme is immobilised inside a porous structure where the pore sizes need to be matched to the enzyme size, it is called encapsulation. To distinguish these two methods, Figure 2.18 illustrates the matrix that immobilises enzymes (entrapment) and the microcapsule support that can cage the enzymes (encapsulation).

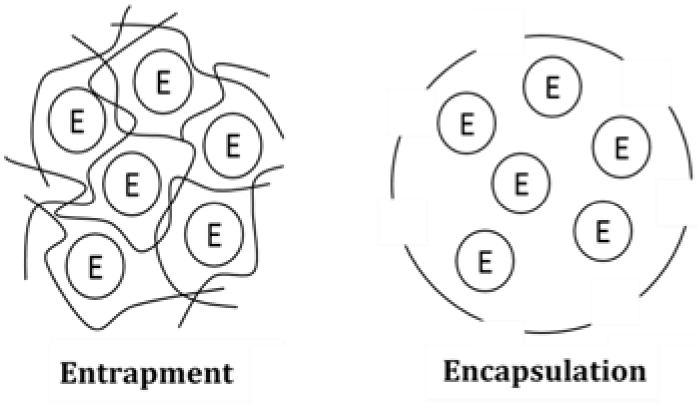

Figure 2.18 – Scheme of entrapped (left) and encapsulated (right) enzymes.

Encapsulation is distinguished from physisorption, because the enzymes do not need necessarily adsorb to the surface. Ideally, only enzymes, with a size similar to the pores, can be encapsulated and fit just inside the confined space maintaining its native conformation. To improve on this enzyme immobilisation process, bulky functional groups that constrict the size of the pore entrance can be introduced after enzyme encapsulation to prevent enzyme leaching.[90]

Cross-linking

Cross-linking is based on the precipitation of enzymes to form aggregates. Cross-linking is related to enzyme immobilisation methods because it is used in combination with other immobilisation methods, but it is considered a carrier-free strategy because the enzyme forms its own nano or microcarrier support.[82,90] This procedure is initiated by precipitating the enzymes (with *e.g.,* salts or organic solvents) and then a conjugation agent is added into an enzyme solution under mild reaction conditions to crosslink the aggregates. Cross-linking potentially allows immobilisation and stabilisation of different enzymes (co-immobilisation) and multimeric enzymes.[3] No leaching from the support is observed because a huge mass of enzyme is interconnected and immobilised. This methodology has some drawbacks related to low mechanical stability and difficulties in handling the cross-linked enzymes. However, these disadvantages can be overcome if this method combines with other immobilisation methods.[3,92] For example, enzymes can form cross-linked aggregates and then be physically adsorbed inside of a porous materials.[90] Other example is shown in section 2.3.3.4.

2.3.2.3 Biochemical and activity considerations

In general, the method used to immobilise enzymes depends on the application, the specific residues that enzyme are available to react with the carrier, and the enzyme parameters that need to be improved and/or the support material already selected. This section will discuss how enzyme activity is influenced by the immobilisation process and the limitations of this process.

Biochemical properties

Biochemical properties, such as storage stability, conformational flexibility, molecular weight, enzyme size, active site, functional groups on the surface, surface charge define how the enzyme is immobilised.[5] Two examples where biochemical properties influence the immobilisation process are: (1) when the enzyme does not fit inside porous supports due to high molecular weight or large size; and (2) when the surface charge of the enzyme is the same as the carrier surface causing electrostatic repulsions. In these cases, the enzyme attachment to the surface is weak because enzymes are not very secured to the support material. Another example is when the enzyme is covalently immobilised and its active site is not accessible to the substrate due to conformation changes. Multi-covalent attachment of enzymes to support material can vary the binding strength as well as the enzyme activity due to reduced enzyme mobility and flexibility.[93]

Kinetic parameters

The profile of stability, specific activity with pH and/or temperature can sometimes be enhanced with the immobilisation processes.[5] These parameters need to be evaluated before (when enzymes are in solution) and after enzyme immobilisation in order to vary the conditions related to the carrier and the immobilisation method that can improve enzyme kinetics. Free enzyme normally has a narrow activity profile when the pH and temperature are varied because deviations from the optimised conditions can lead to inactive conformations or denaturation of the protein. However, when enzymes are immobilised, their 3-dimensional structure is more rigid and is not so susceptible to denaturation by pH and temperature variance, so their activity profile is wider if the active conformation is preserved during immobilisation.[94] A combination of biochemical properties of the enzyme and the chemical/physical parameters of the carrier can improve the activity behaviour of the immobilised enzyme.

2.3.2.4 Chemical and physical considerations of supports for enzyme immobilisation

A support material for enzyme immobilisation needs to be inert, mechanically robust, stable and insoluble in the solution during both immobilisation process and the enzymatic reaction. The support would ideally even enhance the enzyme’s stability and activity and allows it to be reused several times after running each reaction.

Chemical parameters

Chemical parameters, such as chemical composition, functional groups on the surface and hydrophobicity can influence the way how enzymes may be strongly or weakly immobilised. The support material can be inorganic or organic (natural or synthetic) carriers. Silica, magnetic particles, oxides, glass and polymers are some example supports that have been used for enzyme immobilisation.[3] The surface chemical properties of these materials may have specific interactions with the enzyme.

Physical parameters

Physical parameters are also important to control protein loading and catalytic activity. Protein loading refers to the mass of protein immobilised per unit mass of support material. Porosity (pore structure and pore size distribution), morphology, particle size, and surface area can be controlled during or post support synthesis. Porous and non-porous supports show big differences on the amount of protein loading and catalytic activities. Porous supports have a large internal surface area on which more proteins can be immobilised compared with non-porous supports. This topic will be discussed in depth in the next section. The support morphology, *e.g.*, particles, membranes or fibres, influences on the choice of the enzymatic reaction (*e.g.*, batch *versus* continuous flow processes), the stability and recovery of the immobilised enzyme. For example, when the enzymes are immobilised on particles, the abrasion and degradation of the suspended particles during stirring reduces enzyme stability and makes the recovery process harder.

2.3.3 Nanoporous enzyme supports

2.3.3.1 Definition

Porous materials have a large range of pore sizes and they have been classified by the International Union of Pure and Applied Chemistry (IUPAC) as: microporous (< 2 nm), mesoporous (2-50 nm) and macroporous (>50 nm). Of course, the latter two categories are on the nanometer scale, and therefore can be termed 'nanopores'. A new recent classification was proposed based on prefixes defined by the Bureau International des Poids et Mesures under Le Système International d'Unités (SI) (in particular *nano-*, *micro-* and *milli-*). This classification divides the pore sizes into: nanopores (0.1-100 nm), micropores (0.1-100 μm) and millipores (0.1-100 mm).[95]

Porous materials with pore sizes smaller than 2 nm are not suitable to immobilise enzymes because the pores are not large enough to accommodate enzymes inside them (protein molecules sizes typically range between 2-10 nm in diameter). Micropores or millipores are also not suitable for enzyme immobilisation because of the increase in surface area when compared with planar surfaces is small and the leaching that enzymes can face during the enzymatic reaction and immobilisation procedure is significant. Overall, nanoporous supports approximately between 2 and 200 nm pore size are usually used to immobilise enzymes and for these reasons the discussion below will focus on these supports.[89,96] Nonetheless, different pore sizes within this range are associated with different challenges.

Bayne *et al.* investigated the relationships between pore sizes and immobilisation performances of several studies that had been published. One of the correlations found was the protein loading *versus* pore size of the support materials (Figure 2.19). An increase of protein loading was observed with increase of pore size between 1 and 10 nm and then it remained constant up to 90 nm. Above 100 nm, the protein loading decreased.[96]

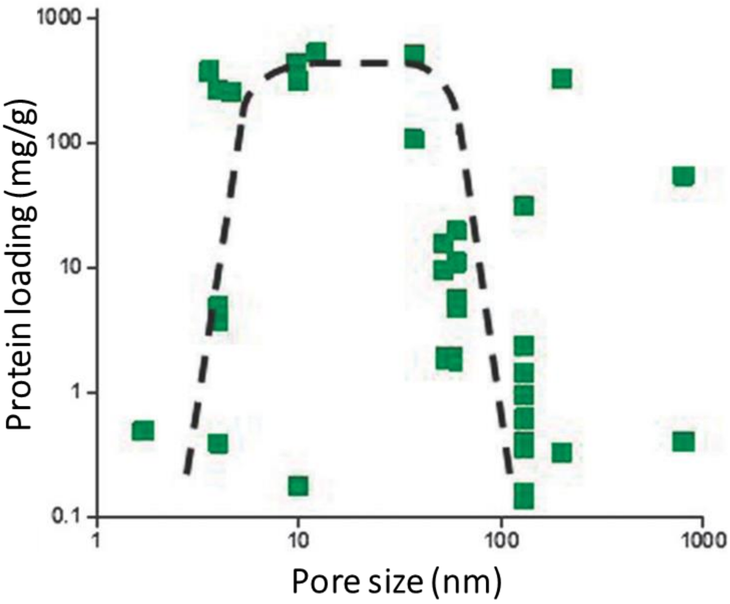

Figure 2.19 – Protein loading *versus* pore size of high confidence in both support and performance data based on the literature analysis made by Bayne *et al*. Trendline on the graph is to guide to the eye. Adapted from [96].

Observing Figure 2.19, when the pores are below 10 nm the surface area is high but the protein loading rate and the stability of these enzymes are limited because most of the enzymes cannot enter into the pores. The enzymes that are immobilised inside the pores are highly stable, but the diffusional limitations of substrate and products are very high.

For pore sizes between 10 and 100 nm, the protein loading per unit mass of material support tends to remain constant. Smaller pore sizes means higher surface area, but some restrictions related to protein-protein interactions and the chemical surface of the support material can influence in some way the enzyme immobilisation process. Increasing the pore size, less amount of enzyme is immobilised because there is less available pore surface area.

When the pores are above 100 nm, the protein loading is significantly less. Even though no steric constraints are present in larger pores, there is less surface area available to immobilise enzymes, so the protein loading is reduced.

In this study, there was no clear relation found between the pore size and retention of activity (ratio of catalytic activity per unit mass protein immobilised to that of the free enzyme in solution). Higher amounts of immobilised enzyme can lead to higher activities but if the immobilised enzyme is not active anymore after the immobilisation procedure, lower activities can be observed. For example, the immobilisation procedure can denatured the enzyme if it loses the conformation or the enzyme can be not accessible to the substrate.

There is much debate as to how large the pore should be in relation to the enzyme molecule. Some authors argue that the pore should be developed to be much larger than the protein, thus minimising potential diffusional restrictions.[96] Others say that pore size should be comparable to the enzyme molecule, thus providing a close fit and reducing the risk of protein leaching.[25] In the end, the application and the purpose of the enzyme immobilisation should control which parameters (protein loading, stability or other) are more important to take into account. For example, if the immobilised enzyme is to be used in a continuous flow process the stability of the enzyme is more important than the protein loading.

The nanoporous supports can be made by different approaches and many chemical compositions can be used. In order to simplify the separation and to reuse immobilised enzymes, different geometries and morphologies (shape and size) can be achieved. These considerations are described in the following sections.

2.3.3.2 Morphology, shapes and geometries of nanoporous supports

The stability of immobilised enzyme on nanoporous particles during operational conditions can be low due to stirring that leads to damage of particle structure and/or loss of immobilised enzyme. For this reason, other morphologies, such as fibres, membranes or capsules with nanopores can be used to avoid harsh washing and recovery procedures to overcome these issues (Figure 2.20).[92,94]

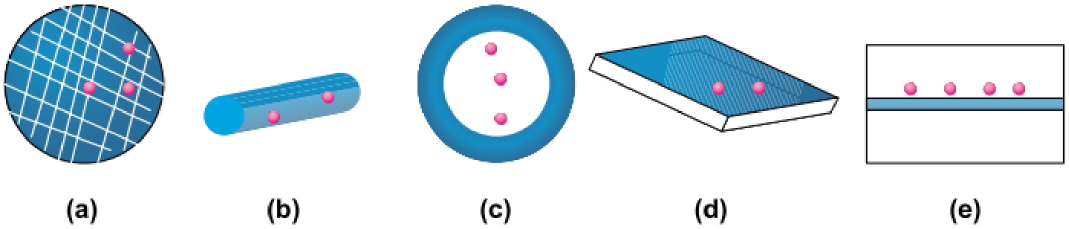

Figure 2.20 – Immobilised enzymes of defined size and shape. Supports vary in their geometric parameters, different shapes and types of enzyme carrier are illustrated: (a) bead, (b) fibre, (c) capsule, (d) film and (e) membrane. Copyright [92].

It was shown that irregular and rough surfaces have higher surface areas than smooth surfaces and consequently higher protein loading rates.[92] Thus the roughness and irregularity of the surfaces can sometimes improve protein loadings and stability, and increase the activity of the immobilised enzyme.

The geometry of the pore also influences the enzyme immobilisation and can improve diffusion rates and reduce leaching (Figure 2.21). 3D channels and foam-like seem to be suitable architectures for protein adsorption because of their 3-dimensional connectivity: the substrate can interact with the enzyme from different sides of the pores, the surface area is large and the probability of leaching is controlled with the pore size. Pore blocking is reduced due to the interconnectedness of the pore channels that allow more effective diffusion.[97]

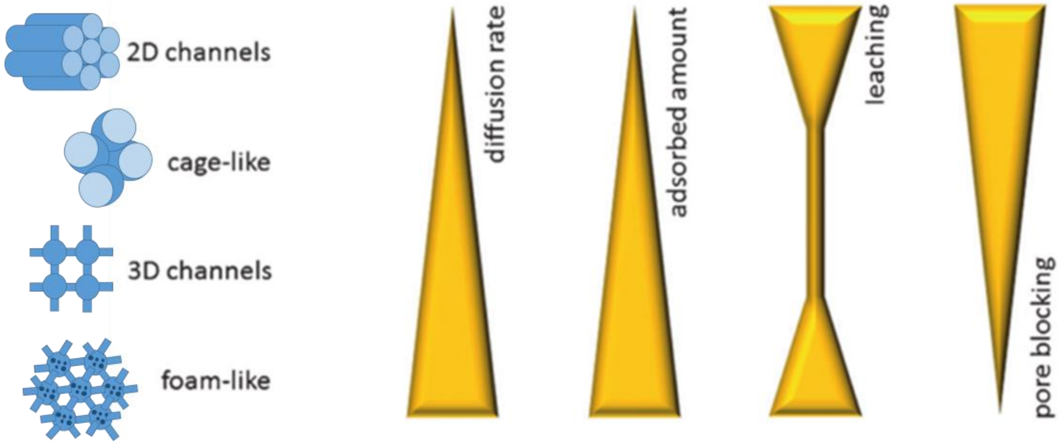

Figure 2.21 – Influence of pore geometry on the adsorption of proteins. Adapted from [94].

Anodic aluminium oxide (AAO) nanoporous membranes, an example of nanoporous support for enzyme immobilisation and other applications

Nanoporous AAO membranes are produced by an inexpensive electrochemical process called anodisation (fabrication description and optimisation stated in detail in Appendix B). Anodisation consists of the conversion process from aluminium into alumina surface layer, by applying an appropriate electrical voltage, resulting in straight cylindrical pores embedded in an alumina matrix.[98] The pores are hexagonally arrayed parallel to each other and can be prepared with diameters between 10 and 400 nm depending on the anodisation conditions (*e.g.*, electrolyte/acid composition and concentration, pH and voltage).[99] The thickness of the AAO layer can be controlled by the duration of the anodisation process.

AAO membranes have advantages and disadvantages when applied to enzyme immobilisation. AAO is a polar oxide surface and it allows enzyme immobilisation and enzymatic reactions in aqueous solutions as well as other polar solvents. The morphology of this support permits continuous processes at a high flow through a high density of nanopores, in contrast to nanoporous silica particles which often have torturous pore structures.[94,100] As disadvantages, this support material is slowly degraded in both acidic and basic solutions (below pH 5 and higher than pH 8), the amount of immobilised enzyme is limited by pore sizes and porosity that are respectively higher and lower than possible with nanoporous silica particles.[94] Also, the allowed applied flow pressure depends on the thickness and mechanical strength of the membrane.

These nanoporous membranes were used as supports for enzyme immobilisation (chapter3) as well as waveguides for measuring diffusion of molecules through nanopores (chapter 4). When using nanoporous materials for waveguiding, the pore sizes need to be smaller than the wavelength of the light. AAO membranes are very convenient to use because their pore size and thickness can be tuned easily. For our stepup the nanoporous AAO needed to be less than 2 μm thick in order to be able to distinguish the different modes and confine the light at different regions of the pore (see the discussion in section 4.2.1). However, thicker AAO membranes (60 μm) were also used for more robust measurements that involved suspending these membranes on a flow cell (chapter 5).

2.3.3.3 Chemical and physical-chemical composition

The surface chemistry affects the strength of the interactions between enzymes and support surface. Different functional groups can change the interaction forces during enzyme immobilisation and hence enzyme performance. The chemistry needs to have a high capacity for enzyme binding and must not lead to denaturation or deactivation of the enzymes. For example, sol-gel synthesis made with the enzyme in solution may result in the denaturation of the enzyme during the immobilisation process.[89]

Hydrophobicity or hydrophilicity of the support may have a strong influence on immobilisation method and catalytic activity of immobilised enzymes. The hydrophobicity of the support influences the electrostatic interactions with the enzyme and its conformation during the immobilisation process.[82]

The pI of a support or enzyme refers to the pH value at which it has a zero net charge. Generally, an attractive interaction between support and enzyme occurs when the pH value during the immobilisation method is below the pI of the enzyme and above that of the support, or vice versa (Figure 2.22).[101] If the solution pH is below the pI of the enzyme, the enzyme has a net positive surface charge, which favours the electrostatic interaction with a support that has a negative charge on its surface. These forces do not only occur between support and protein, but also between protein molecules. The repulsion is minimised when the pH is near that of the pI – the charges of molecules are net zero and there is no repulsion between enzyme molecules. In the regime when the pH values are far below or above the pI, the repulsion between enzyme molecules is much more dominant than the electrostatic attraction to the surface, thus producing the trend in Figure 2.22 with a maximum in adsorbed enzymes around the pI of the enzyme.[94]

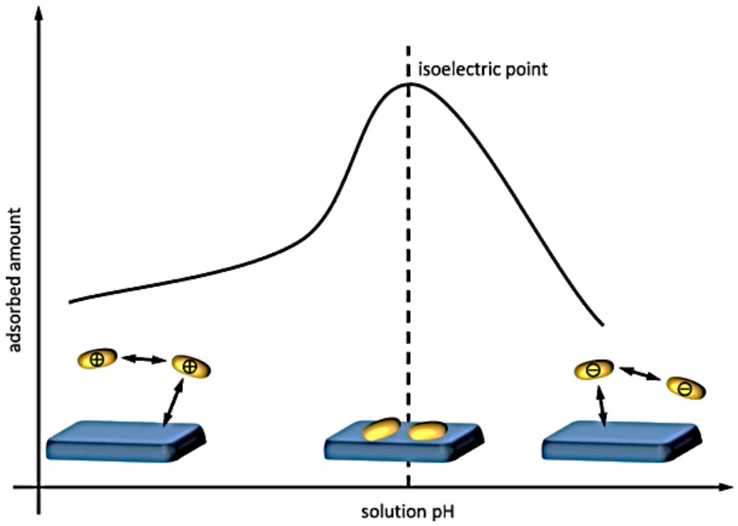

Figure 2.22 – Influence of the pH on the interactions between adsorbed enzyme and silica support during immobilisation. Copyright [94].

2.3.3.4 Novel concepts of enzyme immobilisation on nanoporous supports

In this section, some concepts that have been exploited to enhance the surface attachment of enzymes such as modification of surface wettability to improve enzyme adsorption as well as novel supports for encapsulation and entrapment will be described. These developments did not overcome all the problems that are found during immobilisation processes such as low enzymatic activities however they bring new ideas and concepts for optimising the attachment of enzymes.

Enzyme adsorption by modifying or controlling surface wettability

Immobilisation by adsorption depends especially on the chemical composition of the material support.[101] One example is the work of Wang *et al.* on laccase enzyme immobilisation which varied the surface composition of poly(methyl methacrylate) (PMMA) fibrous membranes with organically modified montmorillonite, PMMA/O-MMT).[102]

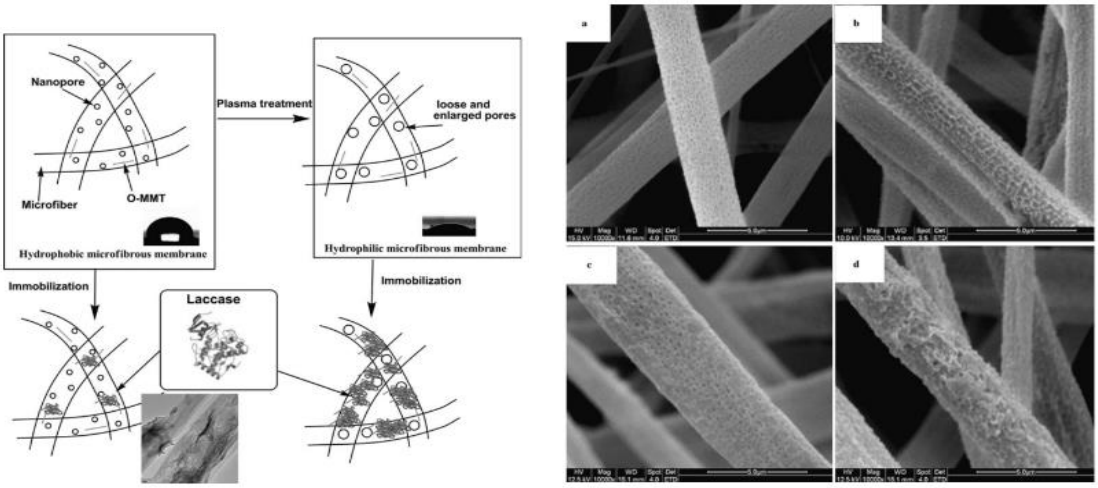

Figure 2.23 – Schematic illustration of the microfibrous membrane fabrication using the electrospinning process and a plasma treatment for laccase immobilisation. SEM of PMMA/O-MMT images: a) original; b) plasma pretreated; c) the original microfibers after laccase immobilisation; d) the plasma pretreated microfibers after laccase immobilisation. Copyright [102].

A plasma treatment was applied to the PMMA/O-MMT membranes and the plasma power and processing duration were changed in order to modify the hydrophobicity/wettability and texture surface morphology of the material, and consequently influence protein loading (Figure 2.23). When the plasma treatment power increased, the hydrophobicity of the samples decreased and then increased due to preferential etching of PMMA, and the protein loading increased (first due to the increase of both size and depth of pores and then due to the increase of the hydrophobicity). The time of plasma treatment had a more important role in improving the enzyme immobilisation yield, since increasing the time from 60 to 90 minutes increased six times more the loading of protein. Figure 2.23 shows that plasma treatment changed the structure of the sample surface, regarding surface porosity, leading to an increase in surface area. Finally, this chemical modification increased the surface free energy by introducing reactive oxygen surface species which although not pointed out by the authors, might have allowed chemical binding of the enzyme to the support surface.[102]

Similar to Wang *et al.*, the idea of Biradar *et al.* was to overcome some problems that solid silica particles have, such as the limitation on the available surface area and pore diameter. Etching silica nanospheres created silica particles with bigger and more accessible cage-like corrugated structures on their external surface (Figure 2.24).[103] Etching for 4 hours resulted in the highest enzyme adsorption due to higher surface area and silanol groups density on the surface. Increasing the number of the silanol groups increases the H-bonding and electrostatic interactions between the enzyme and the silica particles. In this work, where the flavin-containing monooxygenase 1 (FMO1) was immobilised for the first time, nanoporous structures were shown to be advantageous by enabling the immobilisation of enzymes compared with non-porous structures.

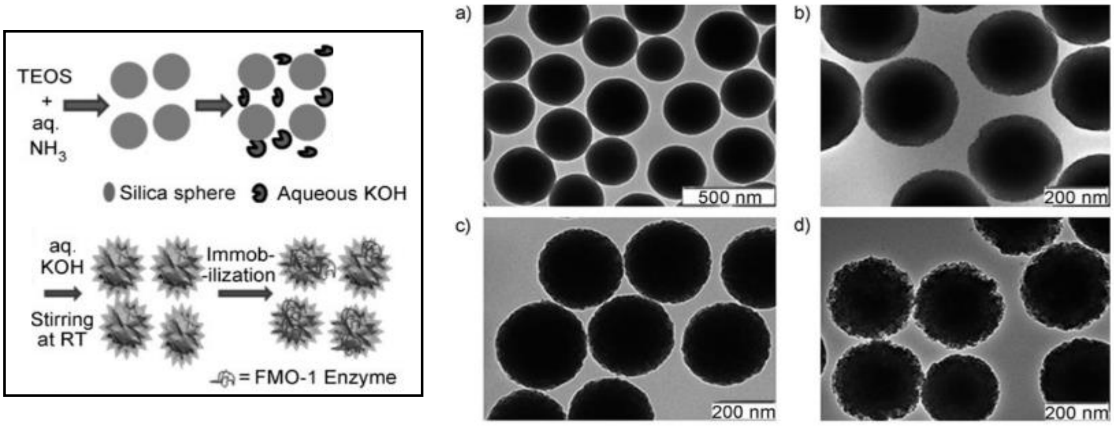

Figure 2.24 – Synthesis of corrugated and nanoporous silica nanospheres by etching nanospheres with dilute aqueous potassium hydroxide (KOH) solution and immobilisation of the flavin-containing monooxygenase 1 (FMO1) on the resulting etched nanospheres [103]. TEM images of silica nanospheres a) before etching and b) after etching for 2h, c) 3h and d) 4h using potassium hydroxide (KOH) solution. Scale bars are a) 500 and b)-d) 200 nm. Copyright [103].

Covalent immobilisation

Chen and co-workers studied the covalent immobilisation of glucose oxidase in nanoporous gold (NPG) films for biosensing applications.[104] They tested the effect of pore diameter on enzyme immobilisation and mainly the effect of a NPG-thiol functionalisation on enzyme immobilisation. In this case, it was observed that the biosensor was more sensitive when thiol linker was presented "due to the enhanced enzyme distribution density and non-destructive enzyme bioactivity on NPG with the aid of the biocompatible thiol linkers". The highest sensitivity did not occur on the NPG with the smallest pore size as the authors expected, because after enzyme immobilisation, the pores were not large enough for easy entrance of substrates.

Novel supports for entrapment

A new strategy to produce nanoporous structures with entrapped enzymes was created by Lu *et al.*. A mixture of horseradish peroxidase (HRP) and ferrocene methanol (FcMeOH) with surfactant cetyl-trimethyl ammonium bromide (CTAB) and sodium chloride (NaCl) as precursor solution (sol) was prepared and passed through glass particles (Figure 2.25).[105]

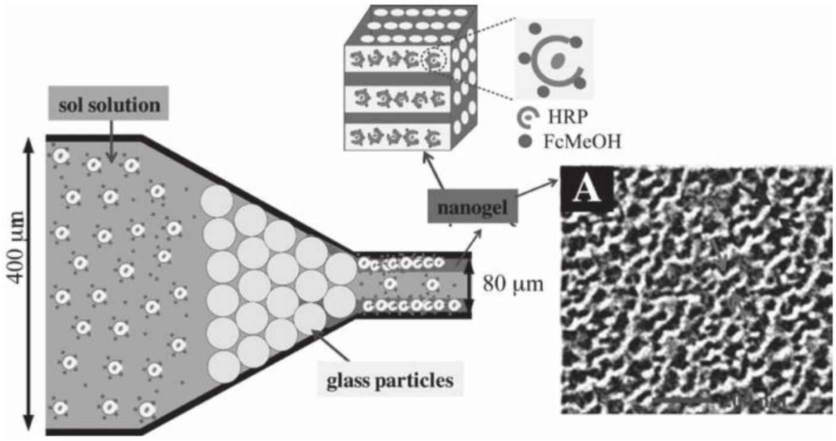

Figure 2.25 – Scheme of flow-induced gelation in a microfluidic filter device. The precursor solution (sol solution) contains CTAB, NaCl, HRP and FcMeOH. Copyright [105].

After passing the precursor solution, a matrix was formed, after the glass particles entrapping the enzymes and FcMeOH inside a porous nanogel structure. The enzymes retained their functional characteristics. It was postulated that the entrapping matrix protected the HRP from leaching. The authors further speculated that this matrix helped retain the enzyme's native stability and reactivity although the preservation of the enzyme structure was not characterised.

Novel supports for encapsulation

Kao *et al.* designed a system where a nanoporous support – mesoporous silica nanoparticles (MSNs) – was used to mimic enzymes in a crowded environment (enzyme inside the cell).[106] The MSNs were selectively functionalised with 3-aminopropyl(trimethoxysilane) (APTS) only on the outer surface. This site-selective specific functionalisation avoided protein adsorption on the surface of these structures, permitting the study of immobilised lysozyme enzymes only inside the pores (Figure 2.26). By varying the pH of MSNs solutions, electrostatic repulsion forces on the surface controlled the uptake of enzymes into the pores. Also, spectroscopic measurements showed that immobilised enzymes were sensitive to the curvature and pore size of the silica materials. The lysozyme adsorption, structure, stability and catalytic activity were studied. The immobilised enzymes were more stable and showed higher activities on concave surfaces because these surfaces provided a better preservation of the native structure of the adsorbed proteins. The authors concluded that higher enzyme activity was observed when the pore size of MSNs was close to the dimension of the proteins.

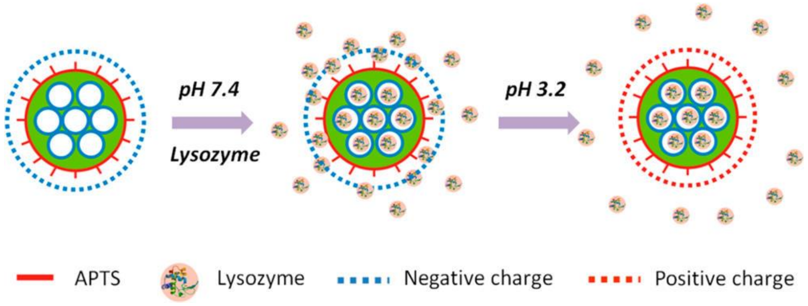

Figure 2.26 – Diagram of Designed Strategy for Lysozyme Adsorption and Desorption from APTS-Functionalised MSNs. Copyright [106].

Itoh *et al.* combined two usual nanoporous materials to build a hierarchical structure to encapsulate formaldehyde dehydrogenase (FDH) and showed its potential as an electrochemical biosensor (Figure 2.27). They prepared silica nanotube with nanochannel-walls using commercial anodic alumina membrane as columnar pores template. This structure was an “artificial biomembrane” to encapsulate FDH inside silica nanopores.[107]

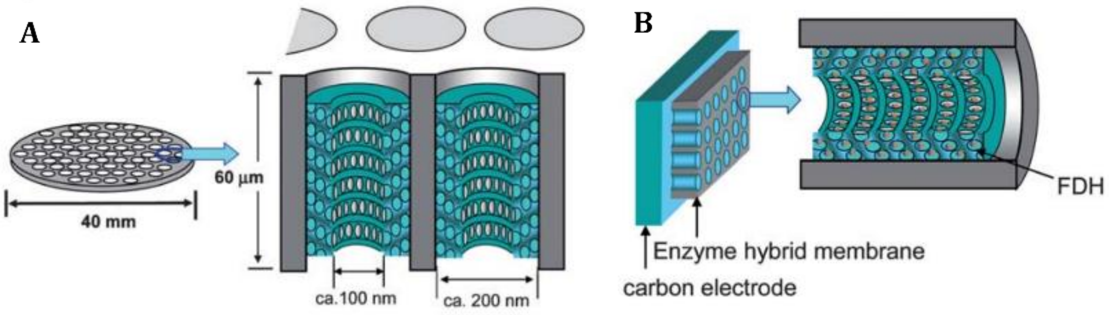

Figure 2.27 – A) Schematic illustrations of the anodic alumina (AAO) membrane and silica-alumina composite membrane. The assembly is made of silica nanotubes (inside tube diameter = ca. 100 nm) with nanochannel-wall (channel diameter = ca. 13 nm) formed inside the columnar alumina pore (pore diameter = 200 nm). B) Schematic diagram of the electrochemical cell step-up. Formaldehyde dehydrogenase (FDH) is immobilised on carbon electrodes with the AAO-silica structure. Adapted from [107].

Another application of encapsulated enzymes in silica nanopores is an enzyme reaction platform for large biomacromolecules— Deoxyribonucleic acid (DNA) (Figure 2.28 A). Matsuura *et al.* studied the effect of the pore size of nanoporous silica on the DNA amplification activity using Taq DNA polymerase (hydrodynamic diameter of ca. 9.2 nm) (Figure 2.28 B).[108]

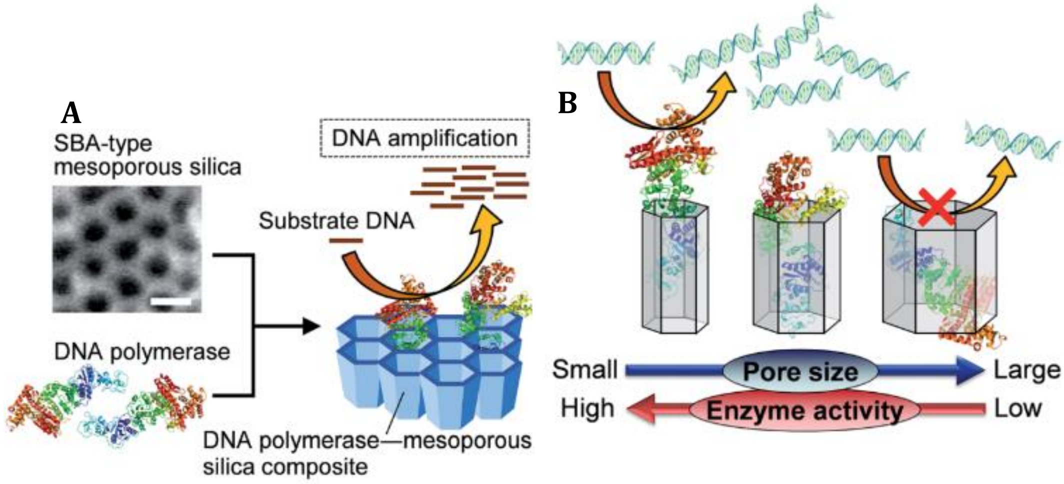

Figure 2.28 – A) Schematic representation of DNA amplification by DNA polymerase immobilised on the channels of mesoporous silica. SEM image shows mesopores with a 7.1nm pore diameter (scale bar = 10 nm). B) Schematic illustration of the relationship between mesoporous silica pore size and the enzymatic activity of immobilised Taq DNA polymerase. Adapted from [108].

They tested different pore diameters of mesoporous silica to immobilise DNA polymerase. The enzyme activity was evaluated and the relationship between pore size and the enzyme activity was assessed. In this particular case, higher enzyme activities were found when the pore diameter was smaller – DNA polymerase could fit better inside the pores and retain 50% of activity (maximum activity achieved). The authors suggested that half of the active centres of DNA polymerase were oriented towards to the deep portion of pores during enzyme immobilisation, whereas the other half of the enzymes interacted with the substrate.

Cross-linking and other immobilisation methods

Different oxidase enzymes were immobilised on magnetic nanoparticles (MNPs), entrapped in large-pore-sized mesoporous silica and cross-linked with glutaraldehyde (Figure 2.29). The cross-linking agent prevented enzyme leaching from the pores and increased the amount of immobilised enzyme. The enzymatic reaction produced coloured products so that this system can be used as a colorimetric sensor. Since different enzymes can be immobilised using this strategy, the potential applications of this technology range from "biosensors to multi-catalyst reactors".[109]

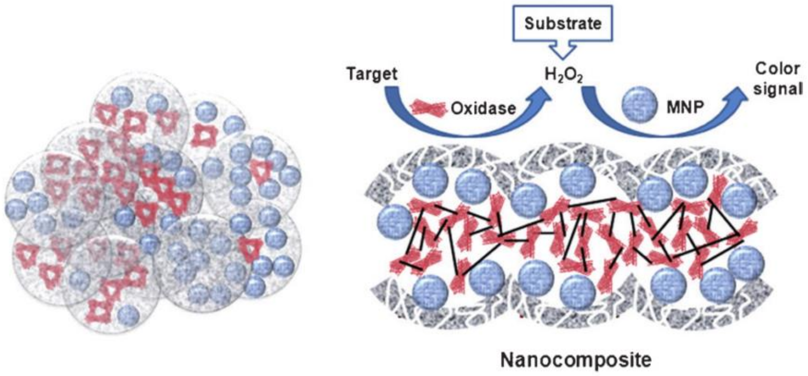

Figure 2.29 – Scheme of the nanocomposite entrapping and cross-linking both Fe_3O_4 magnetic nanoparticles (MNPs) and oxidases in mesocellular silica. Adapted from [109].

Combination of several methods

Laveille *et al.* presented two different concepts that "combines the sol-gel method with a templating process using bilayers of phospholipids to provide an organised network of phospholipids inside the silica and at the same time protect the embedded enzyme, as if they are entrapped in a biological membrane supported on silica" (Figure 2.30 A).[110] The first concept is a sponge-like structure with lipase enzyme and phospholipids inside the structure (sponge mesoporous silica – SMS) (Figure 2.30 B).

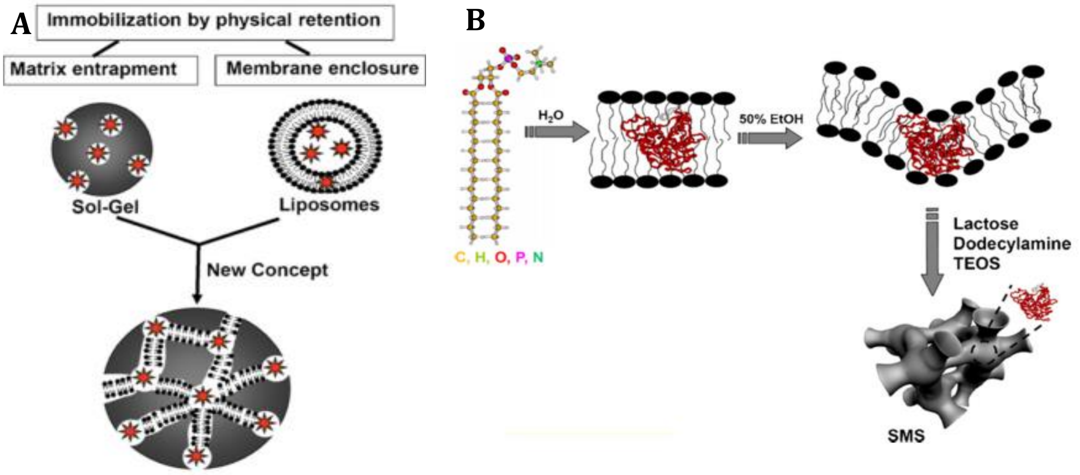

Figure 2.30 – New design to immobilise enzymes that combine encapsulation and entrapment methods. Sponge Mesoporous silica (SMS) tetraethoxysilane (TEOS) Adapted from [110].

To optimise this first system and to use haemoglobin as biocatalyst, a new approach was made by the aggregation of nanoporous silica capsules (NPS) (Figure 2.31). The immobilised lipase showed higher activities compared to the same lipase immobilised in commercially available supports.

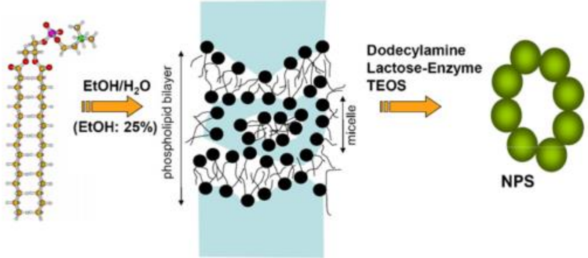

Figure 2.31 – Formation of nanoporous silica capsules (NPS), from phospholipids bilayers and micelles. Copyright [110].

Another different concept on enzyme immobilised was presented by Zhang and their collaborators. They were able to microencapsulate enzymes for catalysis in organic media (Figure 2.32). “An aqueous solution of laccase was successfully encapsulated in silica colloidosomes by linking nanoparticles at the water/oil interface using hyperbranched polyethoxysiloxane (PEOS) in an aqueous-laccase-solution-in-toluene Pickering emulsion. The weight ratio between silica particles and water (Rs/w) was changed in order to adjust the shape and size of the colloidosomes shell".[111]

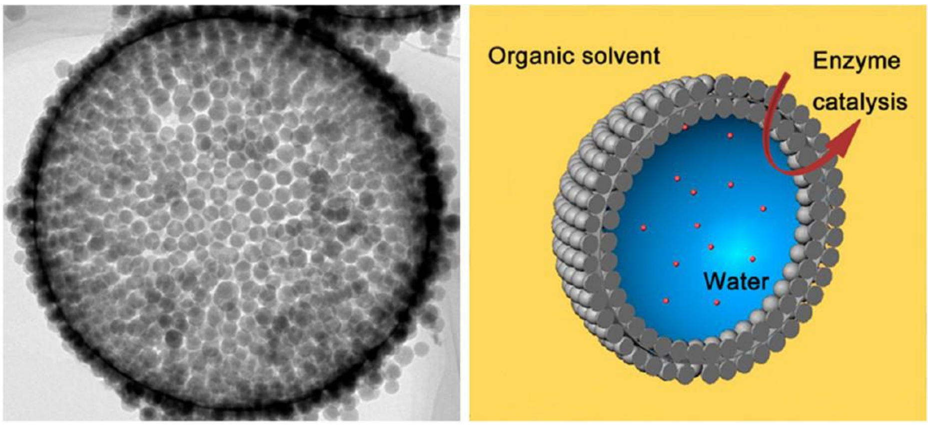

Figure 2.32 – FE-SEM (left) and schematic draw (right) of a colloidosome where an enzyme in an aqueous solution can be encapsulated. Copyright [111].

The authors showed that the Rs/w influences the performance and stability of the enzyme. At Rs/w = 0.4, the structures encapsulate enzymes with the highest reusability but the lowest activity. These two parameters were always affected in opposite ways when the Rs/w was changed. The applications of these structures can be for controlled release systems due to their composition and properties. A significant advantage of this system is biphasic catalysis, where the enzyme is in an aqueous solution and the substrates of organic reactions are soluble in an organic solvent.[111]

2.4 Summary

This literature review covers the most common methods of surface modification, describing in more detail universal coatings. In this thesis, polyphenol coatings were exploited for immobilising proteins, for the first time, and as anchors for grafting polymer brushes. As discussed previously, there are many challenges for attaching molecules to the surface of the materials. For example, for enzyme immobilisation, it is difficult to achieve an ideal system where the surface of the material is totally covered by enzymes and that all the immobilised enzymes are active and available for enzymatic reaction.

The polyphenol coatings were also used to graft polymer brushes for antifouling surfaces. The aim of that was to minimise adsorption events for allowing the characterisation of the diffusion of molecules through nanopores. This helped to enable the optical waveguide spectroscopy (OWS) studies on nanoporous membranes by controlling the transport of molecules with different molecular weight and net charge.

3. Plant-based polyphenol coatings for surface functionalisation with proteins and enzymes

3.1 Introduction

Proteins are biomacromolecules that perform many of the functions of life at mild pH and temperature conditions and can be exploited for practical applications.[20,52,89] Enzymatic proteins, in particular, can catalyse chemical reactions with high specificity and high rates in aqueous as well as non-aqueous media.[59] For these reasons, enzymes are environmentally and economically attractive industrial biocatalysts,[5] as well as molecular sensing elements for applications where the reaction products are easily detectable.[6] Other proteins, *e.g.*, immunoglobulin and avidin, bind to other molecules with high specificity and/or affinity, and are extensively used for sensing of their binding partners in biosensing, biomedical diagnostic, and targeted drug delivery applications, or for assembling molecular components to form complex biointerfaces in research.[105,112]

Immobilisation of proteins on solid support "carriers" is often critical in the aforementioned applications because they may be conveniently handled or delivered with the material substrate, or be readily separated from the solution phase. For example, in industrial biocatalysis, facile separation of enzymes from the reactant substrates and products reduces waste and cost by reducing the need for purification[1,2] and through recovery and reuse of the enzymes.[3–5] In biosensing and biomedical applications, the immobilisation physically links the proteins to the rest of the material system such that protein binding may, *e.g.*, guide theranostic nanoparticles to appropriate biological targets, or confer the optical, electrochemical or structural changes necessary for generating a detectable sensor signal.[20,113]

Immobilisation methods can generally be classified into physical and chemical approaches. Physical adsorption onto surfaces by non-specific intermolecular forces such as van der Waals forces, hydrogen bonding, and hydrophobic or electrostatic interactions (*i.e.*, physisorption) is often the simplest and most convenient method.[87] However, this non-specific binding can be too weak to prevent proteins from leaching off the carrier over time when the protein is soluble in the overlying solution.[114,115] Protein entrapment is another popular physical method, in which proteins are physically confined in an insoluble matrix formed around them.[4] However, finding suitable chemical transformations for forming the matrix without covalently binding the proteins or interfering with their biofunctionality can be challenging, depending on the type of protein.[116,117]

Chemical approaches rely on a specific and strong type of binding between a surface and the protein, *e.g.*, covalent coupling, chelation, and specific protein binding (biorecognition).[6,117] These approaches entail modification (or coating) of a surface with appropriate functional groups for protein binding.[3,82] To enable covalent coupling, for example, carbodiimide-activated carboxyl and maleimide groups may be introduced on the support surface to react, respectively, with amines (lysine residues) and thiol (cysteine residues) that may be present on a protein's surface. Other common functionalities include nickel-chelating His-tags, biotin, lectin-carbohydrate, disulphide bonds, etc.[6,117] However, this methodology almost always requires the development of either i) specialised bifunctional linkers with chemically orthogonal groups for protein binding at one end and surface binding at the other (*e.g.*, silanes for glass and some oxide surfaces, thiols for copper and noble metal surfaces, etc.), or ii) specific methods to derivatise different surfaces in order to leave reactive groups to bind with the protein (*e.g.*, cyanogen bromide or ethyl chloroformate conversion of hydroxyls, plasma, ozone and UV treatments, oxidation, hydrolysis of polymers, etc).[17,20,118–120] Some hybrid chemical-physical approaches, *e.g.*, crosslinking of enzymes to form "carrier-free" reactive particles, are also available.[82,90] However, adapting, developing and/or optimising the aforementioned techniques for different proteins and material surfaces can take significant time and effort.[3,85,93] A simple and convenient way to immobilise different proteins on a variety of materials without leaching would be highly desirable.

A "universal" polyphenol coating approach has been reported for surface modification of a great variety of materials without surface preparation, including metals, oxides and plastics through multiple covalent and non-covalent interactions.[35,38,41,49,53,54,58,121] Polyphenols such as tannic acid and catechins are organic compounds, high in dihydroxyphenyl (catechol) and/or trihydroxyphenyl (galloyl/gallic acid) content, that are abundant in natural plant sources (*e.g.*, green tea and some plant fibres). These coatings were inspired by the popular polydopamine (pDA) coating, in the sense that pDA is also abundant in hydroxyphenyl groups and relies on the multifaceted chemical and physico-chemical properties of these groups. First, hydroxyphenyl groups bind with an underlying material surface as well as with themselves (under an oxidative environment) to form coatings, and then bind with other functional molecules such as polymers and proteins for surface immobilisation. Like pDA, our initial polyphenol coatings were also conveniently formed on different materials simply by short-term (*e.g.*, 10-60 min) immersion in mildly basic aqueous solutions of the (poly)phenol precursor. Other groups have pursued a coordination chemistry approach to create coatings through the chelation of Fe(III) with polyphenols.[58,122] In either case, unlike with pDA, the precursors of polyphenol coatings can (potentially) be sourced from (waste) plant materials that are (drastically) much lower cost than the catecholamine precursors of pDA or its variants.[55,123] Polyphenol coatings are also reasonably transparent through the visible wavelengths (*i.e.*, colourless), so its potential in light-related applications is less restricted than pDA, which is optically opaque due to its chemical similarity with melanin.[55] Furthermore, polyphenol coatings may also be formed using a larger variety of functional polyphenol precursors as well as a larger range of pH conditions, thus potentially widening its applicability.[56]

In this chapter, we demonstrate polyphenol coatings as versatile interfacial layers for the immobilisation of a panel of common mono- and multimeric proteins, including enzymes. We show that polyphenol coatings expand the applicability of "universal" coatings for biomolecular functionalisation to a greater range of surfaces and processing conditions than accessible with pDA. Although polyphenols are often associated with enzyme inhibition, this is true mainly with respect to certain digestive enzymes.[124–126] Furthermore, the polyphenol cannot inhibit a reaction if it is already a part of a solid material surface unless the protein's active site is oriented "upside down" in contact with the coating, which is only encountered by a minor fraction of the immobilised proteins. After realising this, we recently reported on the immobilisation of thermolysin using two polyphenol coatings composed of tannic acid (pTA) and pyrogallol (pPG) (to spatially confine enzyme-catalysed nanofibre formation to a surface).[36] Encouraged by this success, we herein present results on exploiting these polyphenol coatings for the immobilisation of a range of proteins (Figure 3.1) useful for biosensing (immunoglobulin G, avidin, and horseradish peroxidase) and biocatalysis applications (acid phosphatase, chymotrypsin, lactate dehydrogenase). We included in our investigation materials that have not yet been demonstrated for polyphenol coatings – nanoporous alumina, polyester, cellulose, and stainless steel. Cellulose and steel, in particular, are common engineering materials for which standard protocols for their functionalisation with biomolecules have particular limitations.[127,128]

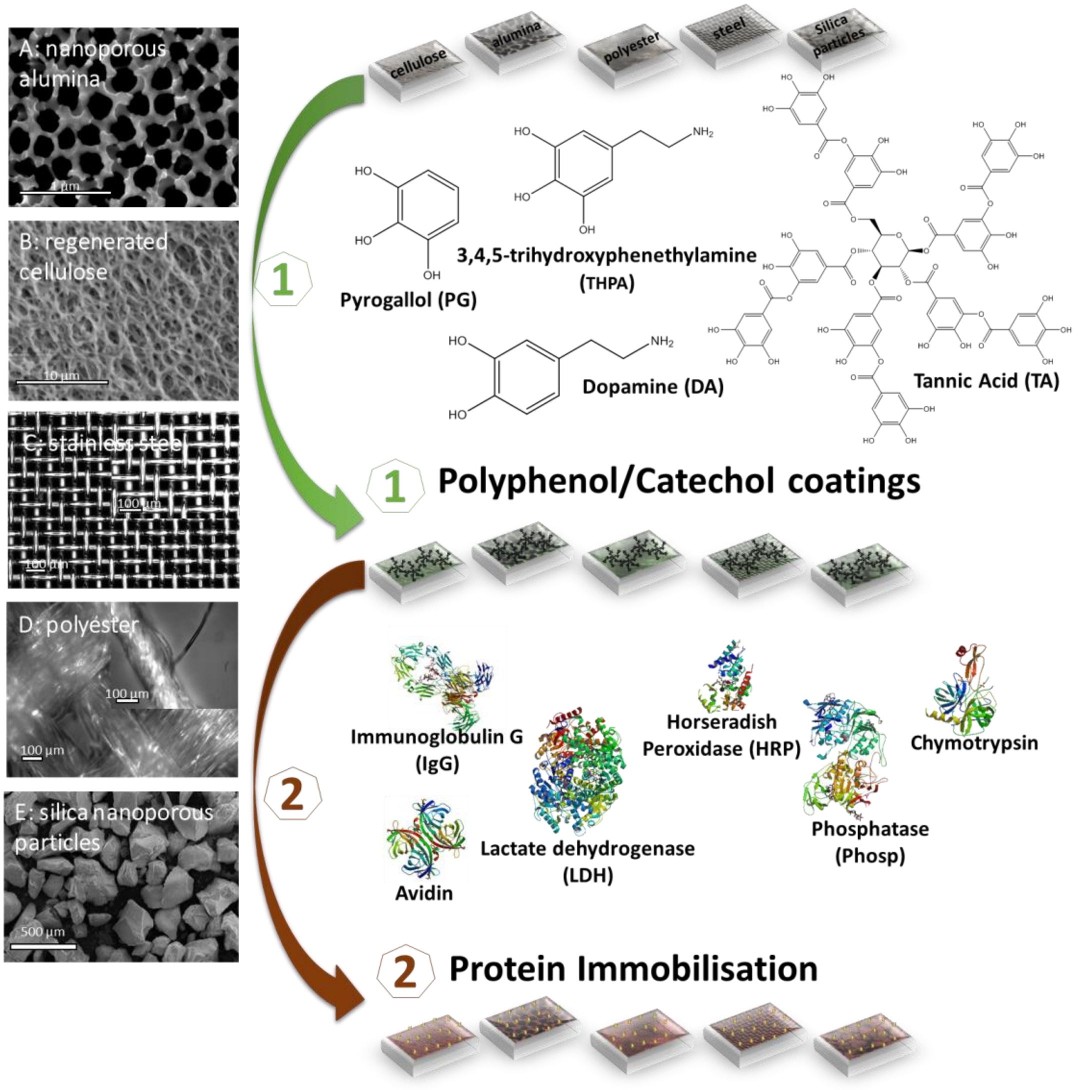

Figure 3.1 – Scheme of polyphenol/catechol (tannic acid (TA), pyrogallol (PG), dopamine (DA), 3,4,5-trihydroxyphenethylamine (THPA)) coating and immobilisation steps of acid phosphatase (Phosp), chymotrypsin, lactate dehydrogenase (LDH), horseradish peroxidase (HRP), Immunoglobulin G (IgG) and Avidin on different supports. SEM images of different supports used: (A) alumina, (B) regenerated cellulose, (C) stainless steel, (D) polyester and (E) silica nanoporous particles. Protein structures from PDB Database: 1XZW, 1MTN, 1I10, 1HCH, 1HZH and 2AVI, for phosphatase, chymotrypsin, LDH, HRP, IgG and avidin, respectively.

A range of conditions for both coating and immobilisation such as pH and precursor were tested. The effectiveness of the polyphenol approach was evaluated mainly by measuring the immobilised enzyme activities. The results were compared with physical adsorption on uncoated versions of the same support materials as well as with immobilisation via pDA and its variant 3,4,5-trihydroxyphenethylamine (THPA). The presence and thickness of the coating and enzyme layers were further quantified by silver staining, contact angle measurements and X-ray photoelectron spectroscopy (XPS).

3.2 Results and Discussion

3.2.1 Effectiveness of polyphenol coatings for the immobilisation of proteins

We chose tannic acid (TA) and pyrogallol (PG) as the model phenolic precursors to evaluate the general effectiveness of the polyphenol coating immobilisation approach. TA is commonly composed of pentadigalloyl ester groups covalently attached to a central glucose core and is highly abundant in a number of plant materials.[57] It is also a commercially important, low-cost compound.[55] PG is 1,2,3-trihydroxybenzene, a simple phenolic mimic. We chose polyphenol coating precursors with only trihydroxyphenyl units to compare our results with the popular polydopamine coatings (pDA), which is prepared from dopamine that consists of a dihydroxyphenyl group (catechol) linked to a primary amine, and hence investigate the difference in coating and protein coupling properties between polyphenols and pDA. In further experiments, we also prepared a previously reported pDA variant constituted from 5-hydroxydopamine, *i.e.*, poly(3,4,5-trihydroxyphenethylamine) (pTHPA) to probe the effect of linking a primary amine to the trihydroxyphenyl chemistry.[123]

Figure 3.2 shows the activities of a panel of proteins immobilised by poly(tannic acid) (pTA) and poly(pyrogallol) (pPG) coatings, compared with the effectiveness of immobilisation by pDA coatings. The proteins were immobilised by a 2-step process. The pTA, pPG, and pDA coatings were first prepared by immersing the solid support materials in the precursors solutions following previously reported protocols in these initial experiments – coating at pH 7.8 for polyphenols and pH 8.5 for dopamine and THPA; a 0.03 mg/mL precursor solution was prepared and the materials were immersed in this solution for one hour (see details in section 3.4.2).[55] Then the coated supports were immersed in the corresponding protein solutions to attempt protein immobilisation. Successful application of the coatings was confirmed, following previously established protocols,[38,55,56] by silver staining and contact angle measurements. The atomic composition and thickness of representative coatings were also characterised by XPS (see Figure I.1 to Figure I.5).

The immobilised activity was quantified using common aqueous enzyme assays performed with a modified cuvette, in which the solid supports may be affixed parallel to the measurement light path (see Figure I.6, Appendix A), to measure the wavelength specific absorbance change from the conversion of a suitable enzyme substrate molecule into its strongly absorbing product. In order to compare the immobilised activities of the same enzyme on different materials, the activity (μmoles/min) per the sample size and surface of the material (see surface areas in Table 3.2 in section 3.4.4). All the results shown throughout this report were obtained from triplicate repeats or more.Cellulose and steel were chosen as the examples of solid material support due to the challenge of functionalising them by previously reported methods.[127–130] The samples were in the form of either a high surface area nanoporous membrane or microfibre mesh to increase the amount of proteins immobilised and simplify protein characterisation (see below). Limited tests were also performed on silica, as well as on alumina and polyester in later parts of this study (see sections 3.2.2 and 3.2.3), and polyphenol coatings have been previously shown on a range of other polymeric and oxide materials.[55]

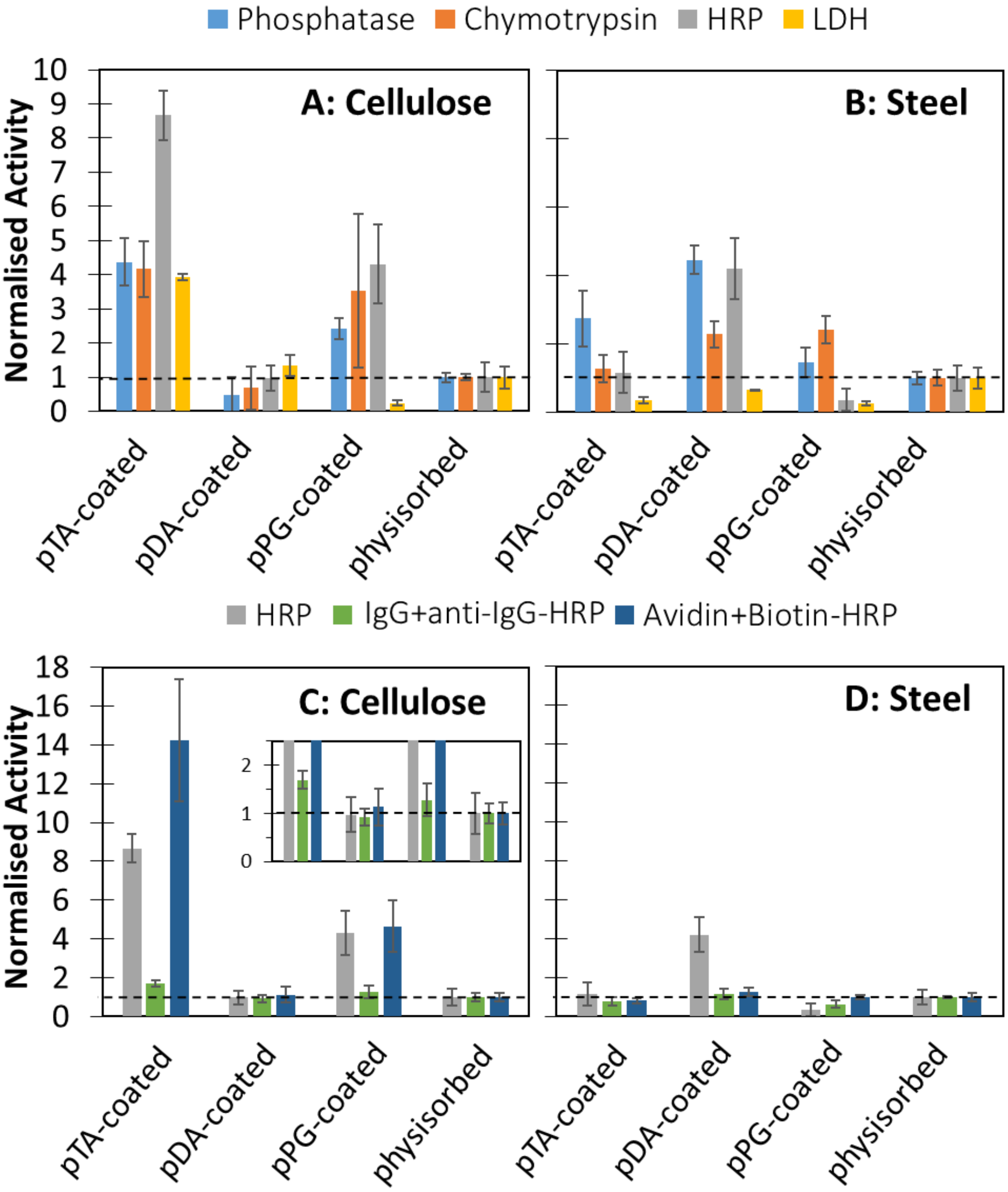

Figure 3.2 – Normalised activity of acid phosphatase, chymotrypsin, horseradish peroxidase (HRP) and lactate dehydrogenase (LDH) on coated- or uncoated- (A) cellulose and (B) steel. Different HRP systems were tested. Poly(tannic acid) (pTA), polydopamine (pDA) and poly(pyrogallol) (pPG)-coated- and uncoated- (C) cellulose and (D) steel were immersed in IgG or avidin solution (immobilisation) before adding anti-IgG-HRP or biotinylated-HRP, respectively. The normalised value 1 is equivalent to the physisorbed enzyme activity of 80, 2.1, 2.1, 0.5, 13 and 3.8 nmoles/min.m^2 (on cellulose) and 192, 3.1, 0.1, 0.7, 37 and 2.3 nmoles/min.m^2 (on steel) for phosphatase, chymotrypsin, HRP, LDH, IgG+anti-IgG-HRP and Avidin+Biotin-HRP. See reference values also in Table I.1 (Appendix A).

A diverse range of 4 enzymes were immobilised on cellulose and steel. They have different isoelectric points (pI ranging over *ca.* 5 to 9), molecular weights (from 44 to 140 kDa) and structural typologies (globular to multidomain/multimeric), and they catalyse a range of different reactions. The measurement of immobilised enzyme activity in these initial experiments rather than the immobilised mass or surface coverage is aimed at evaluating the effectiveness of the coatings for preserving the functional state of a protein, together with their abilities for coupling the protein on a surface. To aid the comparison, all results were normalised with respect to the activities measured for control samples on which the enzymes were physically adsorbed with no coating treatment. Information on the measured activity values are listed in Table I.1 (Appendix A) and can also be referenced from Figure 3.2.

Overall, the use of the polyphenol coating as a protein-coupling layer improved the immobilised activity on cellulose, especially on the pTA samples. For instance, the immobilised HRP activity was 8.5 times higher than that achieved on pDA. For the other enzymes (phosphatase, chymotrypsin and LDH), the activity on pTA coated cellulose was 4 times higher than on pDA. In fact, activities on the pDA coated cellulose were either the same as or lower than the physisorption control. The benefit of using PG for immobilising enzymes on cellulose was less dramatic than using pTA but, except for LDH, the activities were still 2 to 4-fold higher than the physisorption control. Although chymotrypsin may be inhibited by polyphenols in solution,[131,132] this effect is less relevant for immobilised enzymes because the polyphenols are part of the solid surface and cannot interfere with the enzyme's active site, except in the minority of cases when the immobilised protein is oriented with the active site down.

On the coated steel, pTA and pPG were observed to improve the immobilised activity by up to 2.5 times for phosphatase and chymotrypsin, respectively. In comparison, the pDA coating had the same effect as pPG for chymotrypsin, while pDA improved phosphatase and HRP immobilisation 4-fold. Interestingly, an LDH activity lower than the physisorption control was observed on all the coatings. Overall, the coatings mostly increased the immobilised activities on steel compared to the control, but the relatively small improvement shows the fact that physical adsorption was already partially effective by physisorption (*i.e.*, 192 nmoles/min.m^2 for adsorbed phosphatase on steel) while adsorption on cellulose was generally much lower (*i.e.*, 80 nmoles/min.m^2 for phosphatase).

Figure 3.2C and D show the effectiveness of immobilising immunoglobulin G (IgG) and avidin, two proteins often used in biosensing, also on cellulose and steel. We assayed the level of IgG and avidin immobilisation by performing an immunoassay with HRP-functionalised anti-IgG and binding with biotin functionalised HRP, respectively. Through a subsequent regular enzyme assay of HRP activity as above, we were able to compare the IgG and avidin results with the immobilisation of enzymes. The respective protein "sandwich" structures are labelled "IgG+anti-IgG-HRP" and "Avidin+Biotin-HRP". These structures are commonly used for biosensing, and the associated enzyme activities indicated the amount of functional IgG and avidin immobilised with the coatings.

Similar to the enzyme results, the pTA coating on cellulose produced the most dramatic improvement. A 14-fold increase over the physisorption control was observed for avidin immobilisation. The PG coating improved the immobilisation 4-fold while pDA performed no better than the physisorption control. In comparison, little improvement was observed on any of the coatings for IgG immobilisation, with only pTA being able to increase the activity *ca.* 1.5 times on cellulose. The coatings on steel also did not improve the immobilisation process for either IgG or avidin. IgG is a relatively large 160 kDa protein with a non-compact 3-lobed quaternary structure and high protein surface area that is conducive to surface-induced denaturation as well as physical adsorption. Thus, a significant activity was already obtained in the controls while the protein may also participate in multi-point covalent coupling with the coatings that can contribute to structural distortion and functional degradation. However, the case for avidin immobilisation on steel is less clear.

Immobilisation of phosphatase was also attempted on silica nanoporous particles. Similar activities were observed with and without the use of the coatings (Figure I.7). In contrast, it has previously been shown that thermolysin immobilisation by pTA, pPG and pDA on flat glass surfaces was similarly effective (estimated at 40 ng/cm^2 immobilised active enzymes) as opposed to physical adsorption.[36] At the same time, we recognise that polyphenols and pDA coatings of silica are relatively less effective,[47] especially under the present "thin coating conditions" needed to avoid clogging of the nanopores. Silanization is also an effective approach for functionalising silica, so this material was not pursued further.

The overall high immobilised activities obtained by using pTA coatings could indicate that the branched multivalent molecular architecture of TA could be especially suitable for the immobilisation of (bio)molecules. Each TA molecule alone already has multiple galloyl groups to interact with the underlying surface, react with neighbouring TA to form a strong cohesive coating, as well as to couple with proteins. The large TA molecules may also adhere more strongly on a solid surface to more efficiently form a coating via non-specific forces such as π-π stacking, hydrophobic effect and van der Waals interactions.

In the case of pPG and pDA, a coating with unreacted catechol or galloyl sites must first be formed on the material for binding with proteins. Thus between pTA and pPG, both rely on the chemical properties of the trihydroxyphenyl groups, pTA may have an advantage, as seen in the higher activities measured on the corresponding samples. However, the lack of LDH activity juxtaposed with good immobilised activities for the other enzymes measured on the PG samples is intriguing. It suggests that, although the polyphenol (and pDA) coatings generally perform at least as well as physical adsorption, enzyme properties play an important role in the immobilisation process. Moreover, the fact that different activities are measured on the different materials, even though all surfaces were shown to be coated (see Appendix A), suggests that the underlying solid material can influence the coating properties. Therefore, we further investigated how various material, coating and protein properties, as well as the solution parameters of both the coating and immobilisation processes, may influence the effectiveness of protein immobilisation. We focused on characterising enzyme immobilisation because the effectiveness of the process can be conveniently indicated by activity assays, and corroborated the results with the direct characterisation of the coating and protein layers by XPS.

3.2.2 pH effect during the coating

We found that pH is the main parameter that can strongly influence the coating and immobilisation processes. In a first set of experiments (Figure 3.3), we examined the effect of the pH used during the polyphenol coating formation, while fixing the pH of the solution used for protein immobilisation (all at pH 5.2). In a second series of experiments (see section 3.2.3), the pH during coating was fixed while the pH during phosphatase immobilisation was changed. Phosphatase was chosen for this part of the pH studies because it is the easiest to assay and was readily available. Our discussion will focus more on pTA coatings for comparison with pDA coatings because they were generally more effective than PG and THPA coatings. At the same time, we additionally looked at two other solid material supports – polyester fibre meshes and nanoporous alumina membranes. As before, these porous formats provided high surface areas and relatively high enzyme assay signals. Polyester was chosen as another example of an uncharged polymer, often used as a fabric. Alumina was chosen as another oxide material because it is compositionally simpler than the native oxide of steel, which is a complex alloy of Fe/Cr/Mn/Mo/Si/C/P/S, and the pI ~ 9 of alumina well characterised.[133]

It has been reported that a pH within around 2 pH values lower than the first phenolic pKa of the polyphenol should be used during the coating process (the pKa's are 7.7, 9.3 and 10.6 for pTA, pPG and dopamine, respectively).[56,59] For consistency between the two sets of experiments and to cover both the pKa of the polyphenol precursors and the isoelectric point of phosphatase (pI = 5), a pH range from 5 to 10 was chosen for the experiments. However, a slightly restricted range from pH 5 to 8.5 was chosen for alumina and steel because the former undergoes significant etching above pH 8.5 and preliminary tests showed that the activity was negligible also above pH 8.5 on coated steel. Measurements on cellulose and polyester were carried out from pH 5 to 10.

Interestingly, the results (Figure 3.3) showed that the immobilised enzyme activity depended significantly on the underlying material support as well as the pH used for coating formation. In particular, optimal pH values for coating preparation on the different materials that corresponded to maxima in the measured surface activities could be clearly identified. The maxima were observed on pTA coatings at a coating pH ~ 8.5 on both cellulose and polyester (Figure 3.3A and C). On steel and alumina, the highest activities were observed for pTA coatings prepared at pH ~ 7.8 and pH 7, respectively (Figure 3.3B and D). At these maxima, the improvement in surface activities obtained by immobilisation with pTA coatings over the physisorbed enzymes ranged from a high of *ca.* 13 times on cellulose (at $\mathrm{pH_{coating}} = 9$), to 1.3 times on alumina (at $\mathrm{pH_{coating}} = 7$). Except for alumina, these values did not correspond to the pH previously reported for the most efficient formation of thick pTA layers (from pH 6 to 7).[56]

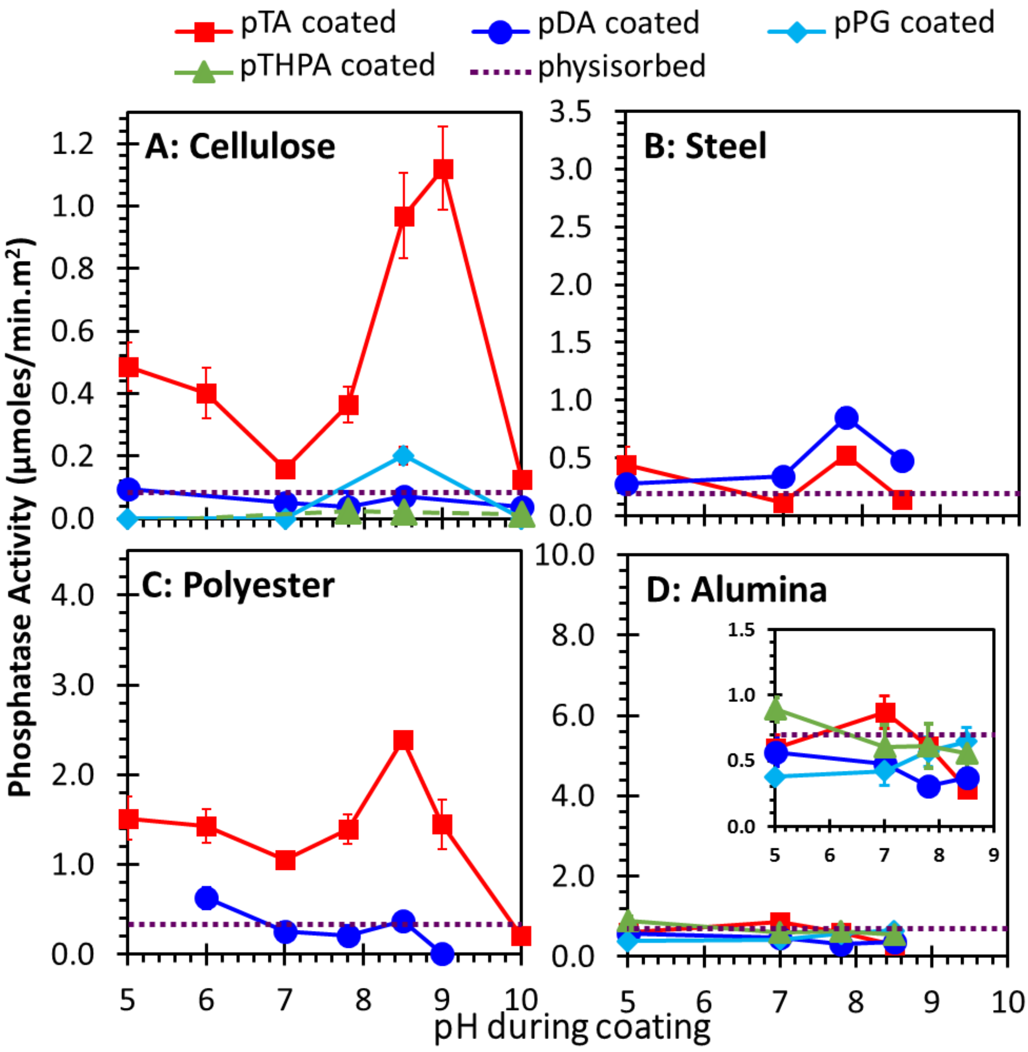

Figure 3.3 – Coating pH effect on phosphatase activity on uncoated and coated- (A) cellulose, (B) steel, (C) polyester and (D) alumina. The coatings used were: poly(tannic acid) (pTA), polydopamine (pDA), poly(pyrogallol) (pPG) and poly(3,4,5-trihydroxyphenethylamine) (pTHPA). The scales of the graphs were set to match side to side the physisorbed activities of the different materials.

The immobilised phosphatase activities were also generally higher on pTA than on pDA coatings (except for steel). In fact, very similar activities were generally observed for physisorbed and pDA immobilised phosphatase and clear optima in the coating pH were also not observed. There was an exception for pDA coated steel, on which a maximum improvement in activity at *ca.* 4 times higher than the physisorbed was observed at a coating pH = 7.8, which is lower than the pH previously reported as optimal for coating (pH 8.5).[38] On cellulose and polyester, although local maxima were observed at pH 8.5, even higher activities were actually observed as the coating pH decreased from pH 7 towards $pI_{phosphatase}$ = 5. Thus overall it appears that the pH optimum for coating formation does not necessarily produce coating surfaces that were more able to immobilise active proteins.

We also performed a smaller set of comparison with PG and THPA coatings on cellulose and alumina. The maximum activity on PG was observed at $pH_{coating}$ = 8.5 on cellulose, at only 2 times higher than the physisorption control. The immobilised phosphatase activities on PG-coated materials had the same trend as pTA-coated materials, but the activities were significantly lower, consistent with the initial results for tests using the broader panel of proteins shown in Figure 3.2. PG is a smaller molecule than pTA, there are fewer groups per molecule available to interact with the enzyme, lower amount of enzyme is immobilised resulting in lower activities. Phosphatase activities on THPA coatings were as low as on pDA coatings, suggesting that THPA behaves more like pDA than PG. The additional hydroxyl group in THPA structure (when compared to dopamine structure) did not improve the immobilisation and the amine group actually change the chemical character of the coatings.

In general, a higher activity in the measurements could be attributed to either a higher amount of enzymes immobilised and/or a lower amount of denatured proteins. Measurements of the amount of proteins immobilised on the present (nano)porous or fibrous solid supports are challenging because common surface measurement tools used for characterising proteins layers such as surface plasmon resonance spectroscopy and quartz microbalances are not directly applicable to thick, non-flat materials. Proteins have a relatively high nitrogen content because of their amino group side residues, therefore the protein content was qualitatively characterised by calculating the N1s/C1s ratio of XPS signals to highlight the changes on the surface after the immobilisation step. The protein and other layer thicknesses were also determined by XPS where a clear substrate signal is available (alumina and steel).

The N1s/C1s ratio of phosphatase layer on pTA and pDA layers on cellulose and alumina is shown in Figure 3.4A and B, respectively. The trends of the N1s/C1s are remarkably very similar to phosphatase activity trends (Figure 3.3) showing that the immobilised phosphatase activity is related to the amount of enzyme on the coating layers.

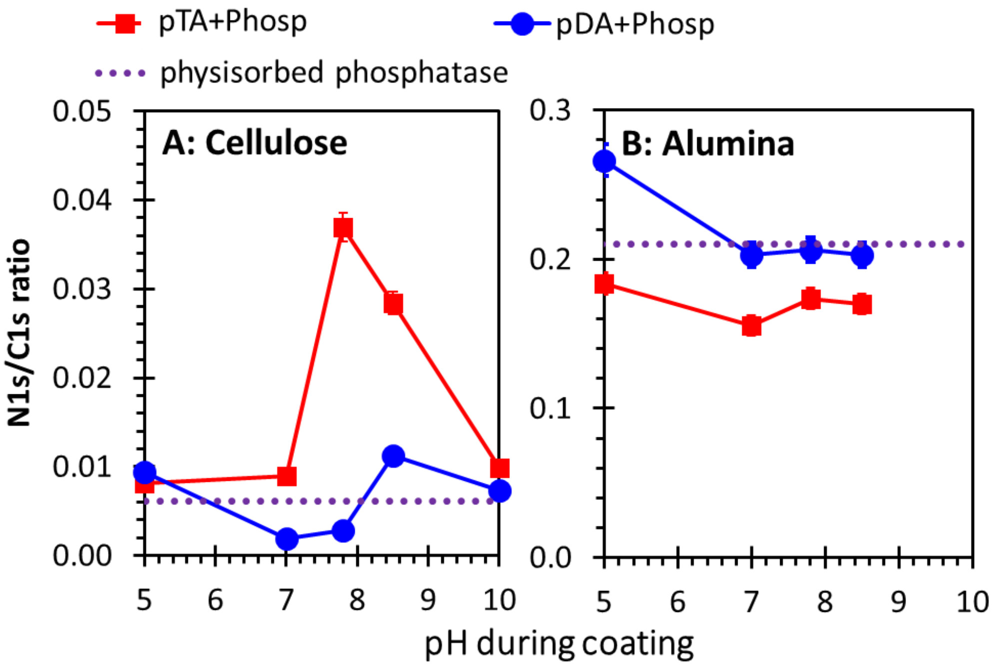

Figure 3.4 – Coating pH effect on the ratio N1s/C1s of phosphatase (Phosp) layer on poly(tannic acid) (pTA)-, polydopamine (pDA)-coated and uncoated (A) cellulose and (B) alumina.

On cellulose, the highest signal was obtained when phosphatase was immobilised on pTA coating at pH 7.8 (differently from the previous results at pH 8.5/9, Figure 3.3A). It is clear that the amount of enzyme decreases at pH 7 and 10, suggesting that the coating effectively works for phosphatase immobilisation between pH 7.8 and 9. The signal of phosphatase on pDA coating was not that different from the signal of the physisorbed enzyme on cellulose, which exactly matched with the immobilised activities (Figure 3.3A). It is worth to note that the signal of phosphatase on pDA coating was also not dissimilar when comparing the signal of pDA coating layer on cellulose (Figure I.8A). This suggests that the N1s signal obtained after immobilising phosphatase on pDA coating was from the pDA layer itself and only a little amount of enzyme was immobilised.

The reason for a low amount of proteins immobilised on pTA and pDA could be due to the interactions between the surface of the material, which may not fully covered with the coating and the enzyme. Higher amounts of enzyme can lead to higher activities (mainly on cellulose), but coatings prepared at different pH values can also be qualitatively different to modify the surface interaction.

There is no clear match between the activity and XPS signal on alumina. The amount of physisorbed and immobilised phosphatase on pTA and pDA coatings were very similar (Figure 3.4B). The N1s/C1s ratio was higher on pDA than on pTA coating, which is the opposite of the activities results shown before (Figure 3.3D). It can be concluded that, in this particular case, for alumina, the analysis of the N1s/C1s ratio is not suitable for comparison. After the immobilisation, the C1s signal was very high and increased, while the N1s also increased, but remained very low (Figure I.9). The C1s signal is much higher for pTA than for pDA coating so, even after the immobilisation, the C1s signal was much higher. Consequently, the N1s/C1s ratio for phosphatase on pTA coating does not correspond to the amount of the enzyme because there is a high influence of the previous layer (pTA coating). In the case of alumina, the estimated thickness values of phosphatase on pTA and pDA coatings are more applicable for evaluating the amount of immobilised enzyme that can be comparable to the activity results.

The thickness values of phosphatase on (un)coated alumina are shown in Figure I.10A. There was a thicker layer of phosphatase on pTA coating (around 2 nm) than on pDA coating (< 1 nm). There was an increase of thickness when increasing the pH, but an increase in phosphatase activities was not observed. For phosphatase on pTA coating, the activity had a maximum, but then it decreased with the increase of pH, which suggests that enzyme denaturation by pTA immobilisation occurred. We believe that enzyme denaturation by pDA immobilisation was not observed for two main reasons. The first was because the pDA coating was very little and the second was because pDA has less available groups to bind with the enzyme than pTA. TA has multiple groups where enzymes can be attached to and, as mentioned before, multiple attachments can lead to the denaturation of the enzymes.

The relatively low improvement of the coatings on alumina could be attributed to the fact that a relatively high level of physisorbed activity was observed, so little improvement over physical adsorption could be expected.[99] However, the use of pTA coating was observed to help maintain the activity after storage of the immobilised enzymes (see section 3.2.4).

Thickness results on coated steel are shown in Figure I.10B. The thickness values for the enzyme (< 2.5 nm) and coatings (1 nm) are much lower than on alumina (up to 7.3 and 5.5 nm for enzyme and coating, respectively) and that can be due to the fact that steel is a more challenging material to be functionalised.[99,128,129] Interestingly, higher amounts of phosphatase but lower activities were obtained on pTA than on pDA coatings, suggesting that pTA immobilisation again had an effect on the enzyme immobilisation. To minimise the denaturation by pTA immobilisation, it would be interesting to control the thickness of pTA coating in order to have just enough to coat the material that is suitable to immobilise enzymes without denaturation.

We also calculated the C1s/O1s ratio to qualitatively characterise the pTA and pDA coatings on cellulose (Figure 3.5A) before the immobilisation step. This ratio was chosen because cellulose has more oxygen in its structure than pTA and pDA coatings. When the surface is coated with pTA and pDA, the content of carbon increases and oxygen decreases, so the C1s/O1s increases when the coatings are on the surface of cellulose. There was a slight increase of the C1s/O1s for pTA, which suggests that the coating was on the surface. Bigger changes were expected, so not all the surface of cellulose was fully covered and/or only a thin layer of coating was present. The ratio for pDA coating was not significantly different from the cellulose reference, meaning that there was no coating present. These results confirm that the poor signal obtained for phosphatase layer on pTA and pDA coatings (Figure 3.4A) was because of the low amount of pTA/pDA molecules on the surface of cellulose.

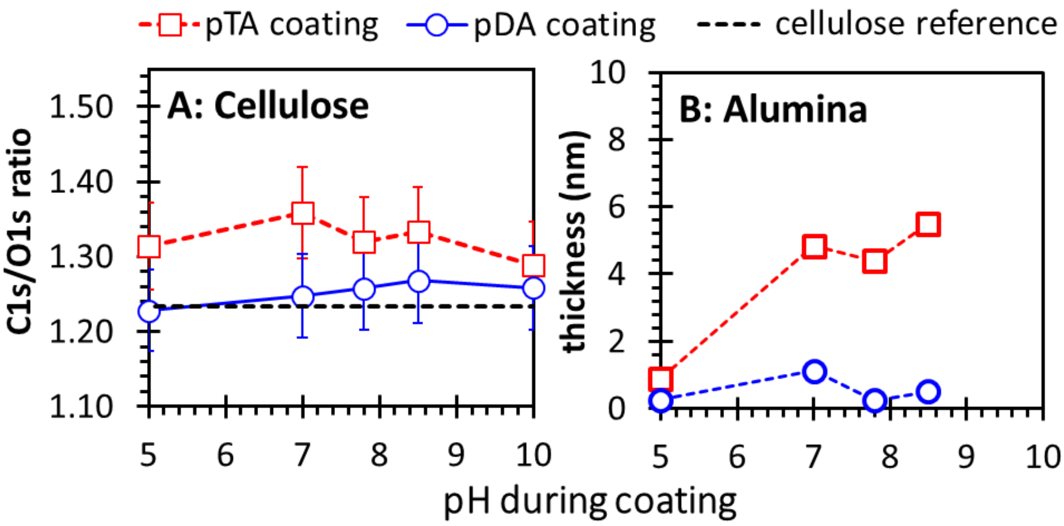

Figure 3.5 – Coating pH effect on poly(tannic acid) (pTA) and polydopamine (pDA) coatings. (A) C1s/O1s ratio of the coatings and cellulose reference. (B) Thickness values of pTA and pDA coatings on alumina.

The thickness of pTA and pDA layers on the alumina was determined (Figure 3.5B). The pTA coating was very thin at pH 5 (< 1 nm) but increased up to 6 nm between pH 7 and 8.5. There was a pH effect for the coating, probably due to electrostatic interactions between the alumina surface (pI 9) and TA (pKa 7.7).[134,135] With pH increase, there are more deprotonated species of TA, so the interaction between TA and alumina can be stronger. This trend did not match with the amount of immobilised enzyme (Figure 3.4B), but it was close to the results on immobilised enzyme activities, which again confirms the denaturation of the enzyme on pTA coating. In the case of pDA coating, there was no increase or change with pH, and only a thin coating was present (less than 2 nm). Overall, both pDA and pTA coatings work even though thicker coating layer was obtained for pTA but physisorption has a major effect on enzyme immobilisation.

For both cellulose and alumina, the pTA coating did not have any maximum corresponding to the maxima observed for phosphatase activity, meaning that the quality in addition to the thickness of coating influences the amounts of the immobilised enzymes. The electrostatic interactions between the coating, the surface of the material and the enzyme are other factors that affect the immobilisation process.

Overall, the amount of immobilised enzyme is an underlying factor for obtaining higher activities. The maxima activities were achieved when the enzyme was immobilised on pTA-coated materials at pH 7 for alumina, pH 7.8 for steel and pH 8.5 for polymeric surfaces (cellulose and polyester). Another parameter that can also influence the amount and activity of immobilised phosphatase is the pH during the immobilisation procedure.

3.2.3 pH effect during the immobilisation

In the previous section, it was observed that the pH influenced both quantity and quality of the coating, but that was not the only factor that contributed to higher or lower immobilised phosphatase activities. In this part of the study, the coating pH was fixed at pH 7.8 while the pH during phosphatase immobilisation was varied between 3.8 and 8. pTA and pDA were able to coat cellulose and alumina at 7.8 (Figure I.1 and Figure I.2). Besides the fact that higher activities were not always achieved at pH 7.8 for both coatings, for consistency, pH 7.8 covers the best condition for both pTA and pDA coatings for both cellulose and alumina.

Phosphatase conformation and its interactions with the surface will be different when varying the pH. At pH 5 (phosphatase pI), the enzyme has a neutral surface charge, so it is important to study the immobilisation process around this pH. The low enzyme activity can be due to the low amount of immobilised enzyme thanks to electrostatic interactions. However, it can also be due to the enzyme unfolding at certain pH values, losing the activity but remaining immobilised on the surface. In this case, large amounts of enzyme can actually be present but if the immobilised enzyme is denatured results in low enzyme activities. For these reasons, in this section, it is even more important to compare the activity with the N1s/C1s ratio results. We only focused on cellulose and alumina because they were the polymeric and oxide materials that showed more interesting results in the previous section.

The effect of pH during the immobilisation step on phosphatase activity on uncoated- and coated-cellulose and alumina is shown in Figure 3.6A and B, respectively. The ratios N1s/C1s of immobilised phosphatase layer on these two materials is shown in Figure 3.6C and D. The ratio N1s/C1s represents the amount of immobilised enzyme on the surface of the materials. The references for coatings on cellulose and alumina are also represented in the graphs.

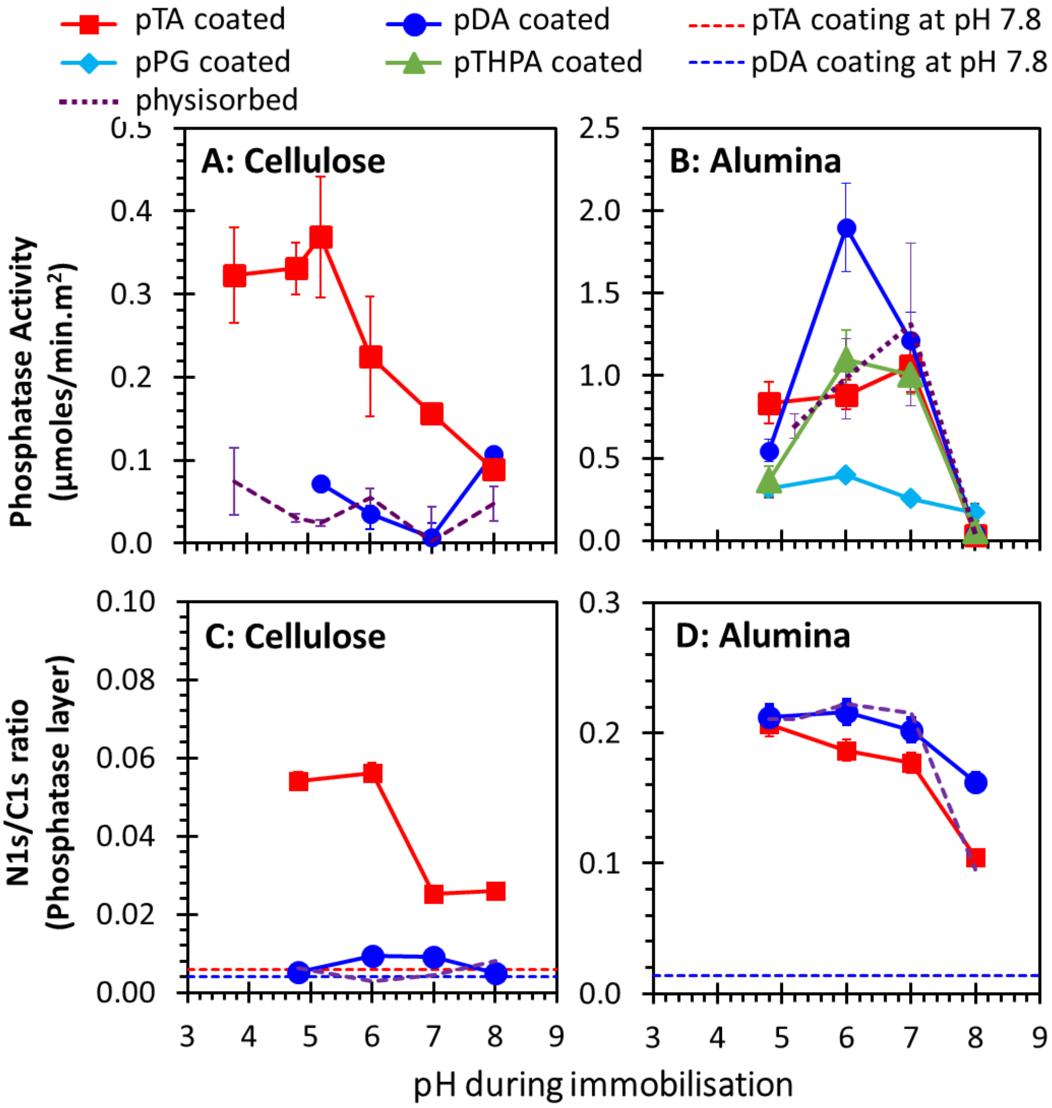

Figure 3.6 – Immobilisation pH effect on phosphatase activity on uncoated and poly(tannic acid) (pTA), poly(pyrogallol) (PG), poly(3,4,5-trihydroxyphenethylamine) (pTHPA) and polydopamine (pDA) coated- (A) cellulose and (B) alumina. Ratio N1s/C1s of the coatings and phosphatase layers on uncoated and coated- (C) cellulose and (D) alumina.

When phosphatase was immobilised on pTA-coated cellulose, higher activities were observed between pH 3.8 and 5, but then the activity decreased with the pH increase (Figure 3.6A). This trend was also observed on N1s/C1s (Figure 3.6C), suggesting, in this case, that phosphatase activity on pTA-coated cellulose is related to the amount of immobilised enzyme. From the previous results (Figure 3.3A), it is now known that pTA coating works better than pDA on cellulose. It is possible that the immobilisation pH can be used to improve the immobilisation on pDA coatings (changing immobilisation pH could increase the activity). However, this was not the case: once again, lower activities were observed for phosphatase on pDA and uncoated-cellulose at all the tested pHs. These results were in agreement with the N1s/C1s that showed very low or no presence of phosphatase on pDA and uncoated cellulose surfaces (Figure 3.6C).

The immobilised phosphatase activity trend on coated and uncoated alumina is slightly different. There is a maximum in activity for each condition: pH 6 for pDA and THPA coatings; pH 7 for pTA coating and physisorbed. The variation of pH during the immobilisation enhanced the activity of the enzyme to a higher extent on pDA and THPA coatings than pTA coatings, proving that the $pH_{immobilisation}$ is another parameter to take into account on immobilisation improvement on alumina.

The activity falls to a low level for all the coatings and physisorption at pH 4.8 and 8, but the effect was more accentuated at pH 8. At pH 4.8, this result is intriguing because both N1/C1s ratio (Figure 3.6D) and thickness (Figure I.11) results show the presence of the enzyme on the surface. In this case, the lower enzyme activity can only be due to the immobilisation procedure that reduces the activity of a large amount of enzymes. At pH 8, both N1/C1s signal and thickness decrease, which means that the reduced activity at pH 8 is due to the low amount of enzyme present at the surface. This can be due to the electrostatic repulsions between the negatively charged enzyme and the coatings/alumina surface, that are also negatively charged. However, when the same study was performed with chymotrypsin enzyme (pI = 8) and the activity also dropped at pH 8 (Figure I.12), which suggests that the pI is not the only factor that influences the immobilisation.

These experiments show that the pH, the chemical structure of the coating and the material are all very important and have an influence on the activity and amount of immobilised enzyme. With this study, we now should be able to optimise both coating and immobilisation pH separately on different materials in order to obtain the highest activities. From this section, we can affirm that the immobilisation of phosphatase should be performed around pH 5 for pTA-coated cellulose and between pH 6 and 7 for uncoated- and coated-alumina.

3.2.4 Storage and reuse of immobilised phosphatase

Phosphatase was immobilised on pTA, pDA and uncoated-alumina and the immobilised enzyme activities were measured (as previously shown). The samples were rinsed with deionised water, and the activity was measured again after 1h, 2h, 24h, one week and one month of sample preparation. Between the measurements (except for the first three uses up to 2h, as they were consecutive measurements), the samples were stored at 4 °C. The activity measured on the first use was normalised to 100 %. The reference activities are shown in Table I.2 and in the caption of Figure 3.7.

Immobilised phosphatase samples were reused several times and stored for one month in order to assess if the immobilised enzyme samples were able to be reused and stored. This part of the study was important to verify if the TA and pDA coatings could help on the stability of the immobilised enzyme. This would be attractive for different purposes by preventing enzyme leaching, after which the enzyme's use is unfeasible due to a complete loss of the enzyme to the solution.

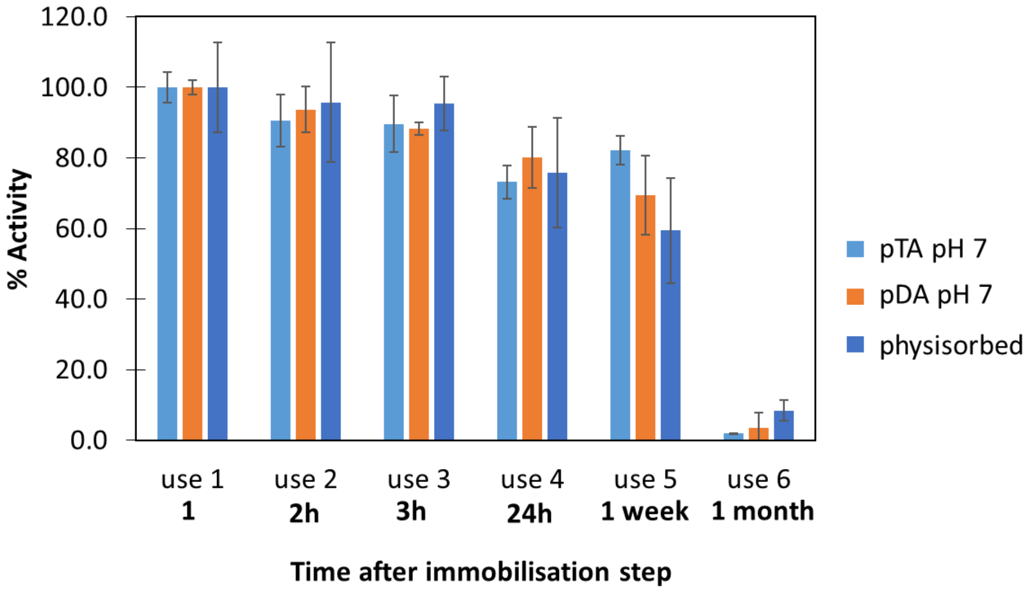

Figure 3.7 – Physisorbed and immobilised phosphatase activity after several uses and stored for one month. 100 % activity is equivalent to the activity measured in the first use of 30, 22 and 27 nmoles/min.m^2, for phosphatase on poly(tannic acid) (pTA)-, polydopamine (pDA)-coated and uncoated alumina. Reference values are also stated in Table I.2 (Appendix A).

After one-week storage and 5 usages, phosphatase retained its activity between 60 and 82 % (Figure 3.7). The activity seemed to decrease with the number of uses during the first week, however the activity drastically drops below 8 % after one-month storage, suggesting that the activity of the immobilised enzyme is related to both the number of uses and the storage time or conditions. The gradual reduced activity could happen because of the enzyme inactivation or leaching during the enzyme assay or rinsing process. For the long-term storage (1 month), the activity of the enzyme is reduced. Salt, glycerol addition or storage of the samples in the freezer at -80 °C are other alternatives to improve the storage conditions.

Overall, the physisorbed phosphatase activity varied more over time than the phosphatase activity immobilised on pTA coating, which is also observed from the error bars. This shows that the polyphenol coating can help to maintain the activity and/or prevent enzyme leaching. The pTA coating might improve the stability of the alumina surface and the enzymes can be more strongly attached to the surface over time, delaying the denaturation and leaching events to occur.

3.3 Conclusions

We presented results on exploiting plant-based polyphenol coatings on different materials such as alumina, cellulose, stainless steel and polyester. These coated materials were used for the immobilisation of different enzymes – phosphatase, chymotrypsin, HRP, LDH. Different conditions for both coating and immobilisation such as pH and precursor were tested. It was found that polyphenol coatings were able to immobilise a wide range of proteins from antibodies to enzymes, and they were more effective than both pDA coatings and physisorption in many situations. On cellulose, HRP activity was 8.5 times higher when immobilised on pTA coating than on pDA coating. The other enzyme activities were 4 times higher on pTA coatings than physisorbed and pDA coatings. Immobilisation by pPG coating did not improve activities so much as pTA coating although the activities were still 2 to 4 times higher than physisorbed, except for LDH. On steel, pTA and pPG improved activity up to 2.5 times for phosphatase and chymotrypsin immobilisations when compared to the control (physisorbed). It was also possible to immobilise proteins that are commonly used in biosensing – IgG and avidin. Once again, pTA coating showed more improvement in the activities of the immobilised proteins. Nevertheless, these immobilisations can be improved if further optimisation.

The pH during coating and immobilisation were found to be key parameters influencing enzyme activity. The effectiveness of the immobilisation also depended on the material support, the coating and the pH during the coating and immobilisation procedures. Higher activities were shown when polymeric and oxide surfaces were coated around pH 7.8 and at pH 7, respectively. For the immobilisation procedure, maxima were reached when phosphatase was immobilised at pH 7, 7.8 and 8.5 on coated alumina, steel and polymeric surfaces, respectively. The pTA coating also showed improvement on the reuse and storage of immobilised phosphatase, retaining 82 % of the activity during the first week of storage.

In summary, we demonstrated that polyphenol coatings can provide unique advantages ranging from their plant-based availability and optical transparency to their extended range of preparation pH and enhanced effectiveness on specific materials. With this work, we proved that the concept of “universal coating” for enzyme immobilisation is difficult to succeed, even though a lot of progress in this field was achieved.

3.4 Materials and Methods

3.4.1 Materials

Tannic Acid (TA), pyrogallol (PG), 3,4,5-trihydroxyphenethylamine (THPA), dopamine hydrochloride, acid phosphatase from potato (Phosp), chymotrypsin from bovine pancreas, lactate dehydrogenase (LDH), horseradish peroxidase (HRP), immunoglobulin G (IgG) from human, anti-human IgG–peroxidase antibody produced in goat (IgG-HRP), avidin from egg white, bovine serum albumin (BSA) and biotinylated peroxidase (biotin-HRP) were purchased from Sigma-Aldrich (UK). The enzyme substrates such as 4-methylumbelliferyl phosphate disodium salt (4-MUP), N-benzoyl-L-tyrosine ethyl ester (BTEE), sodium pyruvate, β-nicotinamide adenine dinucleotide (NADH), 2,2′-azino-bis(3-ethylbenzothiazoline-6-sulfonic acid) diammonium salt (ABTS) and hydrogen peroxide (H_2O_2) were purchased from Sigma-Aldrich (UK). 4-nitrophenyl phosphate disodium salt hexahydrate (pNPP) was purchased from AlfaAesar (UK). All buffers and sodium chloride (NaCl) were purchased from VWR (UK). Anodisc, alumina nanoporous membranes (Whatman, 0.2 µm), regenerated cellulose membranes (RC55, 0.45 µm) were purchase from Sigma (UK), polyester (100 % Polyester Microfibre) from Amazon (UK), stainless steel (SS316 Grade - TWILL - Woven Wire Mesh, 0.026 mm aperture, 0.025 mm wire diameter) from The Mesh Company (Warrington, UK) and silica nanoparticles (Davisil silica gel grade, 100-300 µm, 450 nm pore size) from Grace (Belgium).

3.4.2 Coating procedure

The precursors (TA, pDA, PG or THPA) were dissolved (0.03 mg/mL) in a buffer (with 0.6 M NaCl) at certain pH (the solution was prepared within 30 seconds). The pH coating varied from 3 to 10, so different buffers were used: pH 5 0.1 M acetate, pH 6-7 0.1 M BisTris, pH 7.8-9 0.1 M Bicine, pH 10 0.1 M CAPSO. The materials were immersed in the coating solution and stirred for 1h. After the coating, the samples were rinsed three times with deionised water (DIW), sonicated in the coating buffer without precursors for 15 min and rinsed again with DIW in order to remove unreacted/physisorbed precursors. When the pH during the immobilisation step was varied, the coating was performed at pH 7.8.

3.4.3 Enzyme immobilisation

A 1 mg/mL solution of acid phosphatase in immobilisation buffer (with 0.1 M NaCl) was prepared on the day before the immobilisation and stored at room temperature. The pH for the immobilisation step was varied between 4.8 and 8, so different buffers were used: pH 4.8-5.2 0.1 M acetate, pH 6 and 7 0.1 M BisTris and pH 8 0.1M Bicine. Before the immobilisation, the solution was filtered with a 0.2 µm PES filter and diluted to 0.1 mg/mL with the immobilisation buffer. When the pH during the coating was varied, the immobilisation was performed at pH 5.2. For other enzyme immobilisations, the solutions were prepared in the same day at 0.3 mg/mL for chymotrypsin and 0.03 mg/mL for LDH and HRP at pH 7. Uncoated and coated samples were immersed in the enzyme solutions for 1h. The samples were rinsed three times with DIW, sonicated in immobilisation buffer without the enzyme and rinsed again with DIW in order to remove unreacted enzyme. For IgG+IgG-HRP and Avidin+Biotin-HRP systems, the immobilisation steps were performed in the same way using phosphate buffered saline (PBS) at pH 7.4. For IgG+anti-IgG-HRP system, a BSA layer was added before the enzyme immobilisation (anti-IgG-HRP) step.

3.4.4 Immobilised enzyme assay by UV-Vis spectrophotometer

The solid materials were held by a holder that was inserted into the cuvette to keep the samples on the side of the cuvettes and away from the path length. A magnetic stir bar was added to the cuvette to promote the diffusion of the substrate/product into/from the support (see Figure I.6, Appendix A). Phosphatase: 2 mL of pNPP substrate (15 mM in 1 M sodium acetate buffer pH 5) was added to the cuvette. After 10 min, the absorbance at 405 nm was measured every 5 min for 40 minutes (UV-Vis spectrophotometer, V-660, Jasco, Essex, UK). Chymotrypsin: 1.4 mL of 1 mM BTEE and 1.5 mL of 80 mM Tris-HCl, 0.1 M $CaCl_2$ buffer at pH 8.5, absorbance measured at 256 nm every minute for 10 min. LDH: 1.87 mL of 0.13 mM NADH, 70 µL of 34 mM pyruvate and 70 µL of 0.1 M sodium phosphate buffer pH 7.5, absorbance measured at 340 nm every 5 minutes for 40 min. HRP: 1.93 mL 9.1 mM ABTS, 70 µL of 0.3 % w/w H_2O_2 and 35 µL of 0.1 M potassium phosphate buffer pH 5, absorbance measured at 405 nm every 2 minutes for 20 min. Control samples were coated or uncoated materials without immobilised enzyme. All the enzymatic reactions were monitored by measuring the absorbance of the enzyme product (at the specific wavelength as stated above). The enzyme assays were all optimised (substrate concentration, size of sample, duration and frequency of the measurement) so that the measurements were only performed during the linear initial rate of the enzymatic reaction. By Beer-Lambert law, the absorbance of the product was converted to concentration (using the molar absorptivity of the converted product) and the activity of the immobilised enzyme was then calculated dividing the concentration of converted product by the time of the reaction (moles/min). To assure the correct sample size, after the enzymatic assay, the samples were placed on a flat surface next to a ruler and a photo was taken. The area of each sample was measured using ImageJ software. The immobilised enzyme activity of each sample was divided by the sample area as well as the surface area of the correspondent material (moles/min.m^2). The activities of the immobilised enzyme were corrected by subtracting the activity of the control (no enzyme).

3.4.5 Immobilised enzyme storage

The samples were measured 3 times on the same day and then they were left in air at 4 °C. After one day, one week and one month of the immobilisation, the samples were measured again. The activity was normalised to 100 % for the first use of the samples.

3.4.6 Surface area measurement

The surface area of the different uncoated materials was measured by nitrogen adsorption using Brunauer–Emmett–Teller (BET) isotherm, micromeritics ASAP 2020.

3.4.7 Surface characterisation

Field-Emission Scanning Electron Microscope (FE-SEM) was used to characterise the morphology of the different materials. The FE-SEM images were obtained using a Hitachi SU-6600 operated at an accelerating voltage of 5.0 or 20.0 kV and an extraction voltage of 2-1.80 kV. Microscope optical images were obtained using a black and white Photometric Coolsnap HQ camera, 10x magnification objective (Photometrics, Tucson, USA). Alumina and regenerated cellulose samples were also analysed by X-ray photoelectron spectroscopy (XPS), VersaProbe II from Physical Electronics. All the measurements were done with Al Kα X-rays, 45 degree measuring angle, under low energy electron and Ar$^+$ surface charge neutralisation, with 23.5 eV pass energy for individual peaks and 117.4 eV for survey spectrum. The presence of polyphenol coating was also revealed by immersing the samples in a 20 mM silver nitrate solution for 1h. This process resulted in the deposition of a dark metallic silver film on the surface, through a redox reaction between silver ions and the polyphenolic coating. 285.0 eV for binding energy of the main C1s (CHx) was used to correct of charging of speciement under irradiator. Attenuation of the underlying substrate signal and the C1s/O1s ratio were used as an indicator for the presence of coating. The N1s/C1s ratio was used as indicator for enzyme layer.

The size of the samples used in each cuvette for the activity measurements is described in Table 3.1. The surface area of the samples is stated in Table 3.2. The surface areas were used to normalise the activity measurements as described in section 3.4.4.

Table 3.1 – Size of sample in each cuvette for the activity measurements.

Material/ Enzyme	Phosphatase	Chymotrypsin	LDH	HRP	IgG+anti IgG-HRP	Avidin+biotin -HRP
Cellulose	2x2 cm	1x2 cm	1x2 cm	1x1 cm	1x1 cm	1x2 cm
Stainless steel	2x8 cm	2x4 cm	2x4 cm	2x2 cm	1x1 cm	2x2 cm
Alumina	1x2 cm	1x1 cm	-	-	-	-
Polyester	2x8 cm	-	-	-	-	-
Silica	40 mg (~90 mg wet)	-	-	-	-	-

Table 3.2 – Surface area of the different materials used for enzyme immobilisation. ^{a}BET and ^{b}microscope measurements.

Material	Surface Area (m^2/cm^2 of sample)	Langmuir surface area (m^2/g)
Cellulose	0.0107	2.96^a
Stainless steel	0.002	0.26^b
Alumina	0.035	4.73^a
Polyester	0.0015	0.26^b
Silica	-	10.30^a

4. Nanoporous alumina as optical waveguides for characterising molecular diffusion in nanopores

4.1 Introduction

Biological cells have many different types of pores and channels that enable the highly specific and efficient separation, sequestration, and release of diverse biomolecules for the regulation of life processes. Some examples, ranging in pore diameter from a few angstroms to tens of nanometres, include ion channels, pores inserted into the cell membrane and organelles and the nuclear pore complex (NPC).[136]

The NPC is a ring-like protein assembly forming a central channel ~40 nm that separates out, over the millisecond time-scale, specific proteins and polynucleotides for transport between the cell nucleus and the cytosol, and rejects non-specific biomacromolecular passage.[137,138] NPC only transports molecules that have attached their protein carriers (PC) and do not allow the passage of small molecules even though they could fit in the pores (no size constraint). NPC also resists clogging although large amounts of proteins cross the pores.

Inspired by all these advantages, researchers have been developing nanoporous systems to mimic biological nanopores and as a tool for sensing, detecting, characterising and monitoring molecular transport.[139,140] Solid substrates, such as silicon nitride, aluminium oxide, titania and graphene have been explored for fabricating synthetic nanopores for different applications (*e.g.*, nanopore analytics) due to their well-defined geometries and dimensions, mechanical robustness, ease of modifications, and compatibility with various optical measurement techniques.[136,141,142] The pore size can be controlled from sub-nanometers to hundreds of nanometers, but there is a need to functionalise the pores in order to achieve highly selective transport and chemical specificity.[143] For example, functional polymers are used on commercially separation filters to separate molecules based on size, charge, or hydrophobicity.[144] However, these membranes easily clog after the passage of high number or large molecules and cannot be used again.

Many approaches have been investigated for mimicking some of the NPC's functions.[145–148] For example, poly(N-isopropylacrylamide) (PNIPAM) functionalised nanoporous membrane filters have been tried to mimic the receptor-mediated transport of the NPC. The translocation of a single-stranded DNA (ssDNA) attached to pNIPAM was faster than the smaller ssDNA alone.[145] Building blocks of proteins of the NPC (phenylalanine-glycine (FG)-nucleoporins) as well as poly(ethyethylene glycol) (PEG) (as a control) have been immobilised on polycarbonate membranes. The fluxes of a bovine serum albumin (BSA) and a PC through these pores were measured using confocal microscopy. For both molecules, the flux was identical when the pores were functionalised with PEG but the flux of BSA was significantly lower through the membranes coated with FG-nucleoporins.[147] This work demonstrated that the combination of the coated nanopores and protein regulates selectively the transport of molecules. However, neither study investigated the relationship between the polymer architecture within the grafted FG-nucleoporin structure and protein transport. Other attempts for mimicking the NPC was by preparing bulk hydrogels with sequences of FG-nucleoporins but the selective transport through the pore-like in the NPC was not studied.[146,149]

Although direct replication of the NPC nanostructure appears beyond current scientific capabilities, to mimic this system it is also necessary to have techniques that are able to characterise the pores, their functionalisation and the molecular transport.

The recent developments in this field are based on measuring changes of current during the transport of different molecules through pores or porous membranes.[139,141,150–152] In addition, spectroscopic and microscopic techniques such as UV-Vis, pulsed field gradient NMR, confocal, interference and infrared microscopy can also measure molecular diffusion through and/or inside long nanopores channels (*e.g.*, depth larger than their pore size) or nanoporous membranes.[100,152–155] Kumeria *et al.* developed smart membranes for on-demand molecular transport by attaching light-sensitive peptides on nanoporous anodic aluminium oxide (AAO) membranes. They characterised the molecular transport of a dye through a membrane but the diffusion inside the pores was not described.[155] Hohlbein *et al.* assessed the movement of fluorescent molecules also through AAO by fluorescence correlation spectroscopy (FCS). This technique presents a disadvantage as the light focus is too wide comparing with the pore size, limiting the spatial resolution of the diffusion measured at different pore depths to several microns.[154]

Optical waveguide spectroscopy (OWS) associated with planar optical waveguides of nanoporous AAO membranes have been used to characterise the deposition of molecules within pores. These have a large internal surface sensitive to external stimuli and to the precise conditions necessary for guiding light.[156,157] Consequently, nanoporous OWS has a highly enhanced sensitivity compared to conventional surface techniques such as surface plasmon resonance (SPR) spectroscopy and the quartz crystal microbalance

(QCM). The relatively low cost of OWS and simple home-built experimental setup over conventional analytical tools (*e.g.*, microscopic and scattering methods) are other advantages of this technique.[158]

In nanoporous OWS, the ability of molecules to diffuse inside the pores can be inferred from the results based on refractive index change from adding a molecular layer on the pore walls. On the other hand, OWS can control the distribution of light at different depths of the waveguide film. In fact, processes that occur inside and outside of the pores can be distinguished and monitored *in situ*.

Researchers have been combined OWS with other techniques such as fluorescence microscopy and surface-enhanced Raman scattering (SERS).[159–161] These studies explored the high sensitivity of OWS achieved from the high surface area for sensing and the ability of controlling the distribution of light. Gu *et al*. used optical waveguides to concentrate and confine the light, and silver nanoparticles to enhance the signal of SERS measurements. The waveguide improved the SERS signal by at least two orders of magnitude according to the simulation and experimental results.[160] Fan *et al.* used fluorescent-labelled protein for real-time detection of DNA hybridisation and to study protein adsorption behaviour.[159,161] Lau *et al.* have employed a reductionist approach utilising synthetic AAO membranes with a pore size of 30 nm. The AAO membranes were functionalised with various soft matter structures,[162] investigating key parameters related to the deposition of polymers and proteins into nanopores.[23] With this work, it was possible to monitor BSA adsorption and desorption processes with subangstrom sensitivity[156] as well as measure thickness of the films deposited on pore surfaces.[31,163]

In this chapter, we demonstrate the use of OWS for the development of nanopores that control the transport of biomolecules. This technique brings a new concept of measuring molecular diffusion through nanopores, where the diffusion of fluorescent-labelled molecules is characterised by controlling the distribution of light at different depths of the pore as well as above the nanoporous waveguide (bulk). AAO waveguides with pore sizes matching the lumen of the NPC found on the nuclear envelope (30-50 nm) were fabricated and functionalised with poly(ethylene glycol) (PEG) to decrease the non-specific binding of proteins. The diffusion of molecules of different sizes and net charges was characterised. Pores were also constricted (closed) by addition of a cross-linked organic matrix (poly(tannic acid)) in order to compare the diffusion of the molecules inside the pores (open pores) to the diffusion only on the surface of the AAO film.

4.2 Results and Discussion

4.2.1 Nanoporous optical waveguiding and data analysis

The combination of OWS, nanoporous materials and attenuated total reflection (ATR) setup is reported extensively in the literature.[157,164] In this chapter, we used OWS as a technique, so a brief explanation will be given to highlight only the main features that are important for the design and analysis of our experiments.

Optical waveguide is a material that is able to guide the light. This material can be planar, strip or fibre, be made of glass, polymer or semiconductor and be solid or nanoporous. The planar (or also called slab) waveguide consists of three layers of materials with different refractive indexes. If the middle layer (waveguide) has a higher refractive index than the surrounding layers, the light can be confined in the middle layer by total internal reflection (TIR).[157,165] For TIR to occur the light needs to pass from a dense medium (higher refractive index, n_1) to a less dense medium (lower refractive index, n_2) ($n_1 > n_2$) at an angle larger than a critical angle with respect to the normal to the surface and the light is reflected. By Snell’s law, this critical angle (θ_{TIR}) is when the refraction angle is 90° with respect to the normal. At angles higher than this critical angle ($\theta > \theta_{TIR}$), the light is reflected back to the denser medium. In fact, when TIR occurs, even though the light is reflected back to the medium, there is some light penetration into the second medium at the boundary interface – evanescent wave. This penetration can be used to confine the light between these two media.

Nanoporous materials can be used as waveguides if their refractive indexes are high enough for waveguiding and if the pores are smaller than the wavelength of the propagating light, so that scattering is minimised. For planar nanoporous waveguides, the light propagates through the nanoporous layer normal to the length of the pore and not from the bottom to the top the pores.

In our system, a nanoporous planar waveguide (AAO) was mounted on the top of a semi-transparent metal layer (gold) that was on a glass surface (so the pores of the waveguide were closed at the bottom). The refractive index of the AAO film is much higher than the gold layer and the air/aqueous media, so at certain angles higher than the TIR, the light can be coupled into the nanoporous AAO waveguide layer. A prism was used to couple light both in and out of the waveguide in order to be able to detect the reflectance (intensity of reflected light). At these certain angles when the light is confined ("zigzags") inside the nanoporous waveguide layer, the light is not reflected out of the waveguide, so the reflectance reaches a minimum – waveguide mode. To identify the angles (position) of the modes, an angle scan was recorded where the incident light was varied. In Figure 4.1 is shown that reflectance reached a minimum at 52.25°, 59.40°, 65.60°, 70.65° and 74.19°, labelled as 5th, 4th, 3rd, 2nd and 1st modes, respectively.

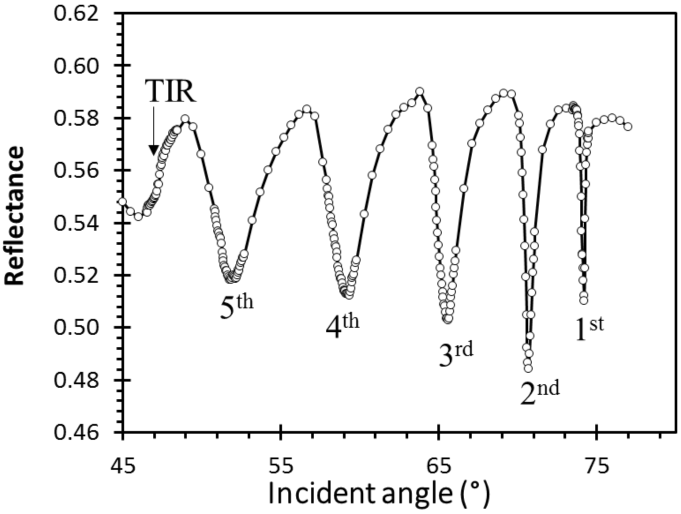

Figure 4.1 – Example of an angle scan of a nanoporous anodic aluminium oxide (AAO) waveguide (30 nm pore size, 1.6 μm thick). At certain angles (higher angles than TIR) the light is channelled (modes – 1st to 5th).

At these angles, the light is confined at specific regions of the nanopores due to their different electric-field distribution. To obtain these distributions and observe how the light is confined at different pore depths and leaked above the nanoporous layer, the angle scan data needs to be introduced into software that can simulate the electric-field distribution. Many pieces of software have been developed to visualise and fit the angle scans for similar systems (*e.g.*, commercial SPR and ellipsometer systems). The software that we used is called Winspall developed at the Max Plank Institute for Polymer

Research, Germany.[166] The illustration of the electric-field intensity distribution of the different modes of our system after Winspall simulation is represented in Figure 4.2.

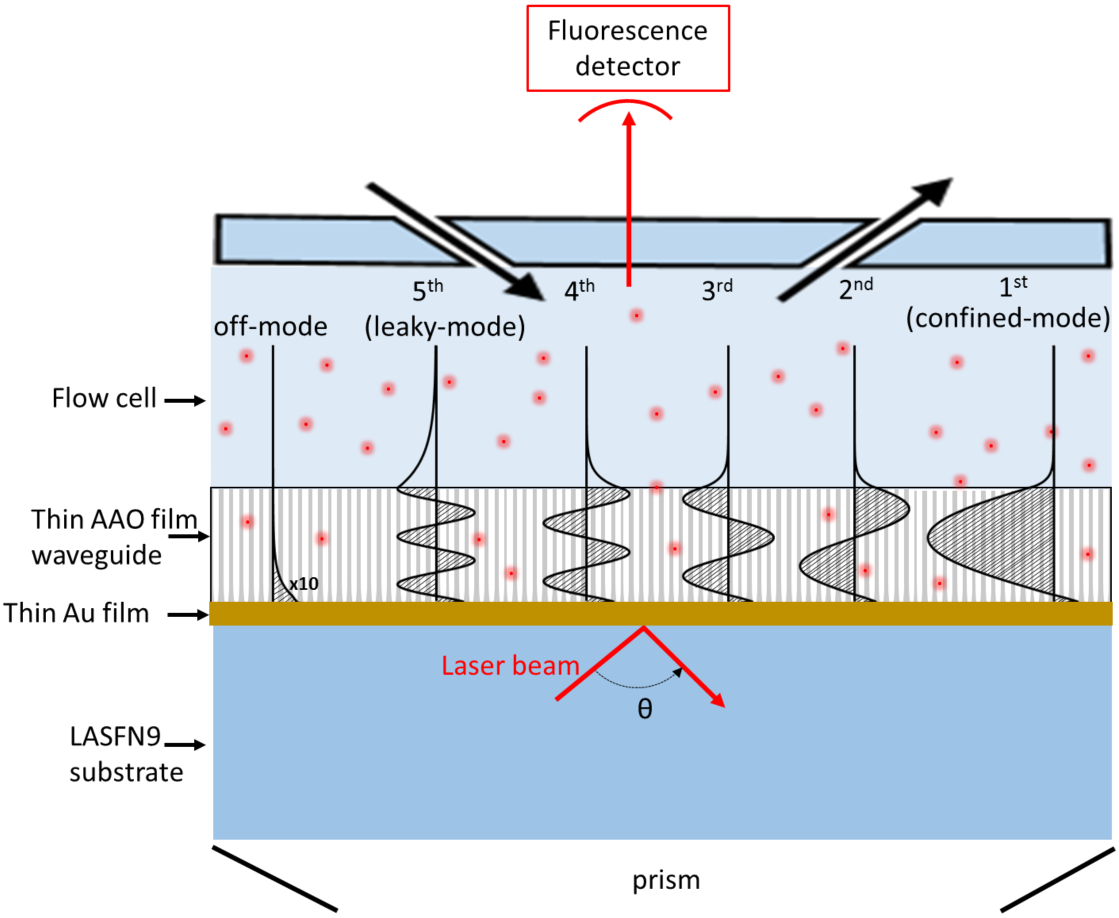

Figure 4.2 – Optical waveguide spectroscopy setup with the simulated electric-field intensity distribution at different modes (from Winspall simulation).[166] The fluorescence molecules (red dots) flow into the flow cell and inside of the nanopores, and the fluorescence detector records the intensity of the fluorescence (not to scale). 30 nm pore size and 1.6 µm thick waveguide.

The 1st mode is represented on the rightmost end of the Figure 4.2 and the 5th mode is represented on the left, right after the off-mode. The electric-field intensity distribution at 1st mode has a maximum in the middle of the nanopores and decays towards the flow cell and the glass surface. The electric-field has zero amplitude once very close to the gold surface. This zero amplitude in the electric-field is called a "node". This mode only has one node, so it can be called "1st mode". However, it is worth noting that the distribution of the electric-field is mostly confined in the middle of the pores so, for that reason, we also call this mode "confined-mode".

The last mode (5^{th} mode) (second electric-field distribution on the left of Figure 4.2) has a sinusoidal shape from the bottom to the top of the pores and has a large decay into the flow cell. It is possible to find five nodes in this mode, *i.e.*, five times when the electric-field distribution amplitude is zero (inside the nanopores). Therefore, it is called "5^{th} mode". This particular mode leaks a significant amount of light to the flow cell (above the nanoporous layer) so we call it "leaky-mode".

It is important to mention that the light at 1^{st} and 2^{nd} modes is only concentrated in the middle of the pores whereas at 4^{th} and 5^{th} modes the electric field is more evenly distributed throughout the pores and including around the pore entrances (above the nanoporous layer). As we go from the confined- to the leaky- modes, there is an increment in the electric-field distribution leak above the nanoporous layer.

When the incident light is not at the modes, the light is total internally reflected and, as explained above, there is an evanescence wave at the boundary interface. When this occurs, we are "off-mode" and the light "illuminates" only the bottom of the pores (200 nm of the pore bottom) (see electric-distribution at off-mode in Figure 4.2). For consistency of experiments at off-mode, we decided to perform the measurements at 5 degrees higher than the 1^{st} mode to make sure that the light was confined only at the bottom of the pore.

Fluorescence can be combined with OWS so that it is possible to measure the fluorescence intensity inside and outside of the pores. Different fluorophores can be used for this type of measurements (*e.g.*, the AlexaFluor and Atto brands of fluorophores), but the light source needs to be able to excite the fluorophores, and the fluorescence detector should filter out the emission wavelength of the fluorophores. In our setup, we used a 632.8 nm standard laser as light source and Alexa/Atto647(N) as fluorophores. These fluorophores have a broad excitation peak centred at a wavelength of 647 nm so a 632.8 nm laser can be used for the excitation. Fluorescence scans and the intensity of the different modes are represented in Figure 4.3 where Alexa647 was flowed to the flow cell (injection) and then after a stable signal, buffer was flowed to the flow cell (rinsing).

From the fluorescence scans, further information about adsorption processes (if they happen), including quantity of fluorophores and distribution of adsorbed molecules, could be obtained. For example, if the fluorescence intensity reaches higher values on the modes at the confined-mode, it can suggest that the molecules are concentrated at the middle and bottom of the pores. The fluorophores can adsorb on the pore surface (inside the pores and/or above the nanoporous layer) or simply dissolve in the media occupying the pores. The scan in Figure 4.3 represents the ideal experimental conditions – after rinsing, the fluorescence dropped back to the fluorescence intensity recorded before the injection, indicating that no irreversible adsorption processes occurred on the surfaces of the pores.

The change on the fluorescence intensity at the modes was used for inspection of adsorption events as well as controlling the quality of the fabricated waveguides by observing the sharpness and angle position of the modes. To see examples of fluorescence scans where the nanoporous waveguide surface did not prevent protein adsorption, see Figure I.20 in Appendix C.

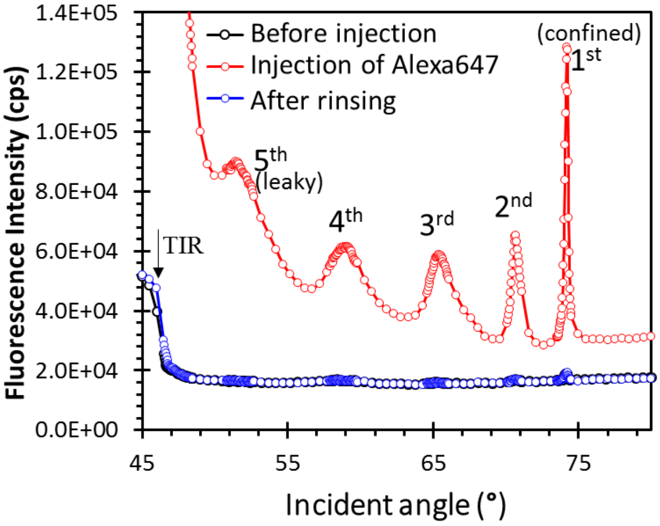

Figure 4.3 – Fluorescence scans of the AAO waveguide (30 nm pore size, 1.6 µm thick) showing the fluorescence intensity increase after injecting with the dye Alexa647 (0.7 µM) and decrease after rinsing. The different modes are labelled on the scan.

As mentioned before, at the modes, the light can be confined at different regions of the nanoporous waveguide, so for that reason waveguides have the ability to differentiate and enhance the detection of processes that occur within the pore structure from those occurring above the nanoporous layer.[157] In this chapter, we will show for the first time that it is possible to characterise the diffusion kinetics of different molecules at different regions of the pores by confining the light at the bottom, middle or entrance of the pore. This diffusion kinetics is the result of the movement of molecules from one area of high concentration to an area of low concentration (see Appendix D for an extended explanation of the different processes that occur and result on an empirical fit) and the time constant of that kinetics describes the duration of the process.

When the light is confined at the bottom of the pore (off-mode), we expect slower kinetics because the molecules take more time to reach the bottom of the pore (where they are detected). On the other hand, at the leaky-mode, the light is leaked above the nanoporous layer so faster kinetics is expected because the molecules are detected earlier. In fact, the concentration of fluorophores above the nanoporous layer takes less time to reach equilibrium, so the kinetics is faster.

For diffusion kinetics measurements, the light was confined at a specific region of the nanoporous waveguide, we injected fluorophores to the flow cell and then we rinsed them. A fluorescence timecourse measurement was performed where the fluorescence intensity (counts per second, cps) was recorded over time (Figure 4.4). This change on fluorescence intensity is then related to the concentration of molecules inside or outside of the pores (depending where the light is confined).

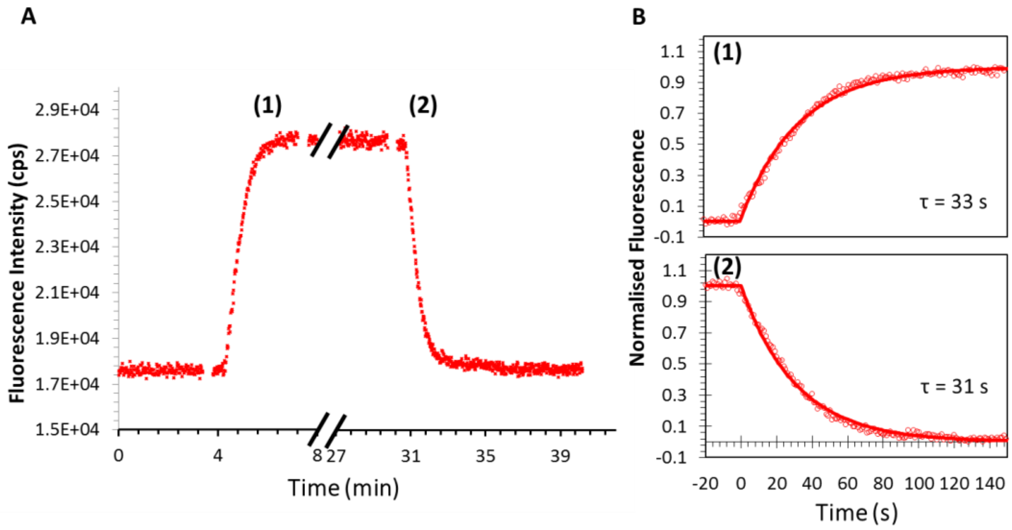

Figure 4.4 – (A) Fluorescence timecourse measurement of (1) injecting and (2) rinsing of 0.17 µM Streptavidin-Alexa647 (Sv) on open pores (30 nm pore size, 1.6 µm thick) at off-mode. The measurement was interrupted for an angle scan. The data were analysed by normalising the fluorescence intensity and by fitting the data to an exponential decay. (B) Respective normalised fluorescence kinetics and time constant values of Sv (B(1)) injection and (B(2)) rinsing.

To aid analysis and comparison of the kinetics of the different molecules, the fluorescence signal was normalised so that the maximum intensities measured were scaled to 1 and the baseline fluorescence intensities due to scattering and any previously surface-attached fluorophores were scaled to 0. The time constants were calculated from single exponential fits (*i.e.*, $I = 1 - e^{-t/\tau}$ for injection and $I = e^{-t/\tau}$ for rinsing, where I is the normalised fluorescence, t the time from the start of the injection/rinsing step and τ the time constant of the diffusion kinetics). As explained in Appendix D, this empirical fit combines all the processes that occur during the diffusion of molecules. There is no model to describe all the processes in one, so an exponential fit was used.

To minimise adsorption of the diffusing species to occur, poly(ethylene glycol) (PEG, 40,000 g/mol) was grafted on a polyphenol coating (tannic acid layer; see section 4.4.1) on the AAO nanoporous waveguides. Adsorption events slow down the kinetics because if there are molecules adsorbing on the surface, other molecules will need to diffuse to equilibrate the system. It is important to emphasise that the diffusion of the dyes and proteins mediated by surface chemistry is minimised with this antifouling layer. To further ensure that (irreversible) molecular adsorption does not influence the results presented in the next sections, we focused on analysing only the data during rinsing (*i.e.*, molecules exiting the pores).

4.2.2 Exploiting of the confinement of light on open and closed pores

The first two experiments consisted in characterising and differentiating diffusion inside the nanopores from diffusing above the nanoporous layer. To accomplish that we used open and closed pores samples to measure the diffusion of the molecules. If the pores are closed, the molecules cannot be inside the pores and they can only diffuse above the nanoporous layer. On the contrary, when the pores are open, the fluorophores can diffuse both inside the pores and above the nanopores.

For open pores, the waveguide was coated with a low concentration of tannic acid (TA) (0.01 mg/mL) and for a short time (15 min) to deposit a thin layer of poly(tannic acid) (Figure 4.5A). When a higher concentration of TA (0.1 mg/mL) was used for a longer time (1h, twice), a thicker layer of TA was deposited at the entrance of the pores so the pores became closed (Figure 4.5B). In Figure I.21 (Appendix C) is shown the reflectance scans of the waveguides before and after the poly(tannic acid) (pTA) coating. It was observed a bigger shift when higher concentrations of TA were used and the shifts were more accentuated on the higher modes (5th mode) than on 1st mode meaning that the pores were closed at the entrance of the pores. As previously mentioned, after this coating, PEG was grafted to prevent protein and dye adsorption.

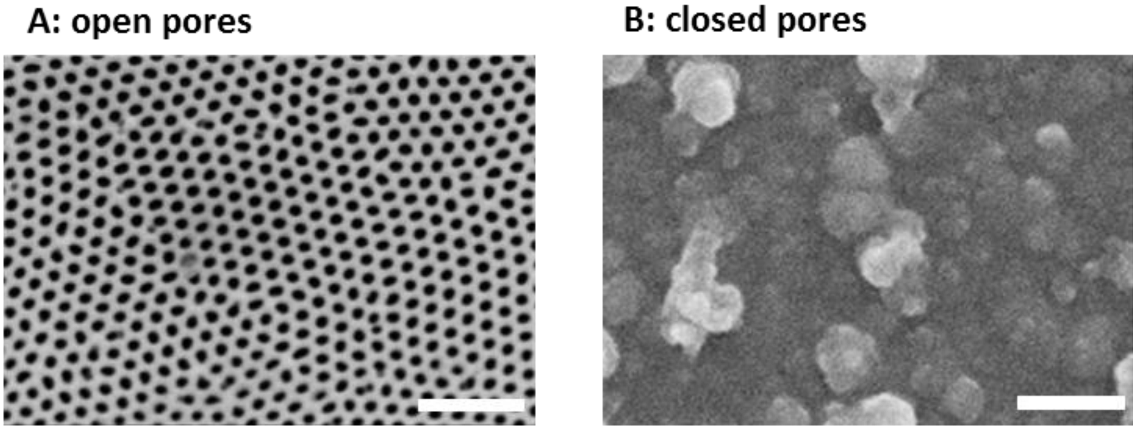

Figure 4.5 – FE-SEM images of (A) open and (B) closed pores after poly(tannic acid) (pTA) coating. The pores remained open after the pTA coating (0.01 mg/mL for 15min). The pores were closed when the pTA coating was performed at higher concentration and for a longer time of pTA. Scale bar of 500 nm.

The diffusion inside and above the pores was characterised using Alexa647 and Streptavidin-Alexa647 (Sv) (the size and the chemical structure represented in Figure 4.6). Streptavidin is 5 times bigger (in diameter) than Alexa647 and for that reason, these two molecules were chosen to demonstrate that small and large molecules, such as proteins, can diffuse inside the pores. These measurements will prove that it is possible to use this technique for measuring diffusion kinetics for molecules with different molecular weight.

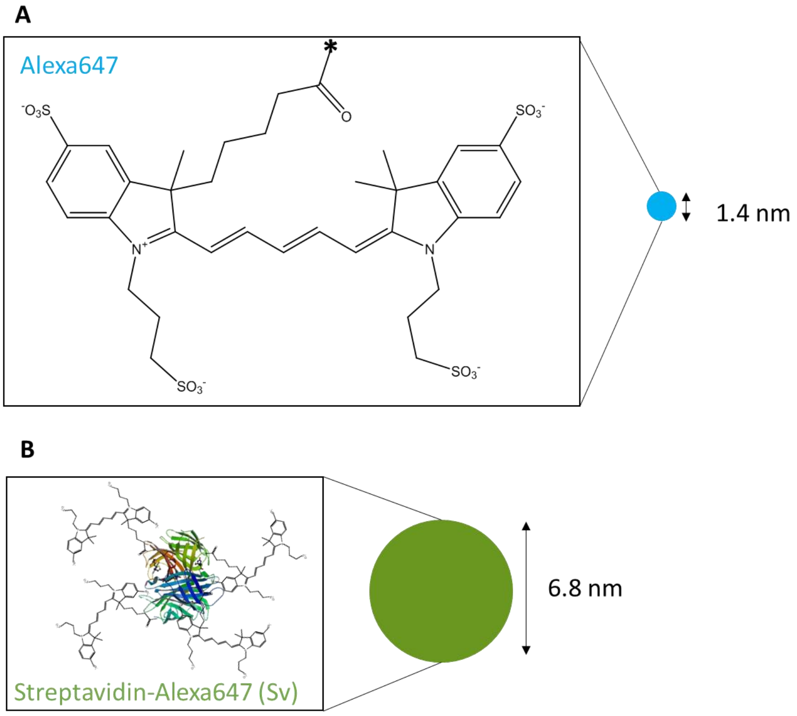

Figure 4.6 – Chemical structures of (A) Alexa647 and (B) Streptavidin-Alexa647 (Sv) and a schematic comparison of the size of these two molecules (blue dot – Alexa647 and green dot – Sv). The * represents where the dye can be bonded to other molecules (*e.g.*, Sv, immunoglobulins, biotin). Measurements with the dye (nonlabelled molecule) were performed with the Alexa647 carboxylic acid. Sv structure from PDB database (4YVB). Each Sv can be functionalised with 2 to 4 Alexa647 molecules.

These two molecules were flowed into a flow cell with open or closed pores (see scheme at the top of Figure 4.7). In the first case, the fluorophores were inside as well as above the nanoporous layer. In the second case (closed pores), the fluorophores were only above the nanoporous layer. Then, a buffer solution was flowed to the flow cell and the fluorophores were rinsed out. Before and after rinsing the fluorophores, angle scans were recorded in order to measure the fluorescence intensity at each mode (leaky- to confined-mode) and off-mode. We refer to the difference in fluorescence intensity before and after rinsing as the “fluorescence decrease baseline” because the fluorescence intensity decreases to the baseline after rinsing the fluorophores. The distribution of fluorescence at the different regions of the pores is presented in Figure 4.7C-F.

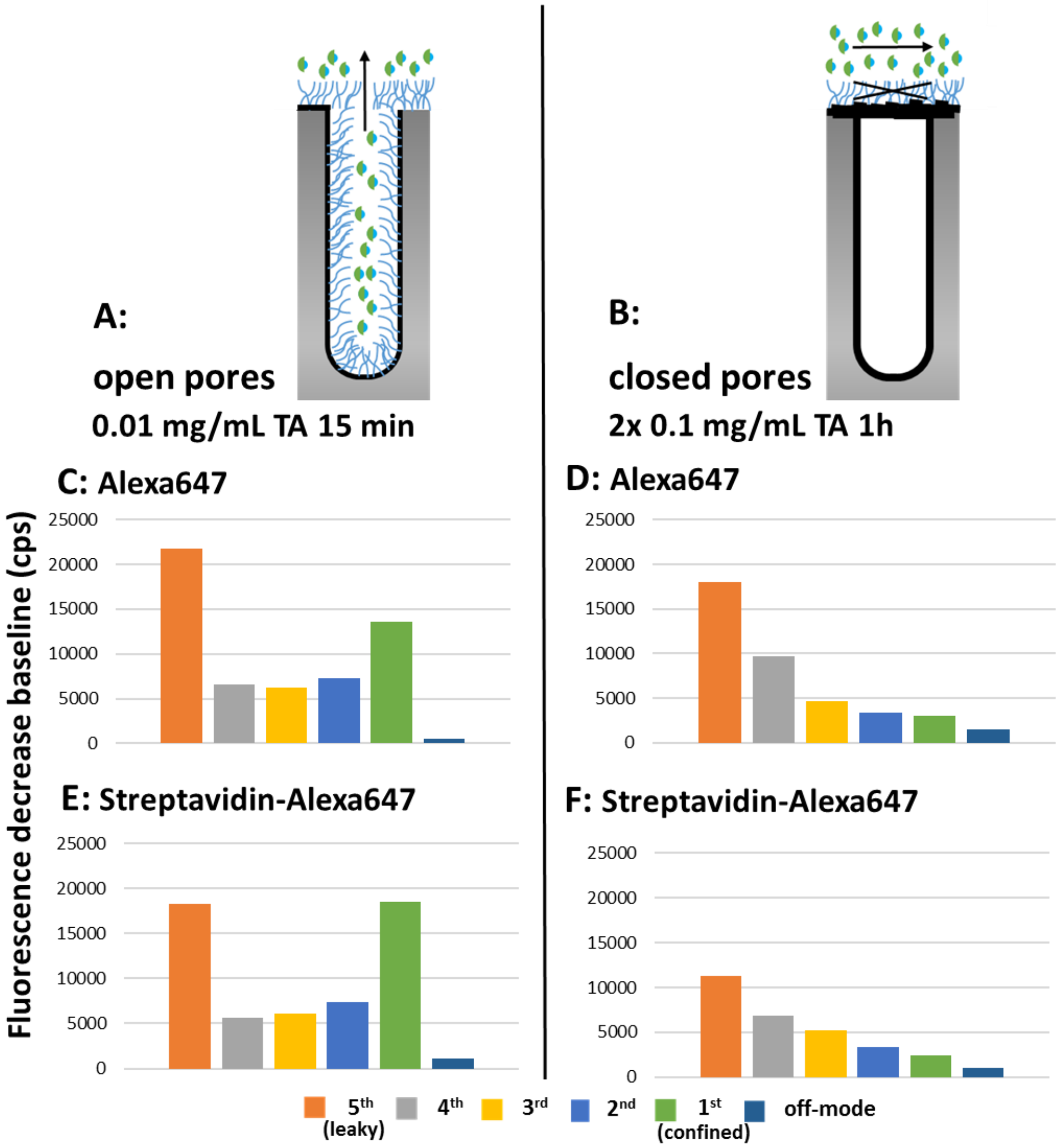

Figure 4.7 – Representative schemes of (A) open and (B) closed pores coated with pTA and PEG layers and diffusion out of Alexa647 (blue half dot) and Sv (green half dot). (C-F) Fluorescence decrease baseline of Alexa647 (0.7 µM) and Sv (0.17 µM) on open (C) (E) and on closed (D) (F) pores, respectively. 30 nm pore size and 1.6 µm waveguide.

We observed very different patterns of relative mode intensities when the pores were open or closed. When the pores were open, the fluorescence intensity was high at the leaky-mode and the fluorescence intensity at the subsequent modes increased (from the leaky- to the confined-mode) (Figure 4.7C and E). In fact, the fluorescence intensity at the confined-mode was as high as at the leaky-mode. When the pores were closed, the fluorescence intensity at the modes decreased from the leaky- to the confined-mode (Figure 4.7D and F). The intensity at the confined-mode was very little unlike when the pores were open.

The observed difference in the relative mode intensities is consistent with what was expected. When the pores are open, the fluorophores can be inside of the nanopores and above the nanopores entrance (middle and top of the nanoporous layer). The relative intensity should be high at the confined-mode due to a larger confinement of light in the middle of the pore (see electric-field intensity distribution of confined-mode in Figure 4.2). The light was mostly confined at the confined-mode, and increasingly leaked to the outside of the nanoporous layer from the confined- to the leaky-mode. For all these facts, this explains why we observed the fluorescence intensity increase from the leaky- to the confined-mode. At the leaky-mode, the light is confined inside the nanopores but is also leaked above the nanoporous layer and since it is very close to when starts occurring TIR, not all the light is completely total internally reflected, so high fluorescence intensities were observed at this region. Many fluorophores are in the bulk, so it is also possible to excite that fluorophores leading to a higher fluorescence intensity.

When the pores are closed, the fluorophores cannot enter inside the pores so they only flowed and diffused above the nanoporous layer. In this case, high fluorescence intensities can only be observed when the light is leaked above the entrance of the pores which is most prominent at the leaky-mode. The fluorescence intensity at the other modes and off-mode should be low and decrease with the decrease of mode (leaky- to confined-mode) because there is less light leaking outside of the nanoporous layer (as explained above and in section 4.2.1). This was observed in this experiment showing that the fluorophores were above the nanoporous layer because the pores were actually closed. In principle, the fluorescence intensity measured at the off-mode position should be even lower than the intensity observed, but the scattered light can excite the fluorophores that are present above the nanoporous layer increasing the fluorescence signal.

Another noticeable feature is the relationship between the fluorescence at the confined-mode and off-mode. The ratio between the intensities at these two regions was 20 and 2 when the pores were open and closed, respectively. When the pores are open, the fluorophores are inside of the pores and the fluorescence is much higher at the confined-mode than at the off-mode because the light is largely confined in the middle of the pores and the fluorescence is enhanced. The light is more coupled inside the pores than leaked by TIR (off-mode). When the pores are closed, the overall intensity at the two regions is very low as well as its ratio, which confirms that the fluorophores are above the nanoporous layer and not in the middle or at the bottom of the pores.

This experiment confirmed the differences on the distribution of light between when the fluorophores are inside and on the top of pores or only above the nanoporous layer.

4.2.3 Differentiating diffusion out and passing above the nanopores

As demonstrated above it is possible to distinguish where the fluorophores are – inside and on the top of the pore or only on the top of the pores. This was shown by comparing the fluorescence intensities at different regions of the nanoporous waveguide. In this section, we focus only on the diffusion kinetics through nanopores of a small model molecule: Alexa647. The light was confined at different regions of the nanopores, illuminating the bottom, the middle and the entrance of the pores: off-mode, confined- and leaky- modes, respectively. Fluorescence timecourse measurements were recorded at one region at a time (at one specific incident angle that corresponded to the off-mode, confined- or leaky-mode), and the diffusion kinetics of rinsing Alexa647 at these different regions for open and closed pores was evaluated.

Different time constant values of Alexa647 were observed at off-mode, confined- and leaky-mode when the pores were open (21, 17 and 15 s) (Figure 4.8A), showing smaller time constant values for the leaky-mode when compared to the off-mode. These results mean that the rinsing of dyes was detected earlier when the light was leaked above the entrance of the pores rather than when was confined at the bottom of the pores. On the other hand, when the pores were closed, Figure 4.8B showed very similar time constant values (21, 18 and 20 s) for off-mode and the different modes. This suggests that the rinsing took the same time to reach the equilibrium independently of where the light was confined. The fluorophores were only above the nanoporous layer and when they were rinsed out similar time constant values were obtained, as expected.

As explained in Appendix D, when the pores are closed there is only diffusion on the diffusion layer and flow of fluorophores above the nanoporous layer. For this reason, when the pores are closed, the time constant values are similar even when the light is confined at different depths of the pore because no process is occurring inside the pores (only above the nanoporous layer). When the pores are open, both processes happen and diffusion through the nanopores also occurs. It takes longer to reach the equilibrium because the fluorophores need to diffuse inside of the nanopores so when the light is confined at different regions of the pore, different time constant values are obtained.

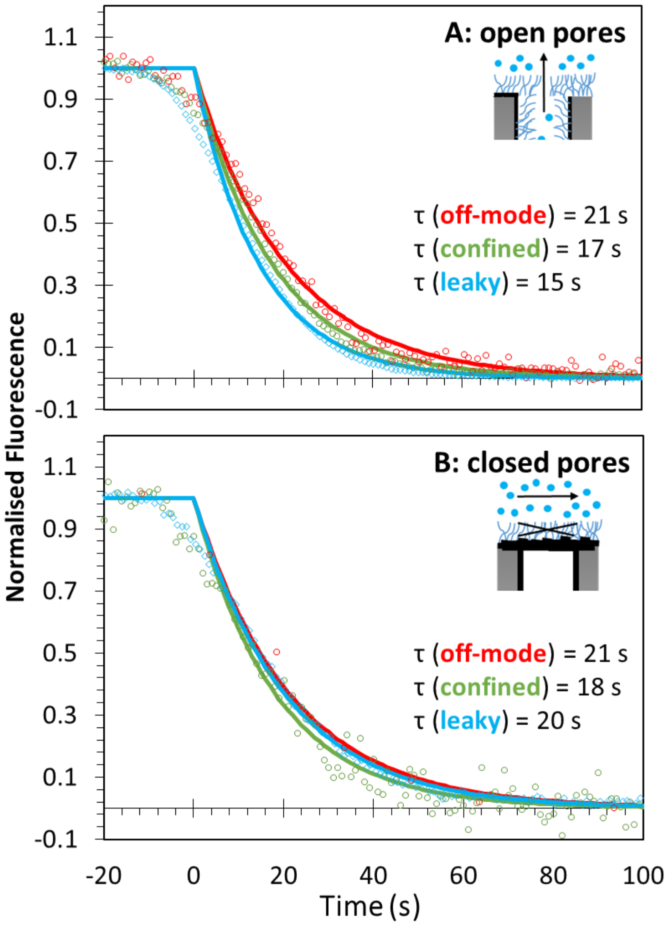

Figure 4.8 – Kinetics of 0.7 µM Alexa647 rinsing at off-mode (red), confined- (green) and leaky- (blue) modes on (A) open and (B) closed pores (30 nm pore size and 1.6 µm thick waveguide). Dots – normalised data, full line – fitting of the normalised data. Representative schemes of open and closed pores of diffusion out of Alexa647 (blue full dots).

As a control, the waveguide film was mounted in a different configuration: the bottom of the pore was faced up to the flow cell (the pores were physically closed with an alumina barrier layer). This control was performed to compare to the results obtained for Alexa647 kinetics when the pores were closed with pTA coating.

The kinetics of Alexa647 at different regions of the pores was again characterised, showing similar time constant values – 14, 15 and 14 s for off-mode, confined- and leaky-modes (Figure 4.9).

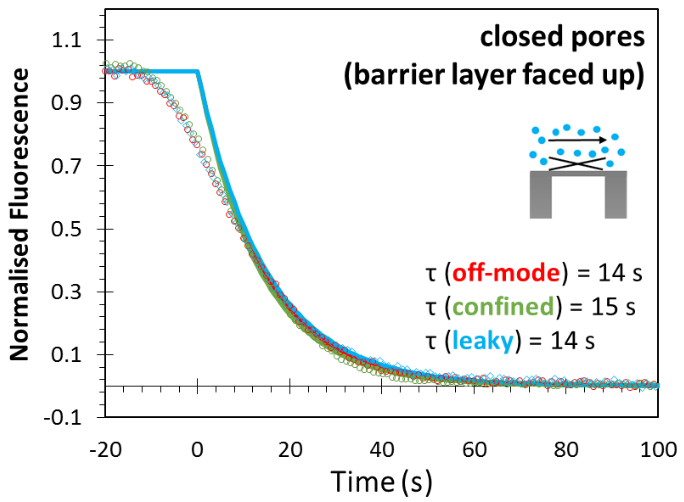

Figure 4.9 – Kinetics of 0.7 µM Alexa647 at off-mode (red), confined- (green) and leaky- (blue) modes on closed pores (barrier layer) film (30 nm pore size and 1.6 µm thick waveguide mounted upside down). Dots – normalised data, full line – fitting of the normalised data. Representative scheme of closed pores of diffusion of Alexa647 (blue full dots).

The similar time constant values at different regions of the nanoporous layer confirmed that the fluorophores were above the nanoporous layer, and the measurement is the result of the diffusion of Alexa647 on the diffusion layer. The time constant values of Alexa647 diffusion when the light was confined at different regions of the pore for the control were slightly smaller than the time constant values obtained when the pores were blocked with the pTA coating (Figure 4.8B). In theory, the time taken should be the same in both cases. However, these are two different samples and the roughness on the top of the nanoporous layer influences the diffusion kinetics.

This experiment demonstrated that is possible to distinguish diffusion kinetics at different depths of the pores. It also proved the pTA coating can actually close the pores and the fluorophores cannot diffuse inside when the pores are closed.

4.2.4 Dependencies of nanopore diffusion on molecular size

In the following experiment, our aim was to show that with this technique is possible to measure diffusion kinetics of molecules with different molecular sizes. The use of molecules with different molecular sizes will prove that the process that we measure is the kinetics of diffusion and not the flow. The diffusion is influenced by the molecular weight of the molecules but the same is not applied to the flow (no dependence on molecular weight). In this respect, the diffusion of molecules with different molecular sizes was characterised. We used immunoglobulin G (IgG), streptavidin (Sv) labelled to Alexa647, and Alexa647 that have a molecular weight of 150, 60 and 1.2 kDa, respectively.[167–170] We focused only at one region of the pore – bottom of the pore – at off-mode, to clearly show the differences on the diffusion of these molecules. The comparison between diffusion when the pores were open or closed was made to confirm again that the configuration of the pores influences the diffusion of different molecules.

In this experiment, when the pores are open, we expect that smaller molecules diffuse faster than larger molecules (IgG is 100 times bigger than Alexa647, regarding molecular weight), which can reflect in smaller time constant value. Also, pore effects can also contribute for slower diffusion kinetics. There is a reduction on the effective pore size due to the molecule size (40 % reduction for Sv). On the other hand, when the pores are closed, the time constant values should be smaller as observed in the previous section and the difference between the time constant values of the different molecules should be less disparate because the molecules can only diffuse above the nanoporous layer, not reaching the pore bottom.

Figure 4.10A shows the kinetics of Alexa647, Sv-Alexa647 and IgG-Alexa647 when the pores are open. The time constant values were 32, 28 and 23 seconds with the decrease of molecular weight – IgG, Sv and Alexa647. These results were consistent with what it was expected: smaller molecules diffuse faster.

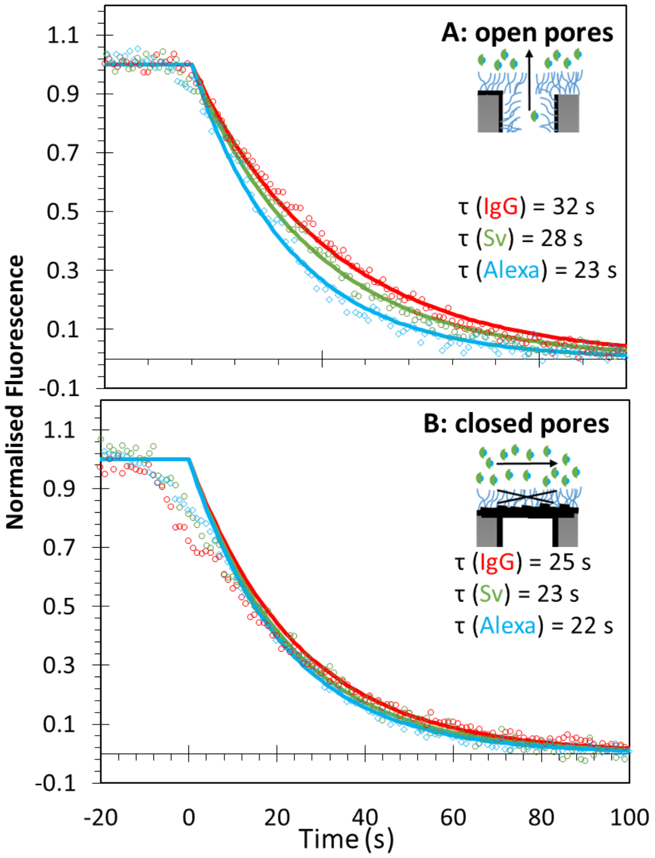

Figure 4.10 – Kinetics of 0.4 µM IgG-Alexa647 (IgG) (red), 0.17 µM Streptavidin-Alexa647 (Sv) (green) and 0.7 µM Alexa647 (blue) at off-mode on (A) open and (B) closed pores (30 nm pore size and 1.6 µm thick waveguide). Dots – normalised data, full line – fitting of the normalised data. Representative schemes of open and closed pores of diffusion out of Alexa647 (blue half dots) and Sv (green half dots).

When the pores were closed, the time constant values for the different molecules did not differ that much – 25, 23 and 22 seconds for IgG-Alexa647, Sv-Alexa647 and Alexa647, respectively (Figure 4.10B). The time constant values were smaller than when the pores were open. When the pores are closed, the molecules can flow only above the nanoporous layer and diffuse on the diffusion layer. For that reason, the kinetics is very similar and not as dependent of the molecular weight as it was observed.

To compare these results with the literature, we calculated the effective diffusion constants of Alexa647, Streptavidin-Alexa647 and IgG-Alexa647 based on the time constant values obtained in this experiment. We related the diffusion constant values with the molecular weight of the molecules. In the literature, it is stated that the diffusion is inversely proportional to the cube root of the molecular weight ($D \propto MW^{-1/3}$).[171]

To obtain the time constant of the diffusion that occurred only inside the pores, we subtracted the time constant values of the molecules when the pores were open (23, 28 and 32 s) by the time constant values when the pores were closed (22, 23 and 25 s) to eliminate the time that corresponds to the flow and diffusion above the nanoporous layer. The diffusion constants for each molecule (D, μm^2/s) were then calculated using Einstein equation: $\langle x^2 \rangle = q_i D t$, where x is mean-square displacement (2 μm pore length), q_i the numerical constant (q_i = 2 for 1 dimensional diffusion), D is diffusion coefficient (μm^2/s) and t is the time (in seconds).[140,168] See Table I.3 (Appendix C) for detailed calculations. We plotted the effective diffusion constants *versus* the molecular weight of Alexa647, Streptavidin and IgG (Figure 4.11). The slope of the relationship between the molecular weight and the diffusion constant was -0.378, which is approximated to the relationship described in the literature – -0.33(3).[171]

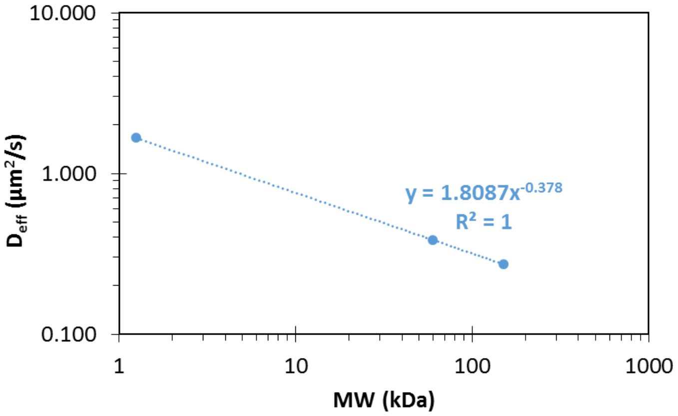

Figure 4.11 – Relationship between diffusion constant (μm^2/s) of Alexa647, Streptavidin-Alexa647 and IgG-Alexa647 and their molecular weight (kDa). The plotted values are on a logarithmic scale. The diffusion constants of the molecules was calculated based on the Einstein equation.[140,167–170]

4.2.5 Dependencies of nanopore diffusion on protein net charge

Despite the fact that adsorption events are not desirable to determine time constants of the diffusion of molecules through the pores, we proceeded to show how sensitive OWS is to adsorption processes at different depths within the pores. In this experiment, a bare nanoporous AAO waveguide was coated with a protein with a net charge to promote adsorption events by electrostatic interactions and observe how different molecules can adsorb on the surface depending on their charge.

Avidin was the protein used due to its isoelectric point (pI = 10). The protein was attached to the surface using a thin pTA coating (same approach as in chapter 3, section 3.4.2). When the waveguide is covered with the avidin layer, the surface is positively charged because at pH 7 (pH of the HEPES buffer used for the measurements) the net charge of the protein is positive (pH is below the pI of the protein). After covering the surface with the protein, we used two other proteins with different net charges to observe their adsorption behaviour within the pores.

Proteins can be labelled with a range of fluorophores as previously described. Alexa647, Atto647N and Atto647 have a net electric charge of -3, +1 and 0, respectively (Table 4.1). The fluorophores replace the positively charged amine groups of the proteins, so the protein net charge will depend on the type of fluorophore that it is attached.

Table 4.1 – Net charge of Alexa647, Atto647N, Atto647 fluorophores.

Fluorophore	Surface charge
Alexa647	-3
Atto647N	+1
Atto647	0

Streptavidin-Atto647N (Sv-Atto647N) and Bovine Serum Albumin-Alexa647 (BSA-Alexa647) were chosen for these measurements because they have similar molecular weights, but their overall net charge is different so their interaction with the surface is expected to be not the same. At pH 7, Sv-Atto647N and BSA-Alexa647 are positive and negatively charged, respectively. It is expected that BSA-Alexa647 is attracted to surface and adsorbs on the avidin layer by electrostatic interactions whereas Sv-Atto647N is less attracted to the surface so it would be able to diffuse inside of the pores. As mention before, the fluorescence intensities at the different modes are sensitive to the different regions of the pore. If there is more adsorption of molecules on the top of the nanopores, the fluorescence intensity at the modes where the light leaks more outside of the nanoporous layer (leaky-mode) will be higher than the fluorescence intensity of the other modes. After rinsing the fluorophores and if they remain adsorbed on the top of the pores, the fluorescence intensity will still be higher at the modes where the light is leaked outside of the nanoporous layer. These changes in fluorescence intensity can be observed when fluorescence scans are recorded. Figure 4.12 shows the fluorescence scans of BSA-Alexa647 and Sv-Alexa647.

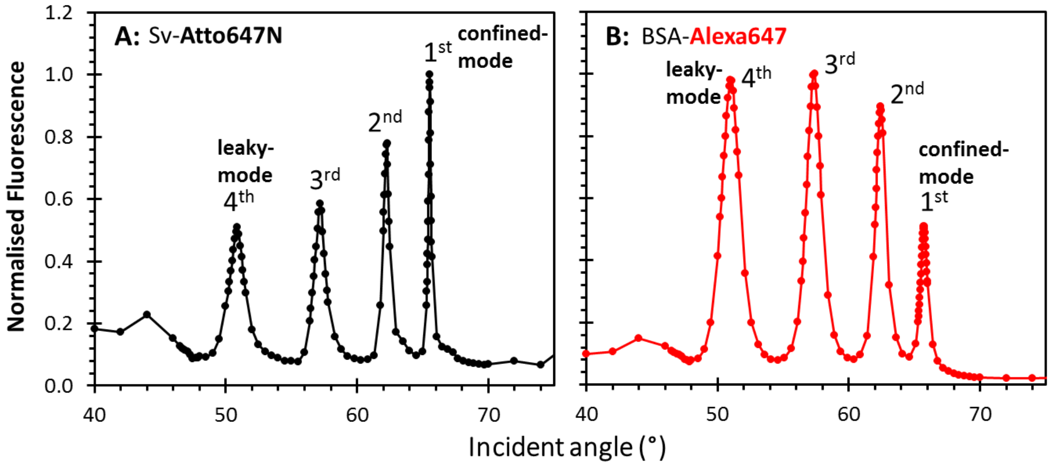

Figure 4.12 – Fluorescence scans after (A) Streptavidin(Sv)-Atto647 and (B) Bovine Serum Albumin(BSA)-Alexa647 diffusion inside the pores. The waveguide (30 nm pore size, 1.6 µm thick) was coated with tannic acid and with avidin. 0.14 µM Sv-Atto647N and BSA-Alexa647 were injected and rinsed. The fluorescence scans were recorded after rinsing the labelled-proteins.

In Figure 4.12A it is shown that the fluorescence intensity is well distributed over all the modes suggesting that Sv-Atto647N was evenly adsorbed from the bottom to the top of the pores. On the other hand, when BSA-Alexa647 was used, the fluorescence intensity at the leaky-mode was higher than at the confined-mode (Figure 4.12B) meaning that the BSA was attracted to the surface and adsorbing at the entrance of the pores. The proteins start to adsorb when they find a surface (top of the pore) and more molecules diffuse inside the pores. After some time, the entrance of the pore is covered by adsorbed proteins and the protein layer has a repulsive effect on the successive proteins that are diffusing so they cannot enter inside the pores.

This experiment shows how small interactions of different labelled-molecules with distinct net charges at the surface of the pores can be tracked by OWS. As shown in this experiment, the electrostatic interactions between molecules and the surface of the waveguide films are important for controlling the transport of molecules through the pores.

4.3 Conclusions

Optical waveguide spectroscopy was used to characterise the diffusion of different molecules inside nanopores. The confinement of the light at different regions of the pores allowed us to distinguish how the fluorophores travel inside the pores. For a measurement at off-mode, the light is concentrated at the bottom of the pores, while at the leaky-mode the light is quite evenly distributed through the pores, including around the pore mouths. Kinetics of different molecules when the pores were open or closed was analysed. For open pores, the kinetics was slower at off-mode as the molecules needed to travel inside the nanopores, while the diffusion kinetics was faster at the leaky-mode. When studying the diffusion of molecules with different molecular weights, larger time constant values were observed for bigger molecules. In contrast, the molecules could not diffuse inside the nanopores when the pores were closed. Similar time constant values were obtained for different molecules, independently of where the light was confined because the diffusion inside did not occur. Our OWS technique brings a new concept of characterising molecular diffusion through nanopores, which can be useful for the development of biomimetic macromolecular transport.

4.4 Materials and Methods

4.4.1 AAO waveguide membranes

AAO membranes were prepared by two-step anodisation process – a more detailed description of the different steps of the fabrication of AAO films and the different parameters that were varied to accomplish ordered and uniform straight pores is presented in Appendix B. The final procedure is described in this section. Aluminium pieces of high purity (99.999 %) (Advent Materials, UK) were mechanically polished (E W Jackson & Sons LTD (Germany) (motorised polisher using a 1200 grade sandpaper) and placed on a sample holder (Figure I.13, Appendix B) and in an electrolytic cell. Electropolishing was performed (40% v/v phosphoric acid, H_3PO_4 (Sigma-Aldrich, UK), 38 % v/v ethanol (Sigma-Aldrich, UK) and 22 % v/v deionized water) at a temperature of 45 ˚C at 1 A. The first anodisation was performed in 0.3 M oxalic acid (VWR, UK) at 30 °C for 2 hours. The unordered alumina nanopores were etched in a 1.8 wt % chromium trioxide, CrO_3 (Sigma-Aldrich, UK) and 6 wt % of H_3PO_4 solution at 70 °C for one hour. The second anodisation was performed at 0 °C for 45 min to obtain 25-30 nm pore size and < 2 µm thick film (Figure I.15 and Figure I.16, Appendix B). After anodisation, the unreacted aluminium was selectively etched (3.4 wt % copper (II) chloride in 1:1 H_2O:10M hydrochloric acid (Sigma-Aldrich, UK)) to obtain free-standing AAO (Figure I.18, Appendix B). LASFN9 substrates (Hellma Optics, Germany) were coated with 2 nm thick chromium film and 50 nm thick gold layer by vacuum thermal evaporation. Then, the free-standing AAO films were glued on the gold-coated LASFN9 substrates using an optical adhesive (NOA81, Norland, USA). The films were coated with tannic acid (TA) (Sigma-Aldrich, UK) (open pores – 0.01 mg/mL TA in 0.1 M bicine, 0.6M NaCl (VWR, UK) pH 7.8 for 15min; closed pores – 0.1 mg/mL TA for 1h twice), rinsed three times with deionised water and coated with PEG-SH (5 mg/mL in water for 40h) (molecular weight 40,000 g/mol, JenKem, USA). For the last experiment (avidin coating), the waveguide (30 nm pore) was coated with 0.01 mg/mL TA (0.1 M Bicine, 0.6 M NaCl) for 15 min and then with avidin (0.01 mg/mL using 10 mM HEPES, 150 mM NaCl at pH 7.0).

4.4.2 Optical waveguide spectroscopy (OWS) setup

OWS measurements were performed using the AAO films on gold-coated LASFN9 glass substrates and operating at 632.8 nm (He-Ne laser (PL610P, Polytec, Germany)) in the Kretschmann configuration. The substrate was matched to a glass prism by optical immersion oil (Cargille, USA) and then a flow-cell composed of poly(dimethylsiloxante) (PDMS) gasket and a transparent quartz slide with input and output ports was attached (flow cell of 0.6 mm height, 10 mm length and 2 mm width). The liquid cell was connected to a peristaltic pump (Regio, Ismatec, Switzerland) to flow the liquid in and out of the cell (34 µL/min). The whole device was mounted on a rotation stage (Hans Huber AG, Germany) to control the incidence angle. The intensity of the light beam reflected at the prism base was detected using a photodiode and a lock-in amplifier (Model 5210, Princeton Applied Research, USA).[172] The emitted fluorescence was collected by a lens (focal length 30mm, numerical aperture of NA=0.2), passed through two bandpass filters (FBF, transmission wavelength 670 nm, 670FS10-25, Andover Corporation Optical Filter USA) and a notch filter (LNF, central stop-band wavelength 632.8nm, XNF-632.8-25.0M, CVI Melles Griot, USA).

4.4.3 Fluorescence timecourse measurements

Alexa647 (0.7 µM), Streptavidin-Alexa647 (0.17 µM), IgG anti-human Alexa647 (0.4 µM) (ThermoFisher, UK) were dissolved in buffer (10 mM HEPES, 150 mM NaCl) at pH 7.0. The sample was positioned at a certain angle: off-mode and at confined- or leaky-modes. The off-mode measurements were at 5 degrees higher than the angle of the confined(1st)-mode to make sure that the light was confined at the bottom of the pores. The fluorescence timecourse measurement started with the pores filled with buffer and the fluorescent molecules were added to the flow cell. After a stable signal (loaded pores), the measurement was interrupted for an angle scan. After the reflectance and fluorescence scans, the fluorescence timecourse measurement was continued, the loaded pores were rinsed out and an angle scan was recorded again. To aid analysis and comparison of the kinetics of the different molecules, the fluorescence signal was normalised: maximum intensity = 1 and baseline = 0. The time constants were calculated from single exponential fits (*i.e.*, $I = 1 - e^{-t/\tau}$ for injection and $I = e^{-t/\tau}$ for rinsing, where I is the normalised fluorescence, t the time from the start of the injection/rinsing step and τ the time constant of the diffusion kinetics). There was some variance between measurements and samples but for the measurement that had a higher difference between the observed value and the fitted value (squared sum of the residual error = 1.4, see Figure I.22, Appendix C), the t-test showed a small p-value ($p < 0.001$) meaning that we could be confident about the fitting that we used. It was also observed a normal distribution (bell-curve) (see Figure I.23, Appendix C).

4.4.4 Characterisation of the nanopores

To verify if the pores were open or closed after the polyphenol coatings, we used Field Emission Scanning Electron Microscopy (FE-SEM) (Hitachi SU-6600). We also fitted the reflectance data (before and after the coatings) in Winspall (Max Plank Institute for Polymer Research (version 2.20)) to verify the pore size and thickness of the waveguide.

5. Diffusion of molecules through nanoporous suspended membranes

5.1 Introduction

In the previous chapter, the characterisation of different molecules travelling on the top and inside of nanopores with pores open on one side was assessed. It was possible to distinguish the diffusion of molecules inside the pores and above the nanopores entrances by confining the light at different depths of the pores.

In this chapter, characterisation of the diffusion through nanopores open on both sides within a flow cell is investigated. The concept of waveguiding was no longer applied because the AAO layer was not attached to a gold surface anymore. Instead, a nanoporous alumina membrane was placed between two gaskets (made of polydimethylsiloxane, PDMS) (see Figure 5.1) so the membrane was suspended on the flow cell. The light was confined to only the bottom surface of the flow cell by total internal reflection (TIR). As explained in the previous chapter (section 4.2.1), at angles higher than the critical angle, the light is total internally reflected. There is some light penetration into the less dense medium (water) at the boundary interface (glass-water) – evanescence wave. In our system, this wave can illuminate the bottom of the flow cell (bottom chamber) and excite fluorophores (see scheme of Figure 5.1). For consistency, all the measurements were performed at 0.5° higher than the TIR.

The aim of this work was the characterisation of the diffusion of molecules through the nanoporous suspended membranes when varying different parameters such as the surface charge and pore size. The "new" configuration was chosen to demonstrate how simple and versatile this technique is for following diffusion through a suspended membrane when using an attenuated total reflectance (ATR) system. This system was also used for monitoring *in situ* pore opening and biocatalytic reactions. An ultimate goal of this thesis is mimicking the NPC (as explained in the previous chapter). To achieve this goal, we used a responsive polymer on the nanoporous membrane to control the molecular transport. However, this experiment is just a demonstration of controlling the transport of molecules and it is still far from mimicking the NPC.

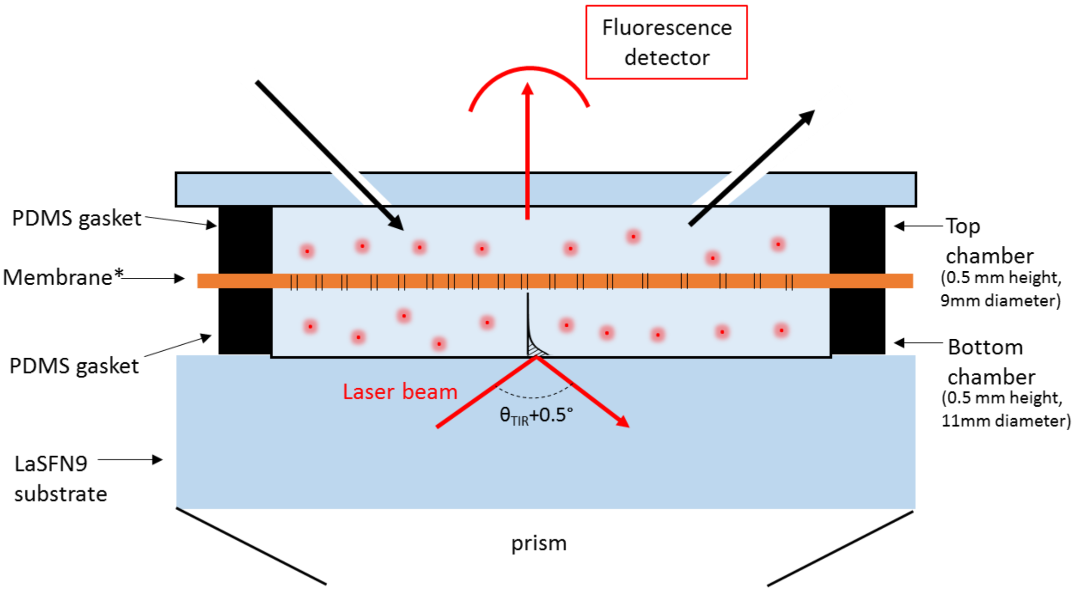

Figure 5.1 – Scheme of the device used for timecourse measurements. *60 µm membranes were used with a pore size of 50 or 200 nm. As controls, no membrane or a membrane with closed pores was placed in the flow cell (diffusion only in the top chamber). For consistency, the measurements were performed at θ_{TIR}+0.5° where the flow cell was illuminated only at the bottom of the bottom chamber.

To start, different controls were performed. First, the diffusion of a small molecule (Alexa647) flowing only in a (top) chamber was measured – it was used a membrane with closed pores so that the dye molecules were not able to cross through the pores or diffuse to the bottom chamber (section 5.2.1). In this chapter, Alexa647 was the only molecule used on our measurements (1 kDa molecular weight, 0.7 nm radius). The first control was performed to determine the time constant of the fluorophores flowing in the first chamber only. For the second control, the diffusion of the Alexa647 was characterised when there was no membrane in order to determine the time constant of filling the whole flow cell. After these controls, the diffusion of Alexa647 through membranes with open pores was assessed.

When there was a membrane, we expected that the molecules (1) flowed to the chamber, (2) diffused on the top chamber on the proximity of the membrane, (3) diffused through the pores and (4) diffused to the bottom of the chamber (see a more detailed explanation in Appendix D). In our measurements, these four processes occurred (at the same time) and the change in fluorescence intensity is the response of the fluorophores moving from higher to lower concentration areas during these processes. For these reasons, the data that we collected is a combination of all these processes and the analysis was performed taken into account an empirical fit.

When there was a membrane, the time constant value should be larger than when the molecules diffused without a presence of membrane because there are more processes occurring, which delays the diffusion kinetics. We expected smaller time constant values upon increasing the pore size of the membranes, as more molecules can cross the pores per unit time. The effect of surface charges on the diffusion of the fluorophore was also assessed. The interactions of the fluorophores with the surface of the membrane can slow down the kinetics if the molecules are attracted to the surface.

5.2 Results and Discussion

5.2.1 Control experiments

The first two experiments were performed as controls to characterise the diffusion of Alexa647 when (1) there was a membrane with closed pores – the dyes only flowed in the top chamber (not diffusing through the membrane); and when (2) there was no membrane – the dyes flowed in a “big” chamber (illustrative schemes at the top of Figure 5.2).

Figure 5.2A and B show the fluorescence intensity increase of Alexa647 as it started flowing into either just the top chamber or the whole flow cell, respectively. In the first case, the dyes flowed in the top chamber (31.81 mm^3) and in the second case they flowed in the whole chamber (79.33 mm^3, double of the height of the first case) (see chamber size in Figure 5.1). Diffusion kinetics was expected to be slower in the second case because the fluorophores need to travel longer distances. When the dye was diffusing to the flow cell, the fluorescence intensity always increased (from the baseline fluorescence intensity), but when there was a membrane with closed pores the increase was much smaller (5.3 times) than there was no membrane (43.5 times). In the last case, greater amount of dyes was excited as they filled the entire (bigger) flow cell. In Figure 5.2C, the fluorescence intensity was normalised: the maximum intensity value was set to 1 and the minimum intensity (baseline) set to 0 in order to compare with the other experiments (in the next sections).

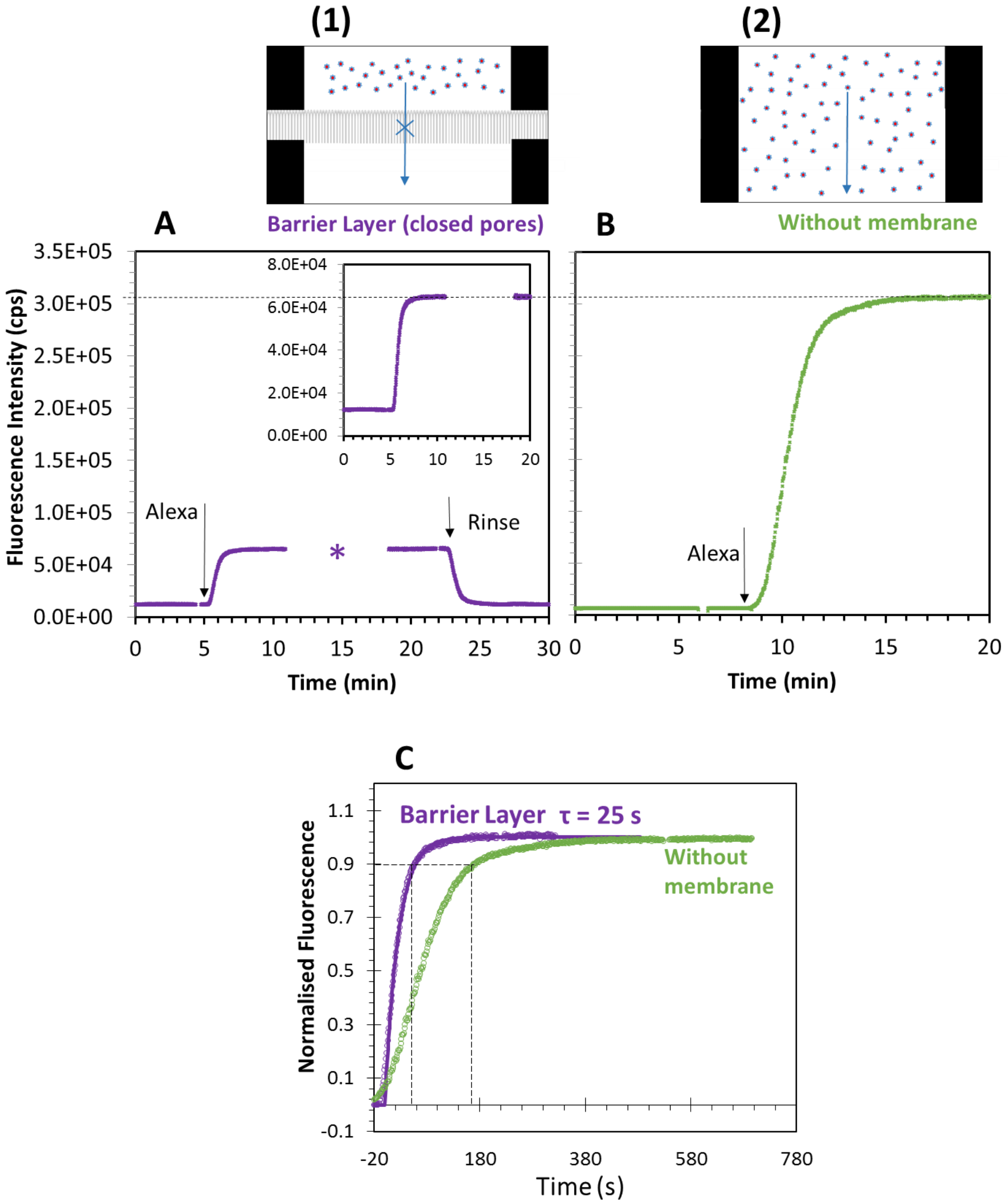

Figure 5.2 – (1) and (2) Representative schemes of the different conditions of the measurement. Timecourse measurements of 0.7 µM Alexa647 (Alexa) when (A) a membrane had closed pores (barrier layer) (uncoated alumina) or (B) there was no membrane and the fluorophores diffuse through the whole flow cell. (*) measurement was interrupted to perform an angle scan. (C) Kinetics of 0.7 µM Alexa647 when there was a barrier layer (purple) or no membrane present (green). Dots – normalised data, full line – fitting of the normalised data.

For the first case, an exponential behaviour was assumed and the calculated time constant was 25 seconds. The meaning of this value is the time that fluorophores take to flow and diffuse in the top chamber to reach a concentration equilibrium inside of the flow cell. In the second case, additional processes occurred and the sum of these processes did not result in an exponential curve. In fact, the flow inside of the flow cell changed because its size. The flow cell was bigger, decreasing the flow speed of the fluorophores and consequently increasing the thickness of the diffusion layer. For that reason, we did not compare the time constants between these two controls. However, it was noticing that when there was no membrane, the system took three times longer to reach 90 % of the equilibrium (see dash lines crossing the 0.9 normalised fluorescence in Figure 5.2C).

These two experiments were performed not only to show the difference between the diffusion on the top and "big" chamber but most importantly to measure the diffusion on the top of the membrane (25 s) to fit the data in the next experiments. In the following experiments, membranes with open pores were suspended and the diffusion of Alexa647 was measured. As explained in the introduction of this chapter, four main processes can occur during the diffusion of molecules crossing from one side to the other of the membranes: (1) flow and (2) diffusion in the top chamber, (3) crossing the nanoporous membrane and (4) diffuse to the bottom of the chamber. The first two processes were characterised when a membrane with closed pores was used – time constant of 25 s. The third process is expected to be longer because the molecules need to find the pores, cross and exit. The fourth process should be as fast as the first and second processes (25 s) and almost negligible in comparison with the third process, because it takes more time for the fluorophores to diffuse through the pores than diffuse in the flow cell. For that reason, the third and fourth processes can be combined in one. To sum up, in the next section, the diffusion of Alexa64 through nanoporous membranes was characterised by two time constants: τ_1 = 25 s and τ_2 that depends on the different parameters that we investigated (*e.g.*, pore size).

5.2.2 Diffusion of Alexa647 using different solution conditions

In this section, the diffusion of Alexa647 through a suspended membrane 60 μm thick with pore sizes of 200 nm (commercially available membrane) was characterised. The first measurement was performed when the flow cell was filled with buffer (10 mM HEPES, 150 mM NaCl pH 7.0) and Alexa647 was also dissolved in buffer. At pH 7, Alexa647 and alumina (pI 8) are negative and positively charged, respectively. The kinetics of Alexa647 was characterised by measuring the fluorescence intensity over time. In contrast, the second measurement was performed when the flow cell and Alexa647 were in deionised water (deionised water pH around 5~6) and the diffusion of Alexa647 through the pores was also characterised.

The first measurement was performed to characterise the diffusion of Alexa647 through a nanoporous suspended membrane and compare with the diffusion when there was a membrane with closed pores (section 5.2.1). As mentioned before, it was expected that the presence of pores slowed down the diffusion kinetics of Alexa647 when compared to the diffusion kinetics when there is no membrane.

The second measurement was performed to verify if the diffusion was influenced by changing the conditions of the solution (buffer *vs.* deionised water). The decrease in pH (from the buffer to deionised water) can increase the electrostatic interactions between the dye and the surface of the membrane and consequently slow down the diffusion of the dye (larger time constant value).

Figure 5.3A shows the kinetics of Alexa647 through nanoporous suspended membrane when dissolved in HEPES buffer or deionised water. When Alexa647 was dissolved in buffer (Figure 5.3A, red line) the diffusion was characterised by τ_1 = 25 s and τ_2 = 270 s. This means that it took 270 s for the system to reach the equilibrium (includes all the processes of the dyes crossing the pores and diffuse to the bottom chamber) (Figure 5.3, red line). This second time constant (τ_2) value is larger than the τ_1 because more than one process occurs (diffusion through the pores and diffusing in the bottom chamber) and these processes take longer than flowing and diffusing in the top chamber.

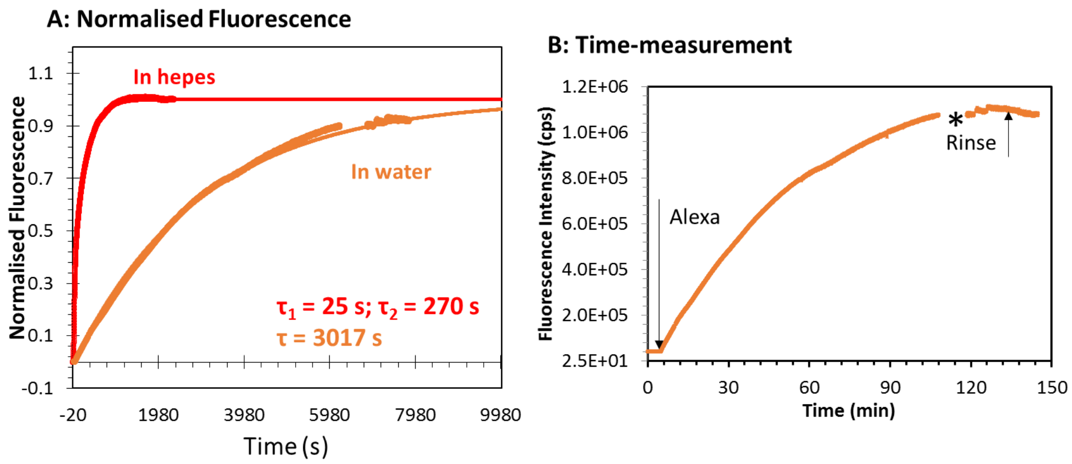

Figure 5.3 – (A) Kinetics of 0.7 µM Alexa647 through a membrane 60 µm thick with 200 nm pore size (uncoated alumina). Alexa647 was dissolved in buffer (HEPES pH 7) (red) or water (orange). Dots – normalised data, full line – fitting of the normalised data. (B) Timecourse measurement of adding and rinsing 0.7 µM Alexa647 (Alexa) dissolved in water through a 60µm thick and 200 nm pore size membrane. (*) measurement was interrupted to perform an angle scan.

Interestingly, when Alexa647 was dissolved in water, the kinetics was slower (Figure 5.3, orange line) and, in this case, a reasonable fit was only obtained when using only one exponential with a time constant. The time constant for diffusion kinetics of Alexa647 when dissolved in water was 3017 s. Figure 5.3B shows the timecourse measurement of Alexa647 dissolved in water and it shows that the fluorescence intensity did not decrease after rinsing the dye with water. This observation suggests that the dye was adsorbed on the nanoporous membranes and for that reason the kinetics was slower.

As shown in Figure 5.3A, the kinetics of Alexa647 in the buffer and water and the calculated time constants were very different. This can be possibly explained by the fact that there were different interactions between the dye and the surface of the nanoporous membrane in the two separated cases. Possibly, the dyes in water were more attracted to the surface – adsorbing – and consequently, the diffusion kinetics was slowed down.

From the results above, we then decided to perform the next experiments with Alexa647 dissolved in buffer to reduce possible events of dye adsorption.

5.2.3 Diffusion of Alexa647 using membranes with different pore sizes

The transport of molecules through pores can also be influenced by physical and chemical properties of the membranes, such as pore size and thickness. For that reason, anodic aluminium oxide (AAO) membranes 60 µm thick and 50 nm pore size, were fabricated in order to compare to the previous diffusion kinetics of Alexa647 through 200 nm pore size membrane (commercially available membrane). The former membrane previously used has an interpore distance of 273 nm and pore size of 200 nm. The AAO membrane fabricated in our laboratory has an interpore distance of 100 nm and pore size of 50 nm (see the comparison in Figure I.33, Appendix E). The pore density of the fabricated AAO membrane (50 nm pore size) is 7 times higher than the 200 nm pore size membrane. However, for the same sample area, the 200 nm pore size membrane has 2 times more cross-sectional area than the fabricated AAO membrane. Therefore, for the same amount of time, 2 times more molecules can cross the pores of the 200 nm pore size membranes. In other words, it was expected that the flux of Alexa647 through 200 nm pore size membrane was 2 times faster (smaller time constant value) than through 50 nm pore size membrane because there is no confinement effect due to the pore and Alexa647 size. Excluded volume in this case does not affect the diffusion of Alexa647 through the pores, because the Alexa647 is much smaller than the pore size. In order to have a 10 % effect, the pore size had to be reduced to 20 nm.

Figure 5.4 shows the diffusion kinetics of Alexa647 through membranes with 200 nm (red line) and 50 nm (blue line) pore sizes. For both cases, τ_1 was fixed to 25 s because the flow and diffusion of the dye on the top chamber is the same for both membranes. The rest of the data was then fitted to a second exponential as mentioned before (section 5.2.1). The second time constants (τ_2) obtained for Alexa647 diffusion through 200 and 50 nm pore size membranes were 270 and 1005 s, respectively.

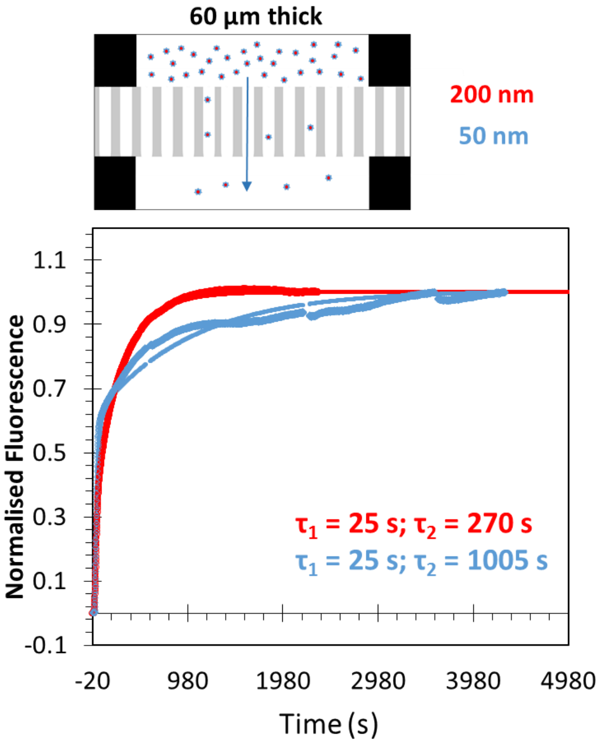

Figure 5.4 – Kinetics of 0.7 µM Alexa647 through a membrane 60 µm thick with pores of 200 nm (red) or 50 nm (blue) (uncoated alumina). Dots – normalised data, full line – fitting of the normalised data.

The kinetics of Alexa647 through 50 nm pore size membrane was 3.7 times slower than when using then larger pore membrane. As expected, the kinetics was slower for smaller pores, but it was even more reduced than the actual relationship between the cross-sectional area and the number of molecules crossing the pores per time that was previously discussed. This discrepancy led us to conclude that were other factors (apart from the pore size) that influenced the diffusion of molecules through membranes with different pore sizes, which deserve further investigation.

5.2.4 *In situ* monitoring of pore transport "switch-on"

As shown in section 5.2.1, when we used a membrane with closed pores (presence of a barrier layer) the molecules were not able to diffuse through the pores. However, if we remove this barrier layer, the pores of the membrane are open – "switch-on" – and the molecules can cross the pores (as shown in the section 5.2.3). In this section, we demonstrate how we can monitor *in situ* the switching-on of the pores by characterising the transport of Alexa647 when the pores are closed and then when the pores start to be open.

The fabrication of AAO membranes finishes with the etching of the unreactive aluminium to expose the nanoporous alumina film (see sections 4.4.1, 5.4.1 and Appendix B). After removing the unreactive aluminium, this side of the membrane does not have open pores due to the presence of the barrier layer obtained under certain anodisation conditions (0.3 M oxalic acid, 40 V, 30 °C) (see the SEM picture of barrier layer at the bottom of the AAO in Figure I.34, Appendix E). To open the pores, the barrier layer side of the membrane needs to be exposed to an etchant. However, if it is exposed for too long, after the barrier layer is removed, the etchant is in contact with the pores so the pores start to be etched as well (pore widening) until the alumina film is completely dissolved. Also, if the barrier layer removal occurs without protecting the other side of the membrane (anodised side) that already has open pores, the etchant widens the pores, which leads to different pore sizes on the two sides of the membrane.

Several approaches for removing the barrier layer have been reported such as ion-milling, or coating the anodised side with a protective (polymer) layer and immersing the whole membrane in an acid solution for certain time.[173–175] The use of a protective polymer was attempted in our laboratory, but it was noticed that the barrier layer removal time was not reproducible and varied for each fabricated membrane. Also, after removal of the protective polymer, some debris remained on the top and inside the pores (see Figure I.35 in Appendix E) in such a way that these membranes were not suitable for the diffusion measurements.

In this section, to switch-on the transport of molecules through the pores two different approaches were used – impedance and fluorescence-ATR measurements (Figure 5.5A and B). For the first approach, the setup and the technique are based on the impedance – electrolyte transport across the membrane. Impedance measurement was simply used to compare with the second method. For that reason, the impedance measurement will not be discussed in depth.

In the first method, a membrane (with barrier layer) was placed between two chambers with salt solutions (see the setup in Figure I.36, Appendix E). Water with salt was added to one chamber, while 5% of phosphoric acid (H_3PO_4) solution (the etchant) with salt (same concentration as the water-salt chamber) was added to the other chamber. The impedance through the membrane was measured (see Materials and Methods section 5.4.4). The etching process to remove the barrier layer took about 60 minutes (the pores were opened when the value theta (°) at a frequency of 10,000 Hz dropped – see Figure 5.5A and Figure I.37 in Appendix E).

In the second method, another membrane with the barrier layer was placed in this ATR suspended membrane device (like in the previous experiments in section 5.2.3). The barrier layer of the membrane was faced up to the top chamber so that the flow cell connected to a peristaltic pump was able to flow Alexa647 continuously. The experiment started by filling the top chamber with Alexa647 in water. Since the barrier layer was present, the Alexa647 was only able to flow in the top chamber. After a stable signal (the concentration of Alexa647 inside the flow cell reached an equilibrium), Alexa647 dissolved in acid (5 % H_3PO_4) was flowed into the flow cell. Water was exchanged by the acid to etch the alumina barrier layer. When the acid started to remove the barrier layer and the pores were open, Alexa647 was able to diffuse through the nanopores and the fluorescence intensity increased because more fluorophores could fill both chambers. At that moment, the acid solution was removed by adding Alexa647 dissolved in water to stop the pore widening.

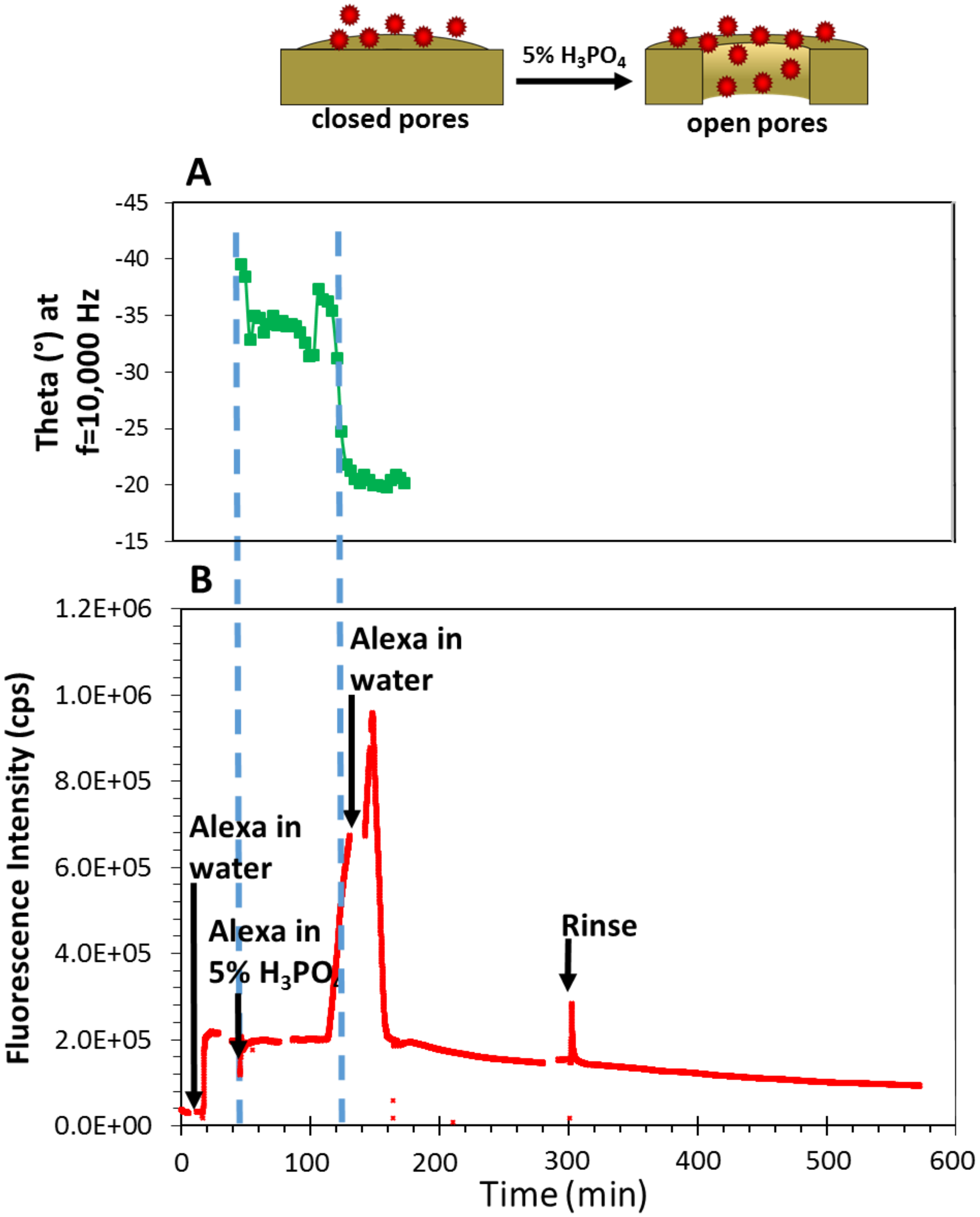

Figure 5.5 – (A) Impedance and (B) ATR measurements of opening pores of a 60 µm thick membrane (uncoated alumina). In the ATR measurement, 0.7 µM Alexa647 (Alexa) was dissolved in water and 5% phosphoric acid (H_3PO_4). The acid solution was used to remove the barrier layer and consequently open the pores of the membrane.

These two methods complemented each other and demonstrated that it takes about 60 minutes to remove the 70 nm thick barrier layer (1.17 nm/min). However, this can vary between 5-10 minutes (6-11 nm of barrier layer), depending on the final thickness of the barrier layer due to variations in the membrane fabrication steps: unreactive aluminium removal is performed in concentrated acid that can unselectively start etching the alumina, removing a few nanometers of the barrier layer. After removing the barrier layer, the pores start to widen, so it is important to stop the barrier removal in order to be able to control the pore size.

The ATR-fluorescence approach showed that coupling the suspending membrane together with the evanescent wave fluorescence enhanced detection enabled monitoring the transport of molecules while pores are being opened – “switching-on”.

5.2.5 *In situ* monitoring of biocatalytic reactions with a nanoporous membrane

Another way to monitor the diffusion through the pores was by detecting species that are generated from inside the pores, instead of being flowed from above.

Enzymes can be immobilised on alumina membranes (as shown in chapter 3). These membranes with immobilised enzymes can be suspended on the flow cell and the conversion of a non-fluorescent substrate to a fluorescent product can be followed *in situ*. In contrast to conventional methods where the substrate is dissolved in solution and needs to find the enzyme, in this system the enzymatic reaction is confined inside the pores and on the surface of the membrane. On the other hand, in this approach, there are more concerns about the flow rate, pore size and the time that the enzyme substrate takes to diffuse to the pores and is converted. For these reasons, *in situ* monitoring of biocatalytic reactions using suspended membranes is very challenging and the different parameters that can influence the feasibility of this system should be investigated.

In chapter 3, the immobilisation of acid phosphatase on pTA-coated alumina membranes was successful. In this chapter, we immobilised the same enzyme on a pTA-coated AAO membrane (60 µm, 50 nm pore size) (immobilisation procedure described in Materials and Methods section 5.4.6). The substrate 9H-(1,3-dichloro-9,9-dimethylacridin-2-one-7-yl) phosphate (DDAO) was used because after acid phosphatase conversion, its product can be excited with the laser of our setup (632.8 nm). DDAO was added to the flow cell, and its conversion was monitored by measuring the fluorescence intensity (Figure 5.6). The diffusion of the substrate and product in this system can be described as shown in

Figure 5.7. The substrate can flow and diffuse on the top chamber. It can also diffuse through the nanopores and in the bottom chamber (there is no flow in the bottom chamber). The substrate is converted and the product is detected when diffusing inside the pores. The fluorescence intensity increased while the enzyme converted the substrate to the product.

As a control, a membrane without any immobilised enzyme was used and DDAO was added into the flow cell to show that there was no fluorescence signal from the substrate itself (blue line in Figure 5.6).

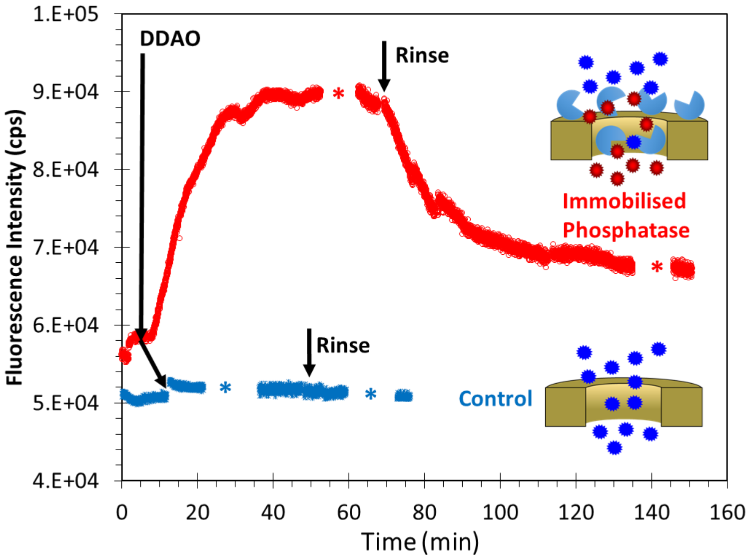

Figure 5.6 – Timecourse measurement of the conversion of 50 µM 9H-(1,3-dichloro-9,9-dimethylacridin-2-one-7-yl) phosphate (DDAO) when acid phosphatase was immobilised (red). Experimental control of DDAO injection with no immobilised enzyme present (blue). (*) measurement was interrupted to perform an angle scan.

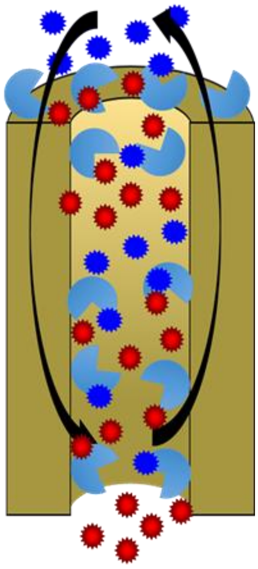

Figure 5.7 – Illustration of the conversion of the substrate in a suspended membrane system. Substrate and product are represented as blue and red dots, respectively. The arrows represent the diffusion direction of the product, where the substrate diffuse on the top and inside the pores and the product is detected.

Ideally, a better scenario would be using a cross-flow cell (Figure 5.8) where there is flow in and out on the top chamber feeding substrate (liquid 1) and a second flow in and out with only buffer (liquid 2) at the bottom. Then, the substrate molecules in the top chamber would diffuse to the bottom chamber and the diffusion would be aided by the setting up of a constant concentration gradient maintained by the constant flowing. This approach was attempted in our laboratory, but several problems such as air bubbles and leaks led to an unsuccessful measurement. A more appropriate design of the flow cell needs to be developed.

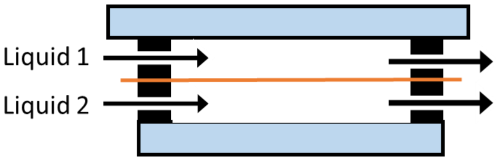

Figure 5.8 – Scheme of a cross-flow cell.

Another aspect that needs to be improved in this setup is the prevention of molecule adsorption on the suspended membranes. In Figure 5.6, it is shown that after rinsing the fluorescence did not decrease/back to the baseline, suggesting that fluorescent product was adsorbed on the membrane. It is important to reduce adsorption events as these influence the kinetics diffusion and activity rate. In the future, it would be interesting to calculate immobilised enzyme activity using the ATR system based on the fluorescence intensity increase and measuring the product concentrations.

5.2.6 *In situ* monitoring of nanopore transport control

The nanopore transport control was also monitored *in situ* by using a responsive grafted polymer. A stimuli-responsive polymer was grafted to a nanoporous AAO membrane (60 μm thick, 50 nm pore size) using SU-8 epoxy resist (see section 5.4.7). This membrane was suspended in a flow cell and mounted on the top of a temperature controller. The grafted polymer, poly(N-isopropylacrylamide) (PNIPAM) can respond to the temperature by becoming water-insoluble at temperatures above the lower critical solubility temperature (LCST) (35 °C) and consequently collapse. Below LCST, the grafted-polymer allows the molecules to pass through the pores. Above LCST, the polymer becomes water-insoluble and collapses to a hydrophobic structure. If there are a high grafting degree and density of polymer brush, the polymer chains become more compact and do not allow the passage of molecules. In case of low grafting density, the polymer can form a hydrogel that can restrict the passage of molecules and when the temperature is raised, the diffusion of molecules is slowed down. For these reasons, it was expected that different kinetics of Alexa647 would be obtained when the diffusion was measured at room temperature or 45 °C. When the temperature was raised, Alexa647 should not be able to diffuse through the pores so the diffusion kinetics of Alexa647 should be faster (smaller time constant value) because the dye can only diffuse in the top chamber.

The experiment started at room temperature (temperature controller set to 25 °C) and Alexa647 was added to the flow cell. The fluorescence intensity increased to 133 times the fluorescence intensity baseline (Figure 5.9). The diffusion kinetics of Alexa647 was also calculated (Figure 5.10 red curve). After rinsing the dye, the temperature controller was set to 45 °C, Alexa647 was again added to the flow cell and the fluorescence intensity increased 13 times relative to the fluorescence intensity baseline and the kinetics was also determined (Figure 5.10 green curve).

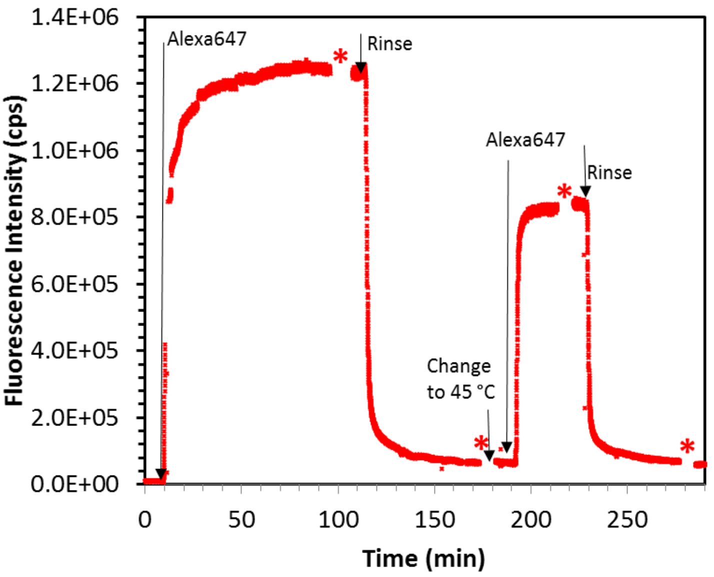

Figure 5.9 – Timecourse measurement of 0.7 µM Alexa647 through a membrane 60 µm thick with pores of 50 nm functionalised with a responsive grafter polymer.

The difference in the increase of fluorescence intensity at room temperature and at 45 °C can be compared with what was observed in the control experiments. As shown in section 5.2.1, the fluorescence intensity did not increase very much when the pores of the membrane were closed because the fluorophores only diffused in the top chamber. In the experiment controls (Figure 5.2A, section 5.2.1), the fluorescence intensity did not increase so much as in this experiment (Figure 5.9). This observation can be due to the fact that in the former experiment, the dyes were actually able to cross the membrane, reach the bottom chamber and be excited. The fluorescence intensity increased even though no molecules reached the bottom chamber but the fluorophores were probably excited by scattered light. In this case, with the increase of temperature, the polymer on the pores of the membrane can restrict the passage of molecules so that the fluorophores diffuse only in the top chamber. As a result, the fluorescence intensity did not increase as much as when the experiment is performed at room temperature.

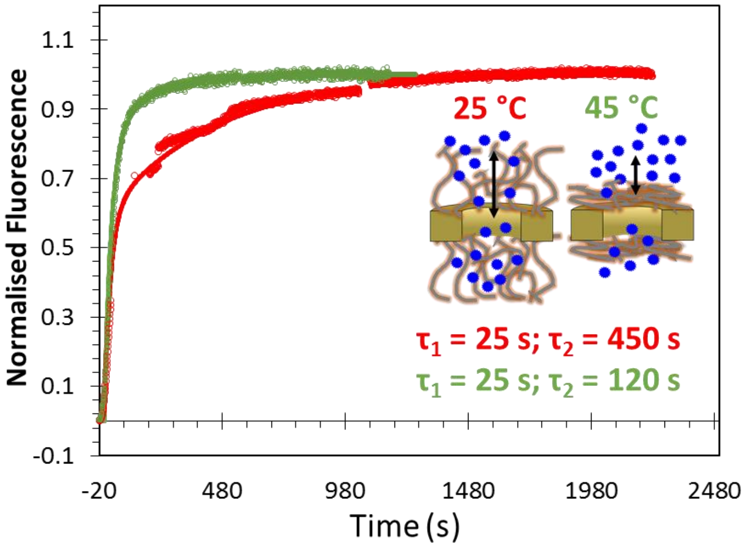

Figure 5.10 – Kinetics of 0.7 µM Alexa647 through a 60 µm thick membrane (50 nm pore size) coated with a responsive polymer at 25°C (red) and 45°C (green). Dots – normalised data, full line – fitting of the normalised data.

Nevertheless, the most important feature of this system is the change of Alexa647 diffusion kinetics when the temperature was increased. The diffusion kinetics at higher temperature approximated to the diffusion kinetics when the pores were closed (first control experiment, section 5.2.1), suggesting that the polymer was able to control the transport of Alexa647 by restricting the pores. The diffusion kinetics at 45°C was not exactly the same as when the pores were closed, meaning that some fluorophores were able to diffuse through the pores.

The time constant calculated for Alexa647 diffusion through 50 nm pore size membrane at room temperature was 450 s. From section 5.2.2, the time constant obtained for 50 nm pore size was 1005 s. The discrepancy between these values was due to the presence of the grafted polymer (that reduced the adsorption events) and because the bottom chamber of this system was smaller than the previous flow cell (in order to fit in the temperature controller device). These two factors led to faster kinetics and consequently smaller time constant value when compared to the previous experiments.

The difference in time constants (120 s [45°C] *versus* 450 s [25°C]) and the difference in the fluorescence intensity increase are evidence that this system with a responsive grafted polymer was able to control the molecular transport and its monitoring could be done *in situ*. Further investigation on this grafted-polymer membrane must be done in order to characterise the pores with this polymer at different temperatures. SEM or atomic force microscopy (AFM) could be used to directly show if the pores were physically closed with the polymer. The use of different molecules with different sizes and charge surface would be useful to show once again the ability to control the transport of molecules. It would also be interesting to monitor *in situ* the reversibility of this system showing the on-demand molecular transport.

5.3 Conclusions

This work demonstrated the potential of a simple ATR optical configuration to be used for measuring diffusion of molecules through a nanoporous membrane. Our work showed that AAO membranes represent a versatile platform with tunable pore size and thickness and the alumina surface can be easily functionalised with a polyphenol coating. This system was used in several applications such as *in situ* monitoring of pore transport “switch-on” and a biocatalytic reaction. It was possible to follow the barrier layer removal and consequently the transport of molecules through the suspended membranes by monitoring the fluorescence intensity increase. The conversion of a substrate to a fluorescence-product by confining the biocatalytic reaction inside the pores of a membrane with immobilised enzymes was also observed. As for last aim of this thesis, the molecular transport was controlled by using responsive grafted-polymer on a suspended membrane and this transport was also monitored *in situ*.

This work can lead to the development of smart devices that can selectively control the transport of molecules. This device could, for example, be used for encapsulating enzymes by functionalising the membranes with polymer brushes (Figure 5.11). These polymers could be able to repel the enzyme to confine it between the membranes and, at the same time, allow enzyme substrate molecules and reaction products to pass through the membranes. This system could also be used in industrial applications for the continuous flow of an enzymatic reaction.

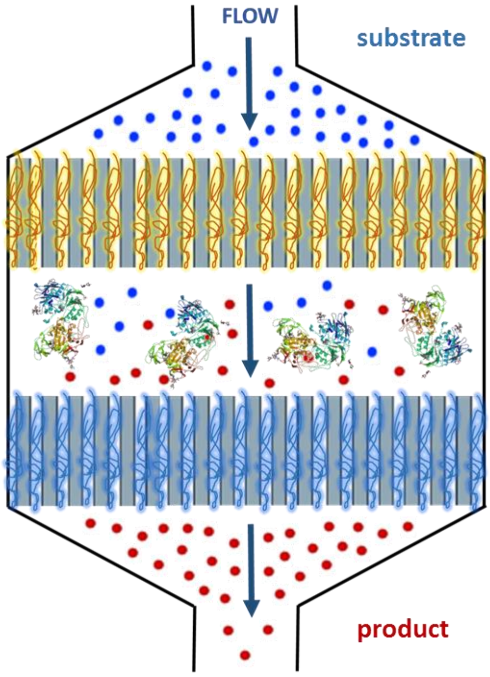

Figure 5.11 – Scheme of suspended membranes for enzyme encapsulation. Polymer brushes on nanoporous AAO membranes could allow substrate and product transport and block the passage to the enzyme. PDB protein structure was used as illustrative representation of protein, blue and red dots represent the substrate and product molecules, respectively.

5.4 Materials and Methods

5.4.1 Fabrication of anodic aluminium oxide (AAO) membranes

Detailed description of the fabrication steps in Appendix B. In this chapter, more development on the fabrication of AAO membranes was performed so a more detailed about the conditions is given.

Sample Preparation

Aluminium discs of high purity (99.999%) were purchased from Advent Materials (UK) and were cut into pieces of 1.5x1.5 cm. To have a smooth flat surface, the samples were mechanically polished using an E W Jackson & Sons LTD (Germany) motorised polisher and a 1200 grade sandpaper. The samples were kept wet throughout the process in order to avoid both scratches and roughness. After the mechanical polishing, the samples were rinsed with deionised water (DIW), ultrasonicated in acetone (Sigma-Aldrich, UK) for 5 minutes, rinsed in ethanol (Sigma-Aldrich, UK) and dried in a nitrogen stream.

In order to give a mirror-like finish to the surface of the sample, an electro-polishing process was performed. Three samples were mounted onto the sample holders' copper tape base unit. Each sample had 0.95 cm^2 exposed to the outside (see Figure I.13, Appendix B). The samples holder and a stir bar were inserted into a small beaker containing the electro-polishing solution (40 v/v % phosphoric acid, H_3PO_4 (Sigma-Aldrich, UK), 38 v/v % ethanol, EtOH (Sigma-Aldrich, UK) and 22 v/v % DIW). The temperature was set to 45 ˚C by using a stir/hot plate (Stuart, heat-stir CC162). The current was set to 1 A which was calculated from sample surface area and the optimum current density of 0.350 A/cm^2 (i.e. 2.85 cm^2 x 0.350 A/cm^2), using a DC power supply (TDK Lambda GEN1500W). Current was applied for 5 minutes and after that, the samples were rinsed with DIW and placed into a glass cell surrounded by a water jacket and coupled with a refrigerating/heating circulator (Julabo F12) on the top of a stirrer (Fisher Scientific, FB15001).

First step of Anodisation

A solution of 0.3 M oxalic acid (Sigma-Aldrich, UK) was prepared and poured into the glass cell and the temperature was set up to 30 ^{0}C. The anodisation lasted 2 hours where the pores became to be ordered at the metal/oxide interface through the time. A thin barrier layer and porous alumina film were formed on the aluminium substrate. During this process, the pores were ordered and parallel at the base but irregular and disordered at the surface (the initial region of pore formation). The solution was discarded, the sample and cell were rinsed with DIW.

Etching the alumina film

In order to remove alumina film to leave an imprint of the ordered pores, the samples were dismantled from the holder and immersed in an etching solution of 1.8 wt % chromium trioxide, CrO_3 (Sigma-Aldrich, UK) and 6 wt % phosphoric acid (H_3PO_4) (VWR, UK) at 70 ^{0}C for 1h. The chromium oxide helps to speed up the etching process as well as the high temperature and the mixture between chromium oxide and phosphoric acid etched only the alumina film, protecting the aluminium substrate from etching. After 1h, the samples were rinsed and sonicated with DIW and remounted onto the samples' holder.

Second step of Anodisation

The samples were placed again into the glass cell with the anodisation solution at 0 °C and the voltage was set to 40 V. The template left after the etching was used to grow a hexagonally ordered porous alumina film during this second anodisation. The temperature was reduced in order to control the growth of the pores and have a denser alumina film. Different times (60, 120 and 210 minutes) were tested during this step in order to calculate the growth rate of the alumina film (see Figure I.15, Appendix B). For 60 μm thick membrane, the anodisation was left for 30 hours.

Etching aluminium

After anodisation, the unreacted aluminium was selectively etched to obtain free-standing AAO films. The pores of the AAO were prevented from coming into contact with the etching solution by securing the AAO/Aluminium samples on the sample holder, where only the aluminium layer was facing the etching solution. Aluminium was etched by immersion in a 3.4 wt % copper (II) chloride, $CuCl_2$ (Sigma-Aldrich, UK) in 1:1 H_2O:10 M hydrochloric acid, HCl (Sigma-Aldrich, UK) solution. The sample was immersed into the solution until some AAO became visible (transparent membrane). Then the sample was transferred to a solution that was diluted with an equal volume of ethanol. This reduces the surface tension and prevents AAO film rupture by the hydrogen produced during acid etching. After the etching was completed, the samples were demounted from the holder and carefully rinsed several times with ethanol and left to dry in air.

Widening the pores

In order to increase the pore size of the sample, an etching solution (8.4 % wt H_3PO_4 in DIW) was prepared. The sample was immersed in this solution for different times (5, 10 and 20 minutes) at room temperature and the etching rate was calculated (see Figure I.17, Appendix B). Further investigation on this matter demonstrated a rate of 0.3 nm/min for a 5 % phosphoric acid solution. To calculate the desirable pore size, the following equation was used: $\emptyset_f = \emptyset_i + 2kt$, where $\emptyset_f$ and $\emptyset_i$ are the final and initial pore size (nm), k the constant rate (in nm/min), and t the time in minutes.

5.4.2 Commercially available AAO membranes (Anodiscs)

Commercially available membranes (Anodiscs) from Whatman (Sigma, UK) were purchased in order to compare the measurements with different pore sizes. Anodiscs with 200 nm pore size and thickness of 60 µm were used. Due to major defects found in commercially available anodiscs with smaller pore sizes – no uniform pore sizes and lateral disorder – we decided to fabricate and use our ones.

5.4.3 Characterisation of AAO membranes

To determine the growth and etching rates and to characterise the AAO membranes morphology, Field-Emission Scanning Electron Microscope (FE-SEM) was used. FE-SEM images were obtained on a Hitachi SU-6600 operated at an accelerating voltage of 5.0 kV and an extraction voltage of 2-1.80 kV. The resolution for each sample varied. ImageJ software was used to analyse the images and calculate the pore size and thicknesses.

5.4.4 Impedance measurements

The fabricated alumina membranes with a barrier layer were placed between two chambers that were clamped together (Figure I.36, Appendix E). In one chamber, a 0.1M potassium sulphate (K_2SO_4) dissolved in water was added and in the other chamber, a 0.1M K_2SO_4 dissolved in 5% of phosphoric acid was added. An electrode was placed in each chamber (working electrode on the acid side) and the resistance/impedance passing through the barrier layer was measured. After a drop in the theta value at a frequency of 10,000 Hz, the membrane was demounted and rinsed with water. By SEM, it was confirmed that the pores were opened on both sides with uniform size (Figure I.38, Appendix E). The measurements over time are plotted in Figure I.37, Appendix E.

5.4.5 ATR measurements

ATR measurements were performed using LASFN9 glass substrates coupled to a prism by optical immersion oil (Cargille, USA) and operating at 632.8 nm (He-Ne laser (PL610P, Polytec, Germany)). One poly(dimethylsiloxante) (PDMS) gasket (0.5 mm height and 11mm diameter) was placed on the glass substrate, the chamber was filled with buffer (10 mM HEPES, 150 mM NaCl pH 7.0), the alumina membrane was placed and another PDMS gasket (0.5mm height and 9 mm diameter) put on the top of the membrane. This chamber was also filled with buffer and the flow cell was then placed on the top of this device. The chambers were filled with water to avoid air bubbles that could be trapped. The liquid cell was connected to a peristaltic pump (Regio, Ismatec, Switzerland) to flow the liquid in and out of the cell (34 µL/min). The whole device was mounted on a rotation stage (Hans Huber AG, Germany) to control the angle of incidence and determine the angle of measurement. The intensity of the light beam reflected at the prism base was detected using a photodiode and a lock-in amplifier (Model 5210, Princeton Applied Research, USA).[172] The emitted fluorescence was collected by a lens (focal length 30mm, numerical aperture of NA=0.2), passed through two bandpass filters (FBF, transmission wavelength 670 nm, 670FS10-25, Andover Corporation Optical Filter USA) and a notch filter (LNF, central stop-band wavelength 632.8nm, XNF-632.8-25.0M, CVI Melles Griot, USA). Timecourse measurements were performed at the angle after TIR (θ_{TIR}+0.5°). A solution of 0.7 µM (0.83 µg/mL) of Alexa647 was prepared and used to characterise the diffusions through the membranes.

5.4.6 Enzyme immobilisation and enzymatic assay using ATR measurement

60 µm thick membrane with 50 nm pores was immersed in 0.01 mg/mL tannic acid (TA) (0.1M bicine buffer 0.6M sodium chloride (NaCl), pH 7.8) for 15 min. The membrane was rinsed with water and immersed in 0.1 mg/mL acid phosphatase solution (0.01 M sodium acetate buffer, 0.1M NaCl, pH 5.2) for 50 min.

The functionalised membrane was placed between the PDMS gaskets filled with 0.01 M sodium acetate buffer pH 5.2. After stabilising the system, 50 µM (21 µg/mL) of 9H-(1,3-dichloro-9,9-dimethylacridin-2-one-7-yl) phosphate (DDAO) dissolved in buffer was added. The increased intensity represented the conversion of the substrate to the product.

As a control, a non-functionalised membrane (no immobilised enzyme) was also placed in this device and DDAO was added to the system. Adding DDAO without any enzyme present did not change the fluorescence signal, showing that the DDAO itself does not have intrinsic fluorescence at that wavelength and proving that the increase in fluorescence in the previous set-up was due to the conversion of the substrate into product only.

5.4.7 Polymer grafting on alumina membranes

An alumina membrane 60 µm thick and 50 nm pore size was spin-coated with an epoxy solution (SU-8 1000 Thinner 1:50, Fisher Scientific, UK) (500 rpm 1 s, 5000 rpm 50 s and then dry in the vacuum oven at 50 °C for 1h). Then a 2.5 wt % poly(N-isopropylacrylamide) (PNIPAM) (polymer supplied by Ulrich Jonas group) (Figure 5.12) solution was spin coated (2000 rpm 60 s) and dried in the vacuum oven at 50 °C for 2h and then cured at 4 J. In dry state at room temperature, the thickness of SU-8 and PNIPAM layers were 1 and 7 nm, respectively.

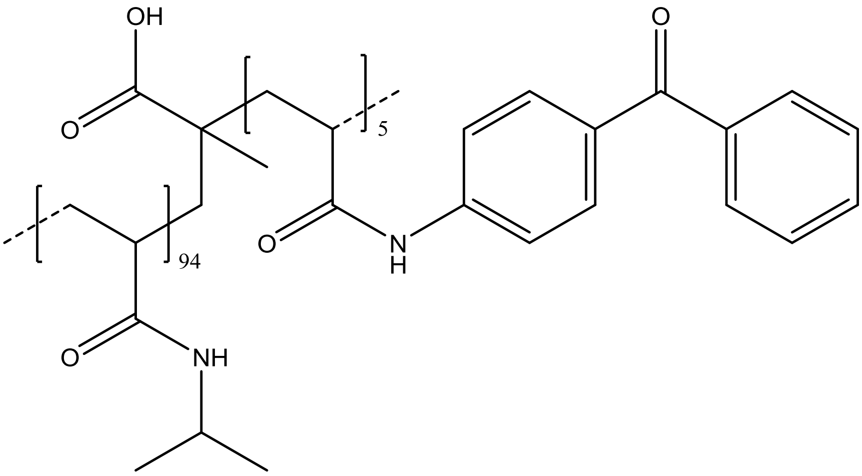

Figure 5.12 – Poly(N-isopropylacrylamide), PNIPAM structure used to functionalise alumina membrane for controlling the transport of Alexa647.

The functionalised membrane was placed between two chambers, with a flow cell on the top, attached to a temperature controller (handmade by Jakub Dostalek group). This device had the chambers a bit smaller than the previous setup, in order to fit all the components to the temperature controller and in the dark box.

6. Conclusions and Future Work

6.1 Summary and Conclusions

This thesis focused on two main topics: development of (1) a new approach to immobilise different proteins and enzymes on various materials and (2) bioinspired, synthetic nanoporous structures for controlling the transport of different molecules through nanopores.

This was accomplished by using polyphenols to functionalise different materials. Polyphenols are available in nature, costless, optical transparent and all in one endows the potential of polyphenol coatings for functionalising different materials, at mild and aqueous conditions, and the coupling of other biomolecules.

Spontaneous polyphenol coatings were used to immobilise a range of proteins and enzymes (avidin, immunoglobulin G, acid phosphatase, chymotrypsin, lactate dehydrogenase (LDH) and horseradish peroxidase (HRP)). The immobilisation was found to be effective on diverse materials, including alumina, polyester, silica, cellulose and stainless steel. The activity of the immobilised enzymes was measured in order to verify the effectiveness of the immobilisation process. The different parameters studied on the coating and immobilisation processes revealed that the pH, the material support and the type of polyphenol molecule are all important factors for the effectiveness of this approach. Polyphenol coatings, especially poly(tannic acid) (pTA) coating, were more effective on immobilising enzymes (higher activities) than polydopamine coating and physisorption method. The activities were 8.5 times higher for HRP and 4 times higher for phosphatase, chymotrypsin and LDH when immobilised on pTA-coated cellulose than when physisorbed. The activities were also higher (up to 2.5 times) for phosphatase and chymotrypsin immobilisation on pTA-coated steel than when physisorbed. The most effective conditions for immobilising phosphatase were observed to be: coating pH of 7 and 7.8 on oxide and polymeric surfaces, respectively; enzyme immobilisation pH of 7, 7.8 and 8.5 for coated alumina, steel and polymeric surfaces, respectively. The pTA coating also helped to maintain the activity of phosphatase when the samples were reused and stored for one week.

In the second part of the thesis, bioinspired and synthetic nanoporous structures for molecular transport were explored. Nanoporous anodic aluminium oxide (AAO) membranes were fabricated with a pore size matching the biological nuclear pore complex. The pore sizes and thickness of AAO membranes were tuned to match the requirements for optical waveguide spectroscopy (OWS), which was used as a tool to measure diffusion of different molecules through the nanoporous membranes. This technique allows the confinement of light at different depths of the pores and thus the differentiation between diffusion inside the pores and diffusion above the nanopores entrances. The polyphenol coating was also used to close the pores and block the diffusion of molecules inside the pores. When the pores were opened, the kinetics at the bottom of the pores were slower (larger time constant values) than in the middle or on the top of the pores. Molecules with different molecular weight were tested and, as expected, larger time constant values were registered for bigger molecules because they diffuse slower. These results were not observed for closed pores because the molecules could not diffuse inside of the pores and the time constant values obtained represented only the molecules flowing in the flow cell. This technique is a new concept of how the molecular diffusion can be characterised, which is important for controlling the transport of biomolecules.

The molecular transport of different molecules can also be controlled by using polymers that control the opening of the pores or that are able to repel only certain and desired molecules. For that, a new configuration and study the diffusion of molecules was carried out. The AAO membranes were suspended (placed between two gaskets) on the flow cell and the diffusion of molecules crossing a nanoporous membrane was characterised. With this work, the simple and versatile combination of ATR and TIR concepts resulted in the *in situ* monitoring of pore transport “switch-on” and biocatalytic reaction (by immobilising an enzyme and follow the conversion of the substrate to fluorescent-product). The nanopore transport control was also achieved by using a responsive polymer that was able to restrict the pore entry and control the transport of molecules.

Overall, the findings provided in this thesis offer a new method to attach molecules on different materials as well as a new strategy to measure molecular transport inside nanopores.

6.2 Future Work

The work presented in this thesis represents a new approach for enzyme immobilisation and a new concept of characterising diffusions through nanoporous membranes. Most of the aims were achieved but many challenges and new ideas can be further developed.

In Chapter 3, the polyphenol coatings were successful on several materials, even though the characterisation of tannic acid and pyrogallol coatings on all the materials was not carried out. It would be interesting to study the type of surface interactions that these molecules have with the material and the enzymes (*e.g.*, solid-state NMR). Only acid phosphatase and chymotrypsin were used to study the pH effect on the immobilisation step. The use of enzymes with different isoelectric points and molecular weights is necessary to find out which biochemical parameter of enzymes influence the immobilisation process with polyphenol molecules. It would be ideal to find a reasonably accurate method to measure the protein loading, in order to compare activity measurements and calculate the percentage of enzyme that was denatured by the immobilisation process. The enzyme conformation on the surface of the materials can be characterised by circular dichroism to assess which conditions during the immobilisation can inactivate the enzyme.

Polyphenols are plant-based molecules so it would be interesting to use tannic acid from different sources and grades, *e.g.*, tea and wine extracts, as well as agricultural waste material to coat different materials. Other polyphenol coating strategies for enzyme immobilisation can be tested, such as multi-layer immobilisation (intercalate enzyme and polyphenol layers in order to have more enzyme immobilised on the surface of the material) and co-immobilisation. Multi-layer approach requires more studies as the substrate access might be restricted, *i.e.*, possible lower activities on the enzyme do not necessarily mean that the enzyme is denatured. Co-immobilisation can be applied in two different ways: (1) through immobilisation of more than one enzyme at the same time, where the electrostatic interactions are even more important depending on the choice of enzymes to be immobilised; or by (2) mixing enzyme and polyphenol solutions and then immersing the material in this solution – the enzyme is crosslinked and covalently immobilised on the surface of the material.

It was shown in chapter 3 that the activity of immobilised phosphatase on coated-alumina was maintained over one week. At longer times, the enzyme activity dropped to less than 8%. Different conditions of storage such as freezing the samples at -20 or -80 °C, or varying the conditions of defrosting, can be performed in order to assess whether the activity is kept.

In chapter 4, OWS was used to characterise the diffusion of molecules through nanopores. However, OWS can also be used on the research topic of chapter 3 by measuring the amount of proteins immobilised on alumina based on the refractive index change. The amount of enzyme on the surface can be controlled by changing the pH, concentration and time of the immobilisation, and this can be monitored *in situ*.

For controlling the molecular transport through nanopores, other grafted-polymer should be tested. It is desirable to find a responsive polymer that is able to functionalise the nanoporous AAO membranes and, at the same time, control the transport of biomolecules. This polymerisation work can be done on flat alumina surfaces to mimic the nanoporous AAO membranes and characterise the polymer layer in terms of structure, surface density, thickness, wettability, protein adsorption and responsiveness by performing ellipsometry and contact angle measurements. It would be interesting to show the reversibility of the system to either allow or block the transport of different molecules on-demand.

In the last chapter, the diffusion of molecules through a nanoporous suspended membrane was characterised. However, different flow speeds, membranes with different thicknesses and pore sizes and cross-flow setup should be tested. This will allow to better understand the different processes occurring during the diffusion of molecules through nanoporous membranes.

Further research on the points stated above would accomplish a better understanding on how molecular transport can be controlled, as well as how to mimic biological systems.

7. References

1. Zhou, Z. & Hartmann, M. Recent Progress in Biocatalysis with Enzymes Immobilized on Mesoporous Hosts. *Top. Catal.* 55**,** 16–18**,** 1081–1100 (2012).

2. Secundo, F. Conformational changes of enzymes upon immobilisation. *Chem. Soc. Rev.* 42**,** 15**,** 6250–61 (2013).

3. Sheldon, R. a & van Pelt, S. Enzyme immobilisation in biocatalysis: why, what and how. *Chem. Soc. Rev.* 42**,** 15**,** 6223–35 (2013).

4. Sheldon, R. A. Enzyme Immobilization: The Quest for Optimum Performance. *Adv. Synth. Catal.* 349**,** 8–9**,** 1289–1307 (2007).

5. Hartmann, M. & Kostrov, X. Immobilization of enzymes on porous silicas--benefits and challenges. *Chem. Soc. Rev.* 42**,** 15**,** 6277–89 (2013).

6. Sassolas, A., Blum, L. J. & Leca-Bouvier, B. D. Immobilization strategies to develop enzymatic biosensors. *Biotechnol. Adv.* 30**,** 3**,** 489–511 (2012).

7. Shahidi, S. & Wiener, J. Surface Modification Methods for Improving the Dyeability of Textile Fabrics. *Intech* 34–54 (2013).

8. McCreery, R. L. & Bergren, A. J. Surface Functionalization in the Nanoscale Domain. in *Nanofabrication* (eds. Stepanova, M. & Dew, S.) 163–190 (Springer Vienna, 2012).

9. Chan, C.-M., Ko, T.-M. & Hiraoka, H. Polymer surface modification by plasmas and photons. *Surf. Sci. Rep.* 24**,** 1–2**,** 1–54 (1996).

10. Tuominen, M. & Lahti, J. The Effects of Corona and Flame Treatment : Part 1 . PE-LD Coated Packaging Board. *11th TAPPI Eur. PLACE Conf.* 15 (2007).

11. Ozdemir, M., Yurteri, C. U. & Sadikoglu, H. Physical Polymer Surface Modification Methods and Applications in Food Packaging Polymers. *Crit. Rev. Food Sci. Nutr.* 39**,** 5**,** 457–477 (1999).

12. Govindarajan, T. & Shandas, R. A Survey of Surface Modification Techniques for Next-Generation Shape Memory Polymer Stent Devices. *Polymers (Basel).* 6**,** 9**,** 2309–2331 (2014).

13. Nath, N., Hyun, J., Ma, H. & Chilkoti, A. Surface engineering strategies for control of protein and cell interactions. *Surf. Sci.* 570**,** 1–2**,** 98–110 (2004).

14. Hermanson, G. T. Chapter 3 – The Reactions of Bioconjugation. in *Bioconjugate Techniques* 229–258 (2013).

15. Sartori, G., Ballini, R., Bigi, F., Bosica, G., Maggi, R. & Righi, P. Protection (and deprotection) of functional groups in organic synthesis by heterogeneous catalysis. *Chem. Rev.* 104**,** 1**,** 199–250 (2004).

16. Desmet, T., Morent, R., Geyter, N. De, Leys, C., Schacht, E. & Dubruel, P. Nonthermal Plasma Technology as a Versatile Strategy for Polymeric Biomaterials Surface Modification: A Review. *Biomacromolecules* 10**,** 9**,** 2351–2378 (2009).

17. Xu, Z., Wan, L. & Huang, X. *Surface Enginnering of Polymer Membranes*. (Springer, 2009).

18. Shrikrishnan, S., Sankaran, K. & Lakshminarayanan, V. Electrochemical Impedance Analysis of Adsorption and Enzyme Kinetics of Calf Intestine Alkaline Phosphatase on SAM-Modified Gold Electrode. *J. Phys. Chem. C* 116**,** 30**,** 16030–16037 (2012).

19. Pujari, S. P., Scheres, L., Marcelis, A. T. M. & Zuilhof, H. Covalent surface modification of oxide surfaces. *Angew. Chemie - Int. Ed.* 53**,** 25**,** 6322–6356 (2014).

20. Gray, C. J., Weissenborn, M. J., Eyers, C. E. & Flitsch, S. L. Enzymatic reactions on immobilised substrates. *Chem. Soc. Rev.* 42**,** 15**,** 6378–405 (2013).

21. Decher, G. & Hong, J.-D. Buildup of ultrathin multilayer films by a self-assembly process, 1 consecutive adsorption of anionic and cationic bipolar amphiphiles on charged surfaces. *Makromol. Chemie. Macromol. Symp.* 46**,** 1**,** 321–327 (1991).

22. Decher, G. & Hong, J. D. Buildup of Ultrathin Multilayer Films by a Self-

Assembly Process: II. Consecutive Adsorption of Anionic and Cationic Bipolar Amphiphiles and Polyelectrolytes on Charged Surfaces. *Berichte der Bunsengesellschaft für Phys. Chemie* 95**,** 11**,** 1430–1434 (1991).

23. Lazzara, T. D., Lau, K. H. A., Knoll, W., Janshoff, A. & Steinem, C. Macromolecular shape and interactions in layer-by-layer assemblies within cylindrical nanopores. *Beilstein J. Nanotechnol.* 3**,** 475–84 (2012).

24. Hermanson, G. T. Chapter 11 – (Strept)avidin–Biotin Systems. in *Bioconjugate Techniques* 465–505 (2013).

25. Al-Warhi, T. I., Al-Hazimi, H. M. A. & El-Faham, A. Recent development in peptide coupling reagents. *J. Saudi Chem. Soc.* 16**,** 2**,** 97–116 (2012).

26. Hermanson, G. T. Chapter 2 – Functional Targets for Bioconjugation. in *Bioconjugate Techniques* 127–228 (2013).

27. Hermanson, G. T. Chapter 4 – Zero-Length Crosslinkers. in *Bioconjugate Techniques* 259–273 (2013).

28. Hermanson, G. T. Chapter 15 – Immobilization of Ligands on Chromatography Supports. in *Bioconjugate Techniques* 589–740 (2013).

29. Gundlach, H. G., Moore, S. & Stein, W. H. The reaction of iodoacetate with methionine. *J. Biol. Chem.* 234**,** 7**,** (1959).

30. Hermanson, G. T. Chapter 13 – Silane Coupling Agents. in *Bioconjugate Techniques* 535–548 (2013).

31. Lazzara, T. D., Lau, K. H. A., Abou-Kandil, A. I., Caminade, A. M., Majoral, J.-P. P. & Knoll, W. Polyelectrolyte layer-by-layer deposition in cylindrical nanopores. *ACS Nano* 4**,** 7**,** 3909–3920 (2010).

32. Andrade, J. D. & Hlady, V. Protein adsorption and materials biocompatibility: A tutorial review and suggested hypotheses. in *Biopolymers/Non-Exclusion HPLC* 1–63 (Springer Berlin Heidelberg, 1986).

33. Kondo, A. & Fukuda, H. Effects of Adsorption Conditions on Kinetics of Protein

Adsorption and Conformational Changes at Ultrafine Silica Particles. *J. Colloid Interface Sci.* 198**,** 1**,** 34–41 (1998).

34. Rivera, J. G. & Messersmith, P. B. Polydopamine-assisted immobilization of trypsin onto monolithic structures for protein digestion. *J. Sep. Sci.* 35**,** 12**,** 1514–1520 (2012).

35. Lee, H., Rho, J. & Messersmith, P. B. Facile Conjugation of Biomolecules onto Surfaces via Mussel Adhesive Protein Inspired Coatings. *Adv. Mater.* 21**,** 4**,** 431–434 (2009).

36. Conte, M. P., Lau, K. H. A. & Ulijn, R. V. Biocatalytic Self-Assembly Using Reversible and Irreversible Enzyme Immobilization. *ACS Appl. Mater. Interfaces* 9**,** 4**,** 3266–3271 (2017).

37. Waite, J. H. & Qin, X. Polyphosphoprotein from the Adhesive Pads of Mytilus edulis †. *Biochemistry* 40**,** 9**,** 2887–2893 (2001).

38. Lee, H., Dellatore, S. M., Miller, W. M. & Messersmith, P. B. Mussel-Inspired Surface Chemistry for Multifunctional Coatings. *Science* 318**,** 5849**,** 426–430 (2007).

39. Jeon, J. R., Kim, J. H. & Chang, Y. S. Enzymatic polymerization of plant-derived phenols for material-independent and multifunctional coating. *J. Mater. Chem. B* 1**,** 47**,** 6501–6509 (2013).

40. Ye, Q., Zhou, F. & Liu, W. Bioinspired catecholic chemistry for surface modification. *Chem. Soc. Rev.* 40**,** 7**,** 4244–58 (2011).

41. Lee, H., Scherer, N. F. & Messersmith, P. B. Single-molecule mechanics of mussel adhesion. *Proc. Natl. Acad. Sci. U. S. A.* 103**,** 35**,** 12999–13003 (2006).

42. Della Vecchia, N. F., Avolio, R., Alfè, M., Errico, M. E., Napolitano, A. & D'Ischia, M. Building-block diversity in polydopamine underpins a multifunctional eumelanin-type platform tunable through a quinone control point. *Adv. Funct. Mater.* 23**,** 10**,** 1331–1340 (2013).

43. Postma, A., Yan, Y., Wang, Y., Zelikin, A. N., Tjipto, E. & Caruso, F. Self-

polymerization of dopamine as a versatile and robust technique to prepare polymer capsules. *Chem. Mater.* 21**,** 14**,** 3042–3044 (2009).

44. Ball, V. Impedance spectroscopy and zeta potential titration of dopa-melanin films produced by oxidation of dopamine. *Colloids Surfaces A Physicochem. Eng. Asp.* 363**,** 1–3**,** 92–97 (2010).

45. Liebscher, J., Mrówczyński, R., Scheidt, H. a, Filip, C., Hădade, N. D., Turcu, R., Bende, A. & Beck, S. Structure of polydopamine: a never-ending story? *Langmuir* 29**,** 33**,** 10539–48 (2013).

46. Ejima, H., Richardson, J. J. & Caruso, F. Phenolic film engineering for template-mediated microcapsule preparation. *Polym. J.* 46**,** 8**,** 452–459 (2014).

47. Ham, H. O., Liu, Z., Lau, K. H. A., Lee, H. & Messersmith, P. B. Facile DNA immobilization on surfaces through a catecholamine polymer. *Angew. Chem. Int. Ed. Engl.* 50**,** 3**,** 732–6 (2011).

48. Black, K. C. L., Yi, J., Rivera, J. G., Zelasko-Leon, D. C. & Messersmith, P. B. Polydopamine-enabled surface functionalization of gold nanorods for cancer cell-targeted imaging and photothermal therapy. *Nanomedicine (Lond).* 8**,** 1**,** 17–28 (2013).

49. Lee, B. P., Messersmith, P. B., Israelachvili, J. N. & Waite, J. H. Mussel-Inspired Adhesives and Coatings. *Annu. Rev. Mater. Res.* 41**,** 99–132 (2011).

50. Dreyer, D. R., Miller, D. J., Freeman, B. D., Paul, D. R. & Bielawski, C. W. Elucidating the structure of poly(dopamine). *Langmuir* 28**,** 15**,** 6428–6435 (2012).

51. Zhang, Z., Zhang, Z., Li, J. & Lai, Y. Polydopamine-coated separator for high-performance lithium-sulfur batteries. *J. Solid State Electrochem.* 19**,** 6**,** 1709–1715 (2015).

52. Cui, J., Ju, Y., Liang, K., Ejima, H., Lörcher, S., Gause, K. T., Richardson, J. J. & Caruso, F. Nanoscale engineering of low-fouling surfaces through polydopamine immobilisation of zwitterionic peptides. *Soft Matter* 10**,** 15**,** 2656–63 (2014).

53. Ball, V. Physicochemical perspective on ‘polydopamine’ and

‘poly(catecholamine)’ films for their applications in biomaterial coatings (Review). *Biointerphases* 9**,** 3**,** 30801 (2014).

54. Salazar, P., Martín, M. & González-Mora, J. L. Polydopamine-modified surfaces in biosensor applications. in *Polymer science: research advances, pratical applications and educational aspects* 1**,** 385–396 (2007).

55. Sileika, T. S., Barrett, D. G., Zhang, R., Lau, K. H. A. & Messersmith, P. B. Colorless multifunctional coatings inspired by polyphenols found in tea, chocolate, and wine. *Angew. Chemie - Int. Ed.* 52**,** 41**,** 10766–10770 (2013).

56. Barrett, D. G., Sileika, T. S. & Messersmith, P. B. Molecular diversity in phenolic and polyphenolic precursors of tannin-inspired nanocoatings. *Chem. Commun. (Camb).* 50**,** 55**,** 7265–8 (2014).

57. Wheeler, S. R. Tea and Tannis. *Science* 204**,** 4388**,** 6–7 (1979).

58. Ejima, H., Richardson, J. J., Liang, K., Best, J. P., van Koeverden, M. P., Such, G. K., Cui, J. & Caruso, F. One-step assembly of coordination complexes for versatile film and particle engineering. *Science* 341**,** 6142**,** 154–7 (2013).

59. Lewis, G. P. the Importance of Ionization in the Activity of Sympathomimetic Amines. *Br. J. Pharmacol. Chemother.* 9**,** 4**,** 488–493 (1954).

60. Banerjee, I., Pangule, R. C. & Kane, R. S. Antifouling Coatings: Recent Developments in the Design of Surfaces That Prevent Fouling by Proteins, Bacteria, and Marine Organisms. *Adv. Mater.* 23**,** 6**,** 690–718 (2011).

61. Krishnan, S., Weinman, C. J. & Ober, C. K. Advances in polymers for anti-biofouling surfaces. *Journal of Materials Chemistry* 18**,** 29**,** 3405 (2008).

62. Damodaran, V. B. & Murthy, N. S. Bio-inspired strategies for designing antifouling biomaterials. *Biomater. Res.* 20**,** 1**,** 18 (2016).

63. Utrata-Wesolek, A. Antifouling surfaces in medical application. *Polimery* 58**,** 9**,** 685–695 (2013).

64. Lin, P., Lin, C. W., Mansour, R. & Gu, F. Improving biocompatibility by surface

modification techniques on implantable bioelectronics. *Biosens. Bioelectron.* 47**,** 451–460 (2013).

65. Ostuni, E., Chapman, R. G., Liang, M. N., Meluleni, G., Pier, G., Ingber, D. E. & Whitesides, G. M. Self-Assembled Monolayers That Resist the Adsorption of Cells. *Langmuir* 17**,** 7**,** 6336–6343 (2001).

66. Herrwerth, S., Eck, W., Reinhardt, S. & Grunze, M. Factors that determine the protein resistance of oligoether self-assembled monolayers - Internal hydrophilicity, terminal hydrophilicity, and lateral packing density. *J. Am. Chem. Soc.* 125**,** 31**,** 9359–9366 (2003).

67. Dalsin, J. L. & Messersmith, P. B. Bioinspired antifouling polymers. *Mater. Today* 8**,** 9**,** 38–46 (2005).

68. Nuzzo, R. G. Biomaterials: Stable antifouling surfaces. *Nat. Mater.* 2**,** 4**,** 207–208 (2003).

69. Zhou, F. *Antifouling Surfaces and Materials*. *Antifouling Surfaces and Materials* (Springer Berlin Heidelberg, 2015).

70. Chapman, R. G., Ostuni, E., Takayama, S., Holmlin, R. E., Yan, L. & Whitesides, G. M. Surveying for surfaces that resist the adsorption of proteins. *Journal of the American Chemical Society* 122**,** 34**,** 8303–8304 (2000).

71. Milner, S. T. Polymer Brushes. *Science* 251**,** 4996**,** 905–914 (1991).

72. Jain, P., Baker, G. L. & Bruening, M. L. Applications of Polymer Brushes in Protein Analysis and Purification. *Annu. Rev. Anal. Chem.* 2**,** 1**,** 387–408 (2009).

73. Minko, S. Grafting on Solid Surfaces: ‘Grafting to’ and ‘Grafting from’ Methods. in *Polymer Surfaces and Interfaces* (ed. Stamm, M.) 215–234 (Springer-Verlag Berlin Heidelberg, 2008).

74. Magin, C. M., Cooper, S. P. & Brennan, A. B. Non-toxic antifouling strategies. *Mater. Today* 13**,** 4**,** 36–44 (2010).

75. Peng, T. & Cheng, Y. Temperature-responsive permeability of porous PNIPAAm-

g-PE membranes. *J. Appl. Polym. Sci.* 70, 11, 2133–2142 (1998).

76. Liu, R., Liao, P., Liu, J. & Feng, P. Responsive Polymer-Coated Mesoporous Silica as a pH-Sensitive Nanocarrier for Controlled Release. *Langmuir* 27, 6, 3095–3099 (2011).

77. Marshall, N., Sontag, S. K. & Locklin, J. Surface-initiated polymerization of conjugated polymers. *Chem. Commun. (Camb).* 47, 20, 5681–9 (2011).

78. Nady, N., Franssen, M. C. R., Zuilhof, H., Eldin, M. S. M., Boom, R. & Schroën, K. Modification methods for poly(arylsulfone) membranes: A mini-review focusing on surface modification. *Desalination* 275, 1–3, 1–9 (2011).

79. Chu, E. & Sidorenko, A. Surface reconstruction by a 'grafting through' approach: polyacrylamide grafted onto chitosan film. *Langmuir* 29, 40, 12585–92 (2013).

80. Enright, T. P., Hagaman, D., Kokoruz, M., Coleman, N. & Sidorenko, A. Gradient and patterned polymer brushes by photoinitiated 'grafting through' approach. *J. Polym. Sci. Part B Polym. Phys.* 48, 14, 1616–1622 (2010).

81. Henze, M., Mädge, D., Prucker, O. & Rühe, J. 'Grafting Through': Mechanistic Aspects of Radical Polymerization Reactions with Surface-Attached Monomers. *Macromolecules* 47, 9, 2929–2937 (2014).

82. Hanefeld, U., Gardossi, L. & Magner, E. Understanding enzyme immobilisation. *Chem. Soc. Rev.* 38, 2, 453–68 (2009).

83. Nelson, D. & Cox, M. *Lehninger principles of biochemistry. W. H. Freeman; 4th Ed.* (John Wiley & Sons Inc., 2005).

84. Guerrier-Takada, C., Gardiner, K., Marsh, T., Pace, N. & Altman, S. The RNA moiety of ribonuclease P is the catalytic subunit of the enzyme. *Cell* 35, December, 849–857 (1983).

85. Datta, S., Christena, L. R. & Rajaram, Y. R. S. Enzyme immobilization: an overview on techniques and support materials. *3 Biotech* 3, 1, 1–9 (2012).

86. Tran, D. N. & Balkus, K. J. Perspective of Recent Progress in Immobilization of

Enzymes. *ACS Catal.* 1**,** 8**,** 956–968 (2011).

87. Scouten, W. H., Luong, J. H. T. & Brown, R. S. Enzyme or protein immobilization techniques for applications in biosensor design. *Tibtech* 13**,** 178–185 (1995).

88. Nelson, J. M. & Griffin, E. G. ADSORPTION OF INVERTASE. *J. Am. Chem. Soc.* 38**,** 5**,** 1109–1115 (1916).

89. Magner, E. Immobilisation of enzymes on mesoporous silicate materials. *Chem. Soc. Rev.* 42**,** 15**,** 6213–22 (2013).

90. Cao, L. *Carrier-bound Immobilized Enzymes: Principles, Application and Design*. (Wiley-VCH Verlag GmbH & Co. KGaA, 2006).

91. Betancor, L. & Luckarift, H. R. Bioinspired enzyme encapsulation for biocatalysis. *Trends Biotechnol.* 26**,** 10**,** 566–72 (2008).

92. Cao, L., Langen, L. Van & Sheldon, R. a. Immobilised enzymes: carrier-bound or carrier-free? *Curr. Opin. Biotechnol.* 14**,** 4**,** 387–394 (2003).

93. Barbosa, O., Torres, R., Ortiz, C., Berenguer-Murcia, A., Rodrigues, R. C. & Fernandez-Lafuente, R. Heterofunctional supports in enzyme immobilization: from traditional immobilization protocols to opportunities in tuning enzyme properties. *Biomacromolecules* 14**,** 8**,** 2433–62 (2013).

94. Fried, D. I., Brieler, F. J. & Fröba, M. Designing Inorganic Porous Materials for Enzyme Adsorption and Applications in Biocatalysis. *ChemCatChem* 5**,** 4**,** 862–884 (2013).

95. Mays, T. J. A new classification of pore sizes. *Stud. Surf. Sci. Catal.* 160**,** 57–62 (2007).

96. Bayne, L., Ulijn, R. V & Halling, P. J. Effect of pore size on the performance of immobilised enzymes. *Chem. Soc. Rev.* 42**,** 23**,** 9000–10 (2013).

97. Bernal, C., Sierra, L. & Mesa, M. Application of Hierarchical Porous Silica with a Stable Large Porosity for β-Galactosidase Immobilization. *ChemCatChem* 3**,** 12**,** 1948–1954 (2011).

98. Md Jani, A. M., Losic, D. & Voelcker, N. H. Nanoporous anodic aluminium oxide: Advances in surface engineering and emerging applications. *Prog. Mater. Sci.* 58**,** 5**,** 636–704 (2013).

99. Kumeria, T., Santos, A. & Losic, D. Nanoporous anodic alumina platforms: engineered surface chemistry and structure for optical sensing applications. *Sensors (Basel).* 14**,** 7**,** 11878–918 (2014).

100. Stroeve, P. & Ileri, N. Biotechnical and other applications of nanoporous membranes. *Trends Biotechnol.* 29**,** 6**,** 259–66 (2011).

101. Sang, L.-C., Vinu, A. & Coppens, M.-O. General description of the adsorption of proteins at their iso-electric point in nanoporous materials. *Langmuir* 27**,** 22**,** 13828–37 (2011).

102. Wang, Q., Peng, L., Du, Y., Xu, J., Cai, Y., Feng, Q., Huang, F. & Wei, Q. Fabrication of hydrophilic nanoporous PMMA/O-MMT composite microfibrous membrane and its use in enzyme immobilization. *J. Porous Mater.* 20**,** 3**,** 457–464 (2012).

103. Biradar, A. A., Biradar, A. V. & Asefa, T. Entrapping Flavin-Containing Monooxygenase on Corrugated Silica Nanospheres and their Recyclable Biocatalytic Activities. *ChemCatChem* 2**,** 8**,** 1004–1010 (2010).

104. Chen, L. Y., Fujita, T. & Chen, M. W. Biofunctionalized nanoporous gold for electrochemical biosensors. *Electrochim. Acta* 67**,** 1–5 (2012).

105. Lu, D., Cardiel, J., Cao, G. & Shen, A. Q. Nanoporous scaffold with immobilized enzymes during flow-induced gelation for sensitive H(2)O(2) biosensing. *Adv. Mater.* 22**,** 25**,** 2809–13 (2010).

106. Kao, K.-C., Lin, T.-S. & Mou, C.-Y. Enhanced Activity and Stability of Lysozyme by Immobilization in the Matching Nanochannels of Mesoporous Silica Nanoparticles. *J. Phys. Chem. C* 118**,** 13**,** 6734–6743 (2014).

107. Itoh, T., Shimomura, T., Hasegawa, Y., Mizuguchi, J., Hanaoka, T., Hayashi, a., Yamaguchi, a., Teramae, N., Ono, M. & Mizukami, F. Assembly of an artificial

biomembrane by encapsulation of an enzyme, formaldehyde dehydrogenase, into the nanoporous-walled silica nanotube–inorganic composite membrane. *J. Mater. Chem.* 21**,** 1**,** 251 (2011).

108. Matsuura, S., Baba, T., Chiba, M. & Tsunoda, T. Nanoporous scaffold for DNA polymerase: pore-size optimisation of mesoporous silica for DNA amplification. *RSC Adv.* 4**,** 49**,** 25920 (2014).

109. Kim, M. Il, Shim, J., Li, T., Lee, J. & Park, H. G. Fabrication of nanoporous nanocomposites entrapping Fe3O4 magnetic nanoparticles and oxidases for colorimetric biosensing. *Chemistry* 17**,** 38**,** 10700–7 (2011).

110. Laveille, P., Phuoc, L. T., Drone, J., Fajula, F., Renard, G. & Galarneau, a. Oxidation reactions using air as oxidant thanks to silica nanoreactors containing GOx/peroxidases bienzymatic systems. *Catal. Today* 157**,** 1–4**,** 94–100 (2010).

111. Zhang, C., Hu, C., Zhao, Y., Möller, M., Yan, K. & Zhu, X. Encapsulation of laccase in silica colloidosomes for catalysis in organic media. *Langmuir* 29**,** 49**,** 15457–62 (2013).

112. Hartmann, M. Ordered Mesoporous Materials for Bioadsorption and Biocatalysis. *Chem. Mater.* 17**,** 18**,** 4577–4593 (2005).

113. O'Connor, E. F., Paterson, S. & de la Rica, R. Naked-eye detection as a universal approach to lower the limit of detection of enzyme-linked immunoassays. *Anal. Bioanal. Chem.* 408**,** 13**,** 3389–3393 (2016).

114. Zhou, Z. & Hartmann, M. Progress in enzyme immobilization in ordered mesoporous materials and related applications. *Chem. Soc. Rev.* 42**,** 9**,** 3894–912 (2013).

115. Kim, J., Jia, H. & Wang, P. Challenges in biocatalysis for enzyme-based biofuel cells. *Biotechnol. Adv.* 24**,** 3**,** 296–308 (2006).

116. Bezerra, C. S., de Farias Lemos, C. M. G., de Sousa, M. & Gonçalves, L. R. B. Enzyme immobilization onto renewable polymeric matrixes: Past, present, and future trends. *J. Appl. Polym. Sci.* 132**,** 26**,** 42125(1)-42125(15) (2015).

117. Brena, B., González-Pombo, P. & Batista-Viera, F. Immobilization of enzymes: a literature survey. *Methods Mol. Biol.* 1051**,** 15–31 (2013).

118. Liston, E. M., Martinu, L. & Wertheimer, M. R. Plasma surface modification of polymers for improved adhesion: a critical review. *J. Adhes. Sci. Technol.* 7**,** 10**,** 1091–1127 (1993).

119. Liu, Y. Application of Surface Functionalization for designing novel interfaces and materials. (University of Delaware, 2014).

120. Sperling, R. A. & Parak, W. J. Surface modification, functionalization and bioconjugation of colloidal inorganic nanoparticles. *Philos. Trans. R. Soc. A Math. Phys. Eng. Sci.* 368**,** 1915**,** 1333–1383 (2010).

121. Dreyer, D. R., Miller, D. J., Freeman, B. D., Paul, D. R. & Bielawski, C. W. Perspectives on poly(dopamine). *Chem. Sci.* 4**,** 10**,** 3796 (2013).

122. Rahim, M. A., Ejima, H., Cho, K. L., Kempe, K., Müllner, M., Best, J. P. & Caruso, F. Coordination-Driven Multistep Assembly of Metal–Polyphenol Films and Capsules. *Chem. Mater.* 26**,** 4**,** 1645–1653 (2014).

123. Hong, S., Yeom, J., Song, I. T., Kang, S. M., Lee, H. & Lee, H. Pyrogallol 2-Aminoethane: A Plant Flavonoid-Inspired Molecule for Material-Independent Surface Chemistry. *Adv. Mater. Interfaces* 1**,** 4**,** 1400113 (2014).

124. Boath, A. S., Grussu, D., Stewart, D. & McDougall, G. J. Berry Polyphenols Inhibit Digestive Enzymes: a Source of Potential Health Benefits? *Food Dig.* 3**,** 1–3**,** 1–7 (2012).

125. Yang, H., Landis-Piwowar, K., H. Chan, T. & P. Dou, Q. Green Tea Polyphenols as Proteasome Inhibitors: Implication in Chemoprevention. *Curr. Cancer Drug Targets* 11**,** 3**,** 296–306 (2011).

126. Roseiro, L. B., Rauter, A. P. & Serralheiro, M. L. M. Polyphenols as acetylcholinesterase inhibitors : Structural specificity and impact on human disease. *Nutr. Aging* 1**,** 99–111 (2012).

127. Lilly, M. D. Enzymes immobilized to cellulose. *Methods Enzymol.* 44**,** C**,** 46–53

(1976).

128. Kang, C.-K. & Lee, Y.-S. The surface modification of stainless steel and the correlation between the surface properties and protein adsorption. *J. Mater. Sci. Mater. Med.* 18**,** 7**,** 1389–1398 (2007).

129. Zhang, L., Cao, X., Wang, L., Zhao, X., Zhang, S. & Wang, P. Printed microwells with highly stable thin-film enzyme coatings for point-of-care multiplex bioassay of blood samples. *Analyst* 140**,** 12**,** 4105–4113 (2015).

130. Cao, R., Tian, W. & Shen, W. Polysaccharides as protectants for paper-based analytical devices with antibody. *Talanta* 165**,** December 2016**,** 357–363 (2017).

131. Smith, D. M., Wang, Z., Kazi, A., Li, L.-H., Chan, T.-H. & Dou, Q. P. Synthetic analogs of green tea polyphenols as proteasome inhibitors. *Mol. Med.* 8**,** 7**,** 382–392 (2002).

132. Nam, S., Smith, D. M. & P. Dou, Q. Ester Bond-containing Tea Polyphenols Potently Inhibit Proteasome Activity in Vitro and in Vivo. *J. Biol. Chem.* 276**,** 16**,** 13322–13330 (2001).

133. Gulicovski, J. J., Čerović, L. S. & Milonjić, S. K. Point of Zero Charge and Isoelectric Point of Alumina. *Mater. Manuf. Process.* 23**,** 6**,** 615–619 (2008).

134. Chen, P., Mitsui, T., Farmer, D. B., Golovchenko, J., Gordon, R. G. & Branton, D. Atomic layer deposition to fine-tune the surface properties and diameters of fabricated nanopores. *Nano Lett.* 4**,** 7**,** 1333–1337 (2004).

135. Rescigno, A., Bruyneel, F., Padiglia, A., Sollai, F., Salis, A., Marchand-Brynaert, J. & Sanjust, E. Structure–activity relationships of various amino-hydroxy-benzenesulfonic acids and sulfonamides as tyrosinase substrates. *Biochim. Biophys. Acta - Gen. Subj.* 1810**,** 8**,** 799–807 (2011).

136. Kowalczyk, S. W., Blosser, T. R. & Dekker, C. Biomimetic nanopores: learning from and about nature. *Trends Biotechnol.* 29**,** 12**,** 607–614 (2011).

137. Lowe, A. R., Siegel, J. J., Kalab, P., Siu, M., Weis, K. & Liphardt, J. T. Selectivity mechanism of the nuclear pore complex characterized by single cargo tracking.

Nature 467, 7315, 600–3 (2010).

138. Raices, M. & D'Angelo, M. A. Nuclear pore complex composition: a new regulator of tissue-specific and developmental functions. *Nat Rev Mol Cell Biol* 13, 11, 687–699 (2012).

139. Li, J., Yu, D. & Zhao, Q. Solid-state nanopore-based DNA single molecule detection and sequencing. *Microchim. Acta* 183, 3, 941–953 (2016).

140. Chmelik, C., Heinke, L., Valiullin, R. & Kärger, J. A new view of diffusion in nanoporous materials. *Chemie-Ingenieur-Technik* 82, 6, 779–804 (2010).

141. Howorka, S. & Siwy, Z. Nanopore analytics: sensing of single molecules. *Chem. Soc. Rev.* 38, 8, 2360–2384 (2009).

142. Liu, N., Yang, Z., Ou, X., Wei, B., Zhang, J., Jia, Y. & Xia, F. Nanopore-based analysis of biochemical species. *Microchim. Acta* 183, 3, 955–963 (2016).

143. Gadsby, D. C. Ion channels versus ion pumps: the principal difference, in principle. *Nat. Rev. Mol. Cell Biol.* 10, 5, 344–352 (2009).

144. Savariar, E. N., Krishnamoorthy, K. & Thayumanavan, S. Molecular discrimination inside polymer nanotubules. *Nat. Nanotechnol.* 3, 2, 112–117 (2008).

145. Caspi, Y., Zbaida, D., Cohen, H. & Elbaum, M. Synthetic mimic of selective transport through the nuclear pore complex. *Nano Lett.* 8, 11, 3728–3734 (2008).

146. Friedman, A. K., Baker, L. A., Shulga, N., Goldfarb, D. S., Wente, S. R., Sali, A., Cowburn, D., Nakano, S. & Kusaka, H. Synthetic hydrogel mimics of the nuclear pore complex display selectivity dependent on FG-repeat concentration and electrostatics. *Soft Matter* 12, 47, 9477–9484 (2016).

147. Jovanovic-Talisman, T., Tetenbaum-Novatt, J., McKenney, A. S., Zilman, A., Peters, R., Rout, M. P. & Chait, B. T. Artificial nanopores that mimic the transport selectivity of the nuclear pore complex. *Nature* 457, 7232, 1023–1027 (2009).

148. Kowalczyk, S. W., Kapinos, L., Blosser, T. R., Magalhães, T., van Nies, P., Lim,

R. Y. H. & Dekker, C. Single-molecule transport across an individual biomimetic nuclear pore complex. *Nat. Nanotechnol.* 6**,** 7**,** 433–438 (2011).

149. Bird, S. P. & Baker, L. A. An Abiotic Analogue of the Nuclear Pore Complex Hydrogel. *Biomacromolecules* 12**,** 9**,** 3119–3123 (2011).

150. Li, S. J., Xia, N., Yuan, B. Q., Du, W. M., Sun, Z. F. & Zhou, B. Bin. A novel DNA sensor using a sandwich format by electrochemical measurement of marker ion fluxes across nanoporous alumina membrane. *Electrochim. Acta* 159**,** 234–241 (2015).

151. Rutkowska, A., Freedman, K., Skalkowska, J., Kim, M. J., Edel, J. B. & Albrecht, T. Electrodeposition and bipolar effects in metallized nanopores and their use in the detection of insulin. *Anal. Chem.* 87**,** 4**,** 2337–2344 (2015).

152. Chmelik, C. & Kärger, J. Imaging of transient guest profiles in nanoporous host materials: A new experimental technique to study intra-crystalline diffusion. *Adsorption* 16**,** 6**,** 515–523 (2010).

153. Heinke, L., Chmelik, C., Kortunov, P., Ruthven, D. M., Shah, D. B., Vasenkov, S. & Kärger, J. Application of interference microscopy and IR microscopy for characterizing and investigating mass transport nanoporous materials. *Chem. Eng. Technol.* 30**,** 8**,** 995–1002 (2007).

154. Hohlbein, J., Steinhart, M., Schiene-Fischer, C., Benda, A., Hof, M. & Hübner, C. G. Confined diffusion in ordered nanoporous alumina membranes. *Small* 3**,** 3**,** 380–385 (2007).

155. Kumeria, T., Yu, J., Alsawat, M., Kurkuri, M. D., Santos, A., Abell, A. D. & Losic, D. Photoswitchable membranes based on peptide-modified nanoporous anodic alumina: Toward smart membranes for on-demand molecular transport. *Adv. Mater.* 27**,** 19**,** 3019–3024 (2015).

156. Lau, K. H. A., Tan, L.-S., Tamada, K., Sander, M. S. & Knoll, W. Highly Sensitive Detection of Processes Occurring Inside Nanoporous Anodic Alumina Templates: A Waveguide Optical Study. *J. Phys. Chem. B* 108**,** 30**,** 10812–10818 (2004).

157. Lau, K. H. A., Cameron, P., Duran, H., Abou-Kandil, A. I. & Knoll, W. Nanoporous Thin Films as Highly Versatile and Sensitive Waveguide Biosensors. in *Surface Design: Applications in Bioscience and Nanotechnology* 383–401 (2009).

158. Kim, D. H., Lau, K. H. A., Joo, W., Peng, J., Jeong, U., Hawker, C. J., Kim, J. K., Russell, T. P. & Knoll, W. An optical waveguide study on the nanopore formation in block copolymer/homopolymer thin films by selective solvent swelling. *J. Phys. Chem. B* 110**,** 31**,** 15381–15388 (2006).

159. Fan, Y., Hotta, K., Yamaguchi, A. & Teramae, N. Enhanced fluorescence in a nanoporous waveguide and its quantitative analysis. *Opt. Express* 20**,** 12**,** 12850–9 (2012).

160. Gu, Y., Xu, S., Li, H., Wang, S., Cong, M., Lombardi, J. R. & Xu, W. Waveguide-Enhanced Surface Plasmons for Ultrasensitive SERS Detection. *J. Phys. Chem. Lett.* 4**,** 18**,** 3153–3157 (2013).

161. Fan, Y., Hotta, K., Yamaguchi, A., Ding, Y., He, Y., Teramae, N., Sun, S. & Ma, H. Highly sensitive real-time detection of DNA hybridization by using nanoporous waveguide fluorescence spectroscopy. *Appl. Phys. Lett.* 105**,** 3**,** 0–4 (2014).

162. Azzaroni, O. & Lau, K. H. A. Layer-by-Layer Assemblies in Nanoporous Templates: Nano-Organized Design and Applications of Soft Nanotechnology. *Soft Matter* 7**,** 19**,** 8709–8724 (2011).

163. Lau, K. H. A., Duran, H. & Knoll, W. In situ characterization of N-carboxy anhydride polymerization in nanoporous anodic alumina. *J. Phys. Chem. B* 113**,** 10**,** 3179–89 (2009).

164. Knoll, W. Interfaces and thin film as seen by bound electromagnetic waves. *Annu. Rev. Phys. Chem.* 49**,** 569–638 (1998).

165. Antun Peic, Daniel Staff, Thomas Risbridger, Bernhard Menges, L.M. Peter, A.B. Walker & P.J. Cameron. Real-Time Optical Waveguide Measurements of Dye Adsorption into Nanocrystalline TiO2 Films with Relevance to Dye-Sensitized Solar Cells. *J. Phys. Chem. C(JPCC)* 115**,** 613–619 (2011).

166. Worm, J. Winspall, version 3.02, http://www.mpip-mainz.mpg.de/groups/knoll/software. (2009).

167. Saltzman, W. M., Radomsky, M. L., Whaley, K. J. & Cone, R. A. Antibody diffusion in human cervical mucus. *Biophys. J.* 66**,** 2 Pt 1**,** 508–15 (1994).

168. Culbertson, C. T., Jacobson, S. C. & Michael Ramsey, J. Diffusion coefficient measurements in microfluidic devices. *Talanta* 56**,** 2**,** 365–373 (2002).

169. Göhler, A., André, S., Kaltner, H., Sauer, M., Gabius, H. J. & Doose, S. Hydrodynamic properties of human adhesion/growth-regulatory galectins studied by fluorescence correlation spectroscopy. *Biophys. J.* 98**,** 12**,** 3044–3053 (2010).

170. Li, J., Czajkowsky, D. M., Li, X. & Shao, Z. Fast immuno-labeling by electrophoretically driven infiltration for intact tissue imaging. *Sci. Rep.* 5**,** April**,** 10640 (2015).

171. Jackson, M. Diffusion and Brownian motion. in *Molecular and Cellular Biophysics* 142–166 (Cambridge University Press, 2014).

172. Dostalek, J., Huang, C. J. & Knoll, W. *Surface plasmon resonance-based biosensors*. *Surface Design: Applications in Bioscience and Nanotechnology* (Wiley-VCH Verlag GmbH & Co. KGaA, 2009).

173. Thormann, A., Teuscher, N., Pfannmöller, M., Rothe, U. & Heilmann, A. Nanoporous aluminum oxide membranes for filtration and biofunctionalization. *Small* 3**,** 6**,** 1032–40 (2007).

174. Schwirn, K., Lee, W., Hillebrand, R., Steinhart, M., Nielsch, K. & Gösele, U. Self-ordered anodic aluminum oxide formed by H2SO4 hard anodization. *ACS Nano* 2**,** 2**,** 302–10 (2008).

175. Lee, W., Ji, R., Gösele, U. & Nielsch, K. Fast fabrication of long-range ordered porous alumina membranes by hard anodization. *Nat. Mater.* 5**,** September**,** 741–747 (2006).

176. Wu, Z. & Chen, G. Q. Axial diffusion effect on concentration dispersion. *Int. J. Heat Mass Transf.* 84**,** 571–577 (2015).

177. Vedel, S., Hovad, E. & Bruus, H. Time-dependent Taylor–Aris dispersion of an initial point concentration. *J. Fluid Mech.* 752**,** 107–122 (2014).

178. Lam, Y. C., Chen, X. & Yang, C. Depthwise averaging approach to cross-stream mixing in a pressure-driven microchannel flow. *Microfluid. Nanofluidics* 1**,** 3**,** 218–226 (2005).

I. Appendices

A. Surface characterisation of different surfaces and materials and experimental details of activity measurements

Surface characterisation of coated materials

Solid materials were immersed in 0.03 mg/mL tannic acid (TA) pH 7.8 or 8.5 for 1h. The unreactive molecules were washed away by sonicating the coating buffer (without TA) for 15 min, the samples were rinsed with deionised water. The presence of poly(tannic acid) (pTA) coating was characterised by immersing the samples in a 20 mM silver nitrate (Sigma-Aldrich, UK) solution overnight, contact angle and/or X-ray photoelectron spectroscopy (XPS). The silver nitrate staining process resulted in the deposition of a dark metallic silver film on the surface, through a redox reaction between silver ions and the polyphenolic coating.

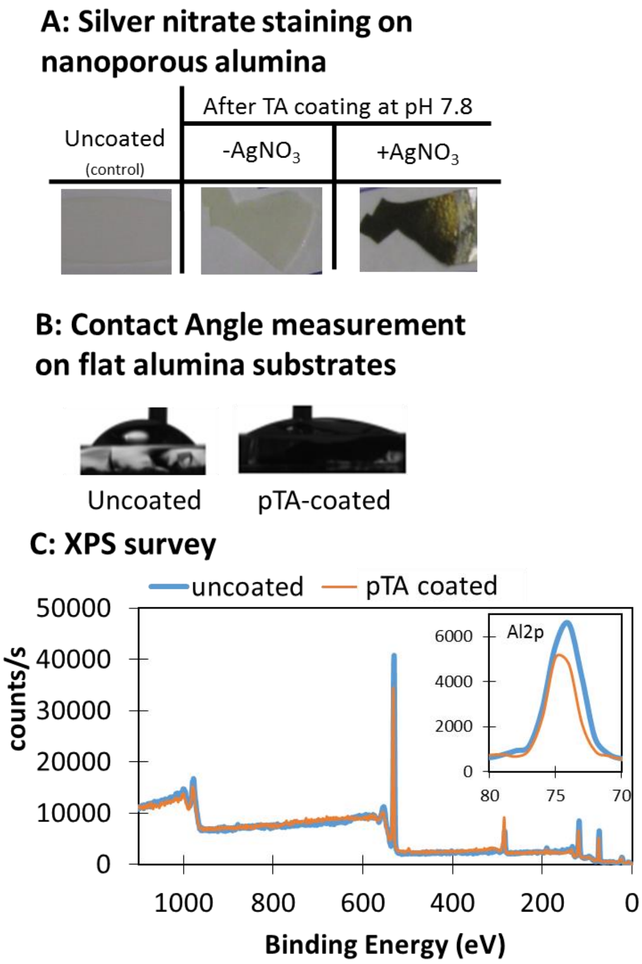

Figure I.1 – Surface characterisation of alumina surfaces after poly(tannic acid) (pTA) coating at pH 7.8. (A) Uncoated alumina and pTA-coated nanoporous alumina before (-) and after (+) silver nitrate ($AgNO_3$) staining. (B) Contact angle measurements with water of uncoated and pTA-coated flat alumina substrates. (C) XPS surveys of uncoated and pTA-coated alumina. The change in Al2p signal after the pTA coating is highlighted in the inset graph.

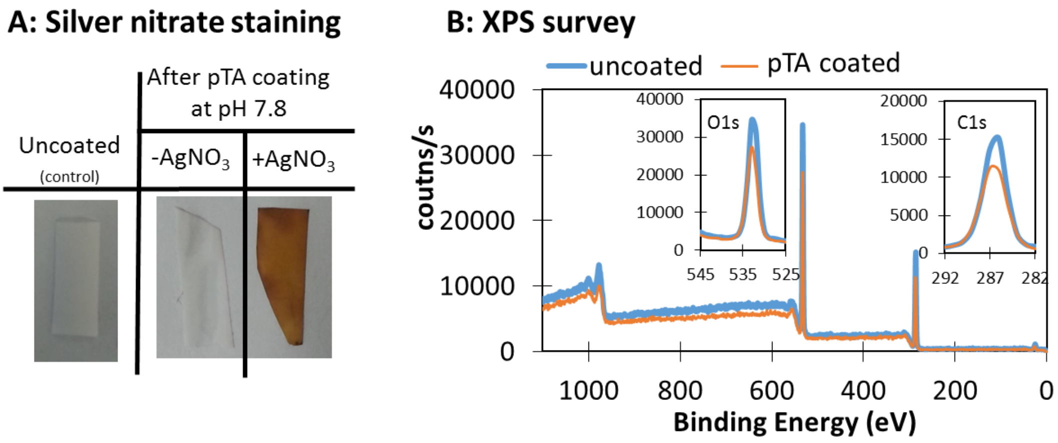

Figure I.2 – Surface characterisation of cellulose surfaces after poly(tannic acid) (pTA) coating at pH 7.8. (A) Uncoated cellulose and pTA-coated nanoporous alumina before (-) and after (+) silver nitrate (AgNO$_3$) staining. (B) XPS surveys of uncoated and pTA-coated cellulose. The change on O1s and C1s signals after the pTA coating is highlighted in the inset graphs.

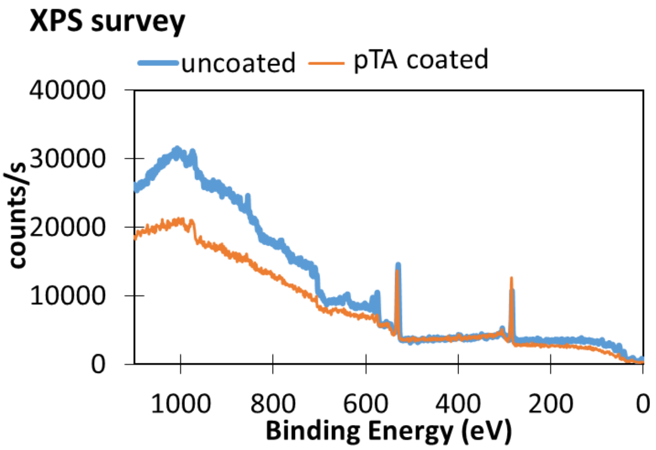

Figure I.3 – Surface characterisation of stainless steel surfaces after poly(tannic acid) (pTA) coating at pH 8.5. XPS surveys of uncoated and TA-coated steel.

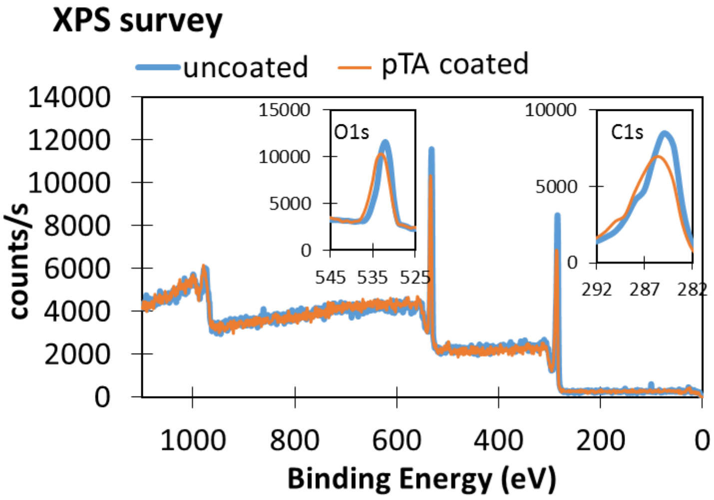

Figure I.4 – Surface characterisation of polyester surfaces after poly(tannic acid) (pTA) coating at pH 8.5. XPS surveys of uncoated and TA-coated polyester. The change on O1s and C1s signals after the TA coating is highlighted in the inset graphs.

Figure I.5 – Uncoated and poly(tannic acid) (pTA) coated silica nanoporous particles (without (-) silver nitrate ($AgNO_3$) staining).

Apparatus used to measure the activities of immobilised enzymes

Cuvette holders were used to perform measurements using a UV-Vis spectrophotometer. The solid supports were fixed inside the cuvette, parallel to the measurement light path (Figure I.6). A stir bar was also inserted into the cuvette to help the diffusion of the substrate to the immobilised enzyme and product in solution.

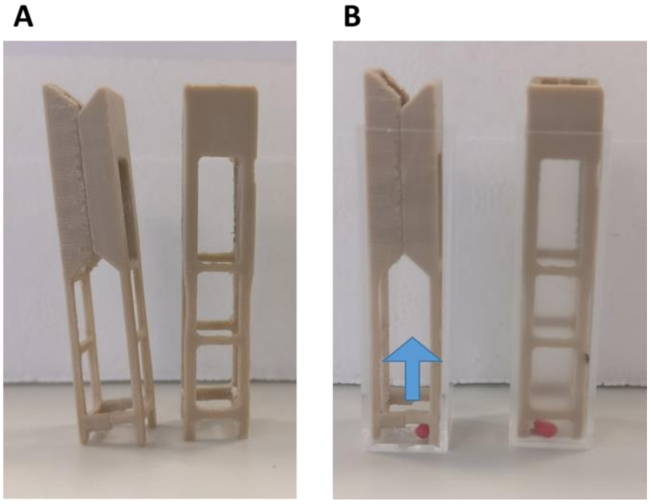

Figure I.6 – (A) Holders to fix solid supports. (B) Holders inside the cuvettes to be parallel to the measurement light path (blue arrow).

Physisorbed enzyme activities on cellulose and steel

Several enzymes and proteins were immobilised on uncoated cellulose and steel as a control. The activities of the physisorbed enzymes were measured and are stated in Table I.1. These activities were then normalised to value 1 in order to compare to the activities of the enzymes immobilised via pTA, pPG and pDA coatings.

Table I.1 – Activity values measured for physisorbed enzyme on cellulose and steel. The activities were normalised to value 1 to compare with other immobilisation methods.

Enzyme/Material	**Physisorbed enzyme activity (nmoles/min.m^2) on**	
	cellulose	steel
Acid phosphatase	80	192
Chymotrypsin	2.1	3.1
Horseradish peroxidase (HRP)	2.1	0.1
Lactate dehydrogenase (LDH)	0.5	0.7
Ig+anti-IgG-HRP	13	37
Avidin+Biotin-HRP	3.8	2.3

Phosphatase immobilisation on silica nanoporous particles

The activity of immobilised phosphatase on silica was measured using a spectrofluorometer. Suspended silica nanoparticles interfere with the UV-Vis spectrophotometer measurement, so a 96-well plate and a fluorometer were used. 120 mg of functionalised particles were suspended in 1.2 mL buffer (1 M sodium acetate pH 5.2) and 350 µL of suspended particles were added to each well. 17.5 µL of 10 mM methylumbelliferyl phosphate disodium salt, 4-MUP was added to the particles and the enzyme assay was followed using a λ_{ex} = 326 nm and λ_{em} = 447 nm, fluorescence spectrophotometer (Cary Eclipse, UK). The activity was determined by the slope of the fluorescence intensity *versus* time. The pTA-coated phosphatase activity was normalised against the physisorbed phosphatase activity (Figure I.7).

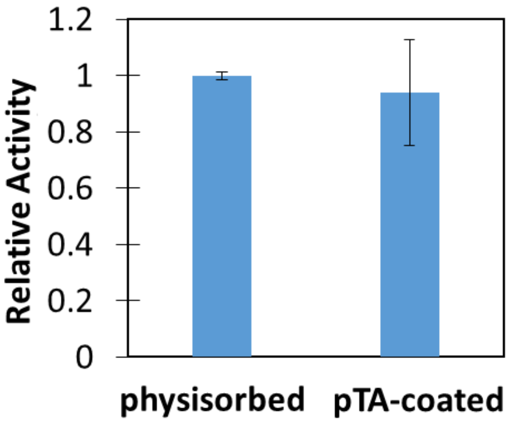

Figure I.7 – Relative activity of fluorescence assay of physisorbed and immobilised phosphatase on uncoated and pTA-coated silica particles.

Surface characterisation of coated materials for phosphatase immobilisation using X-ray photoelectron spectroscopy (XPS)

XPS measurements were performed to evaluate the amount of coating and enzyme on the surface of different materials. The pH effect during the coating of cellulose and alumina was assessed by calculating the ratio N1s/C1s of the pTA and pDA coatings (Figure I.8). The thicknesses of the enzyme layers and pTA/pDA coatings on alumina and steel were also determined by XPS (Figure I.10).

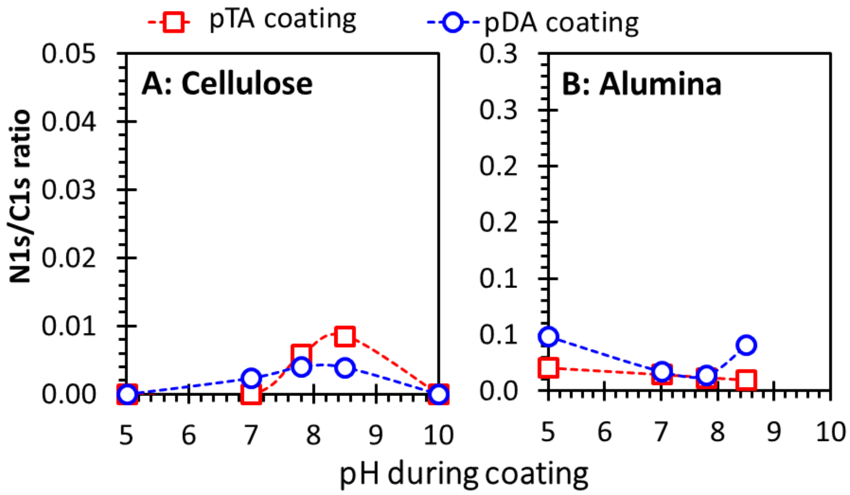

Figure I.8 – Coating pH effect on the ratio N1s/C1s signals of poly(tannic acid) (pTA) and polydopamine (pDA) coatings on (A) cellulose and (B) alumina.

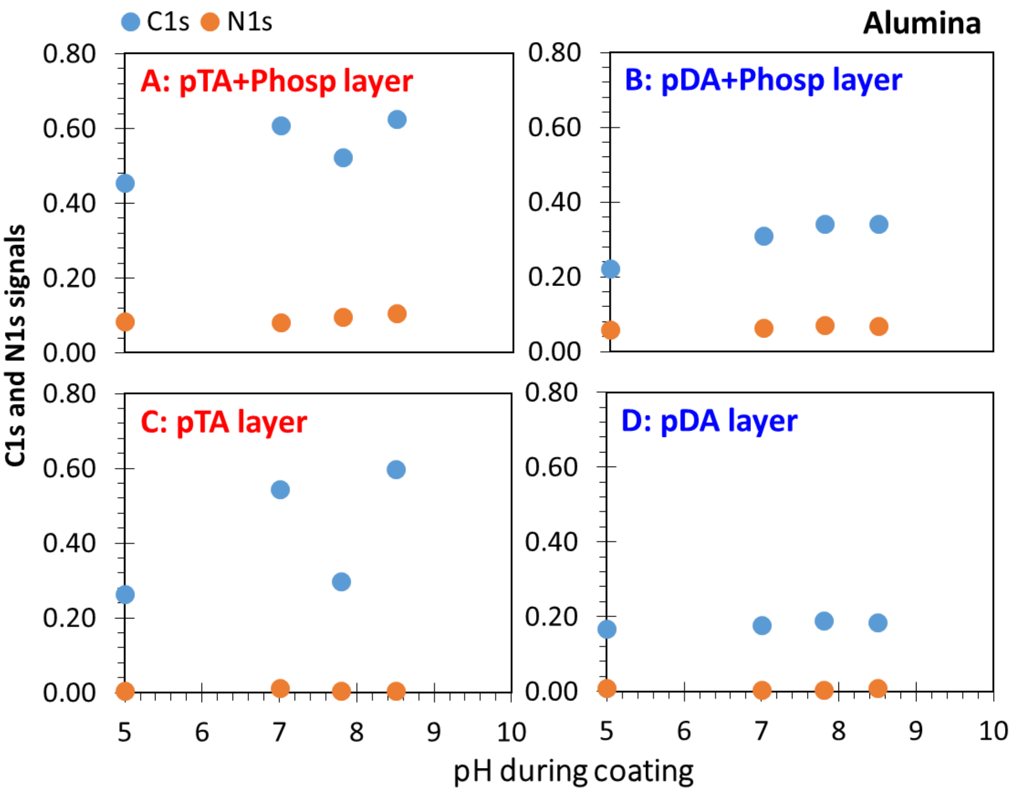

Figure I.9 – C1s and N1s signals from phosphatase layer on (A) pTA- and (B) pDA-coated alumina. The C1s and N1s signals of (C) pTA and (D) pDA coating.

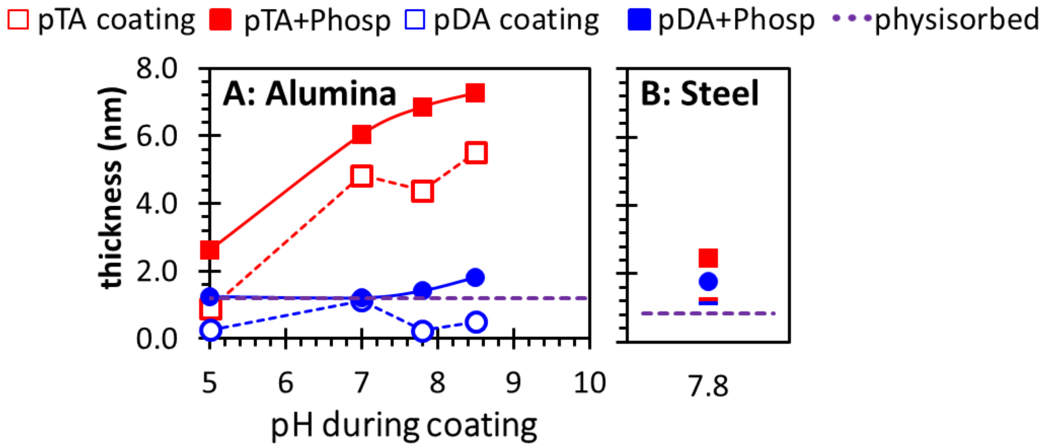

Figure I.10 – Coating pH effect on the thickness of poly(tannic acid) (pTA), polydopamine (pDA) coatings and phosphatase (Phosp) on (A) alumina and (B) steel.

The pH effect during the immobilisation of phosphatase was also assessed by measuring the thickness of the enzyme when it was immobilised on uncoated- and pTA/pDA-coated alumina (Figure I.11).

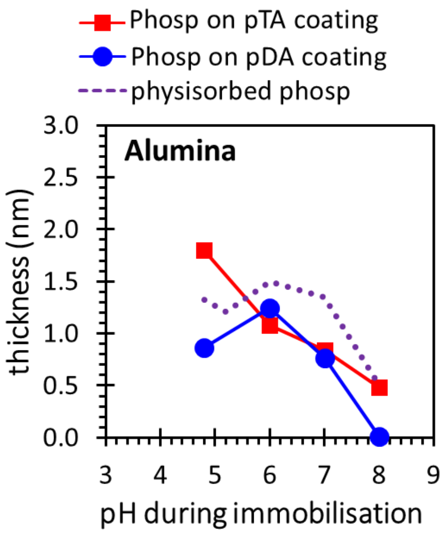

Figure I.11 – Immobilisation pH effect on the thickness of phosphatase (Phosp) layer on poly(tannic acid) (pTA)- and polydopamine (pDA)- coated and uncoated alumina.

Chymotrypsin immobilisation and pH effect during immobilisation

Chymotrypsin was also immobilised on uncoated- and pTA/pDA/pPG-coated alumina and its activities were measured. The pH effect during the immobilisation of chymotrypsin was compared to the activities of immobilised phosphatase.

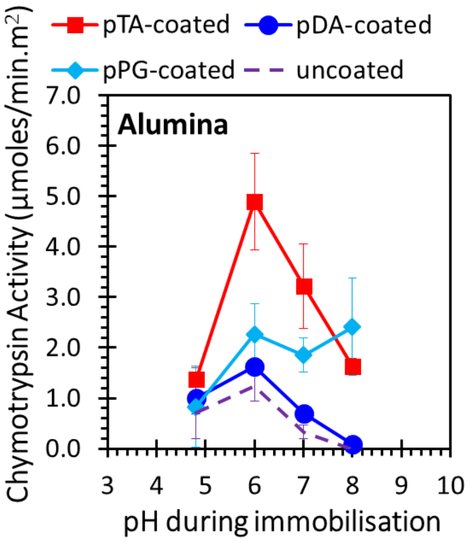

Figure I.12 – Immobilisation pH effect on the activity of immobilised chymotrypsin on poly(tannic acid) (pTA), polydopamine (pDA), poly(pyrogallol) (pPG)-coated and uncoated alumina.

Reuse and storage of immobilised phosphatase on uncoated- and pTA/pDA-coated alumina

After immobilising phosphatase on uncoated- and pTA/pDA-coated alumina, the activity of the enzyme was measured (Table I.2). These activity values were normalised to 100 % in order to be compared to the activities measured in the following hours and days.

Table I.2 – Immobilised phosphatase activity on poly(tannic acid) (pTA)-, polydopamine (pDA)- and uncoated-alumina measured in the first use.

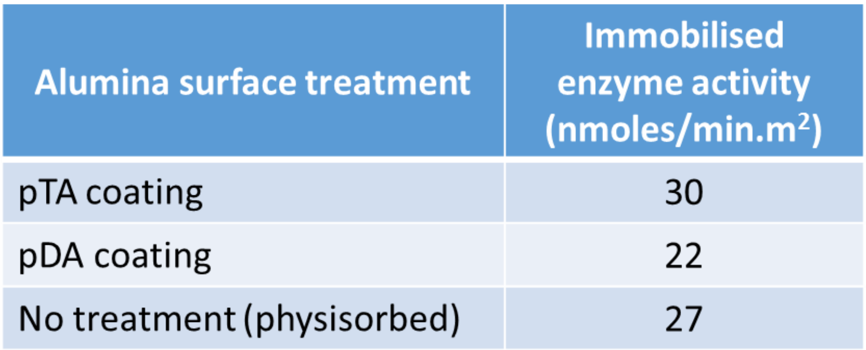

Alumina surface treatment	Immobilised enzyme activity (nmoles/min.m^2)
pTA coating	30
pDA coating	22
No treatment (physisorbed)	27

B. Anodic aluminium oxide (AAO) membranes fabrication

Aluminium pieces of high purity (99.999 %) were mechanically polished and placed on a sample holder (Figure I.13). The sample holder was screwed and placed in an electrolytic cell to perform electropolishing and anodisation procedures.

Figure I.13 – (A) Anodisation holder with a copper tape to connect the electrode to the samples. (B) Holder with 3 aluminium samples.

Different conditions during the anodisation process can control the morphology and pore structure of the membranes. The parameters that characterise the pores structure are: pore organisation, pore size, interpore distance, thickness and barrier layer thickness. The main aim of producing these membranes is fabricating uniform surfaces with well-defined pore size and thickness and without holes, gaps or cracks that can rupture the membranes during their usage. There are two steps to prepare the samples before the anodisation process. These procedures have been reported to control the organisation of the pores and the mechanical stability of AAO membranes. They are: mechanical- and electro-polishing.

Mechanical- and electro-polishing procedures diminish the surface irregularities that have an impact on the pore organisation. The mechanical-polishing was applied in order to smooth and flatten the aluminium surfaces on larger scales while electropolishing etches and flattens the surface at the microscopic level. By FE-SEM images (Figure I.14), we can observe that the sample with both polishing processes generate a more organised structure compared to the sample with no mechanical polishing. Also, it was observed in the laboratory that the mechanical-polishing helps to initiate the electro-polishing process.

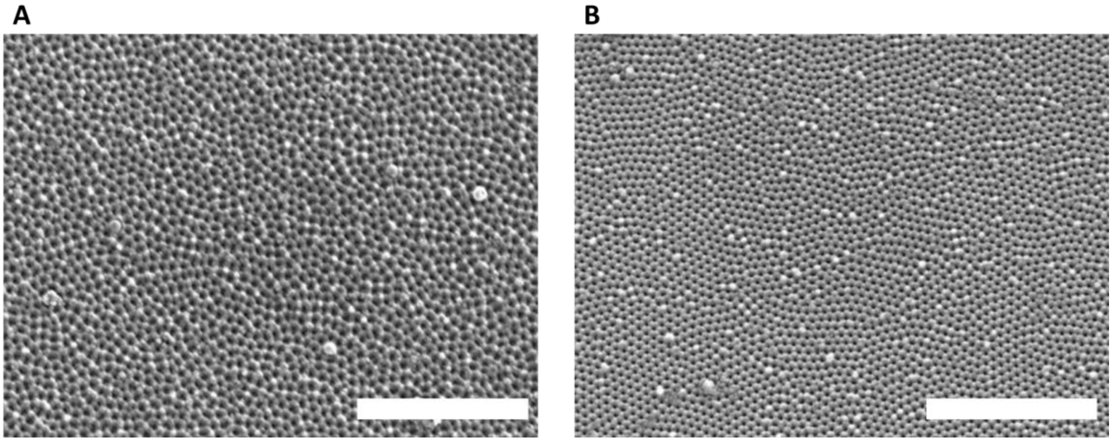

Figure I.14 – FE-SEM images after the second anodisation of AAO membranes with (A) no mechanical- and (B) mechanical-polishing (both electro-polished). Operating voltage of 20.0 kV and magnification of 20,000. Scale bar corresponds to 2 µm.

After preparing the aluminium surfaces, anodisation was performed with oxalic acid solution (0.1 M) as the electrolyte at 30 °C and 40 V. The first step of anodisation and its conditions allow production of a nanoporous surface with 100 nm of interpore distance and 25-30 nm pore size. The anodisation conditions were selected according to the self-ordering voltage and corresponding interpore distance profile described by Lee *et al.*.[175]

This first anodisation followed by the etching step creates a pore template for the second step of anodisation. In this second step, the membrane thickness and mechanical properties can be controlled by varying the time and/or the temperature. The nanopores grow with the time, so the duration of the second anodisation needs to be controlled.

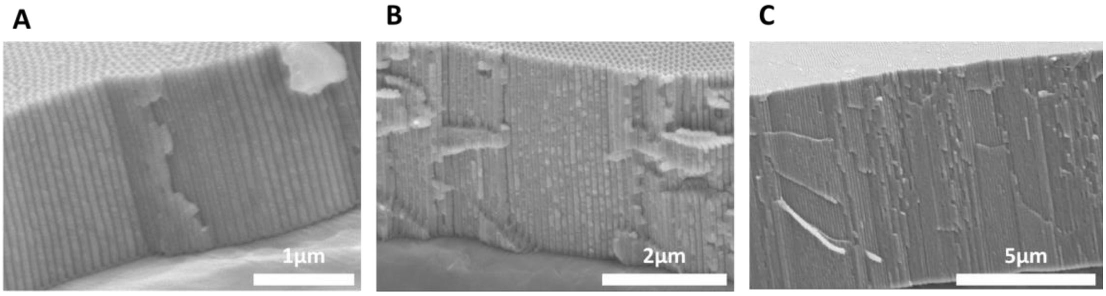

Figure I.15 – FE-SEM images of AAO films cross-section after (A) 60, (B) 120 and (C) 210 minutes of the second anodisation. Operating voltage of 5.0kV and resolution of 35.0. 22.0 and 10.0k.

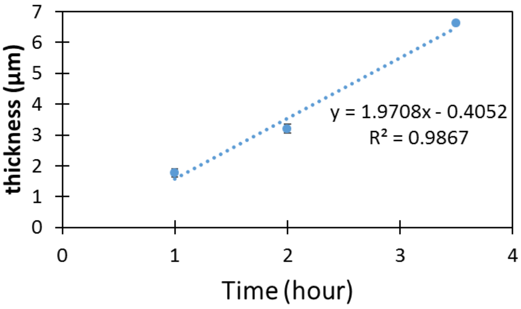

Figure I.16 – Growth rate of the aluminium oxide layer during the second anodisation.

Figure I.15 and Figure I.16 show that the alumina film grows during the anodisation and the growth rate is about 2 µm/min. The second anodisation can be performed using this rate value as a reference to produce thinner or thicker membranes, depending on the application and/or the desired thickness (for waveguide < 2 µm and for suspended membranes around 30 µm).

The initial pore size (after anodisation) is around 27 nm but the pores can be widened by immersing the membrane in a phosphoric acid solution. We immersed membranes, each one for 5, 10 or 20 minutes and the etching rate was calculated by measuring the obtained pore sizes (Figure I.17).

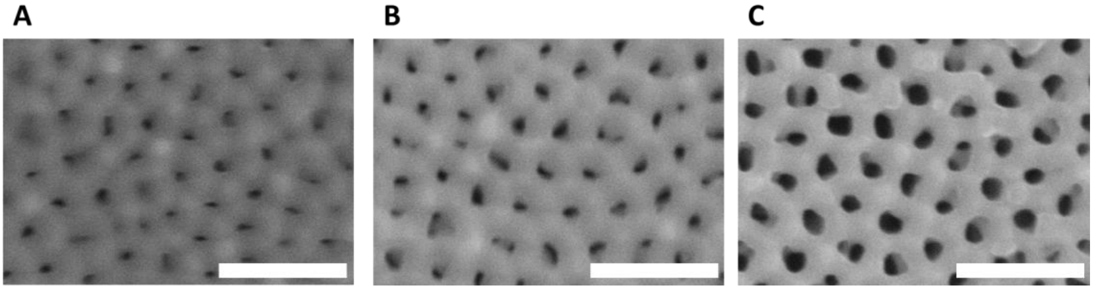

Figure I.17 – FE-SEM images of AAO membranes surface after 5, 10 and 20 minutes in 8.4 % phosphoric acid solution (left to right). Operating voltage of 5.0kV and resolution of 150k. Scale bar corresponds to 300nm.

Further work on this widening process with 5% phosphoric acid was carried out and the calculated rate during etching is of 0.3 nm/min. Since the interpore distance is 100 nm and the initial pore size is 25-30 nm, the pores can be widened up to 40 minutes until the membrane completely dissolves.

The alumina pores (anodised side) were protected from etching and all the aluminium that exposed to the etching solution was removed. After removing Al, the anodised membrane appears clear and transparent and held by an aluminium o-ring (Figure I.18).

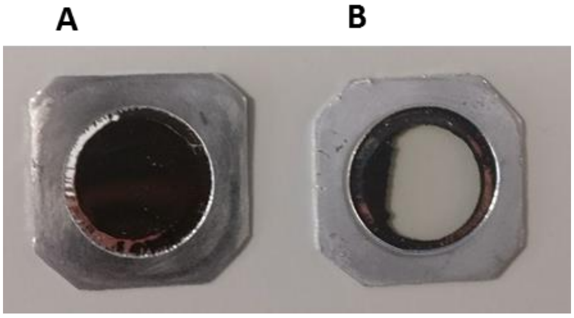

Figure I.18 – Sample before (left) and after (right) the aluminium etching.

FE-SEM images in Figure I.19 summarise the morphology and structure of AAO membranes during the fabrication. The aluminium surface after the electropolishing is smooth and flat (Figure I.19 A) and then, after the first anodisation procedure, straight alumina nanopores are formed (Figure I.19 B). The alumina nanopores are etched in order to create a surface-textured template (Figure I.19 C) from which the growth of well-organised ordered arrays of nanopores can initiate on the second anodisation (Figure I.19 D).

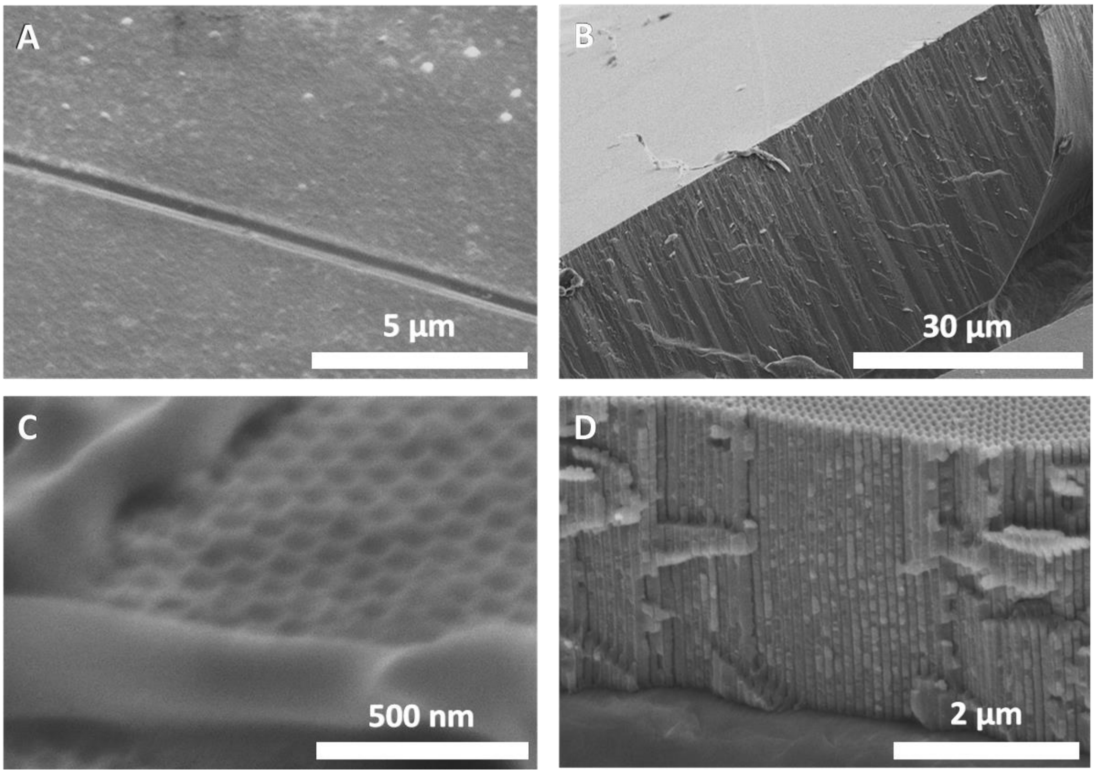

Figure I.19 – FE-SEM images after some steps during the fabrication process of AAO membranes. After (A) electropolishing, (B) 2 hours of the first anodisation, (C) 1 hour of alumina etching and (D) 2 hours of the second anodisation.

C. Nanoporous alumina membranes as optical waveguides

Fluorescence scans of AAO waveguides were performed to assess the presence or absence of adsorption processes. In Figure I.20, the overall fluorescence intensity increased after injecting Streptavidin-Alexa647 (Sv). After rinsing Sv, the fluorescence intensity in some of the modes increased to a larger extent, which means that there was more adsorption on that region of the pores (in this case, bottom and middle of the pores, 1st and 2nd modes).

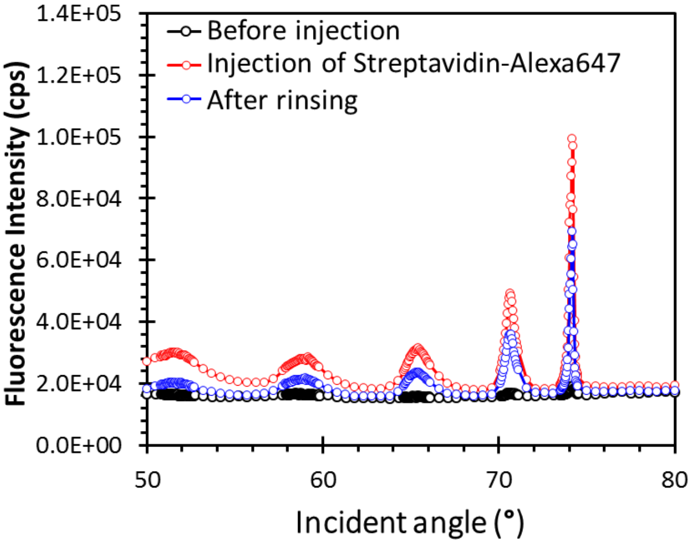

Figure I.20 – Fluorescence scans of the AAO waveguide (30 nm pore size, 1.6 µm thick coated with tannic acid and PEG) showing the fluorescence increase and decrease after injecting and rinsing the labelled protein (0.17 µM Streptavidin-Alexa647). These scans show protein adsorption on the surface and inside of the pores but more at the bottom of the pores (higher angles, more fluorescence intensity increase).

The AAO films were functionalised with poly(tannic acid) (pTA) coating. Figure I.21 shows the reflectance scans of the waveguides before and after the pTA coating when different concentrations of TA and duration of the coating were varied. Low concentration of TA does not change the pore sizes, but higher concentrations can close the pores. In Figure I.21B, the modes at lower angles were shifted much more than at higher angles, which means that the pores were closed at the entrance. By FE-SEM, it was demonstrated that the pores were closed and the time constant values of Alexa647 diffusion confirmed that as well.

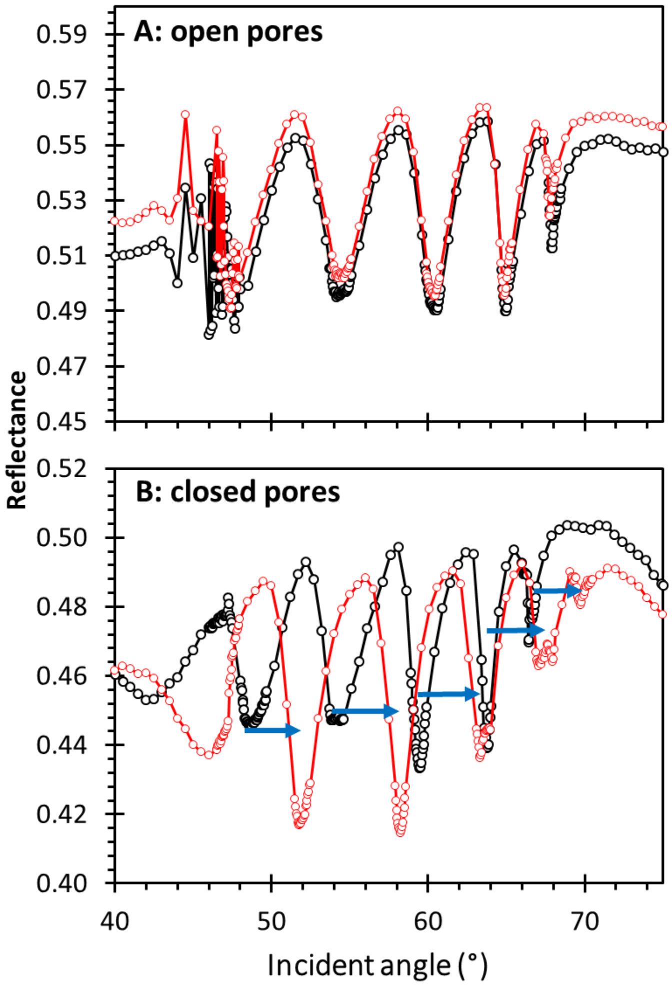

Figure I.21 – Reflectance scans of 50 nm pore waveguide before (black) and after (red) poly(tannic acid) (pTA) coating. (A) When the pores are coated with 0.01 mg/mL TA for 15 min (open pores) and (B) two times 0.1 mg/mL TA for 1h (closed pores).

To compare the experimental results with the literature, the time constant values of Alexa647, Streptavidin-Alexa647, IgG-Alexa647 were calculated based on the diffusion constant (D, μm^2/s) found in the literature and using Einstein equation. The time constant values obtained from the diffusion with open pores were corrected by subtracting the time constant values obtained in the experiments with closed pores (bulk diffusion) (Table I.3).

Table I.3 – Time constant values correction using the time constant values obtained when the pores open and closed.

Molecule	Molecular Weight (kDa)	Radius (nm)	D (μm²/s)[a]	Time constant, τ (s) Open pores	Time constant, τ (s) Closed pores	Time constant, τ (s) with correction
Alexa647	1.25	0.7	1.664	22.77	21.57	1.20
Streptavidin-Alexa647	60	3.4	0.384	28.00	22.80	5.21
IgG-Alexa647	150	5.5	0.273	31.96	24.65	7.32

[a] calculated using Einstein equation, $\langle x^2 \rangle = q_i D t$, where x is mean-square displacement (2 μm pore length), q_i the numerical constant (q_i = 2 for 1 dimensional diffusion), D is diffusion coefficient (μm^2/s) obtained from the literature and t is the time (in seconds).

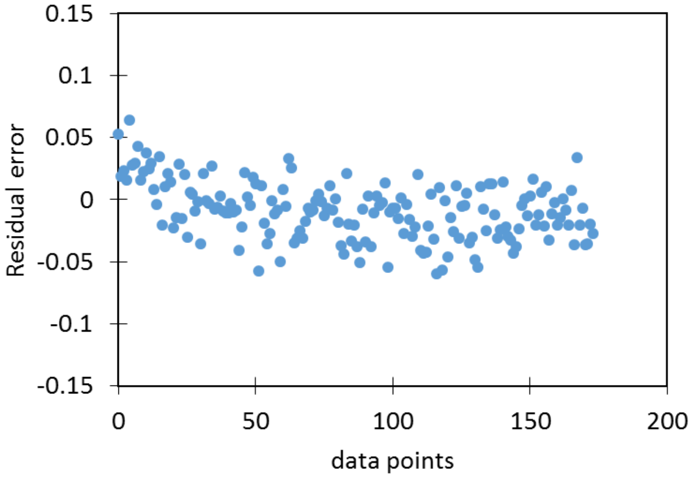

Figure I.22 – Residual error: difference between the observed value and the fitted value.

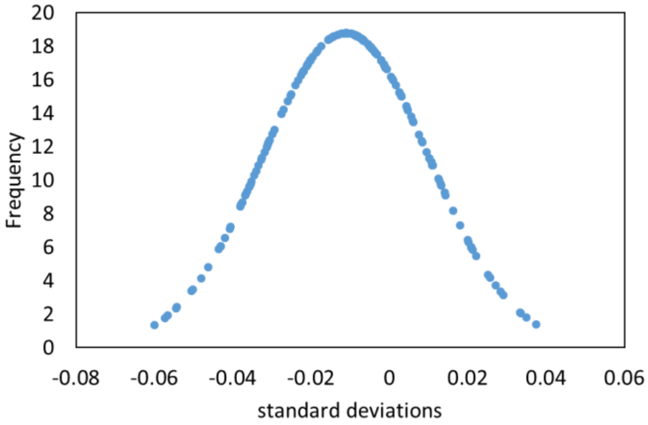

Figure I.23 – Normal distribution of the mean and standard deviation of an exponential fitting used to calculate the time constant (τ).

D. Diffusion Analysis Interpretation

Diffusion is defined by the movement of molecules from one area of high concentration to an area of low concentration. Diffusion is a process resulting from the random movements of atoms. In our study, our aim is to characterise the diffusion of molecules (fluorophores) through the pores which means the fluorophores will diffuse from a region of high concentration to low concentration to reach an equilibrium. During our measurements, different processes are occurring but the sum of those processes characterises the change in concentration of the fluorophores. To be brief, we refer to this as "diffusion kinetics".

Different processes occur during the diffusion of molecules through nanopores. In our system, a flow cell is filled with buffer (flow speed of the pump was set at 34 μL/min) and then we flow fluorophores dissolved in buffer into the flow cell. The fluorophores enter in the flow cell and travel along the flow cell (Figure I.24).

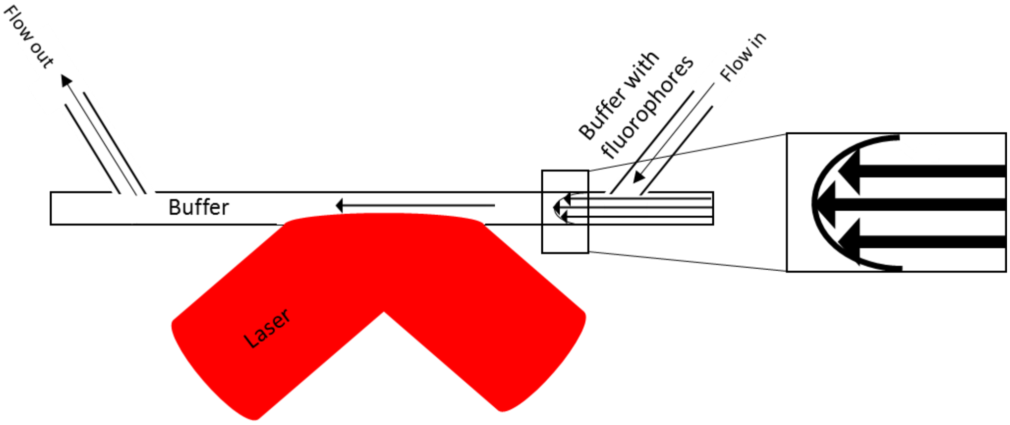

Figure I.24 – Cross-section of the flow cell showing the laminar flow inside the flow cell.

As described by Taylor-axis dispersion for laminar flow in a pipe (see endnote below), the liquid flowing through the flow cell has a parabolic shape over the height of the flow cell and the velocity inside the flow cell is not the same over the height of the flow cell (see inset of Figure I.24). The arrows in Figure I.24 show that the flow at the bottom interface is much slower (technically 0 at the bottom interface) than at mid-height of the flow cell (maximum flow speed): process (1) (Figure I.25).

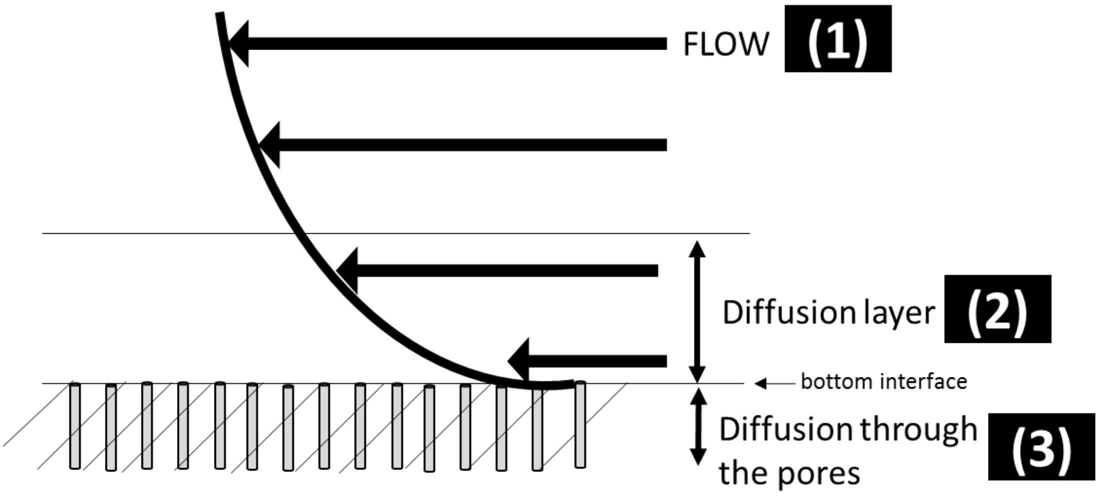

Figure I.25 – Scheme of the different processes that occur when there is flow and diffusion through the pore.

The flow is slow at the bottom interface, so the diffusion dominates the transport of molecules. This is called the diffusion layer, process (2) (thickness of the layer depends on the flow – it is thinner with the flow increment).

Once the fluorophores have diffused to the bottom interface, they can eventually find the pores and diffuse through these, process (3). There is less volume for the fluorophores to diffuse inside the nanoporous layer (reduced volume/cross-section area for diffusion to take place and can also be nanopore effect). Therefore, the effective diffusion constant is smaller inside the nanoporous layer than in the bulk solution above the bottom interface.

Each process has complex equations that characterise the different phenomena (see analysis in the endnote of this appendix). For convenience, the measurement is fitted empirically with a one effective time constant. There is no physical model to fit our data. However, an exponential decay is used and is expressed by $I = 1 - e^{-t/\tau}$ where I is the normalised fluorescence, t the time from the start of the flowing fluorophores and τ the time constant of the diffusion kinetics. This equation describes when the fluorophores are flowed to the flow cell (injection).

In our experiments, we decided to use the data that correspond to the rinsing process. The pores were filled with fluorophores and a buffer was flowed inside the flow cell to remove most of the fluorophores by mass flow (in the bulk of the chamber above the interface). The underlying equation describing the time-dependent concentration change is simpler for diffusion away from the interface than for diffusion to an interface and we do not have to consider (irreversible) adsorption of the diffusion species on the pore walls: $I = e^{-t/\tau}$.

These processes occurred also when we performed experiments with a suspended membrane (chapter 5). In the setup of chapter 5, the thickness of the pores is 60 µm instead of 1.5 µm (chapter 4) so the diffusion through the pores is much slower because the travel distance is bigger. After crossing the pores, the fluorophores diffuse through the second chamber and as a result the time constant values are larger.

Furthermore, a slight delay was observed on the diffusion kinetics with the decrease of concentration (fluorescence intensity). This is due to the delay that the system has to react to changes in concentrations and also because of the time that takes for the buffer to cross the laser spot and interact with the diffusion layer (Figure I.26). The signal is only detected when the front of the buffer crosses the laser spot.

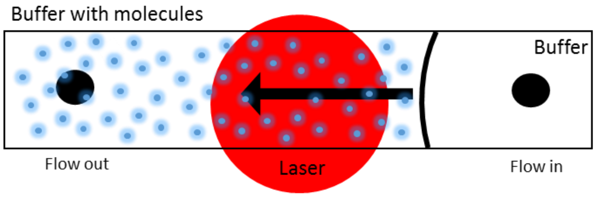

Figure I.26 – Scheme of the top-view of the flow cell. The buffer is flowed in the flow cell in order to rinse out the fluorophores (blue dots). The buffer takes a certain time to cross the laser spot (red circle). Black dots represent the input and output ports of the pump that were used to flow the liquid.

In our experiments with the nanoporous waveguide (chapter 4), we used open and closed pores to characterise the diffusion kinetics of fluorophores during rinsing. In the first case, the fluorophores that are inside the pores can i) diffuse out of the pores, ii) diffuse in the diffusion layer and iii) leave the flow cell from the flow. On the other hand, when the pores are closed, the fluorophores are only on the top of the nanopores, there is diffusion only through the diffusion layer and flow in the flow cell. The fitting of the data for both cases was performed using the same equation even though different predominant processes occur. We decided to fit all with the same equation, an empirical fit, because our measurements are the result of the combination of different processes that cannot be separated during the measurements and there is no simple analytical solution to describe all the coupled processes.

In the future, we would like to characterise each process and have a way to fit all the data including all of the processes however different parameters need to be varied in order to understand the effect of each process on the diffusion of molecules through the pores. For example, if the flow pump speed increases, the diffusion layer is very thin and this process can be ignored. However, at the same time, the flow speed cannot be too high or it will force the movement of molecules inside the flow cell.

Endnote of Appendix D - Analysis by Dr K. H. Aaron Lau. Document prepared by Ana M. L. Sousa

Taylor-Aris dispersion – combined mass flow and diffusive transport in a flow cell

Taylor-Aris dispersion describes the process of pumped laminar flow along a channel.[176,177] Molecular transport in this case is due to both mass flow and diffusion, as the flow speed near the periphery of the channel decreases, in principle, to zero following a parabolic profile with maximum flow speed in the centre of the channel (see Figure I.24). The diffusion layer refers to the thickness next to the channel surface, *e.g.*, on top of the nanoporous sample or bottom interface of the flow cell, at which the diffusion becomes dominant relative to flow. For example, at a pump speed of 34 µl/min in the flow cell used (full height = 0.5 mm) and assuming diffusion constant, $D = 10\ \mu m^2/s$, the ratio between the time scales associated with flow and diffusion (*i.e.*, the Péclet number) equals unity at a height of 5 µm away from the bottom interface.

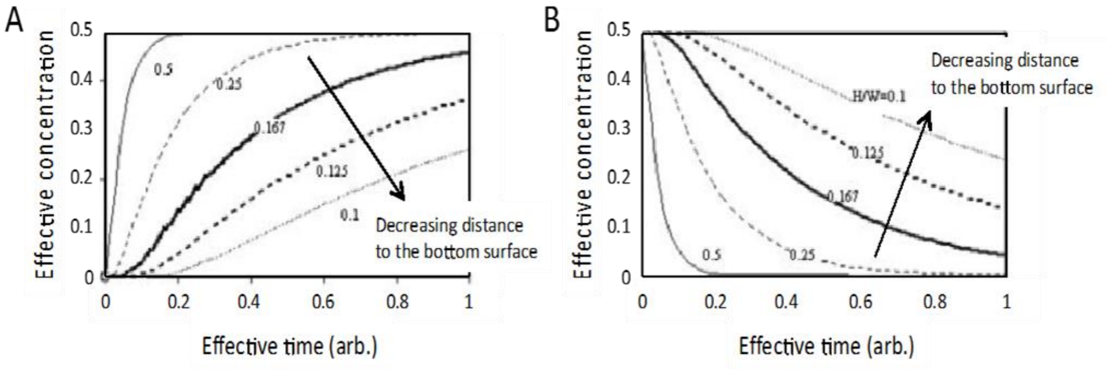

Figure I.27 – Computed time-dependent concentration profiles under Taylor-Aris dispersion at various depths within the diffusion layer towards the no-slip “bottom” surface. The bottom is a non-absorbing (*i.e.*, reflecting) wall. The concentration depends on transport by both mass flow and diffusion. (A) shows the increase in concentration with time as a solution with concentration = 0.5 starts flowing across the observation position. (B) shows the decrease in concentration with time, starting at an initial concentration of 0.5, as an unloaded solution with concentration = 0 flows across the observation position. Adapted from[178] for steady state flow within a microfluidic mixing channel (the travel down the channel is interpreted as the effective time in the figure shown).

The governing equation for the time-dependent concentration profile for Taylor-Aris dispersion is an infinite sum of the sums and ratios of exponential functions in time (t) and distance from the boundary of the diffusion layer where the flow speed is high enough for diffusion to be the minor contribution (x). The computed profiles for a model microfluidic channel is shown in Figure I.27. The shape of the time profiles approximate the solutions to the diffusion to and from a reflecting wall shown in Figure I.28.

Diffusion from a constant source to a reflecting wall – diffusion into closed nanopores

Diffusion into an array of identical cylindrical pores closed at the bottom (*i.e.*, into nanopores of the AAO membrane) is analogous to the classic problem of diffusion in the bulk towards a reflecting wall with an effective diffusion constant (D_{eff}):

$$C(x,t) = C_0 \left\{ \operatorname{erfc}\left(\frac{x}{2\sqrt{D_{\mathrm{eff}} t}}\right) + \sum_{n=1} (-1)^{n-1} \left[\operatorname{erfc}\left(\frac{-(x-2nl)}{2\sqrt{D_{\mathrm{eff}} t}}\right) - \operatorname{erfc}\left(\frac{(x+2nl)}{2\sqrt{D_{\mathrm{eff}} t}}\right) \right] \right\}$$

Equation 1

Equation 1 is plotted in Figure I.28. D_{eff} is expected to be smaller than the value in a bulk solution because of the reduction in cross-sectional area for transport in the membrane layer due to the presence of the solid alumina matrix and because of nanopore effects (*e.g.*, excluded volume effect and any surface specific molecular interactions).

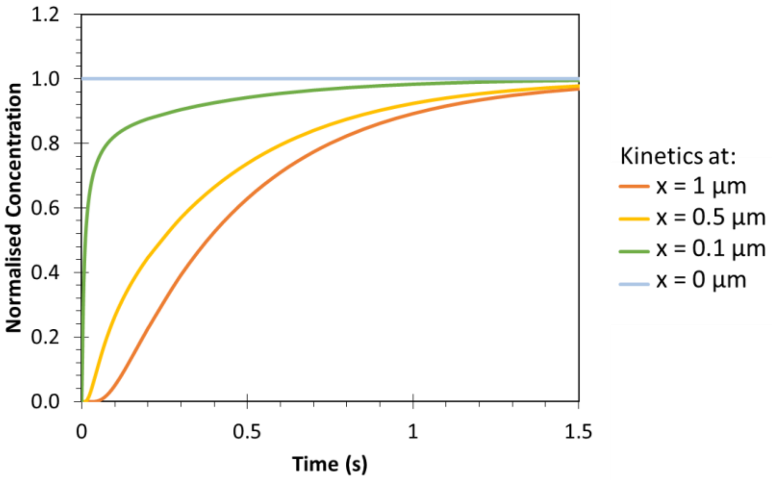

Figure I.28 – Concentration profile at different depths of the nanoporous layer. The full width of the layer is 1. x = 0 µm corresponds to the pore entrance and x = 1 is at the bottom of the pore. Graph is plotted for $D_{eff} = 10\ \mu m^2/s$, layer thickness l = 1 µm.

The concentration at the pore entrance is determined by the combined flow and diffusion of the Taylor-Aris dispersion describing transport in the flow cell. However, the form of the diffusion profile should be self-similar for any initial concentration at the pore entrance, although the actual measured kinetics of the concentration change is slowed by the fact that it takes a finite time to deliver the full concentration of the molecular species (*e.g.*, fluorophore or labelled protein) to the pore entrance due to Taylor-Aris dispersion (see Figure I.28).

Diffusion from the bottom of a suspended nanoporous membrane to the bottom of the lower flow cell chamber enclosed by the membrane and the bottom glass substrate

This is also a case of diffusion in the bulk towards a reflecting wall (Equation 1), except that without the porous membrane, the regular diffusion constant (*D*) should be used.

Diffusion from a finite source to a perfectly absorbing wall – diffusion out of nanopores

The reverse problem of diffusion from an array of identical cylindrical pores that are initially filled with a certain concentration of molecules (*i.e.*, out of the nanopores of the AAO membrane) is analogous to the classic problem of diffusion out into an infinite sink from a filled space closed at one end by a reflecting wall:

$$C(x,t) = C_0 \operatorname{erfc}\left(\frac{-(x-l)}{2\sqrt{D_{\text{eff}}t}}\right)$$

Equation 2

Equation 2 is plotted in Figure I.29. As in Equation 1, D_{eff} is the effective diffusion constant, l is the length of the pores/thickness of the nanoporous membrane. The summation term seen in Equation 1 is no longer needed in Equation 2 because diffusion is towards an infinite sink with molecules removed by the mass flow in the flow cell, rather than towards a reflecting wall (closed pore bottom). The Taylor-Aris dispersion for the removal of the molecule in the flow cell is ignored in this idealised description. As in the case of the diffusion into the pores, the concentration at the pore entrance, in fact, will take a finite time to decrease during flow cell rinsing. Thus also analogous to the diffusion in, this time-dependent rinsing will act to delay the diffusion out of the pores.

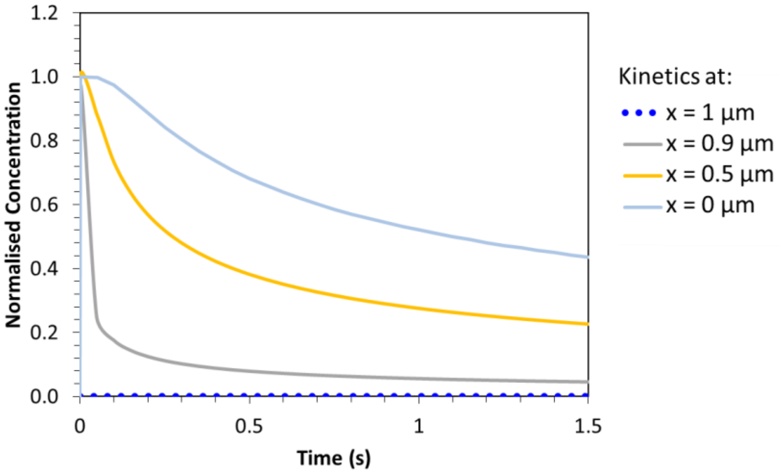

Figure I.29 – Concentration profile at different depths of the nanoporous layer. x = 0 is at the bottom of the pore and x = 1 is at the entrance, where the concentration is always 0 from rinsing. Graph is plotted for Deff = 10 µm^2/s, layer thickness l = 1 µm.

Diffusion through a suspended nanoporous membrane

$$C(x,t) = C_0 \operatorname{erfc}\left(\frac{x}{2\sqrt{D_{\mathrm{eff}}t}}\right)$$

Equation 3

Equation 3 shows the first term of Equation 1, which applies to the case of diffusion from the pore entrance through a porous membrane (*i.e.,* a suspended AAO membrane with nanopores opened on both sides) for relatively short times before the concentration in the bottom flow cell rise appreciably. This first term is simply the inverse of Equation 2, and the time profile is simply the mirror image of Figure I.29 (*i.e.*, flipped top to bottom with trends starting from 0 increasing to 1 with time). The summation term is not relevant at "short times" because the reflecting pore bottom barrier layer is removed. At long times, for a bottom flow cell that is enclosed (no flow out), the solution reverts back to the case of the reflecting wall with a time delay to account for the diffusion in the bottom part of the cell.

Liquid flowing past laser spot (measurement area)

How the laser illuminates the bottom of the flow cell is shown in Figure I.24. The laser has essentially a Gaussian beam profile with maximum intensity in the middle (Figure I.30). The full signal is detected only when the flow of fluorophores has passed entirely over the laser spot. Thus, even without Taylor-Aris dispersion or diffusion effects, the fluorescence signal initially increases slowly as the flow passes the low intensity of the periphery of the beam. As the flow has almost passed over the entire beam spot, the increase in intensity slows as the flow comes again to a low-intensity region of the beam. Similarly, in the rinsing step, as fluorophores are removed, the decrease in intensity simply with flow follows the intensity profile of the laser beam. The overall effect of taking a finite time to pass over the beam spot is the integration over time over a Gaussian profile. The solution of this integral is the error function (Figure I.31).

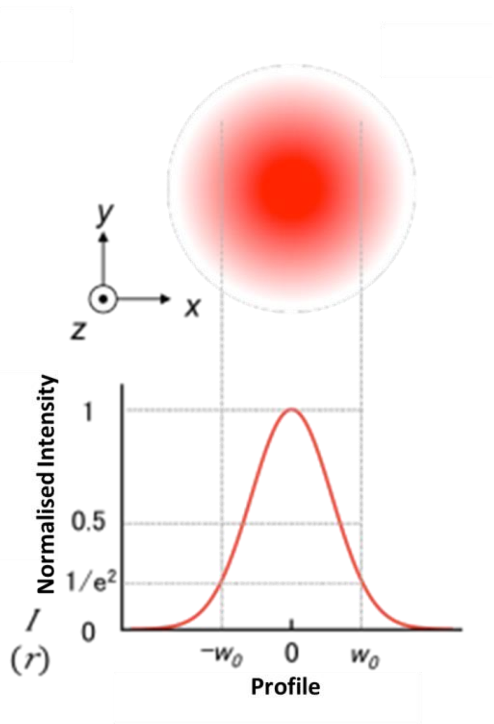

Figure I.30 – Profile of the intensity of the laser spot.

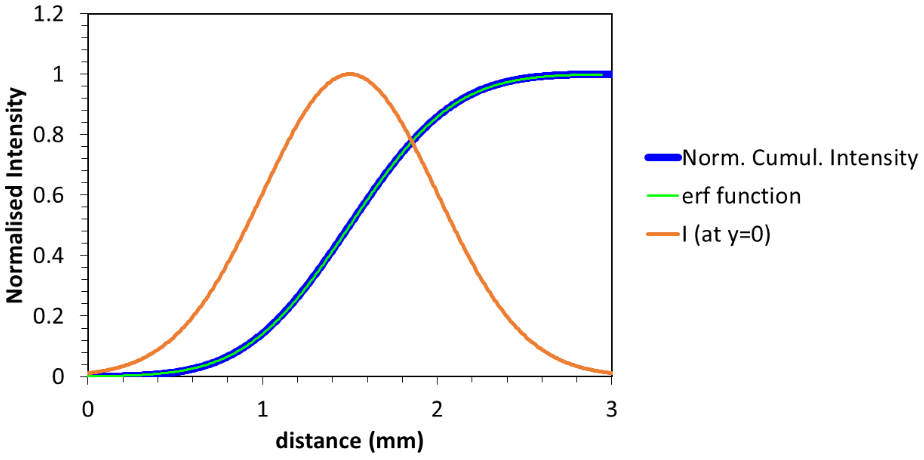

Figure I.31 – Plotted with a beam width of 3 mm, defined as 3x standard deviation of the Gaussian profile (Gaussian is the orange curve).

This delay in the signal intensity reaching a maximum has to be coupled to all the other flow and diffusion processes described in the previous sections. Effectively, the initiation of either the introduction or removal of the fluorophore is shifted in time by an error function corresponding to the beam shape. This effect is illustrated in Figure I.32.

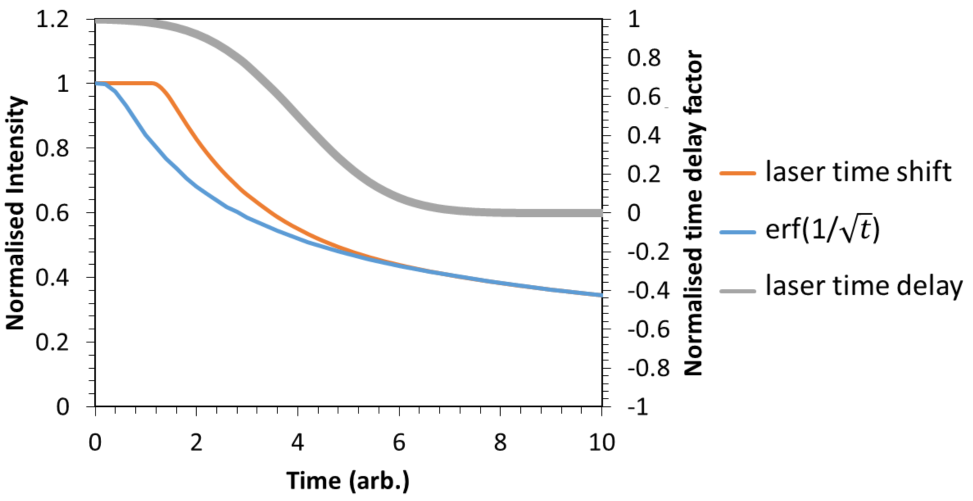

Figure I.32 – Plotted with arbitrary time constants for the flow and diffusion (rinsing case). The right axis indicates the magnitude of the time delay due to mass flow sweeping past a Gaussian beam spot with an arbitrary time constant of 2.

Coupled flow and diffusion in the experimental system

The concentration changes measured at the bottom interface (of either the nanoporous waveguide or the bottom of the flow cell in the suspended membrane setup) is delayed due to the Taylor-Aris dispersion in the flow chamber. This is similar to the delayed and decreased initiate rate of signal intensity change due simply to the effect of flowing fluorophores over the laser beam spot over time described above. As shown in earlier sections, the Taylor-Aris dispersion is not described by simple closed-form analytical solutions. Coupling the diffusion in the nanopores to this transport in the chamber as well as the sweep of the laser beam spot is even more complicated and is not attempted. Nonetheless, it is clear that the time-dependent concentration profile has an initial slow change at an increasing rate, followed by an increase at a decreasing rate of change (see *e.g.*, figures in this endnote). The later part of change at a decrease rate to an asymptotic value in the signal intensity is especially seen to be the dominant part of the process. Therefore, an empirical fit to the data focusing on this part of the process with a limited combination of effective time constants (*e.g.*, 1 or 2) should be a practical means to a quantitative description of the time scale of the transport.

E. Characterisation of nanoporous membranes for impedance and diffusion measurements

Anodic aluminium oxide (AAO) membranes characterisation

The comparison of commercially available alumina (anodiscs) and fabricated AAO membranes regarding interpore distance and pore sizes is in Figure I.33. The pore density on the fabricated AAO membrane (Figure I.33B) is 7 times higher than on the anodisc membranes. However, per sample area, the surface area of anodiscs (Figure I.33A) is 2 times higher than on fabricated AAO membrane.

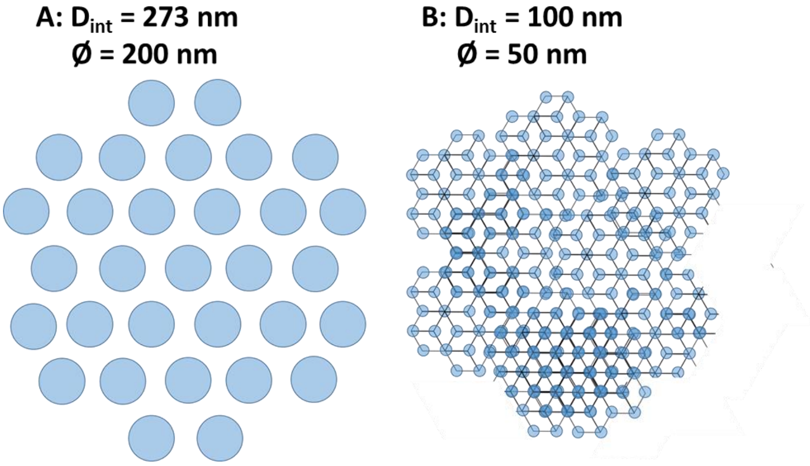

Figure I.33 – Illustration of the pores of a membrane with an interpore distance (D_{int}) and pore size (Ø) of (A) 273 and 200 nm and (B) 100 and 50 nm.

The fabrication of AAO membrane finishes with the removal of unreactive aluminium. When all the aluminium is removed, an alumina barrier layer is exposed (Figure I.34A). This layer also needs to be removed so that the bottom of the pores of the AAO membranes can be open (Figure I.34B).

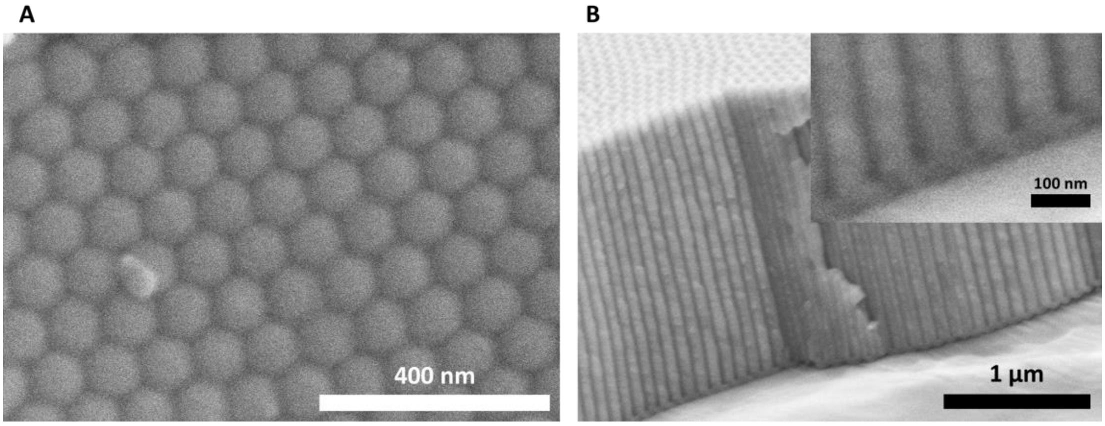

Figure I.34 – SEM pictures showing the barrier layer on the fabricated anodic aluminium oxide (AAO) membranes. (A) After AAO fabrication, the unreactive aluminium was etched and the barrier layer was revealed. (B) Cross-section of AAO membrane showing the barrier layer at the bottom of the pores. Inset = higher magnification image.

To remove the barrier layer, a protective polymer layer was applied on the anodised side of the AAO membrane. This polymer had the aim of protecting the pores from the acid solution used to remove the barrier layer. After removing the barrier layer, the protective layer was also removed from the anodised side and that side of the membranes was characterised by FE-SEM (Figure I.35). The SEM image showed that the polymer left some debris even after cleaning the surface.

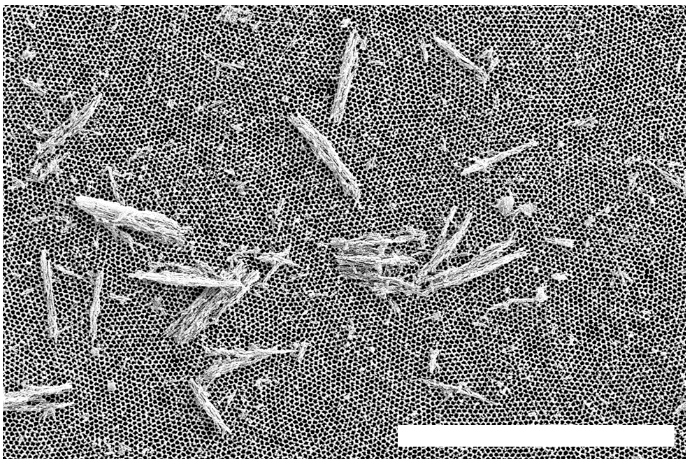

Figure I.35 – FE-SEM images of the pores on the anodised side after removing the barrier layer and the protective polymer. Scale bar = 5 μm. Some debris from the protective polymer remained on the membrane.

Impedance measurements

For impedance measurements and to remove the barrier layer, the fabricated AAO membrane was placed between two chambers. In Figure I.36, it is shown how the handmade chambers were used to place the AAO membrane for the impedance measurements.

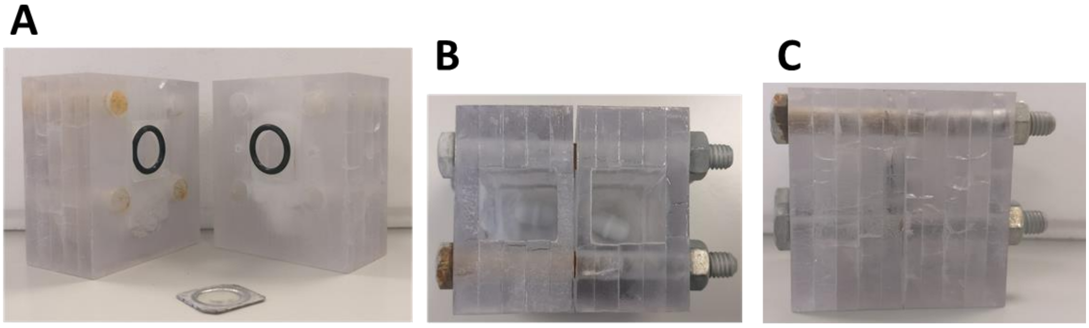

Figure I.36 – Sample holder of impedance measurements. (A) Demounted holder – two individual chambers that are clamped together. An alumina membrane (bottom of the photo) is placed in between the two chambers with an o-ring sealing. (B) top and (B) side views of the mounted holder.

The impedance measurements were followed by monitoring the change of the voltage, and frequency *versus* the theta values (Figure I.37). There are two main states during these impedance measurements: (1) when the pores are being opened, and (2) when the membrane is completely dissolved. In the first state, the voltage decreases when the pores are being opened and the frequency values change from a quadratic to cubic function – change shape from purple curve (47 min) to yellow curve (59 min) (Figure I.37B (1)). After the pores being opened, the frequency values do not change anymore because the pores only being widened (Figure I.37B (2)). In Figure I.37C, the time was plotted *versus* the theta value at the frequency of 10,000 Hz, where can easily see the change during the pore opening.

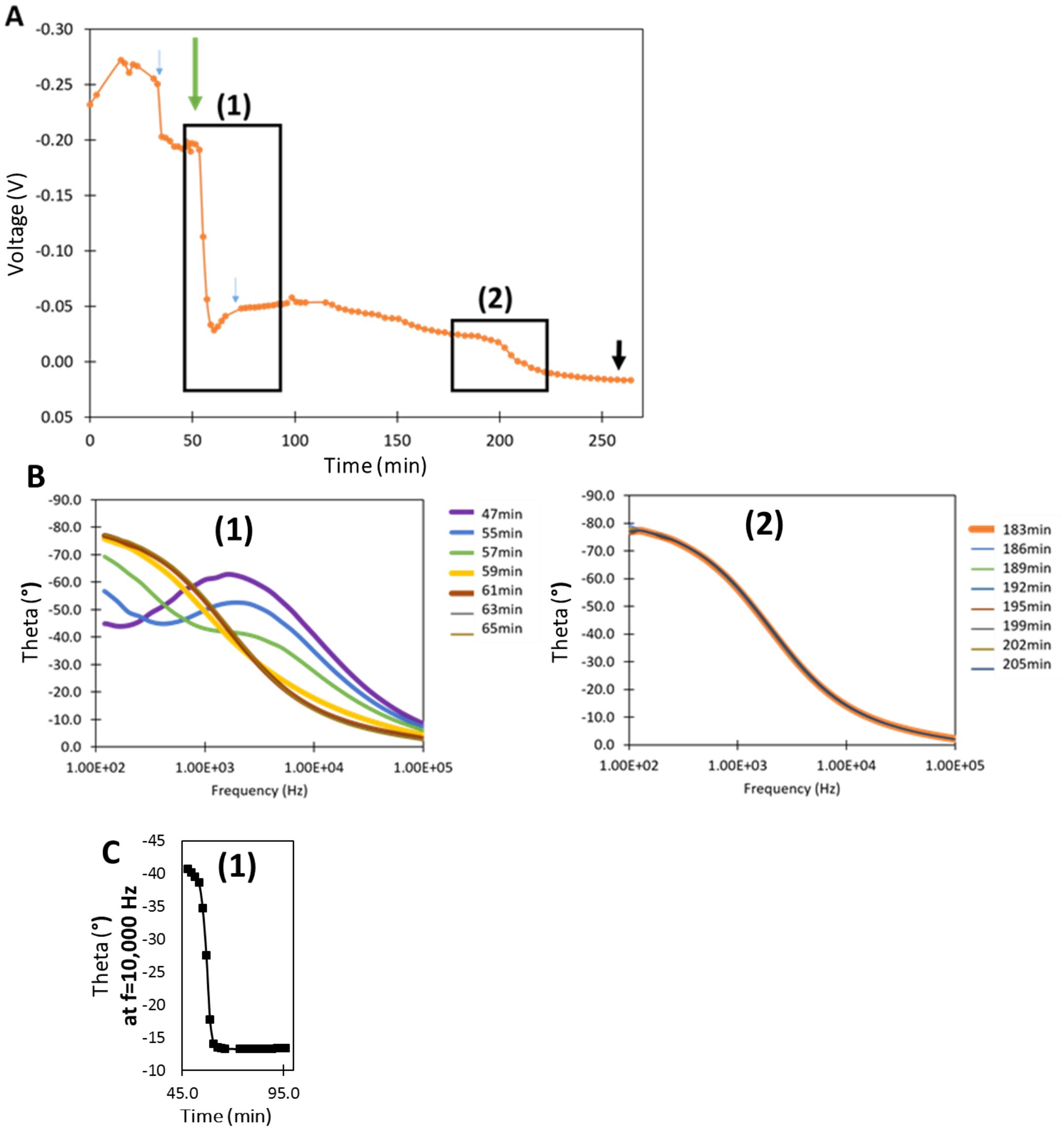

Figure I.37 – Impedance measurements for opening the pores of an alumina membrane. (A) Open circuit voltage measured between the two chambers until the membrane was completely dissolved. Blue arrows represent a new batch of measurements, more solution was added to the chambers, or the electrodes were moved during the measurement which caused a change in the voltage. The green arrow represents the pore opening, and the black arrow represents that the completely dissolved membrane. The data was also plotted theta *versus* frequency and the corresponding graphs for the insets (1) and (2) are B(1) and B(2), respectively. C(1) represents theta at 10,000 Hz during the opening process (A(1)).

Impedance approach did not directly protect the pores of the anodised side. The pores were not covered with any protective layer, but the anodised side was not directly in contact with the acid solution having a negligible effect on the pore widening. Figure I.38 show the pores of a membrane after removing the barrier layer using impedance approach. It is noticeable the same pore size on both sides of the membrane proving that with this setup is not only possible to monitor the barrier removal *in situ* as well as the pore etching on the anodised side of the membrane was minimised, producing membranes with uniform pores.

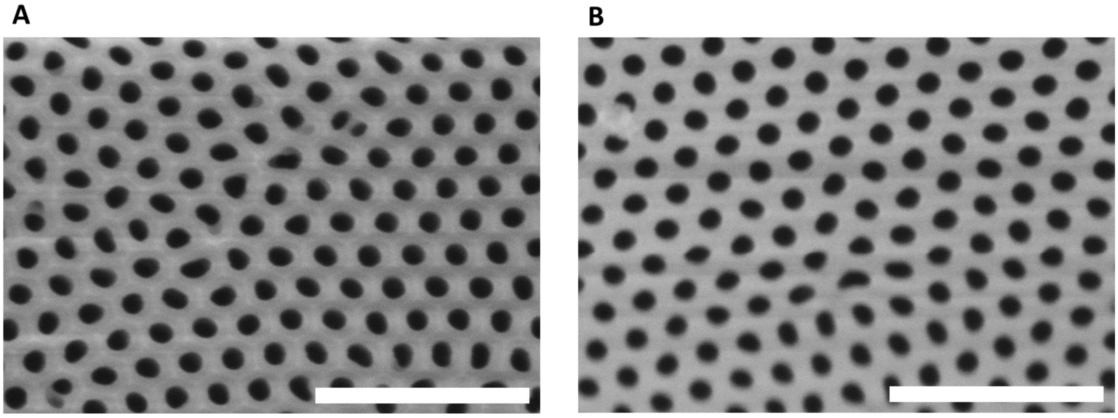

Figure I.38 – FE-SEM images of the pores on the (A) anodised side and (B) backside after removing the barrier layer using the impedance approach. Scale bar corresponds to 500 nm.

List of Figures

List of Tables